

**APPLICATIONS OF LASER INDUCED
PHOTOACOUSTIC EFFECT FOR THE STUDY OF
GASES AND SOLIDS**

A. V. RAVI KUMAR

**THESIS SUBMITTED
IN PARTIAL FULFILMENT OF THE REQUIREMENTS
FOR THE DEGREE OF
DOCTOR OF PHILOSOPHY**

**LASER DIVISION
DEPARTMENT OF PHYSICS
COCHIN UNIVERSITY OF SCIENCE AND TECHNOLOGY
COCHIN - 682 022
INDIA**

CERTIFICATE

Certified that the thesis entitled "APPLICATIONS OF LASER INDUCED PHOTOACOUSTIC EFFECT FOR THE STUDY OF GASES AND SOLIDS" is the report of the original work carried out by Mr. A V RAVI KUMAR in the Department of Physics, Cochin University of Science and Technology, Cochin 682 022, under my guidance and supervision, and that no part thereof has been included in any other thesis submitted previously for the award of any degree.

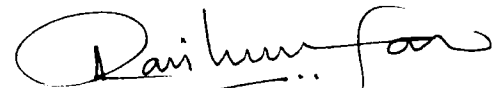
Cochin 682 022,
21 December 1992


Dr. C P Girijavallabhan,
(Supervising Teacher)

DECLARATION

Certified that the work presented in the thesis entitled "APPLICATIONS OF LASER INDUCED PHOTOACOUSTIC EFFECT FOR THE STUDY OF GASES AND SOLIDS" is based on the original work carried out by me in the Department of Physics, Cochin University of Science and Technology, Cochin 682 022, under the guidance and supervision of Dr. C P Girijavallabhan, Professor, Department of Physics, Cochin University of Science and Technology, Cochin 682 022, and that no part thereof has been included in any other thesis submitted previously for the award of any degree.

Cochin 682 022,
21 December 1992



A V Ravi Kumar

PREFACE

Ever since the advent of lasers and the subsequent rejuvenation of the century old phenomenon, namely Photo-Acoustic (PA) effect, discovered originally by Alexander Graham Bell in 1880, it has found innumerable applications in many fields like pure and applied physics, chemistry, biology and industry. Some of the applications range from areas of pure spectroscopy and trace analysis for pollution monitoring to analysis of human blood, cornea and even human skin. Such wide ranging applications arise mainly due to the features which are unique to this technique. These are essentially, fairly simple and straightforward experimentation, high sensitivity and selectivity, ability to give a direct measure of the energy absorbed, and applicability of the technique to a wide range of optical frequencies without changes in the detector. The studies on the phenomenon are based on the detection of the modulated acoustic waves generated in a sample due to excitation by absorption of modulated/pulsed radiation and subsequent relaxation to the initial state through a non-radiative pathways of de-excitation.

The material presented in this thesis is essentially a summary of the research work done by the author in the Laser Division of the Department of Physics at Cochin University of Science and Technology during the last four years. The investigations undertaken in the course of this thesis work involve the applications of the PA technique to detection and analysis of samples in gas phase using a pulsed as well as cw dye laser. The two main gas phase samples studied here are formaldehyde (HCHO) using the pulsed laser and nitrogen dioxide (NO_2) using both pulsed and cw lasers. Emphasis is given to the instrumentation, detection and application to trace analysis with reference to these samples rather than to their detailed

spectroscopic study, although for formaldehyde, some spectroscopic aspects like the one and two photon absorption (TPA) processes have been analyzed in the course of this work. PAS for TPA processes was also applied to samples like sulfur dioxide, acetone and methanol vapour, but this technique was unable to bring out such processes in these samples using the available wavelength for irradiation. Detection of NO_2 using PAS is important since it is a major air pollutant. Both pulsed and cw PAS were used to study the sample. Due to the very complex nature of the visible absorption and PA spectra of NO_2 , serious attempt was not made to analyze them though their spectral signatures were well established using both pulsed and cw PA techniques. The other aspect of PAS investigated in the thesis is the use of same to detect the laser induced damage threshold for surfaces in bulk materials. This brings out the utility and effectiveness of the PA technique for the study of certain physical properties of the solid state.

The thesis is divided into eight chapters and the chapter-wise summary of the same is given below.

The first chapter includes introduction to this technique, the history of photoacoustics, initial work done in this field and a review of some of the important previous work done in condensed as well as gaseous samples using PA technique. The applications of PA effect to gas phase studies, trace analysis and pollution monitoring are given special emphasis since the major work presented in this thesis is related to gas phase PA.

The second chapter describes in detail the process of absorption of radiation by matter and the subsequent generation of the PA signals in gaseous samples. Theoretical analysis of the rate equation for a simple two-level system, excitation of the acoustic wave and subsequent PA signal generation in both pulsed

and cw cases in gas phase have been briefly discussed. The role of dissipative processes in the PA signal generation has been pointed out. The dependence of the PA signal with the various parameters involved in the PA signal generation have been discussed. The Rosencwaig-Gersho theory for PA process in condensed matter in a gas-microphone cell has been discussed briefly. A few other models of PA generation such as the thermal-piston model for optically thick gases and the acoustic transmission line theory for the propagation of acoustic waves are also briefly mentioned. A discussion of parameters like PA signal saturation, Quality factor, skin depths etc form the remaining part of this chapter.

The third chapter deals with the essential instrumentation involved in PA studies. Beginning with a general description of the PA instrumentation, the different light sources, modulators etc. commonly used in PA studies are explained. Various kinds of PA cell, such as the Helmholtz resonator, differential, rectangular, cylindrical configurations, their advantages and specific applications are outlined with emphasis on differential PA detection technique. Different kinds of acoustic transducers, like microphones, piezo-electric detectors and the use of a few other exotic acoustic detectors are discussed in a concise manner. Noise in PA systems and methods for their elimination are also dealt with in some detail.

The pulsed and cw PA detection schemes are elucidated in detail and the principles behind the two signal processing involved in the two techniques namely, the box-car and lock-in detection methods are explained. The importance of the use of pre-amplifiers in PA detection is also mentioned.

Chapter IV describes the actual experimental setup used for PA studies using both pulsed and cw laser sources in the

laboratory. Detailed description of different sub-systems of the pulsed experimental setup namely the pulsed Nd:YAG laser, dye laser, energy meter etc. are given in this chapter. The design and characteristics of the single cavity PA cell used for pulsed studies is outlined. In the cw PA case, the cw argon ion laser, ring dye laser and its components, wave meter for wavelength measurements etc are also described. Following this, the design and characteristics of the dual cavity differential PA cell used for cw studies are illustrated in a detailed manner.

The acoustic characteristics of the dual cavity PA cell have also been investigated using NO_2 gas as the sample. Various response curves for the resonance frequency, Q factor, gas thermal diffusion length, cell constant etc are given here. The variation of these parameters with the gas pressure at high gas concentrations have been investigated and the results presented.

The fifth chapter contains the results of the pulsed PA studies on formaldehyde vapour obtained for the first time. The one and two photon absorption (TPA) processes have been demonstrated, and the normalized TPA PA spectra of formaldehyde vapour have been presented. Analysis of these spectra with reference to the optical absorption spectrum obtained using a UV-VIS-NIR spectrophotometer shows that one photon absorption (OPA) processes is significant at low laser energies while at higher laser energies, the TPA process dominates as observed from the log-log plot of the laser energy vs PA signal amplitude. Studies were done in the 564.5nm as well as the $1.06\mu\text{m}$ wavelength regions and similar results were obtained. The variations of the PA signal with laser energy and the gas pressure have also been studied. Saturation in PA signal was observed at sufficiently high gas pressures.

Chapter VI describes the PAS of NO_2 . It is divided into

two parts viz. A and B. Part A details the results of the PA experiments on NO_2 with the pulsed dye laser in the 560-580nm wavelength region. The normalized PA spectra are given and compared to the normal absorption spectrum of NO_2 in the wavelength region of interest. It was observed that the PA signal shows a minimum at the wavelength at which the absorption spectra show a maximum, thus indicating clearly the occurrence of a radiative path for de-excitation. The gas pressure and the laser energy variations of the PA signals at various wavelengths of interest have been investigated in detail and the results presented.

Part B of this chapter summarizes the results of the PA experiments with the cw laser. The variations of the PA signal with gas pressure and the laser powers of the various discrete lasing frequencies of the argon ion laser have been noted. With high concentration NO_x gas samples ($\sim 98\%$ NO_2 in 90 % NO_x : air mixture), saturation the signal due to both the laser power and gas pressure set in very early as compared to the low concentration gas samples ($\sim 98\%$ NO_2 in 4% NO_x :air mixture). The normalized PA spectrum of the $^2B_2 \rightarrow ^2A_1$ band system of NO_2 in the wavelength region 570-620nm is given. The PA spectrum profile matches with the absorption spectrum but the relative intensities are found to be quite different. Since the thesis attempts to apply the PA effect to gas detection and possible trace analysis, little effort was made to analyze the highly complex spectra of NO_2 . Parameters like the minimum detectable signal, total noise of the system etc. have been evaluated and given.

Chapter seven deals with the application of the PA technique to detect the onset of laser induced damage of surfaces in bulk materials. The chapter discusses the laser damage process, the different mechanism involved, some of the

conventional detection techniques and the difficulties that are encountered in the measurement of this quantity. The advantages of the PA technique over other techniques for laser damage detection are brought out. The detailed experimental setup and the signal monitoring technique for laser damage measurements are described. The versatility of this approach has been demonstrated by applying this technique to determine the laser damage thresholds in a variety of samples like metals, acrylic and thin films. This technique has also been used to monitor the laser induced plasma process. The experimental setup for simultaneous measurement of the plasma emission and the PA signal generated due to plasma formation are given. The plots of the PA signal and the emission intensities of the plasma plume with laser energy density were found to be linear within the region of interest.

The concluding chapter gives a summary and assessment of the scientific results presented in the previous chapters. It also indicates the future possibilities of doing further work in this direction by exploiting the photoacoustic effect.

Part of the results contained in this thesis has been published as research papers in the following journals :-

1. Photoacoustic detection of two photon absorption in formaldehyde using pulsed dye laser
A V RAVI KUMAR, G Padmaja, V P N Nampoori and C P G Vallabhan, Pramana, 33, L621, 1989.
2. Photoacoustic detection of NO_2 using pulsed and cw laser
A V RAVI KUMAR, G Padmaja, V P N Nampoori and C P G Vallabhan, Proc. IEEE National Seminar on lasers in Engineering and Medicine (IEEE-LASEM-89), page 101-105, 1989
3. Photoacoustic detection of two photon absorption in formaldehyde at $1.06 \mu\text{m}$ laser wavelength
A V RAVI KUMAR, G Padmaja, V P N Nampoori and C P G Vallabhan, J. Acoust. Soc. India, 17, 355, 1989

4. Two-photon absorption spectrum of formaldehyde using pulsed gas phase photoacoustic spectroscopy
A V RAVI KUMAR, G Padmaja, V P N Nampoori and C P G Vallabhan,
In the book 'Photoacoustics and Photothermal Phenomena II',
Edited by J C Murphy, Springer-Verlag (Heidelberg), page
360, 1990.
5. Evaluation of laser ablation threshold in polymer samples using pulsed photoacoustic technique
A V RAVI KUMAR, G Padmaja, P Radhakrishnan, V P N Nampoori
and C P G Vallabhan, *Pramana*, 37, 345, 1991
6. A differential photoacoustic cell for gas phase studies
A V RAVI KUMAR, G Padmaja, V P N Nampoori and C P G Vallabhan,
J.Acoust.Soc.Ind., 18, (to appear), 1992.
7. Determination of laser damage threshold using pulsed photoacoustics
A V RAVI KUMAR, G Padmaja, P Radhakrishnan, V P N Nampoori and
C P G Vallabhan, *J.Acoust.Soc.Ind.*, 18, (to appear), 1992.
8. Pulsed photoacoustic spectrum of NO_2 : Pressure and laser power dependence in the 560-570 nm region
A V RAVI KUMAR, G Padmaja, V P N Nampoori and C P G Vallabhan,
J. Acoust. Soc. India, 17, 44, 1990.
9. Pulsed photoacoustic technique for the measurement of laser damage threshold in bulk polymers
A V RAVI KUMAR, G Padmaja, P Radhakrishnan, V P N Nampoori
and C P G Vallabhan, *In the book 'Photoacoustics and Photothermal Phenomena III'*, Edited by Dane Bicanic,
Springer-Verlag (Heidelberg), (in press), 1992.
10. Damage threshold determination of bulk polymer samples by photothermal deflection technique
K Rajasree, A V RAVI KUMAR, P Radhakrishnan, V P N Nampoori
and C P G Vallabhan, *Bull.Mat.Sci.*, 15, 183, 1992
11. Spectral features of laser induced plasma from Y-Ba-Cu-O and Gd-Ba-Cu-O high T_c superconductors
G Padmaja, A V RAVI KUMAR, V Vidyalal, P Radhakrishnan,
V P N Nampoori and C P G Vallabhan, *Pramana*, 32, L693, 1989.
12. Time evolution of laser induced plasma from Gd-Ba-Cu-O high T_c superconductors
G Padmaja, A V RAVI KUMAR, V Vidyalal, P Radhakrishnan,
V P N Nampoori and C P G Vallabhan, *J.Phys.D:(Appl Phys)*, 22,
1558, 1989.

13. Detection of oxide species in the laser ablated plasma of high T_c superconducting sample

G Padmaja, A V RAVI KUMAR, V Vidyalal, P Radhakrishnan, V P N Nampoori and C P G Vallabhan, Proc. IEEE National Seminar on lasers in Engineering and Medicine (IEEE-LASEM-89), page 124-126, 1989

14. Photoacoustic detection of high resolution spectra of $\text{CaF}_2:\text{Nd}^{3+}$ using ring dye laser

S Gopikrishnan, A V RAVI KUMAR, R Navil Kumar, V P N Nampoori and C P G Vallabhan, J.Acoust.Soc.Ind., 17, 69, 1990.

15. Detection of air flow from laser irradiated target using photothermal deflection technique

K Rajasree, A V RAVI KUMAR, P Radhakrishnan, V P N Nampoori and C P G Vallabhan, J.Acoust.Soc.Ind., 17, 24, 1990.

16. Photoacoustic detection of modulated CO_2 laser beam

K Ratnakaran, A V RAVI KUMAR, V Vidyalal and C P G Vallabhan, J.Acoust.Soc.Ind., 17, 48, 1990.

17. Characteristics of laser induced plasma from high T_c superconductors

G Padmaja, A V RAVI KUMAR, V Vidyalal, P Radhakrishnan, V P N Nampoori and C P G Vallabhan, Bull. Mat.Sci., 14, 545, 1991

18. Spatial and Temporal Analysis of Laser Induced Plasma from a Polymer

G Padmaja, A V RAVI KUMAR, P Radhakrishnan, V P N Nampoori and C P G Vallabhan, J.Phys.D:(Appl Phys), 25, (in press) 1992

CONTENTS

CHAPTER I : PHOTOACOUSTIC EFFECT AND ITS APPLICATIONS

	PAGE
1.1. General introduction & history	1
1.2. Applications of the PA effect	6
1.2.1. PA studies in condensed matter	6
1.2.2. PA studies in liquids	12
1.2.3. PA studies in gases	15
1.3. Other phenomena closely related to the PA effect	26
1.3.1. The beam acoustic effect	27
1.3.2. Photothermal calorimetry	27
1.3.3. Photorefractive technique	28
1.4. References	30
1.5. Symbols and notations	36

CHAPTER II : THEORETICAL ASPECTS OF THE PHOTOACOUSTIC EFFECT

2.1. Optical absorption in gases	38
2.1.1. Rate equation for a two-level system	39
2.1.2. Excitation of the acoustic wave	41
2.1.3. Saturation in PA signal	44
2.2. Generation of PA signal in gases : effect of dissipative forces	45
2.3. Other models for gas phase PA signal generation	60
2.3.1. Rosencwaig-Gersho (R-G) theory for gas-microphone generation of PA signals in condensed matter	60
2.3.2. Thermal piston model for PA generation in gases	62
2.3.3. Acoustic transmission line theory	64
2.4. Conclusions	69
2.5. References	70
2.6. Symbols and Notations	71

CHAPTER III : INSTRUMENTATION ASPECTS OF PHOTOACOUSTICS

3.1. Introduction	74
3.2. PA Instrumentation	75
3.2.1. The light source	75
3.2.2. Modulation Techniques	77

3.2.3. PA cells	79
3.3. Detection of the signal	96
3.3.1. Acoustic detectors	96
3.4. Detection Electronics	101
3.4.1. Pre-amplifiers	101
3.4.2. Signal detection, recovery and processing : pulsed and cw detection	102
3.4.3. Noise in PA signal	107
3.5. Scaling laws for PA cells	114
3.5.1. Noise Equivalent Power	117
3.6. Conclusions	118
3.7. References	118
3.8. Symbols and notations	123

CHAPTER IV : EXPERIMENTAL DETAILS OF GAS PHASE PHOTOACOUSTICS

4.1. Introduction	127
4.2. Pulsed PA experimental setup	128
4.3. The cw PA experimental setup	135
4.4. Design and characteristics of the dual cavity PA cell	141
4.4.1. The dual cavity differential PA cell	142
4.4.2. Characteristics of the PA cell	143
4.5. Conclusions	155
4.6. References	155
4.7. Symbols and notations	156

CHAPTER V : PULSED PHOTOACOUSTIC STUDIES OF FORMALDEHYDE VAPOUR

5.1. Introduction	158
5.2. Detection of formaldehyde	160
5.3. Absorption spectrum of formaldehyde	161
5.4. Two photon absorption process	163
5.4.1. Introduction	163
5.4.2. Brief theory of TPA process	165
5.5. PA detection of formaldehyde	170
5.5.1. Experimental details	170
5.5.2. Pulsed PA spectrum of formaldehyde	171
5.6. PA Investigations of TPA processes in other samples	174
5.7. Conclusions	176
5.8. References	177
5.9. Symbols and notations	179

CHAPTER VI : PHOTOACOUSTIC STUDIES IN NITROGEN DIOXIDE

6.1. Introduction	180
6.2. Sources of atmospheric NO ₂	181
6.3. Photochemistry of NO ₂ in the visible region	182
6.4. Detection of Nitrogen Dioxide	184
6.4.1. Calorimetric detection techniques for NO ₂	186
Part A : Pulsed PAS of NO ₂	189
Part B : CW PAS of NO ₂	192
6.5. Conclusions	198
6.6. References	199
6.7. Symbols and notations	201

CHAPTER VII : PHOTOACOUSTIC STUDY OF LASER INDUCED DAMAGE THRESHOLD AND PLASMA PROCESSES

7.1. Laser induced damage process : General introduction	202
7.1.1. Laser beam parameters	204
7.1.2. The test sample	207
7.1.3. Detection technique	208
7.2. Mechanisms of laser induced damage	211
7.3. Forms of Laser induced damage	217
7.3.1. Surface damage	218
7.3.2. Impurity/inclusion damage	223
7.3.3. Bulk damage	224
7.4. Laser induced damage in metals	226
7.5. Laser damage in polymeric materials	226
7.6. Photoacoustic detection of laser induced damage	229
7.6.1. Experimental technique	235
7.6.2. Results and discussion	236
7.7. Photoacoustic monitoring of laser ablation process	240
7.8. Conclusions	242
7.9. References	243
7.10. Symbols and notations	247

CHAPTER VIII : GENERAL CONCLUSIONS

General conclusions	249
Future work	252

CHAPTER I

PHOTOACOUSTIC EFFECT AND ITS APPLICATIONS

ABSTRACT

THIS CHAPTER INTRODUCES THE PHOTOACOUSTIC EFFECT, TRACES ITS HISTORY AND ELUCIDATES SOME OF THE IMPORTANT RESULTS OBTAINED BY EARLIER WORKERS. SOME OF THE MAJOR APPLICATIONS OF THE PA EFFECT IN SOLID, LIQUID AND GASEOUS SAMPLES ARE ALSO GIVEN.

CHAPTER I

PHOTOACOUSTIC EFFECT AND ITS APPLICATIONS

1.1. General Introduction And History

With the emergence of 21st century within a decade, it is anticipated that photons will play a very vital role in several areas of science and technology as they will replace electrons in many technological applications. In fact, light has, already in many ways, found applications in the daily life of mankind. Its use in future is almost certain to range from communications to calculation and medicine to microprocessors.

One of the oldest applications of light, or for that matter, any form of radiant energy, in science has been to the study of properties of substances, and this method can be broadly termed as spectroscopy. It is, by itself, a complete science incorporating various kinds of techniques and applications. The oldest form of spectroscopy is the optical spectroscopy, which involves the interaction of optical photons (x-rays to far IR) with matter. Possessing the advantage of being versatile and non-destructive in nature, optical spectroscopy has found widest applications in the investigation of various properties of matter in all its forms. With the advent of the lasers, the 'light fantastic' in 1960, the discipline of spectroscopy was discovered anew and has hence flourished due to the awesome advantages that a laser could offer over conventional light sources. By the end of two decades since the invention of laser, it has found applications in almost all walks of life. For spectroscopy and

other analytic techniques, properties of lasers such as the high photon flux, monochromaticity, tunability etc enable detection of weaker absorption phenomena, and thus lower the possible detection limits. Also, measurement in shorter time scale are possible using ultra-fast lasers as they can probe non-linear phenomena in matter, all the while, making more accurate measurements [1].

Conventional optical spectroscopy is based on the principle that when photons pass through matter, they are either absorbed, transmitted, reflected or scattered by it. All these phenomena can occur simultaneously in the sample. Most optical spectroscopy are based on the detection and analysis of the photons that are either transmitted or reflected by the sample. In cases where the sample is highly transparent and thus the absorption is very weak, or when the sample is highly opaque, it is very difficult to determine the amount of absorption of the photons by the sample through the conventional technique mentioned above. For the transparent samples, the derivative absorption technique was used but was still found to be quite inadequate. For opaque samples, techniques like Raman scattering [2], diffuse reflection [3], attenuated total reflection [4] etc. were utilized but they too had the limitations that the wavelength regions to which they could be applied and the number of samples that could use these techniques were very small, and moreover, the data from these techniques were difficult to analyze. For such samples, which are weakly absorbing, highly scattering or opaque, and where measurements using conventional optical spectroscopic techniques cannot be used effectively, a new optical technique was introduced to spectroscopic detection and was called the 'PHOTOACOUSTIC SPECTROSCOPY' (PAS). It was only a re-discovery of a century old discovery by Alexander Graham Bell in 1880 [5,6], then termed as the opto-acoustic effect. Names such as the photo-thermal/opto-thermal and opto-acoustic effect are still used to describe

this phenomenon. The basic difference of this effect from conventional optical spectroscopy is that here, the amount of energy absorbed following irradiation of the sample by the optical radiation by the sample is directly measured. The PA effect is essentially the generation and detection of acoustic or other thermo-elastic effects resulting from the absorption of any kind of modulated/pulsed electromagnetic radiation. The absorption in the sample causes excitation of the atoms or molecules to a higher excitation level. When the radiation is removed, (due to modulated/pulsed nature of the irradiation), all or part of the excited atoms/molecules de-excite back to the lower level through various pathways of which the non-radiative de-excitation causes heat, that follows the modulation frequency, to be generated in the sample. This heat generally appears as the kinetic energy in gases and as vibrational energy of ions or atoms in solids or liquids. In PAS, it is this modulated heat that is to be detected, and it is done by placing the sample in an air-tight cell containing a sensitive acoustic transducer. The modulated heat produced in the sample is transferred to the layer of non-absorbing gas medium close to the sample surface filling the cell, causing it to compress and expand. Thus this layer acts as an acoustic piston that drives the rest of the gas in the cell. The pressure variations thus produced are carried to the acoustic transducer that gives an electrical signal which is proportional to the amount of absorption of the radiation by the sample. Following Bell's discovery, the PA effect was pursued for a short while [7,8] in solids and liquids and then was abandoned for the lack of possible applications ! Not until 50 years later was this effect revived by Viengerov [9,10] who applied it, in conjunction with a resonant PA cell to detect the pressure amplitude which was found to be proportional to the concentration of the absorbing gas molecule. This can be considered as the beginning of the application of PAS to trace analysis.

Application of PAS to various aspects of material properties were reported thereon. Gorelik suggested and showed that the phase of the PA signal contained information about the energy transfer rates between the vibrational and translational degrees of freedom in a gas [11]. This was experimentally shown by Slobadaskaya [12] in 1948. The first theory for PAS and thus its official re-appearance since its discovery came about in 1973 with the introduction of the Rosencwaig-Gersho (R-G) theory [13-15], which is a general theory for the generation and detection of the PA signal produced in a sample placed in a gas-microphone cell. It deals with the process of signal generation and its dependence on various parameters like the modulation frequency, relaxation times of the radiative and non-radiative de-excitations and incident optical power in a solid sample. Different cases like optically/thermally thick/thin samples have been dealt with and the results compared to experimental results with a fair amount of coincidence.

Since PAS is essentially detection of heat produced in the sample, it can be referred to as a calorimetric technique. As the sample itself generates the PA signal, this technique can be used over a wide range of electromagnetic radiations with the only limitation that appropriate optical windows corresponding to the wavelength of operation be used in the PA cell. Compared to other calorimetric techniques, PAS is simpler, faster, non-destructive in nature, is more sensitive, has a higher detector rise time etc. It can effectively detect pressure variations that correspond to temperature variations of $\sim 10^{-6}$ $^{\circ}\text{C}$ [16]. With the presently available sensitive transducers and signal processing techniques, a detection limit of parts per billion (10^{-9} or ppbV) in the case of liquids and gases [17] have been experimentally achieved and a theoretical limit of $\sim 10^{-10}$ cm^{-1} for absorption has been predicted for a laser power of 1 watt

[18]. Since absorption of light is required before the PA signal is generated, light that is scattered or transmitted by the sample does not therefore interfere with the inherently absorptive PA measurements. This is important while working with highly transparent samples. This property of PAS to be insensitive to scattered light makes it ideal to study properties of highly scattering samples like colloids. For opaque materials, PAS can provide the absorption spectrum, which is difficult to obtain otherwise. This capacity, coupled with the information in the phase of the PA signal with respect to the modulation frequency finds applications for non-destructive testing (NDT) of solid surfaces and sub-surfaces in bulk as well as in thin film samples. These studies form a branch of PAS called the PA microscopy (PAM) which has found many industrial applications. Since the PAS involves the measurement of how much of the absorbed energy uses the non-radiative de-excitation path, it is complimentary to other radiative and photochemical processes like fluorescence etc. Thus the PAS can also be used to study indirectly the fluorescence and other photochemical processes in the sample. Also, the study of the sample by PAS can provide information, which when coupled to that obtained by measurement of the radiative de-excitations, can provide a complete picture of the energy de-excitation processes occurring in the sample. This technique has been extensively used in gases, liquids and solids for a variety of application, some of which will be discussed later. One of the main applications of PA effect in gases is for trace analysis and pollution monitoring. The drawbacks of this technique are that since the PA signal is detected by a volume responsive detector, the response time is limited to the transit time for the sound wave in the gas within the cell and by the relatively weaker low frequency response of the microphone. These factors limit the response time of a typical gas-microphone PA system to the order of $\sim 100\mu\text{sec}$.

1.2. Applications Of The PA Effect

In the past two decades, PA effect has found many applications in spectroscopy of solids liquids and gases, in medicine and biology, trace analysis, pollution monitoring, remote sensing, physics of semiconductors and amorphous materials, in thin films, and so on. Some of the major applications of the PA effect in these areas will be described in the following pages. Laser PAS has been used to probe phenomena like forbidden transitions as the singlet-triplet electronic transition or vibrational overtone absorptions, which in vapor phase has an extremely low absorption cross section requiring very high laser powers. The application of PA effect has been so widely accepted that photoacoustic microscopy (PAM), Fourier-transform PAS, PA trace analysis, PA magnetic resonance etc. are, by themselves areas of very strong research activity.

1.2.1 PA Studies In Condensed Matter

A variety of properties in solids have been investigated in detail using the PA technique. Investigation of PAS of solids involve both phase and amplitude measurements of the PA signal. Properties of samples like thermal conductivity, thermal diffusivity, heat capacity, phase transitions, laser damage threshold, surface analysis etc. have been investigated using this technique.

The absorptance of mirrors at angles 0 to 90° for both s and p polarized laser has been measured by piezo-electric PA detection technique [19]. The evaluation of both the thermal conductivity and the heat capacity of the solid samples is one of the major applications of PAS and these quantities have been

simultaneously evaluated for liquid crystal samples in their different mesophases [20]. Since normal optical techniques cannot be applied to highly light scattering samples, PA technique was used for such samples and for those having low thermal diffusivity and for samples which were highly opaque [21] and for diffuse samples like powdered semiconductors [22], and metallic powders [22]. The PAS was applied also to rare earths (RE) pentaphosphates [23] and RE doped crystals [24]. Information on the performance of solar cells under open circuit and loaded conditions have been observed by PA studies in the visible region [25]. The theory and experimental studies of PA signatures of particulate matter and the production of acoustic monopole radiation by ultrashort pulses were investigated by Diebold *et al* [26]. Trace species of iron adsorbed on to a single microparticle of solid resin of diameter $300\mu\text{m}$ was detected using PAS by Hsuen *et al* [27]. The use of single microparticle eliminated the possibility of scattering effects. This was further extended to a depth profile analysis of the adsorbed species on the microparticle [28]. Adsorption thickness of $1-10\mu\text{m}$ could be examined. Good agreement between the PA and microscopy data was obtained.

PA microscopy (PAM) is a direct example of the non-destructive evaluation capability of PA effect which has the potential to analyze the various physical properties like optical absorption, and thermal diffusions at various layers of the sample. This technique provides identification of flaws and defects on a surface by the detection and the detailed analysis of the heat flow through the material. By monitoring the amplitude and the phase of the signal, it is possible to probe properties such as the acoustic velocity, elasticity, density, thickness, specific heat, phase transitions etc. The signal amplitude carries information about the surface and the phase of the signal

carries information about the sub-layers. Thus, surface profile, thickness and depth of sub layers, thermal diffusivity of thin films or other irregularities below the surface, depth-dependent optical absorption features etc. can be determined [29]. Experimentally, the PA image is obtained by scanning the modulated cw laser over the sample (mounted on an X-Y translator along with an acoustic detector) and measuring the PA signal and phase by the conventional method. Different depths can be accessed by varying the modulation frequency [30]. PAM was used to detect sub-surface defects in integrated circuits (IC) with an ultimate resolution of less than $5\mu\text{m}$ with a laser spot size of $\sim 2\mu\text{m}$ [31]. At lower modulations, the surface structure is seen and as the frequency is increased, sub-surface features begin to appear. In principle, the amplitude image represents the surface and the phase image reflects sub-surface features. Absolute distribution of the dopant concentrations in ICs' were also determined by this technique [32]. In most of the opaque materials, the thermal wavelength is $\sim 10^3$ times less than the acoustic wavelength at the same frequency. So, to get the same resolution of the sub-surface structure imaging, the operating frequency can be as much less than 10^3 times as that of acoustic microscopy. Also, though PA imaging can be carried out in air for general applications, it must be performed in high vacuum for electron or ion acoustic imaging [33]. Better signal-to-noise ratio (SNR) and resolution are obtained for PAM performed in high pressure and low temperature conditions. The thermal characterization of coal by PAM using PZT detection was performed by Biswas *et al* [34] to characterize *in-situ* the thermo-elastic properties of macerals, (the organic constituents that make up the heterogeneous coal mass) as a function of percentage of carbon. A beam scanning type PAM was used to evaluate magnetic recording media and magnetic recording heads (made of ferrite or calcium titanate ceramics) used in computer disk drives [35,36]. In certain

cases, PAM can detect sub-surface inhomogeneities that cannot be detected by conventional microscopy [37]. Also, PAM studies in multi layered thin films can non-destructively determine the number of layers present by observing the phase change in the PA signal as the modulation frequency is varied. Non-destructive examination of laser mirror coatings can be performed using PAM [38,39]. Sites of surface inhomogeneities in surfaces used in laser optics, which are prone to laser induced damage can be determined using this technique [40]. Many workers have applied the PA technique to determine the laser damage threshold (LDT) and ablation threshold in various samples [41-43]. The abrupt change in the PA signal associated with the damage/ablation process is the basic principle of this technique of determination of LDT. PA technique not only detects the damage threshold, but is also capable of distinguishing between the onset of surface damage and ablation of the sample [44]. The capability of PA method to detect weak absorptions implies that it can be applied to monitor adsorptions due to thin films, which may be on a substrate or free-standing. Further, since it has been experimentally shown that a fractional absorption of $\sim 10^{-6} \text{ cm}^{-1}$ can be detected for a typical 1cm path length, it can be extended to thin films and thus detection of adsorption of thin films $\sim 10^{-8} \text{ cm}$ thick could be possible if the absorption coefficient is 10^2 cm^{-1} or larger [45,46]. Applied to thin layer chromatography (TLC) , PAS can examine the local distribution of dyes adsorbed and identify the separated compounds on the TLC plates. PAS detection was found to be more advantageous due to the highly optically opaque and light scattering nature of the TLC plates [47,48]. Spectroscopic investigations of formation of complexes on metal surfaces with a view for their potential applications in the field of surface chemistry and surface catalysis were carried out using PAS [49,50]. Atmospheric aerosols were studied by collection on teflon filters and then analyzed by PAS [51]. The elemental

carbon concentration in air was estimated by this technique. Similar studies were done on air borne ammonium salt particulates also.

Destructive testing of materials (both bulk and thin film) to study parameters like laser ablation threshold, laser plasma formation, melting etc. have been performed using the optically generated sound in materials. Continuous monitoring of the PA signal pulse amplitude from a transducer placed in the near vicinity or attached to the sample under varying laser energy density conditions can throw light on these parameters [52-55].

Since the thermal parameters of a material undergoing a phase transition change in a drastic manner, monitoring the PA signal from such a sample as a function of temperature will throw light on this phenomenon occurring in the sample. At the first order phase transition, the latent heat strongly influences the PA signal. The amplitude of the signal as a function of temperature runs through a minimum in the transition region whereas the phase of the signal shows different patterns. Various such studies have been performed in many kinds of samples using variable temperature PA cells [56,57].

PA effect has been used to obtain information on the performance of photo-thermal and photo-electric conversion devices. This method provides information on the efficiency of such photo-conversion processes [58].

Different kinds of magnetic resonances (MR) like EPR, NMR, ESR etc. have been detected by the PA technique. The PA-EPR obtained compares well with the conventional techniques. PA-EPR has the advantage of depth sensitivity which can be applied to the study of samples like porphyrins which exhibit different frequency dependence at high and low magnetic field absorptions [59]. Since

the PA signal in these cases varies as $\omega^{-\alpha}$ (α , the exponent is sample dependent) with the modulation frequency ω , and a $T^{-1/4}$ temperature dependence, PA-MR will be as sensitive as conventional ESR when low temperatures and low modulation frequencies are used and thus is a substitute for other thermal detection techniques [60]. By time domain PA detection techniques, the spin lattice relaxations can also be determined [61].

Photo-isomerization is another phenomena that has been investigated using PAS. Studies show an intensity dependent change in the PAS of 3,3 diethyldicarbocynide iodide (DODCI) as observed for reversible photo-isomerization [62].

Fourier Transform PAS (FTPAS) was introduced by Farrow *et al* to overcome the disadvantages of PAS with incoherent light in conjunction with low throughput dispersive optical instruments. The data collection in these cases is point-to-point rather than simultaneous and is thus slow. The FT-PAS is experimentally similar to the normal FT absorption spectroscopy. In FT-PAS, the data at all the spectral wavelengths emitted by the broadband source is simultaneously measured at the throughput of a Michelson's interferometer using a PA detector [63]. It was seen that the combined multiplexing and throughput advantages of the interferometric technique decreases the data acquisition time and increases the SNR of the system considerably [64]. This technique has been extended to the IR regions also, with the PA cell taking the place of the conventional detector in conventional FT-IR spectrometers. The fact that in conventional spectroscopic method of transmission or reflection monitoring of light frequently suffers from the spectral distortions when powdered samples, dispersed in a transparent matrix are examined. Due to decreased light scattering when the refractive index of the matrix equals that of the powdered sample, the transmission is increased

leading to distortion (Christianson effect). The FT-PAS eliminates this problem completely [65,66]. FT-PAS of a wide variety of samples like human blood to laser materials like Nd:glass, La_2O_3 etc. have been studied.

1.2.2. PA Studies In Liquids

The application of PAS to the study of liquids also has ranged from the study of absorption of light by water to analysis of blood and from pollution monitoring to study of laser dyes. In PA studies of liquids, the gas-microphone setup is not employed due to lack of coupling efficiency. A piezo-electric detector placed in contact with the sample is used as the transducer and this has a better efficiency of the coupling of acoustic energy into the transducer [29].

PA trace analysis of suspensions of ultra-trace quantities of suspension particles of BaSO_4 in turbid solutions was performed by Oda *et al* [67]. The PA signal is less affected by the particle size distribution as compared to normal turbidimetric measurements. The detection limit was about 2 orders of magnitude less than that obtained by turbidimetry. A linear concentration range of 3 orders of magnitude was obtained by the PA method. Determination of particulates is also possible in turbid solutions. The sedimentation of molecular or macroscopic dimensions under gravity or ultra centrifuge was detected by pulsed PA technique. The sedimentation data obtained by PAS is not obscured by scattered light as in the case of absorption data [68].

Overtone absorption in liquids was detected by many PA workers, the first reported being in benzene [69,70]. These studies have been extended to H_2O and D_2O to study the weak

absorption in water in the visible region, which is important for underwater laser communication studies [71]. It can also be applied to determine water purity, dissolved microparticles etc. The PA signal in water was found to be highly temperature dependent and it attenuated when the temperature was lowered to 4°C and then increased in opposite polarity for temperatures less than 4°C. Very low temperature PA studies is important in spectroscopy since at low temperatures, the spectral structure of the molecule is simplified owing to the freezing out of the rotational components of the system. Many of the cryogenic solvents (noble gases, N₂ etc.) have high transparency in the IR region. The weak absorptions in these samples can be investigated by PA technique [72,73]. The overall sensitivity of $\sim 10^{-7} \text{ cm}^{-1}$ at a temperature of 125K was obtained using a pulsed laser and piezo-electric detection. Measurements of PA absorption spectra of liquid C₂H₄ (T=113K) in the 0.7 to 1.6μm indicate the general applicability of PAS to investigate the planetary spectra of several gases [74]. Multiphoton absorption is another area which can be efficiently investigated by pulsed PA techniques. Studies in organic solvents and laser dyes have been performed by many workers [75,76]. The quantum efficiency of radiation in a material can be estimated as,

$$\eta = \frac{\nu_e}{\nu_f} \left(1 - \frac{a_1 q_2 P_1}{a_2 q_1 P_2} \right) \quad \dots \dots (1.1)$$

where, ν_e and ν_f are the excitations and the mean frequency of fluorescence emission, q_1 and q_2 the PA amplitudes of the non-fluorescing and fluorescing samples and $a_1 P_1$ is the absorbed power with P_1 being the incident power for the non-fluorescing sample and $a_2 P_2$ likewise for the fluorescing sample. a_1 a_2 are the respective absorption coefficients. It is seen that this technique is more sensitive than conventional calorimetric

techniques.

The quantum yield of emission in laser dyes have also been determined by this technique and was found to give comparable results [77]. PA studies have been extensively applied to the study of biological and medical processes. The photochemical reactions, which necessarily occurs in all plants, can be studied by PA techniques due to the fact that if a fraction of the absorbed energy is consumed by the photochemical process, then the PA spectra differs from the absorption spectra. These measurements can be performed by comparing the PA spectra obtained for a calibrated PA cell for the sample before and after the photochemical process has taken place. Extensive studies were performed on chloroplasts using this technique [78]. PA studies have been done on several biologically important samples [16] like chlorophyll [22], β carotine [79], etc. PAS has been applied to detect the photosynthetic oxygen evolution from leaves and it throws light on the diffusion of oxygen from the chloroplasts to cell boundary and the electron transfer reactions occurring between the photochemical action of oxygen evolution [80,81] by the photosynthesis in whole leaves. The evolution of methane during the flowering process was studied in detail by Harren using PA technique with IR tunable lasers [82].

Since the PA signal in a cell depends on the velocity of the flowing liquid sample, this can be applied to the measurements in flowing blood and has potential applications for *in-vivo* PA measurements on the flowing blood stream [83]. Many applications of the PA effect to medicine have been reported, such as the studies of the effect of sun cream on the epidermal skin [84], effect of drugs on tissues and the study of the intact human and bovine eye lenses to detect cataract, the presence of which induces increased absorption in the UV and IR regions [22].

In-vivo measurements on the penetration of sun-screen cream into the skin was performed by Giese *et al*, using a specially designed PA cell [85]. The *in-vivo* absorbance of human skin was also measured using a differential PA measurement setup [86]. An open PA cell using a piezo-electric transducer was used to study the spectroscopic features of whole human blood [87]. An optical fibre can be attached to the PA cell, making it small in size. The possibility of using such a PA cell, mounted in a cannula for clinical applications has been investigated by McQueen [88].

1.2.3. PA Studies In Gases

PA technique has been widely applied to gas phase studies, specially in the areas of spectroscopy, trace analysis and pollution monitoring. A review of the gas phase PA studies is given below.

i. Applications Of PAS To Trace Analysis And Pollution Monitoring

Since the beginning of the industrial revolution the burning of fossil fuels for energy production increased drastically and consequently, more quantities of pollutants were released into the atmosphere, thus influencing natural physical and chemical regulation cycles which were untouched over long periods. In the earlier periods, the effects of pollution were restricted to industrial areas where the increase in concentrations of the toxic compounds occurred near their sources. More recently, large area damage to nature in the form of acid rain, deforestation, ozone layer depletion etc. are on the rise. Also, these pollutants have found to be harmful to life and are the causes of the alarming prospects of a 'greenhouse effect'. At present, the major pollutants of the lower atmosphere ie, the troposphere are

sulfur dioxide SO_2 , oxides of nitrogen (NO_x) and hydrocarbons (H-C), called the primary pollutants, as well as their respective products like acids and oxidants (secondary pollutants). The SO_2 and NO_x pollutants in the atmosphere are converted to sulfuric and nitric acids which then fall back on the earth as acid rains, thus increasing the acidity of the soil and thereby making the land infertile.

The sensitive and selective detection of numerous trace constituents is a pre-requisite for understanding the various tropospheric pollution processes. Many such detection schemes have been described [89] in numerous reviews on pollution monitoring techniques. These techniques can be broadly classified into spectroscopic and non-spectroscopic techniques. The most widely used non-spectroscopic technique is the gas chromatography. Since most of these techniques do not meet all the requirements with respect to sensitivity, selectivity, kind and number of substances to be detected, temporal resolution practical applicability etc, novel techniques have to be developed in addition to the conventional ones.

Since the advent of powerful and tunable lasers, spectroscopic techniques are finding interesting applications in these fields. Compared to the conventional wet-chemical or chromatographic techniques, the spectroscopic methods generally rely on the absorption measurements. The minimum detectable concentration of a trace gas is thus determined by the minimum measurable absorption coefficient α_{\min} . Since the absorption spectrum is a characteristic for each molecule, these methods often permit simultaneous detection of many substances, depending on the tunability and linewidth of the radiation source and the spectral characteristics of the detector. Figure 1.1 shows the emission ranges of some lasers, their typical output powers, the

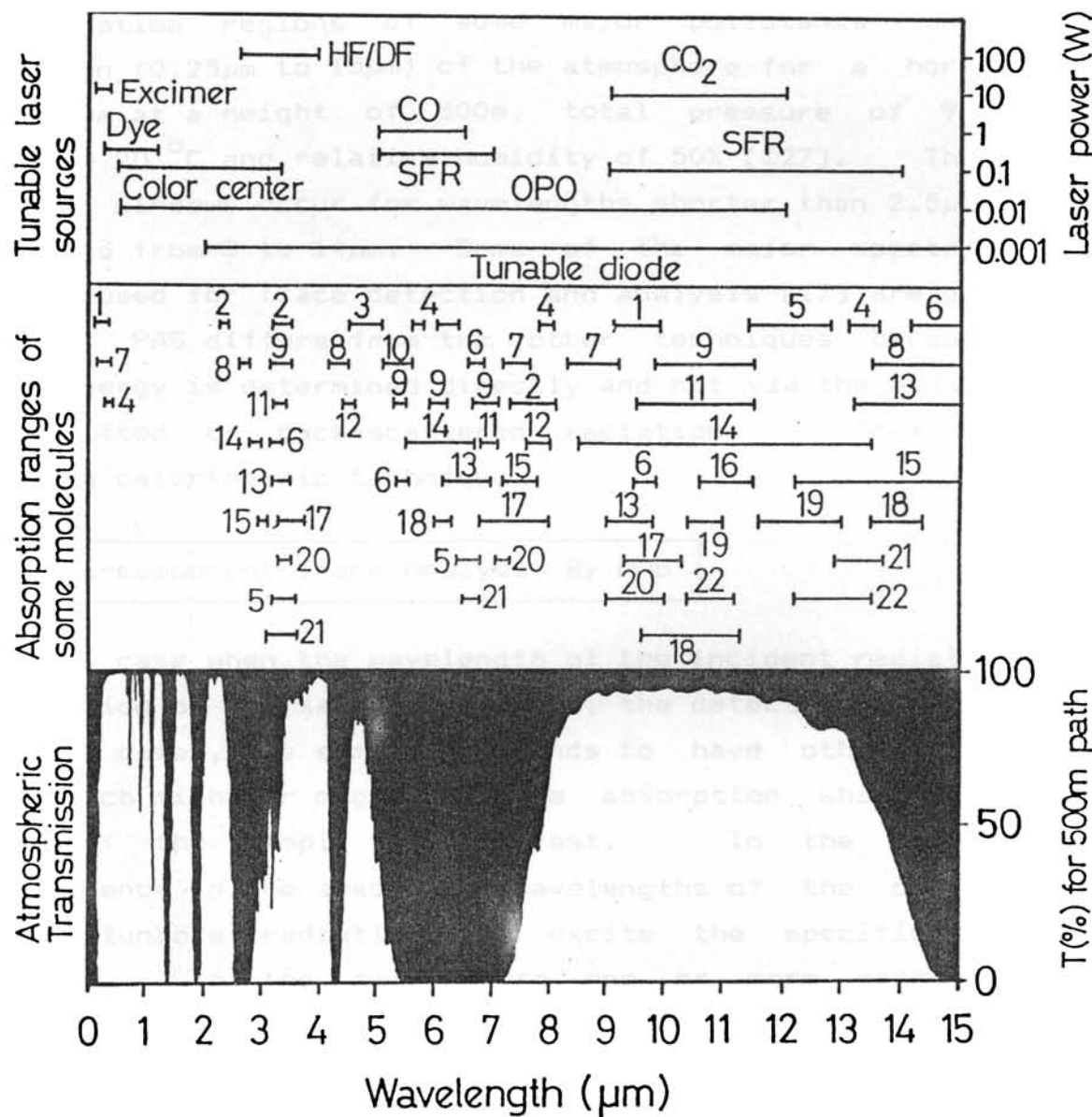


Fig.1.1. Emission ranges of available laser sources, their typical powers, absorption regions of some molecules of environmental concern and the transmission of atmosphere in the 0.25-15 μm wavelength region [127].

1-O₃, 2-CH₄, 3-CO, 4-NO₂, 5-C₂H₆, 6-C₆H₆, 7-SO₂, 8-CO₂, 9-C₃H₆, 10-NO, 11-C₂H₄, 12-N₂O, 13-C₇H₈, 14-NH₃, 15-C₂H₂, 16-C₄H₆, 17-CH₃OH, 18-C₂H₃Cl, 19-C₂HCl, 20-C₂H₅OH, 21-C₃H₈, 22-C₂Cl₄

main absorption regions of some major pollutants and the transmission ($0.25\mu\text{m}$ to $15\mu\text{m}$) of the atmosphere for a horizontal path of 500m at a height of 500m, total pressure of 950mbar, temperature 20°C and relative humidity of 50% [127]. The main atmospheric windows occur for wavelengths shorter than $2.5\mu\text{m}$, from 3 to $5\mu\text{m}$ and from 8 to $14\mu\text{m}$. Some of the major spectroscopic techniques used for trace detection and analysis [17] are given in Table 1.1. PAS differs from the other techniques because the absorbed energy is determined directly and not via the measurement of transmitted or back-scattered radiation. Thus PAS is primarily a calorimetric technique.

a. Multi-component Trace Analysis By PAS

Under ideal case when the wavelength of the incident radiation and the absorption of the sample coincides, the detection is simple, but in most cases, the sample gas tends to have other absorbing species which might or might not have absorption which overlaps with that of the sample of interest. In the case of a non-coincidence in the absorption wavelengths of the constituent species, a tunable radiation can excite the specific species separately. In the case where one or more species have absorption at the same wavelength, it makes discrimination between the species difficult.

In most cases of PA trace analysis, the gas sample will contain more than one absorbing components, which results in a total absorption coefficient α_{tot} so that,

$$\alpha_{\text{tot}}(\lambda) = N_{\text{tot}} \sum c_j \alpha_j(\lambda) \quad \text{with } j = 1, 2, \dots, n$$

.....(1.2)

Table 1.1. Some of the major spectroscopic techniques used for trace detection and analysis

Detection scheme	Main features	Sensitivity	Selectivity
Raman Scattering	Inelastic interaction between photons and irradiated molecules, small cross-sections, selectivity by frequency shift, only one λ needed, better for smaller λ	poor	excellent [90-93]
Laser Induced Fluorescence (LIF)	Fluorescence of irradiated species, small cross-sections, only suitable for detection of atoms or radicals	fair	-----
Differential Absorption Spectroscopy (DOAS) $\alpha_{\min} \approx 10^{-5} \text{ cm}^{-1}$	Broadband source, separated from receiver by open path in the atmosphere, dual λ operation, integrated response, mainly for UV detects SO_2 , NO_2 , O_3	good	good [94]
Long-path absorption spectroscopy	Long, single/multiple pass cells, single/double ended schemes in open atmosphere, integrated response, UV-VIS-IR	good	good
Light Detection And Ranging (LIDAR) $\alpha_{\min} \approx 10^{-6} \text{ cm}^{-1}$	Atmospheric backscatter of laser pulses, 3-D profiling of pollutants, complex, for UV-VIS, detects SO_2 , NO_2 , O_3	fair	good [95-98]
Photoacoustic spectroscopy (PAS) $\alpha_{\min} \approx 10^{-9} \text{ cm}^{-1}$	Measurement of absorbed energy in a cell, sensitive simple, for UV-VIS-IR, selective detection of numerous species possible	excellent	good

N_{tot} is the total number density of the molecules present in the gas mixture, $c_j(\lambda)$ and $\sigma_j(\lambda)$ the concentration and the absorption cross section of the gas component j . Since the PA signal, detected by the microphone is,

$$S = F I N \sigma \quad \dots \dots \dots (1.3)$$

where, N is the molecule density, I the average laser power and F the cell constant given by [82],

$$F = \frac{(\gamma-1) L Q G}{\omega_0 V} \quad \dots \dots \dots (1.4)$$

where, γ is the ratio of specific heats, L the length of the cavity, Q the quality factor at the resonance frequency ω_0 . V is the volume of the cell and G a geometric factor ~ 1

If the σ_j of the components are known, then the corresponding c_j can be evaluated by scanning the wavelength λ of the source and simultaneously recording the signal $S(\lambda)$. The absorption interferences and overlaps of the components is a problem which leads to the reduction of sensitivity and selectivity of this method.

In analogy to the equation 1.2, the total absorption coefficient α_i at a specific laser line i if a gas mixture containing n components is represented by,

$$\alpha_i = \sum_{j=1}^n \alpha_{ij} = N_{\text{tot}} \sum_{j=1}^n \sigma_{ij} c_j \quad \begin{matrix} \text{for } i = 1, 2, \dots, m \\ j = 1, 2, \dots, n \end{matrix}$$

with $n \leq m$

$\dots \dots \dots (1.5)$

σ_{ij} is the absorption cross section of species j at a laser

transition i . The corresponding measured microphone signal being S_i , the absorption coefficients derived from the measurements will be (from Equ.1.3),

$$\hat{\alpha}_i = \frac{S_i}{F I_i} \quad \dots\dots(1.6)$$

F is the cell constant and I_i the incident laser power at transition i . The aim is to extract the n concentrations c_j from the set of m absorption coefficients from $\hat{\alpha}_i$ derived experimentally. The measured and calculated absorption spectra can be represented as vectors $\hat{\alpha}$ and $\underline{\alpha}$ in a m -dimensional space. Thus Equ.1.5 can be written as,

$$\underline{\alpha} = N_{\text{tot}} \sum \underline{c} \quad \dots\dots(1.7)$$

Where, \sum is a $m \times n$ matrix which contains the elements of σ_{ij} of the calibration spectra of the n components in the columns. The vector \underline{c} contains the concentrations c_j . In practice, the calculated $\underline{\alpha}$ always varies from $\hat{\alpha}$ due to the noise of the measured signals and the absorption by components not taken into account for the calculation of $\underline{\alpha}$. Therefore, the absorption is usually measured at $m > n$ laser transitions. Then the concentrations c_j are derived from the overestimated system of equations by minimizing the residuals

$\rho_i = \hat{\alpha}_i - \alpha_i$ in a least squares fit, which yields,

$$\underline{c} = \frac{1}{N_{\text{tot}}} \left(\sum^t \sum \right)^{-1} \hat{\alpha} \quad \dots\dots(1.8)$$

where, \sum^t is the transposed matrix of \sum

The symmetric, positive definite matrix $\left[\sum^t \sum \right]$ is non-singular if Σ contains n linear independent column vectors α_j . This condition is well fulfilled if all the spectra of the n components taken into account exhibit specific features. For various reasons, the residuals ρ_i are weighted by introduction of normalized weighting factors W_i , which are inversely proportional to the uncertainty $\Delta\hat{\alpha}_j$. In addition, these factors are chosen to decrease the weight for those laser transitions for which $\alpha_i > \hat{\alpha}_i$, yet to increase it for the transitions with $\alpha_i \approx \hat{\alpha}_i$. Since these factors W_i depend on the priori unknown concentrations c_j , the solutions of Equ.1.8 is obtained by iteration. This technique permits the determination of individual concentrations even if additional components not considered for the fit, contribute to the measured absorption spectrum.

The major advantages of using PAS for trace analysis and pollution monitoring are [17,99];

1. A high sensitivity which permits the measurement of absorption coefficients of the order $10^{-8} / \text{cm}$ corresponding to densities of $\mu\text{g}/\text{m}^3$ or to concentrations of ppbV (10^{-9}) for most substances. A theoretical detection limit of $\alpha_{\min} \approx 10^{-10} \text{ cm}^{-1}$ has been predicted for a laser power of 1 watt [100].
2. The experimental setup is simple and does not involve detectors that require cryogenic cooling etc.
3. The calibration of the PA system with certified gases and gas mixtures is straightforward, reliable and can be used for different gases in the same system. Tunable lasers permit simultaneous detection and analysis of various components in the sample species.

4. A wide dynamic range of at least 5 orders of magnitude is offered, ie, the same system can be used for low as well as high concentrations.
5. By changing the wavelength of the laser to suit the sample and by using appropriate window materials for the wavelength of laser, different species can be studied using the same system.
6. Short absorption paths of typically tens of centimeters enable measurements even in regions beyond the atmospheric windows.
7. Since PA cells can be made small without compromising on the sensitivity, only small quantities of sample gas are required.
8. Measurements on continuously flowing gases are possible by PAS ie, *in-situ* monitoring with a better temporal resolution than by gas chromatography is possible.

After the pioneering work of the first application of laser PAS to trace analysis by Kerr and Atwood [101] and by Kreuzer [102], many different kinds of gas phase PA studies have been carried out. Different lasers, modulation techniques, cell designs and detection schemes have been employed. Some of the different detection methods employed were, Raman [103], Doppler free [104], Stark [105], saturation [106] and harmonic saturated [107] PAS techniques as well as a combination of PAS and gas chromatography [108,109] or a non-contact method such as the photothermal deflection technique [110,111]. Most of these works involved the use of conventional laser PA detection method and with the major part of them aimed at the detection of single gaseous trace component in a non-absorbing buffer medium like nitrogen. In general, a detection limit in the ppbV

concentration range has been obtained. Table 1.2. lists some of the laboratory studies on trace gas studies using laser PAS.

Actual measurements in real air samples have been carried out by only a few workers. Kreuzer and Patel [122] detected NO in ambient air and in automobile exhausts. NO in the stratosphere was also detected *in-situ* and in real time using a balloon borne PAS system and a spin-flip Raman laser [123-125]. Methane was detected from road-side and from fruit storage chambers using PAS [126]. PA studies on automobile exhausts were extensively carried out by Sigrist *et al* [17,127,128] and by Roessler in diesel exhausts [129]. The PAS was effectively used in biological and agricultural applications by Harren *et al* [82,130].

ii. PA Studies In Flames

The acoustic signals produced by the absorption of the laser beam by the transient species in the flame are detected by a microphone placed in the vicinity of the flame. PA signals in flames was first demonstrated using a pulsed dye laser absorbed by sodium and lithium atoms seeded into the flame by Allen *et al* [131]. The first detection of molecular species was that of NO_2 , both seeded and as a natural product of the combustion product using a pulsed dye laser [132] where ppm sensitivities were obtained. One application of this technique is in combustion diagnostics. Certain transient species such as NH_2 occurring in a $\text{NH}_3\text{-O}_2$ flame cannot be detected by normal fluorescence techniques applied to the flames, but could be detected by the PA technique using a pulsed dye laser in the 630nm region [133].

A novel application of the PA effect was the Photo Acoustic Detection and Ranging (PADAR), which essentially involves sending of a laser pulse tuned to an absorption line of the gas

Table 1.2. Examples of gas samples detected by PA technique

Laser	Wavelength	Species	C _{min}	Ref. No.
He-Ne	3.39 μm	n-butane, CH ₄	1000	[71, 72]
CO	5-6.5 μm	NO, olefines	ppb	[112]
CO ₂	9.2-10.8 μm	NH ₃	< 3	[73]
CO ₂	9.2-10.8 μm	freon, C ₂ H ₄	≤ 4	[77]
CO ₂	9.2-10.8 μm	explosives	1000	[86]
CO ₂	9.2-10.8 μm	SF ₆	0.01	[87]
CO ₂	9.2-10.8 μm	O ₃ , C ₆ H ₆ , SO ₂	ppb/ppm	[80]
CO ₂	9.2-10.8 μm	Hydrazines	< 30	[81]
CO ₂	9.2-10.8 μm	Toxic vapors	< 10	[113]
CO ₂	9.2-10.8 μm	30 species/air	50	[114]
CO/CO ₂	6 μm/11 μm	explosives	1-10	[78]
CO	5.2-6 μm	10 species	< 1	[70]
CO	4.75 μm	CO	150	[84]
HF	2.7-2.9 μm	HF, CO ₂ , NO	1000	[74]
DF	3.8 μm	CH ₄ , N ₂ O	0.5-5	[76]
Ar ⁺	(multiline)	NO ₂ in air	5	[88]
Kr ⁺	(multiline)	NO ₂ in air	2	[115]
cw dye	0.57-0.62 μm	NO ₂	10	[75]
pulsed dye	480-625 nm	NO ₂ in air	4	[116]
pulsed dye	560-570 nm	HCHO	----	[117]
Freq.doubled dye laser	300.5 nm	SO ₂ in air	0.2	[118]
Freq.doubled pulsed dye	303.59 nm	HCHO	51	[119]
Freq.doubled cw dye	290-310 nm	SO ₂	0.12	[120]
PbS _{1-x} Se _x	4.8 μm	CO	10 ⁴	[160]
Excimer	308 nm	Acetaldehyde	25	[121]

species to be detected and ranged [134]. The acoustic pulse generated in the region of the species is detected by a sensitive microphone mounted on a parabolic reflector placed close to the laser source. The range is inferred from the delay in receiving the acoustic pulse. A range resolution of 100 m was demonstrated by detecting and ranging two Bunsen burners acting as localized sources of CH_4 and using an Optical Parametric Oscillator (OPO) laser tuned to the $3.35\mu\text{m}$ absorption line of CH_4 . The system could also locate over a range of 20m, a gas concentration (leak from a gas line) to within a volume of $20 \times 20 \times 200 \text{ mm}^3$. PADAR has similarities with the Differential absorption LIDAR (DIAL) technique [135], in which the range is determined by the propagation time of the light pulses. It is limited to a resolution of $\sim 10\text{m}$ whereas, since the PADAR essentially detects the acoustic pulses, the resolution is approximately three orders of magnitude better than the DIAL technique. PADAR is more suited for measurements ranges below 100m as compared to the long range, low resolution DIAL.

iii. Spectroscopy Using PA Technique

The phase of the PA signal provides much information on the relaxation processes in gases. The vibrational-translational (V-T), vibrational-rotational (V-R) and vibrational-vibrational (V-V) relaxations have been studied in many gas mixtures by the PA technique. Hunter and Avramides [136], studying the phase of the PA signal obtained by using a $3.39\mu\text{m}$ wavelength He-Ne laser, determined the lifetimes of these processes in CH_4 . Relaxations in CO_2 were determined from the observations of the PA signals at different resonance frequencies and the corresponding Q factors of a resonant PA cell containing the sample and using a CO_2 laser [137]. Similar measurements in SO_2 in the IR region obtained the relaxation rates from the relation between the the rates and the

phase shifts of the PA signal [138].

iv. PA Overtone Spectroscopy

Overtone absorption is essentially a very weak phenomenon, which are forbidden by the dipole selection rule or by spin conversion, and its detection, specially in the gas phase is extremely difficult. Its detection by conventional techniques essentially require either very high optical powers, large absorption path lengths or both. Other techniques such as collimated molecular beams and non-linear spectroscopy to reduce the Doppler width cannot be used effectively for such high vibrational overtones because the oscillator strength of these transitions is very small. Bulk gas cooling is another alternative, but it involves the use of multipass cells and requires cooling of a large volume of gas, which can lead to turbulence in the gas [139]. The PA effect is ideally suited for this purpose due to two of its features viz, its high sensitivity and the small size of the PA cell. The small size allows it to be placed inside the optical cavity of a laser so as to utilize the large optical power available there. Also, by using a non-resonant PA cell, the variation of the PA signal with changes in the beam location within the PA cell are minimized during the intra-cavity operation [140]. PA detection of overtone absorption was first demonstrated by Stella *et al*, who used the intra-cavity PA technique to detect the 619nm overtone CH_4 and the 645nm NH_3 bands using a dye laser with possible applications to planetary atmospheres [141]. Many workers have reported the high resolution overtone absorption spectra of the C-H stretch using intra-cavity gas phase PA detection. The overtones in CH_4 , C_2H_4 etc, both normal and deuterated, were observed by many workers [138,142,143], the rotational-vibrational lines being determined with an accuracy of better than 0.003cm^{-1} . The low-temperature

PA cell used in the above studies had the limitation that only samples of high vapour pressure at low temperatures could be studied. The C-H and C-D stretch overtones in benzene (C_6H_6 , C_6D_6 and C_6HD_5) were obtained by Reddy *et al* using this technique [144]. The line positions of the 4-0 and 5-0 overtones of HT (ie, $^1H^3H$) were determined with an accuracy of better than 0.01 cm^{-1} using the PA technique [145]. The ν_3 bands of HCN were determined for the first time using the PA detection and a F-centre laser with an accuracy of 0.002 cm^{-1} [146]. The highly excited vibrational states of HCN in the visible region were recorded using a longitudinal resonant PA cell placed in the modified and extended cavity of a ring dye laser [147]. Measurements of the absolute overtone cross-sections for the stretching overtones of the C-H were determined by the PA technique by Gutov *et al* [148]. High resolution overtone vibrational-rotational lines of HCl using the ultrasensitive intra-cavity PA technique were reported by Reddy [149]. The gas phase C-H and C-O overtone spectra were obtained by Amrein *et al* in CH_3CHO [150] and the N-H and C-H stretching vibrations in several gaseous amines by Fang *et al* [151].

v. PA Studies In Chemically Reactive Gases

Chemically reactive gases may produce transient intermediate chemical species, and the high sensitivity of the PA technique may be useful in identifying some of the intermediate products, and hence provide important information about the reaction channel. The steady state concentration of products in the photolysis of CH_3NO_2 such as NO_2 were monitored by PA technique using a tunable dye laser [152]. The components of the photofragmentation of CH_3I were detected by PA technique by Hunter and Kristjansson using a tunable, modulated light source in the UV region [153].

vi. PA Raman And Multiphoton Absorption Studies

The PA technique is also suited for measurement of non-linear absorption or non-linear optical scattering effects, since some degree of heat deposition (very weak) in the gas usually occurs owing to these phenomena. PA Raman spectroscopy (PARS) was suggested by Nachaev and Ponomarev [154] and was first observed by Barrett and Berry [155] who used this to detect overtone absorption in the 605.4nm band of CH_4 using a cw tunable dye laser and a pump laser. This technique finds applications to measure Raman frequencies and cross sections, specially in luminescent samples or in hostile environments like flames and discharges. Trace amounts of CH_4 or CO_2 in nitrogen were detected by Siebert *et al* using the PARS technique [156].

Multiphoton absorption process was first detected in SF_6 -Ar mixture using a CO_2 laser and PA detection by Cox [157]. A similar setup was used by Fukumi *et al* [158] to detect multiphoton absorption in CH_4 . Brenner *et al* studied the multiphoton absorption in propynal by both PA and fluorescence techniques [159]. Weulersse and Giner have obtained the multiphoton absorption cross sections for CO_2 lines in CF_3I using PA technique [160]. In the work presented in this thesis, the results of the multiphoton absorption in formaldehyde vapour, detected using pulsed PA technique was reported for the first time [117].

1.3. Other Phenomena Closely Related To The PA Effect

In the PA effect, the excitation source is usually optical radiation and the detected quantity is an acoustic wave generated directly or indirectly by heat. There are several other

phenomena that are closely related to the PA effect such as the "beam acoustic effect", "photothermal calorimetry", "drum effect", "photorefractive effect" etc.

1.3.1. The Beam Acoustic (BA) Effect

The BA effect essentially means excitation by means of a beam and detection by acoustic monitoring. The PA effect is also a part of the BA effect. In general, this term is used when the exciting source is a particle beam of electron, ions, meson, x-ray, RF etc. An important application if the BA effect is in the area of microscopy. By modifying a commercial scanning electron microscope to obtain a modulated electron beam which was focused on to the sample surface, the ultrasonic waves generated was monitored acoustically by a piezo-electric transducer attached to the sample. The transducer output is used to obtain a scanned, magnified image of the sample surface. The image contrast comes primarily from the spatial variations in the thermal and elastic properties within a resolution depth which can be typically of the order of a few microns [161,162]. Cracks on sub-surfaces were identified by thermal wave imaging and phase optimization by Brandis and Rosencwaig [114]. This technique was also used to detect and image phosphorus during the doping of silicon wafer [163]. Nunes *et al* [121] detected the acoustic signals of the ferromagnetic resonance in a thin iron film using microwave radiation. Melcher [113] used magnetic field modulation instead of RF amplitude modulation. Such acoustic detection of magnetic resonances have been reported by many workers [118,119,164].

1.3.2. Photothermal Calorimetry (PTC)

The PTC is also, in general terms, production of heat following

absorption of radiation. The PA effect in fact, is a consequence of this. This also produces some other consequences as well. This technique is simply based on the conservation of energy produced, if no luminescence, photochemistry or photoelectric effects occur. The sample is placed in a well insulated vacuum Dewar and is in good thermal contact with only the thermal detector. The wavelength of the optical radiation is scanned and the corresponding temperature rise of the sample is determined precisely. The disadvantage of this system is the extremely slow response of the thermal detector. Hass and Davidson [165] performed such experiments to determine the absolute optical absorption coefficients of water at 20°C using argon laser wavelengths and the results compare well with PA measurements in water. PT radiometry (PTR) is used to determine the thermal changes on the sample by non-contact methods, which is, in certain environments, advantageous over the conventional PA detection. A great deal of work in this aspect was done by Kanstad and Nordal using a tunable IR laser on samples ranging from rare earth compounds to blood and whole leaves. The thermal emission from the sample irradiated with the IR laser is monitored remotely using a sensitive far-IR detector (PbSnTe). This has all the advantages of PA technique and the added remote detection capability [166-169]. This technique applied to imaging and the non-contact mode of detection makes rapid imaging possible of both large and small samples without sample contamination [170]. An important medical application of the PTR being *in vivo* imaging of parts of human body.

1.3.3. Photorefractive Technique

This technique is also called 'Thermal lens' (TL) or 'Photothermal Deflection' (PTD). In PTD, the heat gradient generated in the sample on irradiation with the higher power pump laser affects the

propagation of the weaker probe beam. In the Thermal lens, the propagation of the pump beam is affected by processes like the 'self defocusing' or 'thermal blooming'. Self defocusing usually occurs instead of focusing since the derivative of the refractive index with respect to temperature is usually negative. Thus the photorefractive technique can be monitored either by self-defocusing or by probe-beam deflection methods. Liete *et al* were the first to demonstrate this technique as a spectroscopic tool [171] and the quantitative theory provided by Solimini [172]. The thermal lensing technique was used in conjunction with a collinear probe beam to obtain better sensitivity than the single beam technique [58]. Several workers [172] have developed and refined this technique and applied it to different areas of research ranging from trace analysis [173] to studies of material properties [174].

The work presented in this thesis essentially attempts to study the photoacoustic effect in solid and gaseous samples. CW as well as pulsed PA spectra of nitrogen dioxide and formaldehyde gases have been studied in some detail in this thesis. This is motivated by the fact that the detection and analysis of gaseous samples, specially pollutant ones like NO_2 and formaldehyde, which play a vital role in the environmental chemistry is very important. PA technique provides a versatile tool for detection and analysis of such pollutants due to the many-fold advantages of this method. Multiphoton absorption processes, detected by PA technique is one method of detecting trace gases which do not normally exhibit absorption in the wavelength region of interest (visible). Rather than the detailed spectroscopic studies of these gas samples, the method of detection of the samples and characterization of the PA system for these species have been given more importance. In the case of solids, the study of

laser-material interactions like laser damage, plasma formation etc are of great current interest from the point of view of characterization of materials. Application of the PA technique to such studies have also been presented here. Some simple and *in-situ* methods for the detection and measurements of such parameters have been introduced here and are discussed in the succeeding chapters of this thesis.

1.4. References

- [1] Imasaka T and Ishibashi N, *Prog.Quant.Electr.*, **14**, 131, (1990)
- [2] Wright G B, "Light Scattering of Solids", (Springer-Verlag, Berlin, 1969)
- [3] Wendlandt W W and Hecht H G, "Reflectance Spectroscopy", (Wiley, New York, 1966)
- [4] Wilks P A and Hirschfeld T, *Appl.Spectroc.Rev.*, **1**, 99, (1968)
- [5] Bell A G, *Am.J.Sci.*, **20**, 305, (1880)
- [6] Bell A G, *Philos.Mag.*, **11**, 510, (1881)
- [7] Tyndall J G, *Proc.Royal.Soc.Lon.*, **31**, 307, (1881)
- [8] Rontgen W C, *Philos.Mag.*, **11**, 308, (1881)
- [9] Viengerov M L, *Dolk.Akad.Nauk.SSSR*, **19**, 687, (1938)
- [10] Viengerov M L, *Izv.Akad.Nauk.SSSR*, **4**, 94, (1940)
- [11] Gorelik G, *Dolk.Akad.Nauk.SSSR*, **54**, 779, (1946)
- [12] Slobodaskaya P V, *Izv.Akad.Nauk.SSSR*, **12**, 656, (1948)
- [13] Rosencwaig A, *Opt.Comm.*, **7**, 305, (1973)
- [14] Rosencwaig A, *Anal.Chem.*, **47**, 592A, (1975)
- [15] Rosencwaig A and Gersho A, *J.Appl.Phys.*, **47**, 64, (1976)
- [16] Rosencwaig A, "Photoacoustics and Photoacoustic Spectroscopy" (Wiley Interscience, New York), (1983)
- [17] Sigrist M W, Bernegger S and Meyer P L, *Topics in current Physics*, Vol.46: "Photoacoustic, Photothermal and Photothermal Processes in Gases" Ed: Hess P, (Springer -Verlag, Heidelberg, 1989), p 173

- [18] Zarov V P and Letokhov V S, *Laser Opto-Acoustic Spectroscopy*" Springer series in optical sciences, Vol.37, (Springer-Berlin, 1984)
- [19] Kimura W D and Ford D H, *Rev.Sci.Instrum.*, 57, 2754, (1986)
- [20] Zammit U et al, *J.Phys.:E(Scient.Instr.)*, 21, 935, (1988)
- [21] Tilger R, *Appl.Opt.*, 20, 3780, (1981)
- [22] Rosencwaig A, "Advances in Electronics and Electron. Physics Vol 46", Ed. Martin L, (Academic Press, New York, 1978)
- [23] Strek W et al, *Appl.Spectos.*, 41, 639, (1987)
- [24] Vallabhan C P G et al, *J.Aco.Soc.Ind.*, 18, 69, (1990)
- [25] Patel C K N and A C Tam, *Rev.Mod.Phys.*, 53, 517, (1981)
- [26] Diebold G J, Khan M I and Park S M, *Science*, 250, 101, (1990)
- [27] Hsuen Y M, et al, *Anal.Sci.*, 6, 67, (1990)
- [28] Hsuen Y M, et al, *Anal.Sci.*, 6, 71, (1990)
- [29] Tam A C, *Rew.Mod.Phys.*, 58, 381, (1986)
- [30] Quimbly R S and Lin Z M, *Can.J.Phys.*, 64, 1276, (1986)
- [31] Zhang S Y and Chen Li, *Can.J.Phys.*, 64, 1316, (1986)
- [32] Ash E A, et al, *Electon.Lett.*, 16, 470, (1980)
- [33] Rose D N et al, *Can.J.Phys.*, 64, 1284, (1986)
- [34] Biswas A et al, *Can.J.Phys.*, 64, 1184, (1986)
- [35] Hoshimiya T, conference proceedings of the "6th International Topical Meeting on Photoacoustic, and Photothermal Phenomena" U.S.A, 1989, paper # ThGai, p.340
- [36] Hoshimiya T, Ohta M and Kojima M, conference proceedings of the "7th Topical International Meeting on Photoacoustic and Photothermal Phenomena", The Netherlands, 1991, paper # PII/2, p.264, 1991
- [37] Brandis E and Rosencwaig A, *Appl.Phys.Lett.*, 37, 98, (1980)
- [38] Adams M J, et al, *Appl.Spectrosc.*, 32, 430, (1978)
- [39] Fernelius N C, et al, *Appl.Surf.Sci.*, 7, 32, (1981)
- [40] Busse G, *Appl.Opt.*, 21, 107, (1982)
- [41] Rosencwaig A and Willis J B, *Appl.Phys.Lett.*, 36, 667, (1980)
- [42] Harada Y et al, *J.Phys.D:Appl.Phys.*, 22, 569, (1989)
- [43] Srinivasan R and Braren B, *Chem.Rev.*, 89, 1303, (1989)
- [44] Ravi Kumar A V et al, *Pramana*, 37, 345, (1991)

- [45] Patel C K N and Tam A C, *Appl.Phys.Lett.*, **34**, 467, (1979)
- [46] Tam A C, "Ultrasensitive spectroscopy" Ed:D Kliger, (Academic Press, New York, 1983)
- [47] Castleden S L, *et al*, *Anal.Chem.*, **51**, 2152, (1979)
- [48] Rosencwaig A and Hall S S, *Anal.Chem.*, **47**, 548, (1975)
- [49] Nordal P E and Kanstad S O, *Opt.Comm.*, **22**, 185, (1977)
- [50] Nordal P E and Kanstad S O, *Opt.Comm.*, **24**, 95, (1978)
- [51] McCleny W A and Rohl R, conference proceedings of the "2nd International Conference on Photoacoustic Spectroscopy", U.S.A., (1981)
- [52] Yeack C E *et al*, *Appl.Phys.Lett.*, **41**, 1043, (1982)
- [53] Srinivasan R and Braren B, *Chem.Rev.*, **89**, 1303, (1989)
- [54] Dienstbier M *et al*, *Appl.Phys.B*, **51**, 137, (1990)
- [55] Leung W P and Tam A C, conference proceedings of the "7th Topical International Meeting on Photoacoustic and Photothermal Phenomena", The Netherlands, 1991, paper PIX/14A, p.365, 1991
- [56] Florian R *et al*, *Phys.Stat.Solidi*, **48**, k35, (1978)
- [57] P Korpiun, "P.A. Effect, Principles and Applications ", Eds. Luscher E *et al*, (Friedr.Vieweg & Sohn, Weisbaden, 1984), p.211
- [58] Cahen D, "P.A. Effect, Principles and Applications ", Eds. Luscher E *et al*, (Friedr.Vieweg & Sohn, Weisbaden, 1984), p.271
- [59] Netzelmann U, "P.A. Effect, Principles and Applications ", Eds. Luscher E *et al*, (Friedr.Vieweg & Sohn, Weisbaden, 1984), p.333
- [60] Moore W S, *Pure & Appl.Chem.*, **40**, 211, (1974)
- [61] Mandelis A and Royce B S H, *J.Opt.Soc.Am.*, **70**, 474, (1980)
- [62] Schneider S, Moller U and Coufal H, *Appl.Opt.*, **21**, 44, (1982)
- [63] Farrow M M *et al*, *Appl.Phys.Lett.*, **33**, 735, (1978)
- [64] Lloyd L B *et al*, *Rev.Sci.Instrum.*, **51**, 1488, (1980)
- [65] Teng Y C and Royce B S H, *Appl.Opt.*, **21**, 77, (1982)
- [66] Laufer G *et al*, *Appl.Phys.Lett.*, **37**, 517, (1980)
- [67] Oda S *et al*, *Anal.Chem.*, **52**, 650, (1980)
- [68] Wyllie I W and Lai E P C, *Rev.Sci.Instrum.*, **57**, 1185, (1986)
- [69] Patel C K N and Tam A C, *Appl.Phys.Lett.*, **34**, 467, (1979)

- [70] Patel C K N *et al*, *J.Chem.Phys.*, **71**, 1470, (1979)
- [71] Tam A C and Patel C K N, *Appl.Opt.*, **18**, 3348, (1979)
- [72] Brueck S R J, *et al*, *Opt.Comm.*, **34**, 199, (1980)
- [73] Nelson E T and Patel C K N, *Nature*, **286**, 368, (1980)
- [74] Nelson E T and Patel C K N, *Appl.Phys.Lett.*, **39**, 537, (1981)
- [75] Reji Philip *et al*, *J.Phys.:B*, **25**, 155, (1992)
- [76] Lahmann W and Ludewig H J, *Chem.Phys.Lett.*, **45**, 177, (1977)
- [77] Sathy P *et al*, *Pramana*, **34**, 585, (1990)
- [78] Ross L N *et al*, *Biochem.et.Biophysic.Acta.*, **593**, 330, (1980)
- [79] Lahmann W *et al*, *Anal.Chem.*, **49**, 549, (1977)
- [80] Poulet P *et al*, *Biochem.et.Biophysic.Acta.*, **724**, 433, (1983)
- [81] Bults G *et al*, *Biochem.et.Biophysic.Acta.*, **679**, 452, (1982)
- [82] Harren F J M, PhD thesis "The PA Effect Refined And Applied To Biological Problems" Katholieke University, The Netherlands, 1988
- [83] Quimbly R S and Sheinis A I, *Appl.Opt.*, **363**, (1987)
- [84] Roscencwaig A, *Anal.Chem.*, **47**, 592A, (1975)
- [85] Giese K *et al*, *Can.J.Phys.*, **64**, 1139, (1986)
- [86] Guy M and Bernengo J C, *Can.J.Phys.*, **64**, 1142, (1986)
- [87] Helander P and Lundstrom I, *J.Photoacoustics*, **1**, 203, (1982)
- [88] McQueen D H., *J.Phys.:E.*, **16**, 738, (1983)
- [89] Fox D L, *Anal.Chem.*, **59**, 280R, (1987)
- [90] "Laser Monitoring of the Atmosphere", 'Topics in Applied Physics', **14**, Ed. Hinkley E D, (Springer, Berlin, 1976)
- [91] Patel C K N, *Science*, **202**, 157, (1978)
- [92] Turn I and Waters D N, *Int.J.Environ.Stud.*, **21**, 165, (1983)
- [93] Grant W B and Menzies R T, *J.Air.Poll.Cont.Assn.*, **33**, 187, (1983)
- [94] Edner H *et al*, *Appl.Opt.*, **25**, 403, (1986)
- [95] Killinger D K and Mooradian, "Optical and Laser Remote Sensing", 'Springer series in Optical Science' Vol 39, (Springer, Berlin, 1983)
- [96] Carswell A I, *Can.J.Phys.*, **61**, 378, (1983)
- [97] Measures R M, "Laser Remote Sensing, Fundamentals and Applications", (Wiley, New York, 1984)

- [98] Dubinsky R N, *Lasers Optron.*, 7, 93, (1988)
- [99] Sigrist M W et al, *Infrared Phys.*, 29, 805, (1989)
- [100] Zarov V P and Letokhov V S, "Laser Opto-Acoustic Spectroscopy" Springer series in Optical Sciences Vol.37, (Springer-Verlag, Berlin, 1985)
- [101] Kerr E L and Atwood J G, *Appl.Opt.*, 7, 915, (1968)
- [102] Kreuzer L B, *J.Appl.Phys.*, 42, 2934, (1971)
- [103] West G A et al, *J.Appl.Phys.*, 51, 2823, (1980)
- [104] Marinero E E and Stuke M, *Opt.Comm.*, 30, 349, (1979)
- [105] Di Lieto A et al, *Appl.Phys.:B*, 27, 1, (1982)
- [106] Di Lieto A et al, *Opt.Comm.*, 31, 25, (1979)
- [107] Klimack C M and Gelbwachs J A, *Appl.Opt.*, 24, 247, (1985)
- [108] Nickolaisen S L and Bialkowski S E, *J.Chromatogr.*, 366, 127, (1986)
- [109] Zarov V P, "Laser Opto-Acoustic Spectroscopy in Chromatography" in 'Laser Analytical Spectrochemistry', Editor : Letokhov V S, (Adam-Hilger, Bristol, 1985) chapt.5
- [110] Fournier D et al, *Appl.Phys.Lett.*, 37, 519, (1972)
- [111] Tran C D, *Appl.Spectos.*, 40, 1108, (1986)
- [112] Bernegger S and Sigrist M W, *IR Phys.*, 30, 375, (1990)
- [113] Melcher R L *Appl.Phys.Lett.*, 37, 895, (1980)
- [114] Brandis E and Rosencwaig A, *Appl.Phys.Lett.*, 37, 98, (1980)
- [115] Poizat O and Atkinson G H, *Anal.Chem.*, 54, 1485, (1982)
- [116] Voigtman E et al, *Anal.Chem.*, 53, 1442, (1981)
- [117] Ravi Kumar A V et al, *Pramana*, 33, L621, (1989)
- [118] Coufal H, *Appl.Phy.Lett.*, 39, 215, (1981)
- [119] DuVarney R C et al, *Appl.Phys.Lett.*, 38, 675, (1981)
- [120] Cvijin P V et al, *Anal.Chem.*, 59, 300, (1987)
- [121] Nunes O A C et al, *Appl.Phys.Lett.*, 35, 656, (1979)
- [122] Kreuzer L B and Patel C K N, *Science*, 173, 45, (1971)
- [123] Patel C K N et al, *Science*, 184, 1173, (1974)
- [124] Burkhardt E G et al, *Science*, 188, 1111, (1975)
- [125] Patel C K N, *Opt.& Q.Elect.*, 8, 145, (1976)
- [126] Perlmutter P, et al, *Appl.Opt.*, 18, 2267, (1979)

- [127] Meyer P L and Sigrist M W, *Rev.Sci.Instr.*, **61**, 1179, (1990)
- [128] Meyer P L *et al*, "Photoacoustic and Photothermal Phenomena", Eds. Hess P and Pelzel J, Springer Series in Optical Sciences, **58**, (Springer, Berlin, 1988) p.127
- [129] Roessler D M, *Appl.Opt.*, **23**, 1148, (1984)
- [130] Harren F *et al*, "Photoacoustic and Photothermal Phenomena", Eds. Hess P and Pelzel J, Springer Series in Optical Sciences, **58**, (Springer, Berlin, 1988) p.148
- [131] Allen J E *et al*, *Opt.Lett.*, **1**, 118, (1977)
- [132] Tennal K *et al*, *Appl.Opt.*, **21**, 2133, (1982)
- [133] Smith G P *et al*, *Appl.Opt.*, **22**, 3995, (1983)
- [134] Brasington D J, *J.Phys.D:Appl.Phys.*, **15**, 219, (1982)
- [135] Collis R T H and Russell P B, "Laser Monitoring of The Atmosphere", Ed. Hinkley E D, (Springer, Berlin, 1976)
- [136] Avramides E and Hunter T F, *Chem.Phys.*, **57**, 441, (1981)
- [137] Zarov V P and Montanari S G, *Opt.Spectrosc.*, **51**, 66, (1981)
- [138] Slobodskaya P V and Rityn E N, *Opt.Spectrosc.*, **47**, 591, (1979)
- [139] Scherer G J *et al*, *J.Chem.Phys.*, **81**, 5319, (1984)
- [140] Wong J S and Moore C B, *J.Chem.Phys.*, **77**, 603, (1982)
- [141] Stella G *et al*, *Chem.Phys.Lett.*, **39**, 146, (1976)
- [142] Crofton M W *et al*, *J.Chem.Phys.*, **89**, 7100, (1989)
- [143] Scherer G J *et al*, *J.Chem.Phys.*, **78**, 2817, (1983)
- [144] Reddy K V *et al*, *J.Chem.Phys.*, **76**, 2814, (1982)
- [145] Chuang M C and Zare R N, *J.Mol.Spectrosc.*, **121**, 380, (1987)
- [146] German K R and Gornal W S, *J.Opt.Soc.Am.*, **71**, 1452, (1981)
- [147] Lehmann K K *et al*, *J.Chem.Phys.*, **77**, 2853, (1982)
- [148] Gutow J H *et al*, *Chem.Phys.Lett.*, **185**, 120, (1991)
- [149] Reddy K V, *J.Mol.Spectrosc.*, **82**, 127, (1980)
- [150] Amrein A *et al*, *J.Chem.Phys.*, **90**, 3944, (1989)
- [151] Fang H L *et al*, *Chem.Phys.Lett.*, **108**, 539, (1984)
- [152] Colles M J *et al*, *Nature*, **262**, 681, (1976)
- [153] Hunter T F and Kristjansson K S, *Chem.Phys.Lett.*, **58**, 291, (1978)

- [154] Nechaev S Y and Ponomarev N Y, *Sov.J.Quant.Electron.*, 5, 752, (1975)
- [155] Barrett J J and Berry M J, *Appl.Phys.Lett.*, 34, 144, (1979)
- [156] Siebert D R et al, *Appl.Opt.*, 19, 53, (1980)
- [157] Cox D M, *Opt.Comm.*, 24, 336, (1978)
- [158] Fukumi T, *Opt.Comm.*, 30, 351, (1979)
- [159] Brenner et al, *Chem.Phys.Lett.*, 72, 202, (1980)
- [160] Weulesse J M and Genier R, *Appl.Phys.*, 24, 363, (1981)
- [161] Cargill C S, *Nature*, 286, 691, (1980)
- [162] Cragill C S, "Scanned Electron Microscopy", Editor: Ash E A, (Academic Press, New York, 1980) p.319
- [163] Rosencwaig A and White R M, *Appl.Phys.Lett.*, 38, 165, (1981)
- [164] Hirabayashi I, et al, *Jpn.J.Appl.Phys.*, 20, L208, (1981)
- [165] Hass M and Davidsson J W, *J.Opt.Soc.Am.*, 67, 622, (1977)
- [166] Kanstad S O and Nordal P E, *Powder Technol.*, 22, 133, (1978)
- [167] Kanstad S O and Nordal P E, *Appl.Surf.Sci.*, 5, 286, (1980)
- [168] Nordal P E and Kanstad S O, "Scanned Electron Microscopy", Ed. Ash E A, (Academic Press, New York, 1980) p.331
- [169] Nordal P E and Kanstad S O, *Appl.Phys.Lett.*, 38, 486, (1981)
- [170] Busse G, *Appl.Opt.*, 21, 107, (1982)
- [171] Leite R C C, et al, *Appl.Phys.Lett.*, 5, 141, (1964)
- [172] Kliger D S, *Acct.Chem.Res.*, 13, 129, (1980)
- [173] Higashi T et al, *Anal.Chem.*, 55, 1907, (1983)
- [174] Sell J A et al, *J.Appl.Phys.*, 69, 1330, (1991)

1.5. Symbols and Notations

a_1	Absorption coefficients
$\hat{\alpha}$	Measured absorption spectrum
$\underline{\alpha}$	Calculated absorption spectrum
α_{tot}	Total absorption coefficient

\underline{c}	Vector containing the concentrations of c_j
F	Cell constant
G	Geometrical factor for the cell
γ	Specific heat ratio
I_i	Incident laser power at transition i
L	PA cavity length
η	Quantum efficiency
N_{tot}	Total number density of gas molecules in the mixture
$P_1 P_2$	Incident optical power
Q	Quality factor of the cell
$q_1 q_2$	PA signal
S	PA signal
σ_j	Absorption cross section of gas component j
\sum	Matrix containing the elements of σ_{ij}
$v_e v_f$	Frequency of excitation and fluorescence

CHAPTER II

THEORETICAL ASPECTS OF THE PHOTOACOUSTIC EFFECT

ABSTRACT

IN THIS CHAPTER, AN INTRODUCTION TO THE THEORY OF PA SIGNAL GENERATION IN GASES IS GIVEN, STARTING FROM OPTICAL ABSORPTION BY THE GAS, FOLLOWED BY THE NON-RADIATIVE DE-EXCITATION AND FINALLY THE PRODUCTION OF THE ACOUSTIC SIGNAL. VARIOUS OTHER ASPECTS SUCH AS LOSSES IN THE CELL, PA SIGNAL SATURATION ETC. ARE ALSO DISCUSSED. A FEW OTHER MODELS OF PA SIGNAL GENERATION ARE ALSO DISCUSSED.

CHAPTER II

THEORETICAL ASPECTS OF THE PHOTOACOUSTIC EFFECT

2.1. Optical Absorption In Gases

The absorption of photons by the molecules of a gas sample can produce a variety of phenomena depending mainly on their spectral characteristics. Following the absorption, the level which gets excited may lose their energy by either the radiative or non-radiative de-excitation process, the former process leading to phenomena like fluorescence, phosphorescence etc. and the latter channeling the energy absorbed into translational degrees of freedom resulting in a change of temperature of the gas. If the photon energy is high enough, a direct photochemical decomposition of the molecule is also possible. Inter-system energy transfer occurs due to collision with another or same species in the ground state resulting in their excitation to the higher energy state. In vibrational excitation, the radiative emission and the chemical reactions do not play an important role since the radiative lifetime of the vibrational levels is very long compared to the time needed for collisional de-excitation at ordinary pressures. Also the photon energy is too small to induce such reactions. But in the case of electronic transitions, both emission of radiation and the chemical reactions may compete strongly with

collisional de-activation. The different channels of de-excitation that follow absorption of radiation and the generation of the acoustic signal in a sample are depicted in fig.2.1.

2.1.1 Rate Equation For A Two-level System

Considering a simple two-level system such that r_{ij} represents the rate of radiative transition from level i to level j while c_{ij} represents the non-radiative transition from E_i to E_j as shown in fig.2.2. It is seen that,

$$r_{ij} = \rho_v B_{ij} + A_{ij} \quad \dots \dots (2.1)$$

here, ρ_v is the radiation density at energy $E_v = E_1 - E_0$, E_1 and E_0 being the energies of the excited and ground states respectively. $B_{ij} = B_{ji}$ and it represents the Einstein coefficient for stimulated emission from $i \rightarrow j$ and A_{ij} the Einstein coefficient for the spontaneous emission from $i \rightarrow j$ and thus, $A_{01} = 0$ since $E_1 > E_0$. Let N_1 and N_0 be the number of molecules in the excited and ground states respectively. The rate of change of N_1 with time is the number of molecules entering level 1 minus the number of molecules leaving level 1 per unit time so that,

$$\dot{N}_1 = [r_{01} + c_{01}]N_0 - [r_{10} + c_{10}]N_1 \quad \dots \dots (2.2)$$

$A_{01} = 0$ and $c_{01} \approx 0$ since there is a very low probability of a collisional excitation of an atom from level 0 to 1 at room temperature. Also, $B_{01} = B_{10}$. Thus,

$$\dot{N}_1 = \rho_v B_{10} (N_0 - N_1) - [A_{10} + c_{10}] N_1 \quad \dots \dots (2.3)$$

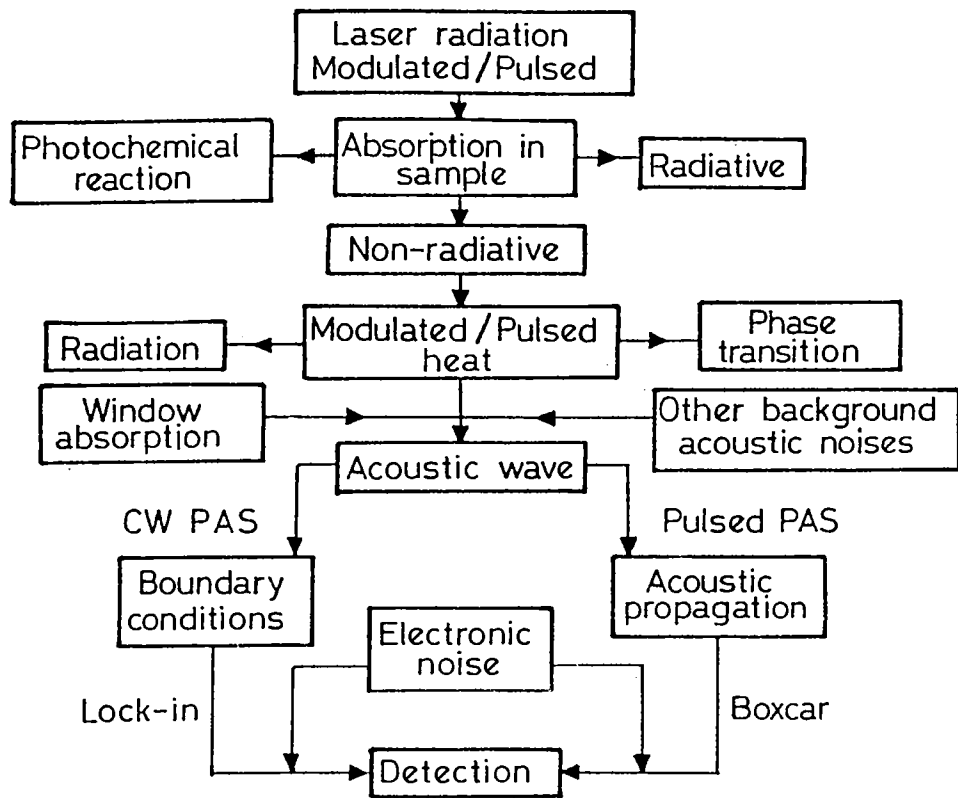


Fig.2.1. The different channels of de-excitation that follows the absorption of radiation by a sample

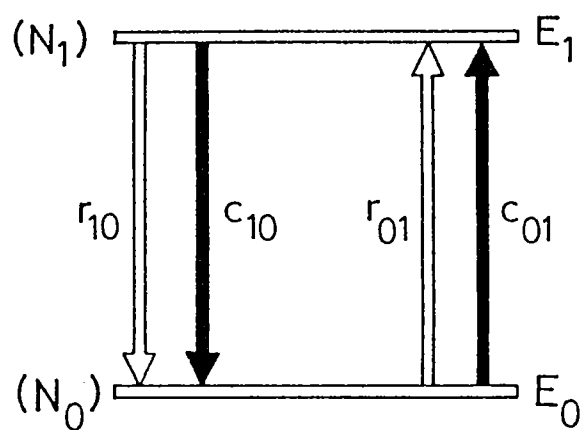


Fig.2.2. The representation of a simple 2-level system and the excitation and de-excitation parameters involved

It can be also represented as,

$$\dot{N}_1 = \rho_v B_{10} \left(N_0 - N_1 \right) - \left(\tau_r^{-1} + \tau_c^{-1} \right) N_1 \quad \dots \dots \dots (2.4)$$

where, $\tau_r = 1/A_{10}$ the relaxation time for radiative transfer from level 1, $\tau_c = 1/c_{10}$ the relaxation time for non-radiative transition from level 1, and The total relaxation time can be defined as,

$$\tau^{-1} = \tau_r^{-1} + \tau_c^{-1} \quad \dots \dots \dots (2.5)$$

Therefore,

$$\dot{N}_1 = \rho_v B_{10} \left(N_0 - N_1 \right) - \left(\tau^{-1} \right) N_1 \quad \dots \dots \dots (2.6)$$

similarly for N_0 in the ground state,

$$\dot{N}_0 = - \rho_v B_{10} \left(N_0 - N_1 \right) + \left(\tau^{-1} \right) N_1 \quad \dots \dots \dots (2.7)$$

thus,

$$\frac{d}{dt} \left(N_1 - N_0 \right) = -2\rho_v B_{10} \left(N_1 - N_0 \right) - 2\tau^{-1} N_1 \quad \dots \dots \dots (2.8)$$

at steady state, the LHS of the above equation is equal to zero so that,

$$N_0 = \frac{\left(\rho_v B_{10} + \tau^{-1} \right) N}{2\rho_v B_{10} + \tau^{-1}} \quad \dots \dots \dots (2.9)$$

$$N_1 = \frac{\rho_v B_{10} N}{2\rho_v B_{10} + \tau^{-1}} \quad \dots \dots (2.10)$$

where N is the total number of molecules/cc so that $N = N_0 + N_1$. ρ_v can be defined as $\frac{I\hbar\nu}{c}$, where I is the intensity of light, ν its frequency and c the velocity of light, and $B = B_{10} \frac{\hbar\nu}{c}$. Thus,

$$N_1 = \frac{BIN}{2BI + \tau^{-1}} \quad \text{and,} \quad N_0 = \frac{(BI + \tau^{-1}) N}{2BI + \tau^{-1}} \quad \dots \dots (2.11)$$

If the incident light is modulated such that,

$$I = I_0 \left[1 + \delta \exp(i\omega t) \right] \quad 0 \leq \delta \leq 1 \quad \dots \dots (2.12)$$

where δ is the modulation depth, then,

$$N_1 = N \frac{BI_0 \left[1 + \delta \exp(i\omega t) \right]}{2BI_0 \left[1 + \delta \exp(i\omega t) \right] + \tau^{-1}} \quad \dots \dots (2.13)$$

2.1.2. Excitation Of The Acoustic Wave

If the incident light pumps a considerable number of molecules from the ground state E_0 to the excited state E_1 , it is seen that when the excited molecules decay back to the ground state by means of collision, the energy difference $\Delta E = E_1 - E_0$ goes into translational energy ie, the velocities of the colliding molecules

increases. Ignoring the rotational and vibrational energies, the internal energy of the absorbing gas/unit volume is ,

$$U = \sum_i (N_i E_i) + K \quad \dots \dots \dots (2.14)$$

Here, K is the kinetic energy. In the two level system considered,

$$U = N_1 E_1 + K \quad \dots \dots \dots (2.15)$$

and,

$$\dot{U} = \dot{N}_1 \dot{E}_1 + \dot{K} \quad \dots \dots \dots (2.16)$$

By conservation of energy, \dot{U} is equal to the difference between the energy absorbed and re-radiated. Then,

$$\dot{U} = \left(r_{01} N_0 - r_{10} N_1 \right) E_1 + c_{10} N_1 E_1 \quad \dots \dots \dots (2.17)$$

where,

$$K = c_{10} N_1 E_1 \quad \dots \dots \dots (2.18)$$

From thermodynamics,

$$dK = \left(\frac{\partial K}{\partial T} \right)_V dT + \left(\frac{\partial K}{\partial V} \right)_T dV \quad \dots \dots \dots (2.19)$$

Where, T and V are the temperature and volume of the gas respectively. Since the volume is taken to be constant,

$$dK = \left(\frac{\partial K}{\partial T} \right)_V dT = C_V dT \quad \dots \dots \dots (2.20)$$

where C_V is the specific heat of the gas at constant volume.

Therefore ;

$$K = C_v T + f(V) \quad \dots \dots \dots (2.21)$$

where, $f(V)$ is a function that is dependent on volume but not on temperature. For an ideal gas,

$$P = NkT \quad \dots \dots \dots (2.22)$$

k = Boltzmann constant

$$P = \frac{k}{C_v} N \left[K - f(V) \right] \quad \dots \dots \dots (2.23)$$

The pressure wave is $\partial P / \partial t$. Thus the derivative of Eqn.2.23 is,

$$\dot{P} = \frac{k}{C_v} NK = \frac{k}{C_v} N \left[c_{10} N_1 E_1 \right] \quad \dots \dots \dots (2.24)$$

from Eqn.2.13,

$$\dot{P} = \frac{k}{C_v} \frac{\frac{N^2}{\tau_c} E_1 BI_o \left[1 + \delta \exp(i\omega t) \right]}{2BI_o \left[1 + \delta \exp(i\omega t) \right] + \tau^{-1}} \quad \dots \dots \dots (2.25)$$

expanding the parts of $\delta \exp(i\omega t)$ and retaining only the $\exp(i\omega t)$ terms, and putting $\omega t = \Phi$,

$$\dot{P} = \frac{kE_1 N^2}{C_v} \left\{ \frac{2\tau_c^{-2} BI_o \delta}{\left[2BI_o + \tau^{-1} \right] \left\{ \left[2BI_o + \tau^{-1} \right]^2 + \omega^2 \right\}^{1/2}} \right\} \exp \left[i(\omega t - \Phi) \right] \quad \dots \dots \dots (2.26)$$

integrating, we obtain the pressure signal as,

$$p = \frac{kE_1 N^2}{C_v \omega} \left\{ \frac{2\tau_c^{-2} BI_o \delta}{\left[2BI_o + \tau^{-1} \right] \left\{ \left[2BI_o + \tau^{-1} \right]^2 + \omega^2 \right\}^{1/2}} \right\} \exp \left[i(\omega - \Phi - \pi/2) \right] \dots \dots \dots (2.27)$$

The PA signal at the microphone output is measured as [1,2],

$$q = -p \dots \dots \dots (2.28)$$

2.1.3. Saturation In PA Signal

At low light intensities, I_o is small and thus the optical pumping term, $2BI_o \ll \tau^{-1}$ and thus the PA signal,

$$q \cong \frac{kE_1 N^2}{C_v \omega} \left(\frac{\tau}{\tau_c} \right)^2 \frac{2BI_o \delta \exp \left[i(\omega t - \Phi + \pi/2) \right]}{\left(1 + \omega^2 \tau^2 \right)^{1/2}} \dots \dots \dots (2.29)$$

The PA signal is proportional to I_o and square of the total number molecules/unit volume.

Since $q \propto \left(\frac{\tau}{\tau_c} \right)^2$, and also as τ_c decreases with temperature, it

is seen that the PA signal generally increases with temperature. For high optical densities (\sim watts/cm²), $2BI_o \gg \tau^{-1}$ and for small ω ,

$$q \cong \frac{kE_1 N^2}{C_v \omega} \left(\frac{1}{\tau_c} \right)^2 \frac{1}{BI_o} \delta \exp \left[i(\omega t - \gamma - \pi/2) \right] \dots \dots \dots (2.30)$$

Here, the PA signal is inversely proportional to I_o and thus,

absorption saturation occurs at high intensities. It is due to the result of attempting to pump harder than the upper level can be de-excited, ie, $B_1 I > 0.5 \tau^{-1}$. Since τ is usually of the order of 10^{-6} to 10^{-4} sec, saturation of the PA signal will set in for most of the absorbing gases at watts/cm² intensities. This saturation behaviour has been clearly observed in the results given in Chapters V and VI.

2.2. Generation Of PA Signal In Gases : Effect of Dissipative Forces

Optical absorption of the incident radiation produces excited states in the molecules of the gas. Considering a simple two level system such that N_0 and N_1 are the densities of the ground and excited states respectively,

$$\frac{dN_1}{dt} = (N_0 - N_1)R_e - N_1(R_e + A_r + A_n) \quad \dots \dots (2.31)$$

where, A_r = radiative decay of the excited state,

A_n = non-radiative decay rate of excited state due to collisions of the excited state and,

R_e = excitation rate due to the light beam of intensity I photons/cm²/sec.

If the absorption cross section is σ cm², then,

$$R_e = I\sigma \quad \dots \dots (2.32)$$

If the modulation frequency is assumed to be sinusoidal and of the order of kHz or less, it is slow compared to the excited state decay rate. Also, since the light intensity is weak enough, $N_0 \gg N_1$ and thus the stimulated emission from the excited state

can be neglected. Under these assumptions,

$$N_1 = \frac{N_0 R_e}{(A_r + A_n)} \quad \dots \dots \dots (2.33)$$

Or, $N_1 = N_0 I \sigma \tau$ $\dots \dots \dots (2.34)$

where $\tau = (A_r + A_n)^{-1}$ is the total lifetime of the excited state. The corresponding heat production rate H due to the excited state density N_1 is given by [3],

$$H(r,t) = N_1(r,t) A_n E' \quad \dots \dots \dots (2.35)$$

Here, H is a function of r (position) and t (time) since I is a function of r and t . E' is the average thermal energy released due to a non-radiative de-excitation collisions of the excited state. If the de-excitation collisions result in converting the excited state to the ground state, then the de-excitation energy E' is simply the energy of the excited state with respect to the ground state. The Eqn.2.35 gives the basis of heat production term in PA experiments using slow modulation. The heat source term in the PA signal is proportional to the product of the molecular density N , photon absorption rate $I \sigma$, the probability for non-radiative relaxation of the optically excited state τA_n and the heat energy released per excitation E' .

Since we assume that the modulation frequency ω of the optical beam is much slower than the total decay rate τ^{-1} , of the excited state and thus, if $\omega > \tau^{-1}$, then dN_1/dt cannot be put equal to 0 in Eqn.2.31. Therefore, Eqn.2.31 can be written as [2],

$$\left(\frac{d}{dt} + \tau^{-1} \right) N_1 = N_0 R_e \quad \dots \dots \quad (2.36)$$

Also, we assume that there is no optical saturation ie, $N_1 \ll N_0$ and $R_e \ll \tau^{-1}$. Since the optical radiation is sinusoidal, it can be represented as,

$$I = I_0 [1 + \exp(i\omega t)] \quad \dots \dots \quad (2.37)$$

where, only the real part has any physical meaning. The constant part in Eqn.2.37. can be neglected since only the modulated heat source contributes to the generation of a corresponding PA signal. Solving of Eqn.2.36 and 2.37 yields,

$$N_1 = \left[\frac{N_0 I_0 \sigma \tau}{\sqrt{1 + \omega^2 \tau^2}} \right] \exp[i(\omega t - \psi)] \quad \dots \dots \quad (2.38)$$

where, $\psi = \tan^{-1}(\omega\tau)$ is the phase lag of the modulation of the excited state density compared to the optical excitation and is large when the excited state decays more slowly than the modulation rate of the light intensity.

To evaluate $H(r,t)$, we start with the inhomogeneous wave equation relating the acoustic pressure p and the heat source $H(r,t)$.

If we introduce heat $H(r,t)$ in the gas (in this case due to the absorbed light), changes in temperature (t) and pressure (p) will occur. We assume that these changes are small as compared to the static total temperature (T) and pressure (P). For such a situation, Morse and Ingard (1968) derived the inhomogeneous wave equation relating the acoustic pressure and the heat source $H(r,t)$ as [4],

$$\nabla^2 p - \frac{1}{c_0^2} \frac{\partial^2 p}{\partial t^2} = - \frac{\gamma-1}{c_0^2} \frac{\partial H}{\partial t} \quad \dots \dots \dots \quad (2.39)$$

Where c_0 is the velocity of the sound in the gas filling the cavity such that $c_0^2 = 1/\rho k_a$, where k_a is the adiabatic compressibility of the gas ($\text{msec}^{-2}/\text{kg}$) and ρ its density. γ is the specific heat ratio. In the above equation, all dissipative forces (due to heat diffusion and dynamic viscosity) have been neglected.

The origin of loss of acoustic energy can be due to the following;

1. Volume losses of thermal origin and internal viscosity of the gas
2. Surface losses due to friction of gas at the walls
3. Losses due to changes in gas behavior from adiabatic to partly isothermal close to the walls
4. Acoustic intensity escaping through the walls and openings
5. Other losses due to wave reflections brought about by the compliance of the chamber walls, by acoustic wave scattering at surface obstructions and deviations (gas inlets, microphone chamber etc in the cavity geometry from the normalized resonant mode shape).
6. Dissipation at the microphone diaphragm.

The reflection losses are a function of density and wave speed of the gas and the reflecting walls and can be easily determined. By selecting appropriately rigid materials for the cell, these losses can be kept at a minimum. [5]. All the dissipative terms due to the heat diffusion and dynamic viscosity have been neglected since the loss from these effects are negligible (for example, a reduction of the acoustic intensity of a factor of 3 over a distance of 10kms). In general, the thermal expansion of the gas is adiabatic, however, near the walls of the

cavity, it changes into isothermal expansion. The temperature variation changes exponentially from adiabatic propagation in the gas to zero at the walls; thus inducing thermal losses. Outside a thin boundary layer of thickness d_h near the wall, these thermal losses can be neglected [4]. The energy losses/unit area are,

$$L_h = \frac{(\gamma-1)\omega}{2\rho c_o^2} d_h |p|^2 \quad \dots \dots \dots (2.40)$$

$$\text{with } d_h = \left(\frac{2k_h}{\rho \omega c_p} \right)^{1/2} \quad \dots \dots \dots (2.41)$$

Here, k_h is the heat conductivity of the gas (J/m sec K), $\omega = 2\pi f$ of the acoustic response (1/sec) and p the pressure variation (N/m²). For viscosity, the gas velocity drops to zero at the cell walls and mainly causes losses in a viscous boundary layer with a width d_v

$$L_v = 1/2 \rho \omega d_v |u|^2 \quad \dots \dots \dots (2.42)$$

$$\text{with } d_v = \sqrt{\frac{2\eta}{\omega \rho}} \quad \dots \dots \dots (2.43)$$

Where η is the viscosity of the gas (Nsec/m²) and u the macroscopic motion of the gas (m/sec). The terms d_h and d_v are called 'skin depths' [1]. At atmospheric pressures, both these boundaries are very small. Except for tubes of capillary diameter and gases with exceptionally high viscosity or heat conductivity. The Eqn.2.39 yields a good approximation under these conditions.

The thermodynamic relationships between the pressure p and other variables can be described as [6],

$$\text{Temperature } T \approx (\gamma-1) \frac{k_a p}{\beta} \quad \dots \dots \dots (2.44)$$

Where, β is the thermal volume expansion coefficient at constant pressure and k_a is the adiabatic compressibility.

$$\text{Velocity } \bar{u} \approx \frac{\bar{\nabla}p}{i\omega\rho} \quad \dots \dots \dots (2.45)$$

$$\text{Mass density } \rho \approx \frac{p}{c_0^2} \quad \dots \dots \dots (2.46)$$

The physical nature of the two losses (L_v and L_h) described here can be understood by the boundary effects imposed by the walls. Since the thermal conductivity of the walls is greater than that of the gas, the gas near the walls is kept at constant temperature and thus the expansion and contraction associated with the acoustic wave occur under isothermal conditions. On the other hand, the expansion and contraction of the gas far from the walls is nearly adiabatic. The acoustic loss from heat conduction occurs in the region where the gas behavior is partly adiabatic and partly isothermal. Similarly at the wall surfaces, the tangential component of the acoustic velocity is zero because of the viscosity, and while far from the wall it is proportional to the gradient of the acoustic pressure. Visco-elastic losses occur in the region where the tangential velocity approaches zero. The total surface loss L_s can be described as,

$$L_{sj} = |A_j|^2 \int \left(0.5R_v |v_{tj}|^2 + 0.5R_h |p_j|^2 \right) dS \quad \dots \dots \dots (2.47)$$

Where v_t is the tangential velocity far from the wall

$$R_v = \sqrt{0.5\eta\omega\rho} \quad \dots\dots(2.48)$$

and,

$$R_h = \frac{\gamma-1}{\rho c_0^2} \left[\frac{k_s \omega}{2\rho C_v} \right]^{1/2} \quad \dots\dots(2.49)$$

The volume loss is simply due to the energy transferred from the acoustic wave to the thermal energy through heat conduction and through the viscosity which acts as a frictional force thus,

$$L_{vj} = |A|^2 \left[\frac{\omega_j}{\rho c_0^2} \right]^2 \left[(\gamma-1) \frac{k_s}{2C_p} + 2/3 \eta \right] V_0 \quad \dots\dots(2.50)$$

The acoustic energy stored in a mode j is given by,

$$E_j = \frac{V_0 |A_j|^2}{\rho c_0^2} \quad \dots\dots(2.51)$$

The quality factor Q of the mode is then,

$$Q_j = \omega_j \frac{\text{energy stored in the mode}}{\text{rate of energy loss for the mode } j}$$

Thus,

$$Q_j = \omega_j \frac{E_j}{L_{sj} + L_{vj}} \quad \dots\dots(2.52)$$

Neglecting the acoustic dissipation forces, the Eqn.2.39 can be solved by expressing the Fourier transform of p in terms of the

"normal acoustic mode" p_{ij} which satisfies the appropriate boundary conditions. Then, the acoustic pressure in the cell is simply the sum over all the normal modes ie,

$$p(r, \omega) = \sum_j A_j(\omega) p_j(r) \quad \dots \dots \dots (2.53)$$

with p_j being the solution of the homogeneous wave equation ie,

$$\left[\nabla^2 + \frac{\omega_j^2}{c_0^2} \right] p_j(r) = 0 \quad \dots \dots \dots (2.54)$$

p_j must be chosen to satisfy the boundary condition that the gradient p normal to the cell wall vanish at the wall, since the acoustic velocity is proportional to the gradient of p and must vanish at the wall. To calculate the amplitude of the induced acoustic signal, it is convenient to decompose the signal into a linear combination of orthogonal modes p_j each of which corresponds to a normal acoustic mode of the PA cavity. These ortho-normal modes in the cylindrical geometry are represented by Morse and Ingard (1968) as [4],

$$p_j(r, \phi, z, t) = g_j \cos(m\phi) \cos\left(\frac{k\pi z}{L}\right) J_m \left(\frac{\alpha_{mn} \pi r}{R_0} \right) \exp(-i\omega_j t) \quad \dots \dots \dots (2.55)$$

with a corresponding frequency ω_j given by,

$$\omega_j = \frac{\pi c_0}{2} \left\{ \left(\frac{k}{L} \right)^2 + \left(\frac{\alpha_{mn}}{R_0} \right)^2 \right\}^{1/2} \quad \dots \dots \dots (2.56)$$

Here, g_j is a normalization constant, L the cavity length, c_0 the velocity of sound in the gas filling the cavity, R_0 is the radius

of the cell. (r, ϕ, z) are the cylindrical co-ordinates of the spatial point, k, m, n are the longitudinal, azimuthal and radial mode numbers respectively. J_m is the Bessel function, α_{mn} the n^{th} zero solution of the equation,

$$\frac{dJ_m}{dr} = 0 \quad \text{at } r = R_o \quad \dots \dots \quad (2.57)$$

From the above discussions, the conditions of vanishing pressure gradient at the cell wall requires that the acoustic pressure $p(r, \omega)$ be expressed as the linear combination of eigen modes p_j for a cylindrical geometry. For a specific case of excitation beam being along the axis of the cylindrical PA cell, and in weak absorption limit, only the radial normal modes can be excited by $H(r, \omega)$, the heat source ie, we need to consider only the radial normal modes

$$p_j(r) = g_j J_0 \left(\frac{\pi \alpha_{0j} r}{R_o} \right) \quad \dots \dots \quad (2.58)$$

With the eigen function ω_j being,

$$\omega_j = \frac{\pi c \alpha_{0j}}{R_o} \quad \dots \dots \quad (2.59)$$

Having delineated the expansion basis p_j , we solve for the expansion coefficient $A_j(\omega)$. Taking the Fourier transform of Eqn.2.39,

$$\left[\nabla^2 + \frac{\omega^2}{c_o^2} \right] p(r, \omega) = \left[\frac{(\gamma-1)}{c_o^2} \right] i\omega H(r, \omega) \quad \dots \dots \quad (2.60)$$

Substituting Eqn.2.53 into 2.60 and using the orthonormal condition for the eigen function p_j we may solve for $A_j(\omega)$ as,

$$A_j(\omega) = \frac{-i\omega \left(\frac{(\gamma-1)}{V_0} \right) \int_V p_j^* H(r) dV}{\omega_j^2 \left\{ 1 - \left(\frac{\omega}{\omega_j} \right)^2 - \left(\frac{i\omega}{\omega_j Q_j} \right) \right\}} \quad \dots \dots \quad (2.61)$$

Where, V_0 is the volume of the cell, Q_j is the Q-factor for the acoustic mode p_j as described by Eqn.2.52. p_j^* is the complex conjugate of p_j and is integrated over the volume of the cell. The overlap between the spatial structure of the acoustic mode and the laser beam profile is described quantitatively by the above integral. For example, this integral is zero for azimuthal modes in a cylinder with the laser beam aligned co-axial to the cylinder axis. Longitudinal modes are only weakly excited in the case of homogeneous absorption of the laser irradiation along the cylinder axis because the positive and negative contributions to the integral essentially cancel out. To achieve strong excitation of the longitudinal modes, asymmetric excitation is needed. Thus the radial mode excitation is ideal for co-axial propagation of the laser radiation through the cell. Similar mode amplitude calculations have been given by Rosengren [7,8] and by Kamm [5]. The frequency dependence of $A_j(\omega)$ contains two resonance parameters namely the resonance bandwidth and the resonance frequency which ultimately determines the Q factor of the cell ie,

$$Q = \frac{\omega_0}{\Delta\omega} \quad \dots \dots \quad (2.62)$$

where, ω_0 is the resonance frequency and $\Delta\omega$ the resonance bandwidth which can be obtained from the cell resonance studies.

Also, the Q factor for a practical cell can be calculated as, [6]

$$Q = \frac{2S}{2\pi R_0 \left(d_v + (\gamma-1)d_h \right)} \quad \dots \dots \quad (2.63)$$

where, S is the cross-section of the resonator tube. The physical quantity measured is the absolute magnitude of the complex pressure function at the microphone position. The complex character of the amplitude which is caused by the phase shift with respect to the source function, is important if the neighbouring modes are not well separated and interferences occur [9]. In cylindrical resonators, the spacing between the excited radial and longitudinal modes is relatively large and thus can be optimized by choosing an appropriate ratio between the radius and length of the cavity. The interference effects need to be taken into account only at low pressures or if very strong relaxation losses are present that considerably broaden the resonance profiles.

The term Q has been included to account for the mode damping and to avoid the physically unreasonable situation of $A_j \rightarrow \infty$ as $\omega \rightarrow \infty$. The Eqn.2.61. can be further simplified for the case of H being given by Eqn.2.35, with I being given by Eqn.2.37. We get,

$$H(r, \omega) = N_0 \sigma A_n E' I_o(r) = \varphi I_o(r) \quad \dots \dots \quad (2.64)$$

Where the coefficient φ contains both the space and time independent coefficients of $I_o(r)$. Assuming the light beam to be Gaussian,

$$I_o(r) = \left(\frac{I_o}{\pi a^2} \right) \exp \left(\frac{-r^2}{a^2} \right) \quad \dots \dots \quad (2.65)$$

(a = beam radius) and that the beam propagates only along the axis of the cell so that only eigen modes of the form of Eqn.7.58. are needed to be considered. These assumptions satisfy most actual cases of PA generation. The amplitude of the lowest order radial pressure mode ($j=1$) will be of the form,

$$A_1(\omega) = \frac{-i\omega(\gamma-1)g_1qI_0L \exp(-\mu_1)}{\omega_1^2 \left\{ 1 - \left[\frac{\omega}{\omega_1} \right]^2 - \left[\frac{i\omega}{\omega_1 Q_1} \right] \right\} V_0} \quad \dots \dots \dots (2.66)$$

where, $\mu_1 = \frac{a^2}{(2\pi\alpha_{01}R_0)^2}$ $\dots \dots \dots (2.67)$

and $\exp(-\mu_1) = \frac{1}{V_0} \int J_0 \frac{\pi\alpha_{01}r}{R_0} \exp\left(-\frac{r^2}{a^2}\right) dV \quad \dots \dots \dots (2.68)$

g_1 = normalization factor for $p_1 = \left[J_0(\pi\alpha_{01}) \right]^{-1}$ $\dots \dots \dots (2.69)$

Close to acoustic resonance, $\omega = \omega_1(1+\Delta)$ and Δ being small,

$$A_1(\omega) = \frac{Q_1(\gamma-1)g_1qI_0L \exp(-\mu_1)}{\omega_1(1-2iQ_1\Delta)V_0} \quad \dots \dots \dots (2.70)$$

This is the basic physics of the operation of a resonant PA cell. The resonance enhancement of the amplitude of the radial pressure ($j=1$) is obtained when the fractional detuning from the resonance δ is $< (2Q_1^{-1})$. Larger acoustic amplitude is obtained for larger γ , larger light power absorbed qI_0L , smaller beam radius (a) and smaller cell volume V_0 .

The above equation is for cases near the resonance of the lowest radial mode. For an opposite case of wide off-resonance (non-resonant mode), the modulation frequency being less than the

lowest order radial resonance frequency ($\omega \ll \omega_1$),

$$A_j(\omega) \simeq -\frac{i\omega(\gamma-1)}{\omega_j^2 V_0} \int p_j^* H(r) dV \quad \dots \dots \dots (2.71)$$

In such a non-resonant mode, the acoustic signal lags behind the modulation by $\pi/2$. The signal dependence is same as that at resonance.

If we assume that the optical beam suffers only a small attenuation traversing the cavity, then, $H(r,t) = \alpha I_0(r,\omega)$ where α is the absorption coefficient (cm^{-1}) and $I_0(r,\omega)$ represents the optical beam intensity ($\text{ergs/cm}^2/\text{sec}$). Then,

$$A_j(\omega) = \frac{-i\alpha\omega \left(\frac{(\gamma-1)}{V_0} \right) \int p_j^* I_0(r,\omega) dV}{\omega_j^2 \left\{ 1 - \left(\frac{\omega}{\omega_j} \right)^2 - \left(\frac{i\omega}{\omega_j Q_j} \right) \right\}} \quad \dots \dots \dots (2.72)$$

If I_0 is spatially constant, ie, $I_0(r,\omega) = I(\omega)$, then,

$$\int p_j^* I_0(r,\omega) dV = 0 \text{ for } j \neq 0 \quad \dots \dots \dots (2.73)$$

The only non zero mode is p_0 with a resonant frequency $\omega_0 = 0$. This is thus a spatially independent pressure change in the cell ie, independent of r . Then,

$$A_0(\omega) = \frac{i\alpha(\gamma-1)I_0}{\omega \left(1 - \frac{i}{\omega \tau_0} \right)} \quad \dots \dots \dots (2.74)$$

where, τ_o = damping time of p_o resulting from heat conduction from the gas to the cell walls. And,

$$A_1(\omega) = \frac{-i\omega\alpha(\gamma-1)I_o}{\omega_1^2 \left\{ 1 - \left(\frac{\omega}{\omega_1} \right)^2 - \left(\frac{i\omega}{\omega_1 Q_1} \right) \right\}} \quad \dots \dots \dots (2.75)$$

If we put beam power as W (watts/cm²) then $I_o = \frac{WL}{V_o}$ and correspondingly we get,

$$A_o(\omega) = \frac{i\alpha(\gamma-1)WL}{\omega \left(1 - \frac{i}{\omega\tau_o} \right) V_o} \quad \dots \dots \dots (2.76)$$

and,

$$A_1(\omega) = \frac{-i\omega\alpha(\gamma-1)WL}{\omega_1^2 \left\{ 1 - \left(\frac{\omega}{\omega_1} \right)^2 - \left(\frac{i\omega}{\omega_1 Q_1} \right) \right\} V_o} \quad \dots \dots \dots (2.77)$$

Comparing the Eqns. 2.76 & 2.77,

$$\frac{A_1(\omega_1)}{A_o(0)} = \frac{Q_1}{\omega_1 \tau_o} \quad \dots \dots \dots (2.78)$$

At low frequencies, $A_o(\omega) > A_1(\omega_1)$, and at higher frequencies, $A_o(\omega) \propto 1/\omega$ while $A_1(\omega)$ is maximum at $\omega = \omega_1$. Also, $A_1(\omega_1) \propto 1/\omega_1$ and since the first radial resonance frequency $\omega_1 \propto 1/R_o$, it is apparent that small diameter cells have higher ω_1 and thus a lower $A_1(\omega_1)$ and should be used in the non-resonant mode ie,

$A_o(\omega)$. Also, since at low frequencies, $A_o(\omega) \cong \tau_o \alpha(\gamma-1) \frac{WL}{V_o}$, and is relatively independent of the frequency ω . Thus at low modulation frequency operations of the PA cell, non-resonant mode of operation is preferred.

For pulsed PA studies, the net heat released up to a time t can be written from Eqns.34 & 35 as,

$$H(t)_{\text{pul}} = GA_n \tau E' \left[1 - \exp(-t/\tau) \right] \quad \dots \dots (2.79)$$

where the incident light is assumed to be of infinitesimal time duration occurring at $t = 0$ and with the total number of photons absorbed being G and neglecting the heat diffusion. Here, $H(t)_{\text{pul}}$ has the unit of energy whereas $H(r,t)$ has the unit of unit energy/unit time. The pressure increase $p(t)$ of the irradiated gas column of volume V_o in the cavity can be estimated from Eqn.2.27 by using gas laws.

$$p(t) = \frac{H(t)_{\text{pul}} R}{MC_v V_o} \quad \dots \dots (2.80)$$

where,

R = universal gas constant

M = molecular gas weight

C_v = specific heat/unit mass of the gas at constant volume

The variation of the PA signals with the corresponding modulated/pulsed optical radiation [7] is shown in fig.2.3(a&b). The time dependence of $p(t)$ for pulsed PA signal is shown in the fig.2.3.(b) for a short optical pulse and long thermal diffusion time τ_D so that,

$$\tau_D \approx a^2/D \quad \dots \dots (2.81)$$

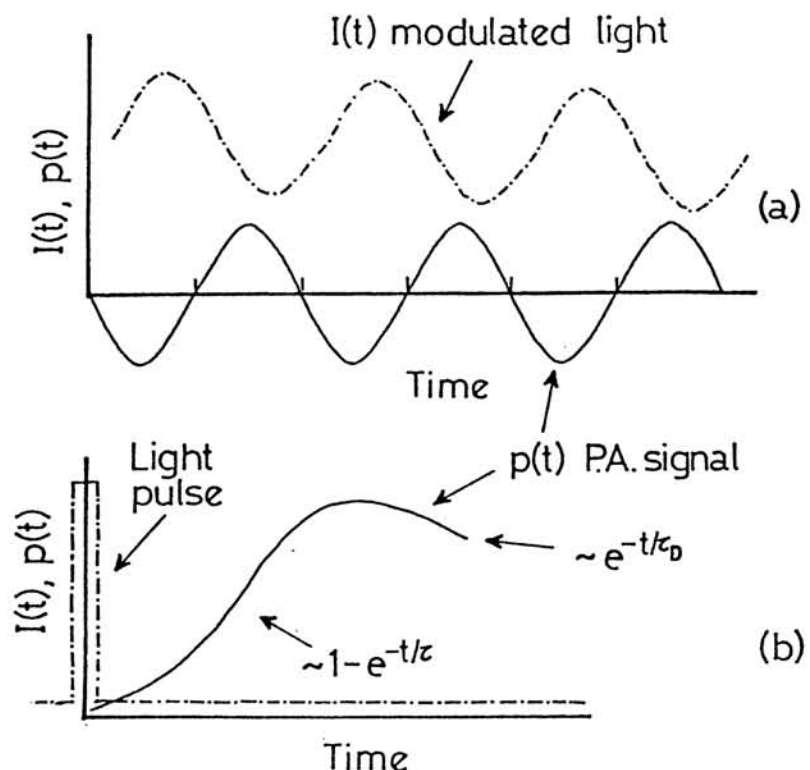
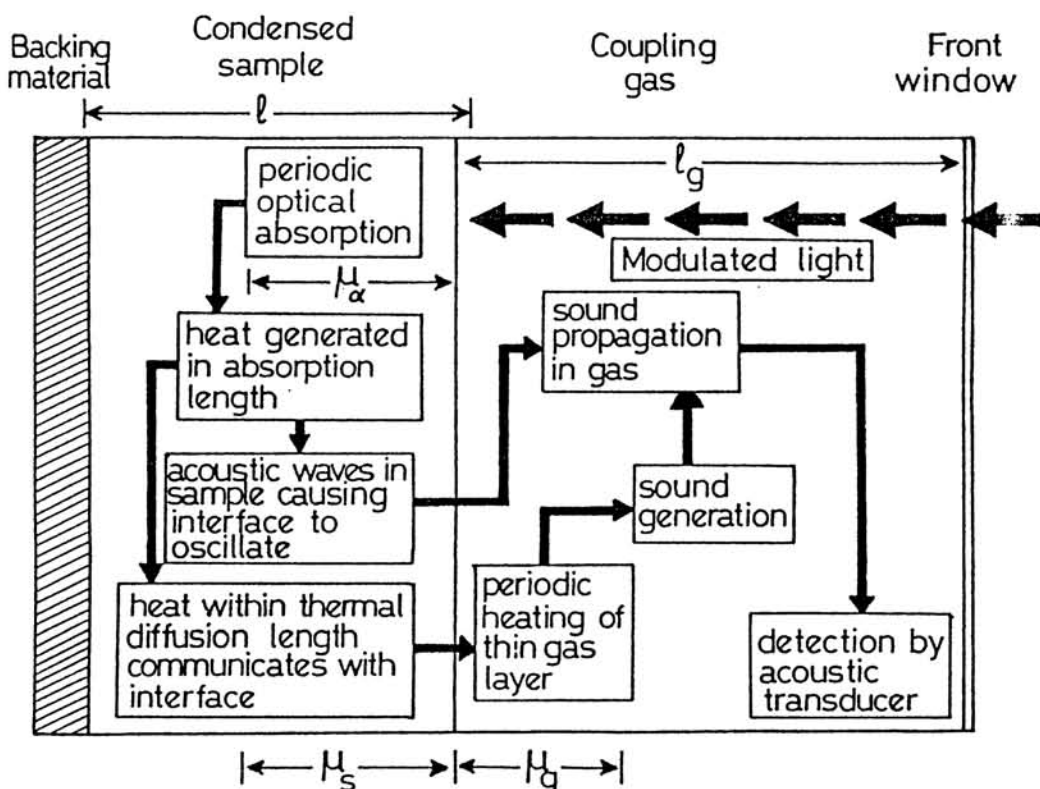


fig.2.3. The PA signals and their corresponding input radiation for (a) cw (b) pulsed detection [7]



2.4. The schematic diagram of the PA signal generation process in condensed matter (from R-G theory) [1,3]

such that, $D = k_t / C_v$ k_t = thermal conductivity
Where a is the beam radius and D thermal diffusivity of the gas.
The initial rise in the pulsed PA signal depends on the lifetime τ
of the excited state involved and the slow decrease of $p(t)$ back
to zero depends on the thermal decay time constant τ_D . The cell
radius determines the thermal time constant of the pressure signal
such that, [10]

$$\tau_D = R_o^2 / 5.76 k_t \quad \dots \dots \dots \quad (2.82)$$

The cell radius must match the beam closely enough to prevent convection currents in the cavity. If they are permitted to start, there would be a discontinuous non-linear rate of transfer of heat to the tube walls which would diminish the signal strength.

2.3. Other Models For PA Signal Generation

Various other models for PA signal generation in condensed and gaseous media have been proposed, depending on the kinds of results obtained by the workers. A few of these models are discussed briefly below. Rosencwaig and Gersho proposed what is now known as the R-G theory for the generation of PA signals in condensed matter. The electrical transmission line analog is another model proposed for PA signal generation in gaseous media.

2.3.1. Rosencwaig-Gersho (R-G) Theory For Gas-microphone Generation Of PA Signals In Condensed Matter

The R-G theory is based on the model of a thermal or acoustic piston. The sample, placed on a backing material is located in a closed cavity containing a non-absorbing gas and the acoustic

transducer. The heat generated due to non-radiative de-excitation in the sample on irradiation of modulated optical radiation is transferred to a thin layer of the gas medium near to the surface of the sample. It is this length of gas that plays an important role in the PA detection. Due to the modulated heat that is generated, this thin layer of gas is compressed and expanded alternatively and thus it acts as an acoustic piston acting on the rest of the gas in the cell. The schematic representation of the PA signal generation process in condensed media is given in fig.2.4. and the various possible detection cases by gas coupling method as a result of this theory is shown in Table 2.1. The ordered brackets (a,b,c) in the table indicates $a > b > c$ with a, b and c being the three lengths μ_s μ_α and l [1,2,11].

In the equations represented in the table, γ is the ratio of specific heats of the coupling gas, P_o and T_o the ambient pressure and temperature of the gas, I_o the amplitude of the incident optical radiation, l_g the thickness of the coupling gas, and l that of the sample, μ with suffixes g , s , and b are the thermal diffusion lengths for the gas, sample and the backing material respectively and k with the same suffixes the thermal conductivities. Optically thin (thick) implies that $\mu_\alpha >$ (or $<$) l and thermally thin (thick) implies that $\mu_s >$ (or $<$) l . Some of the important points of results from this theory are,

1. There is always a phase lag between the sinusoidal PA signal and the modulation. If μ_s is less than μ_α and l , the phase lag is approximately 90° otherwise it is $\sim 45^\circ$.
2. The PA signal is proportional to the absorption coefficient α_a of the sample for all optically thin cases (cases 1-3) and for case 6. It is only these four cases that can be used for spectroscopy. In other cases, PA saturation occurs.

Table 2.1. Possible PA signal generation cases and their respective expressions in the R-G theory of PA effect in condensed matter [1,3]

No.	Condition	Case	Approximate expression for the PA signal
1	(μ_s, μ_α, I)	Thermally thin, Optically thin	$(1-i)\alpha_a I \left(\frac{\mu_b}{k_b} \right) F$
2	(μ_α, μ_s, I)	Optically thin, Thermally thin	$(1-i)\alpha_a I \left(\frac{\mu_b}{k_b} \right) F$
3	(μ_α, I, μ_s)	Optically thin, Thermally thick	$-i\alpha_a \mu_s \left(\frac{\mu_s}{k_s} \right) F$
4	(μ_s, I, μ_α)	Thermally thin, Optically thick	$(1-i) \left(\frac{\mu_b}{k_b} \right) F$
5	(I, μ_s, μ_α)	Optically thick, Thermally thick	$(1-i) \left(\frac{\mu_s}{k_s} \right) F$
6	(I, μ_α, μ_s)	Thermally thick, Optically thick	$-i\alpha_a \mu_s \left(\frac{\mu_s}{k_s} \right) F$

Where, $F = \frac{\gamma P_o I_o \mu_g}{2\sqrt{2} I_g T_o}$

3. Case 5 is best suited for the study of thermo-elastic properties and depth profiling since the PA signal is higher and independent of the backing material. The PA signal in cases 3 and 6 is less than that in 5 and the PA signal is dependent on the backing material in all other cases.

2.3.2. Thermal-Piston Model For PA Generation In Gases

The Thermal piston model for PA effect deals with sound generation in optically thick gas samples. At high concentrations of an absorbing gas, the optical absorption length for the incident radiation can become small compared to the thermal diffusion length of the gas. A description of the PA effect consequently must include the thermal conduction of heat to the cell window since the sound generation takes place in a thin layer of gas adjacent to the entrance window. The remainder of the gas in the cell undergoes passive adiabatic compression and expansion. The thin periodically heated gas layer acts as a piston driving the remainder of the gas. [12]. It was seen that the dependence of amplitude and phase of the acoustic signal as the mole fraction of the sample gas and the modulation frequency were found to be different from those derived for optically thin gas [2,3,12,13] from the solutions of inhomogeneous wave equation for pressure with a thermal source term arising from absorption of radiation [4]. The acoustic signal was found to be,

$$P = \frac{\gamma P_0 I_0 \mu}{\sqrt{2} T_0 \alpha_a L k} \left(1 - \frac{1}{\alpha_a \mu} \right) \exp \left\{ i \left[\omega t - \pi/4 - \frac{1}{\alpha_a \mu} \right] \right\} \dots \dots \quad (2.83)$$

for $\alpha_a \mu \gg 1$ for a thermally thick gas. This is valid for cases

where the thermal diffusion length is much greater than the optical absorption length. Here,

$\mu = \left(\frac{2\alpha}{\omega} \right)^{1/2}$ is the thermal diffusion length, α the thermal diffusivity, k the thermal conductivity, ω the modulation frequency, β the absorption coefficient, γ the ratio of specific heats, I_0 the intensity of radiation and P_0 the ambient gas pressure.

Several unusual dependencies exhibited by this solution in the limit $\alpha_a \mu \gg 1$ were observed, that were peculiar to a highly absorbing gas [12].

1. The signal decreases as α_a^{-1} with increase in the absorption coefficient. This is qualitatively different from the amplitude dependence for an optically thin gas where the signal increases with α_a .
2. The frequency dependence of the signal amplitude (which is contained in μ) decreases as $\omega^{-1/2}$ instead of ω^{-1} as obtained by the solution of the wave equation.
3. The phase lag in the acoustic signal relative to the modulation is $\pi/4$ as compared to $\pi/2$ in the case of optically thin gas obtained from wave equation (the modulation frequency is much less than that compared to the reciprocal of vibration relaxation time).
4. The PA signal has a weak γ dependence and a χ^{-1} dependence as predicted by Eqn.2.83 since $\alpha_a \propto c_g \chi$ where, χ is the mole fraction and c_g the concentration of the gas.

This model becomes invalid as $\alpha_a \mu \approx 1$

2.3.3. Acoustic Transmission Line Theory

If an acoustic wave is transmitted through a tube, we can express the acoustic behavior using the one-dimensional electrical transmission line analog. The basis of the theory [4,14] was applied to this field by Kritchman *et al*, [15] Nordhaus [16] and was further extended by Bernegger [17] with matrix formalism which permits a quantitative description of the PA signal at any position in the cell and at any arbitrary frequency. The requirement of this theory is that the acoustical wavelength should be long compared to the cross dimensions of the cavity so that only the motion of the gas parallel to the tube axis is considered [6].

Within the transmission line description, volumes, constrictions, openings, and cross dimensional variations can be expressed as discreet circuit elements such a impedance R, admittance G, capacitance C and inductance L [18].

<u>Electrical quantity</u>	<u>Acoustic quantity</u>
Electromotive force (V)	Acoustic pressure (p)
Charge (Q)	Volume displacement (X)
Current ($I=dQ/dt$)	Volume velocity (dX/dt)
Resistance (R)	Acoustic resistance (R_a)
Capacitance (C)	Acoustic capacitance (C_a)
Inductance (L)	Acoustic inductance (L_a)

The acoustic analog of the pressure in a tube element is the voltage V across the corresponding point of the filter circuit and the analog of the current I at the same position in the

circuit is the total flux of the gas $I^0 = S u$, where S is the cross sectional area and u the gas velocity. A heat source in the acoustic arrangement, such as the laser energy absorbed by the gas molecules is acoustically equivalent to an electric current of I^0 . For a laser power amplitude of W at circular modulation at a frequency ω and an absorption coefficient α_a of the gas, at a laser wavelength λ , the analog of the electric current source/unit length of the tube is [4],

$$\frac{dI^0}{dx} = \frac{(\gamma-1) W \alpha_a}{\rho c_0^2} \quad \dots \dots \dots (2.84)$$

where, $\gamma = C_p/C_v$, ρ = density of the gas and c_0 the velocity of sound in the gas. The acoustic analog of the inductance, capacitance and the resistance of a tube of cross section area S , perimeter O and length L are,

$$L_a = \frac{\rho L}{S} \quad \dots \dots \dots (2.85)$$

$$C_a = \frac{LS}{\rho c_0^2} \quad \dots \dots \dots (2.86)$$

$$R_a = \frac{\rho L O}{(2S^2) \omega \left[d_v + (\gamma-1) d_h \right]} \quad \dots \dots \dots (2.87)$$

where, d_h and d_v are the 'skin depths' [1] being the thickness of the boundary layers of the thermal and shear modes.

$$d_h = \left[\frac{2\eta}{\rho\omega} \right]^{1/2} \quad \dots \dots \dots (2.88)$$

$$\text{and } d_v = \left(\frac{2k_h}{\rho \omega C_p} \right)^{1/2} \quad \dots \dots \dots (2.89)$$

Where, η is the viscosity and k_h the heat conductivity. The acoustic resistance is proportional to $\omega^{1/2}$ and not frequency independent as in the case of electrical resistance. It must be noted that the above two equations are valid only if d_v and d_h are much less than the cross sectional dimensions of the tube. This condition yields a lower frequency limit, while the upper limit is reached when the wavelength of the sound becomes comparable to the cross sectional dimensions of the tube. If the sound source is well located, then the discrete analog impedances are well suited for calculating the acoustic behavior of transmission lines [4,15,16]. If a tube is divided into two parts, it can be considered as a Helmholtz resonator as seen in fig.2.5. The following parameters of the resonators are obtained,

$$V = \frac{1}{i\omega C_a} \frac{\omega_0^2 - 2\omega^2 + 2i\omega_0\omega/Q}{\omega_0^2 - \omega^2 + i\omega_0\omega/Q} I^0 \quad \dots \dots \dots (2.90)$$

$$\omega_0 = 2 \left[L_a C_a \right]^{-1/2} = \frac{2C_0}{L} \quad \dots \dots \dots (2.91)$$

$$Q = \frac{\omega_0 L_a}{R_a} = \frac{2S}{D \left[d_v + (\gamma-1) d_h \right]} \quad \dots \dots \dots (2.92)$$

From Eqns.2.84, 2.86 and 2.90, the cell constant F can be evaluated as, $F = \frac{P}{\alpha W}$ which relates the pressure amplitude p with the absorbed laser power. For a PA cell operating in the resonance mode, having a volume V_0 and length L , having a resonance frequency ω_0 and a quality factor Q then the cell constant ;

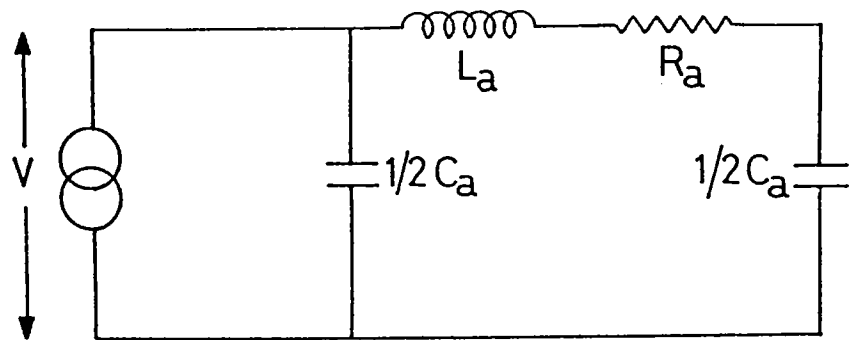


Fig.2.5. The electrical transmission analog of an Helmholtz resonator

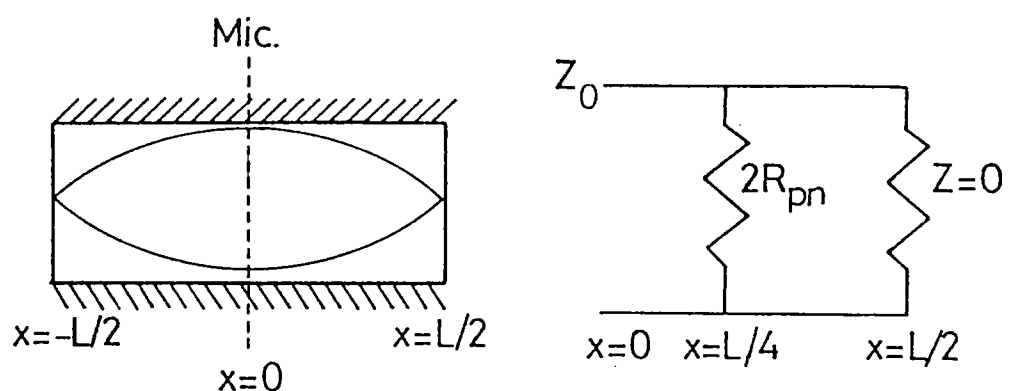


Fig.2.6. The longitudinal resonance mode of the pressure response in an open cylindrical resonator and the corresponding transmission line analog.

$$F(\omega_0) = (\gamma - 1) \frac{L Q G}{i \omega_0 V_0} \quad \dots \dots \dots (2.93)$$

Here G is a geometrical factor of the order 1. A qualitative behavior for ω_0 and Q can also be obtained. The tube length L has to be a multiple of half the wavelength of the acoustic resonance mode. The Q is given by the ratio of the energy stored in a mode to the energy dissipated in that mode in unit time [15,19,20]. These losses are proportional to the cell surface A and to the thickness $d_v \approx d_h \approx d$ of the boundary layers while the total energy is proportional to the cell volume. So for a cylindrical PA cell of radius R_0 and length $L \gg R_0$ operating in the longitudinal resonance mode,

$$\omega_0 \propto L^{-1} \quad \dots \dots \dots (2.94)$$

$$Q(\omega_0) \propto \frac{V_0}{Ad} \propto \frac{R_0 L^{1/2}}{(R_0 + L)} \cong \frac{R_0}{L^{1/2}} \quad \dots \dots \dots (2.95)$$

$$F(\omega_0) \propto \frac{L^{1/2}}{R_0} \quad \dots \dots \dots (2.96)$$

For radial resonance mode,

$$\omega_0 \propto R_0^{-1} \quad \dots \dots \dots (2.97)$$

$$Q(\omega_0) \propto \frac{V_0}{Ad} \propto \frac{L R_0^{1/2}}{(R_0 + L)} \cong R_0^{1/2} \quad \dots \dots \dots (2.98)$$

$$F(\omega_0) \propto \frac{L}{R_0^{1/2} (R_0 + L)} \cong R_0^{-1/2} \quad \dots \dots \dots (2.99)$$

The product $F(\omega_0) Q(\omega_0)$ is nearly independent of cell dimensions for any kind of PA cell. The operation of the cell in the longitudinal mode is more advantageous since it permits for optimization of the resonance frequency and the Q factor independently which is not possible for radial resonance. When the PA cell is long and the generation of the PA signal is distributed over the whole length of the cell, the discrete element analysis does not prove effective. Thus, Brenegger and Sigrist [17], in their model, considered the whole cell as many infinitesimal elements of length ΔL within the length of the tube. The discrete values in fig.2.5 will thus be replaced by corresponding infinitesimal values. Here, the V and I are represented as functions of position x within the tube. By applying appropriate boundary conditions and by using matrix formulation, the total pressure amplitude $p(x)$ at any location x within the tube can be separated into a term independent of x caused by the heating of the gas and into two damped waves propagating in the positive and negative x directions, the coefficients of the obtained equations permit the calculation of the pressure amplitude anywhere in the tube.

The longitudinal resonant mode and the corresponding transmission line analog of then open resonator is given in fig.2.6. The line is short circuited at $x = L/2$ since the pressure node (maximum gas velocity) is obtained there. Out of the heat flow power $W_{heat} = K\Delta T$ to the external walls and the membrane, only $W_{heat} \Delta T/T$ is available as the mechanical power. Using the gas equation to get ΔP from ΔT , the mechanical relation, $W_{mech} = \Delta P^2/R_{pn}$, which is the pneumatic analog of the electrical relation $W_{elect} = V^2/R$, (V is the voltage applied to the resistance R) is derived [15]. Since $K_t = k_h A/d_h$, It can be seen that due to the power dissipation induced by the total heat conductivity K_t of the enclosed gas limited at one end by an ideal

membrane kept at constant temperature, the membrane feels a pneumatic impedance,

$$R_{pn} = \frac{P^2}{K_t T} \quad \dots \dots \dots (2.100)$$

Where, P is the total pressure in the cell. The dominating thermal and viscous losses are distributed along the whole tube. The transmission line is loaded at a single point $x = L/4$ with the pneumatic impedance R_{pn} to account for the thermal losses. Since the thermal losses at the walls is equal to the viscous losses upon the walls and both dominate other losses, we can assume that the total dissipative impedance Z_l loading the transmission line is twice R_{pn} or,

$$Z_l = \frac{2 P^2 d_h}{k_h A T} \quad \dots \dots \dots (2.101)$$

This loading impedance is located at a particular point of the transmission line, depending on the specific type of resonance being considered.

2.4 Conclusions

The general theory of PA signal generation in gases is discussed in detail. The process of optical absorption followed by non-radiative relaxation and the evolution of the acoustic wave are discussed. The loss factors encountered in PA signal generation and the PA saturation effect are also discussed. A few other theories of PA signal generation are also briefly mentioned.

2.5. References

- [1] Rosencwaig A, "Photoacoustics and Photoacoustic Spectroscopy" (Wiley, New York), 1980
- [2] Kreuzer L B, "Optoacoustic Spectroscopy and Detection" Editor Y H Pao, (Academic Press, New York, 1977), chapt.1.
- [3] Tam A C, "Ultrasensitive spectroscopy" Ed. Kilger D S, (Academic Press, New York), 1983, Chapter 1
- [4] Morse P M and Ingard K V, "Theoretical Acoustics" (McGraw-Hill, New York, 1968)
- [5] Kamm R D, *J.Appl.Phys.*, 47, 3550, (1976)
- [6] Harren F J M, PhD thesis "The Photoacoustic Effect, Refined and Applied to Biological Problems", Katholieke University of Nijmegen, The Netherlands, 1988
- [7] Rosengren L G, *Appl.Opt.*, 14, 1960, (1975)
- [8] Rosengren L G, *IR Phys.*, 13, 1009, (1973)
- [9] Hess P, "Topics in Current Physics : Photoacoustic, Photothermal and Photochemical Processes in Gases", Editor Hess P (Springer, Heidelberg 1989), p 85, 106
- [10] Kerr E L and Atwood J G, *Appl.Opt.*, 7, 915, (1968)
- [11] Rosencwaig A and Gersho A, *J.Appl.Phys.*, 47, 64, (1976)
- [12] Stewart R B and Diebold G J, *Appl.Phys.Lett.*, 50, 13, (1987)
- [13] Karbach A and Hess P, *J.Chem.Phys.*, 84, 2945, (1986)
- [14] Morse P M, "Vibration and Sound", (McGraw-Hill, New York, 1948)
- [15] Kritchman E et al, *J.Opt.Soc.Am.*, 68, 1257, (1978)
- [16] Nordhaus O and Pelzl J, *Appl.Phys.*, 25, 221, (1981)
- [17] Bernegger S and Sigrist M W, *Appl.Phys.B.*, 44, 125, (1987)
- [18] Bechthold P S, "Photoacoustic Effect" Ed. E Luscher et al, (Friedr. Vieweg & Sohn, Wiesbaden), 1984, p.400
- [19] Johnson R H, et al, *Appl.Opt.*, 21, 81, (1982)
- [20] Karbach A and Hess P, *J.Chem.Phys.*, 83, 1075, (1985)

2.6. Symbols And Notations

A	Surface area of the PA cell
A_r	Radiative decay of excited state
A_n	Non-radiative decay of excited state
A_{ij}	Einstein coefficient for spontaneous emission from i to j
A_j	Amplitude of the j^{th} acoustic mode
a	Beam radius
α_a	Absorption coefficient of the gas
α	Thermal diffusivity
α_{mn}	Solution of the n^{th} zero solution of the m^{th} Bessel fn.
β	Thermal expansion coefficient at constant pressure
B_{ij}	Einstein coefficient for stimulated emission from i to j
c	Velocity of light
c_0	Velocity of sound in the gas filling the cavity
C_p	Specific heat of the gas at constant pressure
C_v	Specific heat of the gas at constant volume
C_{ij}	Non-radiative transition from level i to j
C_v	Specific heat at constant volume of the gas
C_a	Acoustic capacitance
ΔE	Energy difference between ground and excited states
D	Thermal diffusivity of the gas
d_h, d_v	Gas thermal diffusion length, viscous boundary layer
γ	Ratio of specific heats
δ	Modulation depth
E_1, E_0	Energies of excited and ground states
E'	Average thermal energy due to non-radiative relaxation
g_1	Normalization factor for the acoustic pressure
G	Total number of photons being absorbed
$H(r, t)$	Heat production rate
$H(t)_{\text{pul}}$	Heat released up to a time t in pulsed PA
I, I_0	Intensity of incident light

Current
 m^{th} Bessel function
Boltzmann constant
Total heat conductivity
Kinetic energy
Thermal conductivity
Longitudinal, azimuthal and radial mode numbers
Adiabatic compressibility of the gas
Heat conductivity of the gas
 k Thermal conductivities of gas, sample and backing material
 l_b Lengths of the coupling gas, sample and backing material
Length of the cavity
Total surface loss
Energy loss/unit area
Viscous boundary loss
Acoustic inductance
Molecular gas weight
Thermal diffusion length
 μ_b Thermal diffusion lengths for gas, sample and backing
Optical absorption length
Viscosity of the gas
Total number of molecules/cc
Number of molecules in ground and excited state
Perimeter of the resonator
Pressure, acoustic signal
Ambient gas pressure
Acoustic pressure in the cell
Solution of the homogeneous wave equation
Quality factor of the j^{th} acoustic mode
PA signal
Cylindrical coordinates of the spatial point
Radiative transition from level i to j

Spatial point
Excitation rate
Universal gas constant
Acoustic resistance
Radius of the resonator tube
Pneumatic impedance
Radiation density
density of gas
Cross section of the resonator tube
Absorption cross section
Phase lag
Total relaxation time
Relaxation time for radiative transition
Relaxation time for non-radiative transition
Thermal diffusion time
Thermal time constant
Damping time for the p_0 acoustic mode
time
Temperature of gas
Ambient gas temperature
Macroscopic motion of the gas
Volume of the PA cell
Tangential velocity far from the walls
Frequency of light
Modulation frequency
Resonance frequency
Resonance bandwidth
Volume of gas
Voltage
Input beam power
Volume displacement
Impedance
Total dissipative impedance

CHAPTER III

INSTRUMENTATION ASPECTS OF PHOTOACOUSTICS

ABSTRACT

THIS CHAPTER DEALS WITH THE VARIOUS ASPECTS OF THE PA INSTRUMENTATION. THE SYSTEMS AND SUB-SYSTEMS THAT GO INTO MAKING AN IDEAL PA EXPERIMENTAL SETUP ARE DISCUSSED. THE ASPECTS OF NOISE IN PA MEASUREMENTS AND THE SCALING FACTORS FOR PA CELLS ARE ALSO BRIEFLY MENTIONED.

CHAPTER III

INSTRUMENTATION ASPECTS OF PHOTOACOUSTICS

3.1. Introduction

One of the most vital aspect of experimental measurements is the instrumentation associated with the same. The accuracy and range of the data gathered critically depend on the design and selection of appropriate systems and instruments. The more adapted and optimized the instrumentation is to the particular experimental technique, the more accurate and reliable will be the data thus acquired. Depending on the technique of signal detection that is chosen, appropriate combination of instruments that detect, measure and record the varying parameters with respectable accuracy, resolution and reliability will have to be used in the experiment. It is based on the data thus gathered that the properties of the sample under study are to be analyzed. Though in most cases of optical spectroscopy, the basic components involved are the light source, detector and the electronics, care must be taken, specially while detecting low level signals, to eliminate as much as possible, the noise associated with it in order to obtain a better signal-to-noise ratio (SNR). An ideal experimental system for a particular technique and for a particular application can be evolved only by a tedious process of trial and error. The various advantages and disadvantages, instrumental and otherwise involved in the experimentation have to be thoroughly looked into before finalizing a workable setup. Wherever possible, it is preferable to keep the instrumentation

part as simple as possible. In the recent times, more and more instruments are being used in conjunction with computers, which make system control and data acquisition much easier. This chapter deals with the instrumentation involved in the PA experimentation, and gives a detailed account of the various systems and sub-systems that have been used in the present investigations.

3.2. PA Instrumentation

The basic requirements [1] of the PA detection technique are the following;

- i. Light source,
- ii. Means of modulating the light (for cw sources),
- iii. Appropriate PA cell,
- iv. Suitable acoustic transducer and
- v. Signal detection and processing electronics

Figure 3.1. shows the schematic of the general instrumentation involved in PA studies.

3.2.1. The Light Source

There are two major classes of light sources that have been used for PA studies. The first category consists of arc lamps, filament lamps, glow sources etc. Such sources have a rather broad wavelength output from UV to far IR. These sources have low spectral brightness, incapability of fast modulation and they necessitate the use of external, low throughput spectral selection elements like monochromators to get tunable wavelength output. The low spectral brightness can be more or less compensated by techniques such as Fourier Transform PAS [2-4].

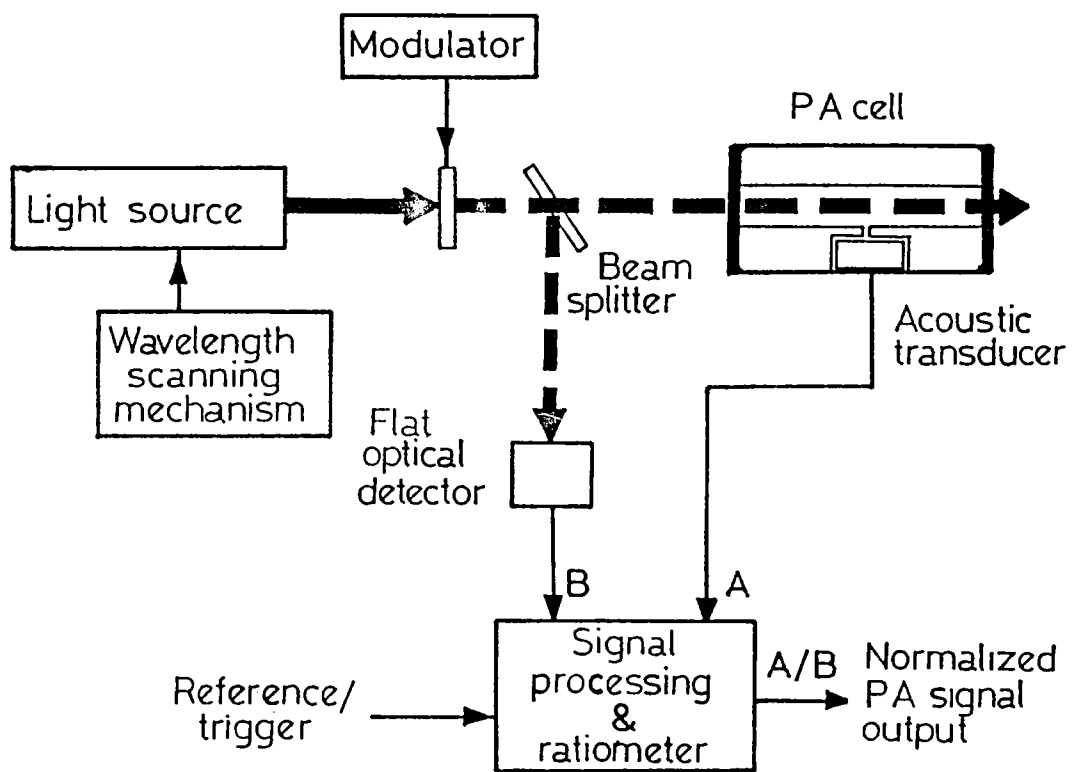


Fig.3.1. The schematic diagram of the general PA instrumentation

The other class of light sources are the lasers. They have high spectral brightness, have narrow spectral line widths and they can be readily modulated by intra cavity or extra cavity means. Different types of solid state, gas and dye lasers have been employed in various kinds of PA studies [5,6]. Pulsed lasers are capable of producing peak powers up to 10^9 Watts or more. Such lasers have been used to study optical non-linear absorption phenomena which cannot be generally probed using the cw lasers. The disadvantage of high peak power lasers is the increase in spurious signals due to window and wall absorptions. Since this background is enhanced by the large photon flux, most studies for sensitive PA trace analysis use cw lasers, though pulsed lasers also are used for the same [7,8] along with gating techniques. Various kinds of pulsed and cw lasers, and dye lasers with different dyes have also been used to obtain wavelengths in regions from UV to far IR. These have enabled a variety of studies ranging from spectroscopy to trace analysis and from pollution monitoring to microscopy using the PA effect.

Secondary laser sources like the spin-flip Raman laser has also been used [9] in certain cases. Solid state light emitting diode and diode lasers have found application in cw PAS. Relatively high power and the narrow emission in the VIS-NIR region, and the advantage that it can be easily modulated by just modulating the voltage to the LED [10], together with the fact that they are compact, cheap and easy to use make it an ideal choice for use in small, sample specific PA cells. With a LED, modulation frequencies of $\sim 40\text{MHz}$ are easily obtainable without loss of average power [11]. The same is true for semiconductor diode lasers up to $\sim 200\text{MHz}$. With respect to laser sources, lead-salt diode lasers have the additional advantage because their wavelength can be rapidly tuned within a few wavenumbers directly by the current variation.

wavelength can be rapidly tuned within a few wavenumbers directly by the current variation.

3.2.2. Modulation Techniques

To generate the PA signal, it is necessary to modulate the light in the case of a cw source. A variety of modulation techniques have been used such as, Q-switching, mode locking, pulsing the flash lamp, wavelength or frequency modulation, acousto-optic / electro-optic modulation and also mechanical modulation [1]. The amplitude modulation is the most popular technique used in the kHz-MHz frequency region. A few of the commonly used amplitude modulators are described below. The modulator also provides the reference signal to the lock-in amplifier for cw PAS detection.

i. Mechanical chopper

It is the simplest form of a modulator consisting of a rotating slotted disk placed in the path of the light beam. It offers 100% modulation depths for frequencies from a few Hertz to 5-8kHz. The disadvantage of this chopper is that at higher frequencies, the mechanical vibrations and sound associated with the fast rotating blade requires the chopper assembly to be isolated acoustically from the PA cell. Sine or square wave modulation is possible by using neutral density filter disk or a slotted disk as the chopping element respectively.

ii. Electrical Modulation

This is generally employed in gas discharge lasers. This technique involves the modulation of the plasma tube current of the laser. 100% depth of modulation is not obtained in this case. Since modulation of current in lasers operating at very high discharge voltages is difficult, the frequency range of this type of modulation is limited to a few hundred Hertz. Since the

spatial beam position depends on the plasma tube current, this technique cannot be used where the laser beam has to be spatially stable as in the case of pumping a dye laser. The only advantage over mechanical choppers is that this technique does not posses the acoustic noise factors associated with mechanical choppers. Lasers like CO, CO₂ and ion lasers can be modulated in this manner.

iii. Electro-optic (EO) Modulation

This technique involves the changing of the plane of polarization of a incoming polarized laser beam in a non-linear crystal like ADP or KDP (Ammonium or Potassium dihydrogen phosphate) with the application of electric field to it. The laser beam exiting from the crystal is passed through a polarizer which is crossed to the initial direction of polarization of the laser beam. Voltages which rotate the plane of the beam by 90° will allow the beam to pass through the polarizer. For all other voltages, the polarizer will not allow the full power of the beam to be transmitted. 100% modulation depths can be achieved for sine, square or triangular modulations. It has a large frequency range from 0-20MHz. The noise level is much less than that introduced by other modulation means. They have the disadvantage that they are costly, need wavelength specific high voltages for operation and cannot be used along with high powered lasers.

iv. Acousto-optic (AO) Modulators

This involves the spatial modulation of the laser by acoustic diffraction of light in a crystal. The light is diffracted by the sound waves in the crystal generated by modulated radio frequency. Extra dense flint glass, lead molybdate and tellurium dioxide are a few of the AO crystals used. This technique is not very popular with PA workers as such. The wavelength or

frequency modulation [12,13] offers an added advantage that it eliminates the continuum background PA signal caused by wavelength independent signals from window and wall absorptions thus increasing detection sensitivity [14,15]. Modulation of absorption characteristics of the sample can be achieved by Zeeman or Stark effects, ie, by applying a modulated electric or magnetic field across the sample. Consequently, the absorption wavelength of the sample is varied, which corresponds to a wavelength modulation method. The result, again, is a suppression of the continuum background signal. A reduction of the background by a factor of 500 was achieved by Stark modulation in comparison to the signal in the same PA cell with conventional amplitude modulation with a chopper [16]. This kind of modulation is well suited for absorbers with narrow linewidth, such as atomic and diatomic species. However, the Stark modulation scheme can be applied only to molecules with a permanent electric dipole moment like ammonia (NH_3), Nitric oxide (NO) etc. Nevertheless, a considerable increase in the sensitivity and selectivity in multi component mixtures can be achieved.

3.2.3. PA Cells

The PA cell is the heart of the whole PA system and thus should be carefully designed for its particular application. Since the sample is to be placed inside the PA cell, the design of the cell depends very much on the nature of sample to be studied. A typical PA cell should have the following characteristics :-

1. Proper acoustic shielding from ambient atmosphere
2. Minimization of unwanted signals due to interaction of the excitation light with cell walls, windows and microphone
3. Proper configuration and placement of microphone, sample and gas inlets
4. Means for maximizing the signal from the PA cell

5. Heating, cooling facilities for temperature variation of the cell (if needed).

i. Resonant And Non-resonant PA Cells

The acoustic characteristics of the PA cell cavity can be effectively used to enhance the PA signal and to eliminate, to a large extend, the unwanted acoustic noise involved in the PA detection.

The frequency response of a PA cell depends on [17] ;

1. The PA generation process in the cell,
2. Losses due to 3-D heat flow to the cell walls and windows,
3. Acoustic response of the PA cell and
4. Response of the transducer detection electronics

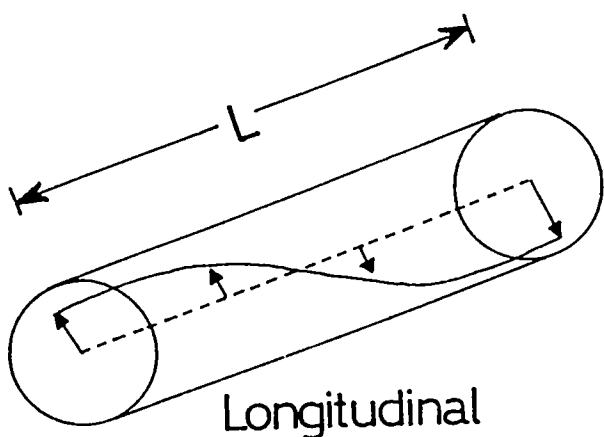
To utilize the acoustic properties of the cell, its acoustic resonance characteristics have to be analyzed and the different modes of resonance that are excited in the cell are to be determined. These characteristics depend on various parameters like the dimensions of the cavity, the power and beam characteristics of the excitation source etc. The frequencies of resonance of a open cavity of cylindrical cross section is given by, [18]

$$f_{kmn} = \frac{\pi c_0}{2} \left\{ \left(\frac{k}{L} \right)^2 + \left(\frac{\alpha_{mn}}{R_0} \right)^2 \right\}^{1/2} \quad \dots \dots \quad (3.01)$$

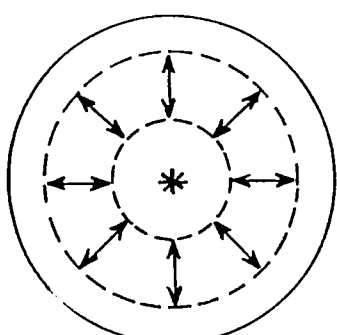
Here, L is the cavity length, c_0 the velocity of sound in the gas filling the cavity, R_0 is the radius of the cell. k, m, n are the longitudinal, azimuthal and radial mode numbers respectively. α_{mn} the n^{th} zero solution of the derivative of the m^{th} Bessel

function. Figure 3.2. shows the longitudinal, azimuthal and the radial resonances that are possible in such a resonator [1]. PA studies have been made by many workers using azimuthal [19], axial, [19,20] and radial [19-22] resonances of a cylindrical resonator. For a typical cylindrical resonator of length $L \approx 2R_o$, [1,23] there are about 12 acoustic modes in the 4-8kHz region but however, in actual measurements, with the laser beam propagating along the axis of the cylinder, and the microphone mounted flush with the inside wall midway between the ends of the cell lead to only about 2-3 detected resonances in this frequency region. Which modes are effectively excited and detected depends on the spatial geometric configurations used for laser excitation and microphone detection. In the case of a favourable overlapping of the laser excitation and the spatial structure of the corresponding mode, a standing wave is formed if the modulation frequency coincides with the resonance frequency of this mode, ie, the PA cell in this case essentially acts as an acoustic amplifier [45]. This means that the symmetry constraints, imposed by the laser excitation and the microphone detection drastically reduce the number of modes actually observed [23]. Azimuthal modes ($m \neq 0$) are not excited by the axial laser beam possessing cylindrical symmetry since for weakly absorbing samples, there is little pressure variation along the cell axis due to light absorption. The resonant operation of the PA cell also enables the following ;

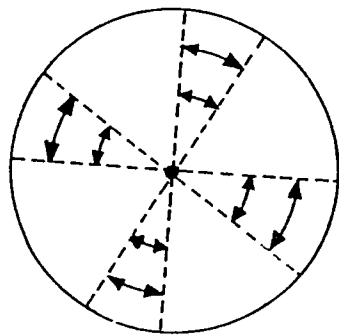
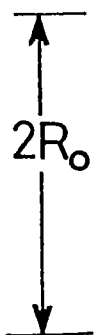
1. window-less operation of the PA cell in certain conditions
2. continuous gas flow to the cell is possible
3. the wall's adsorption of the gas is minimized since the ratio of the wall surface to its volume is comparatively small in a resonant cell
4. Some molecular parameters like relaxation times and thermodynamic characteristics of the sample can be determined.



Longitudinal



Radial



Azimuthal

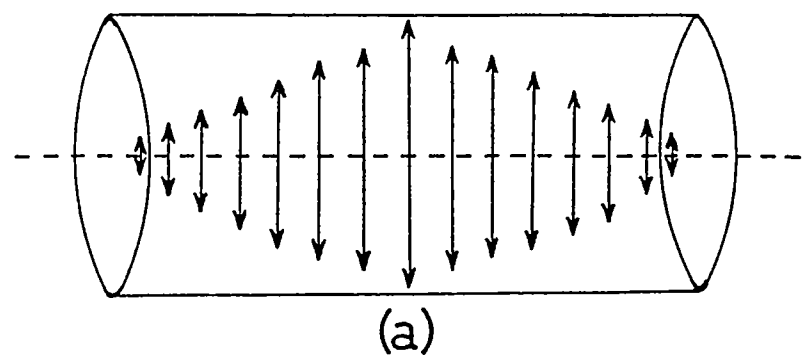
Fig.3.2. The possible acoustic resonant modes in a cylindrical resonator

Non-resonant cells also have been used extensively in PA measurements. Depending on whether or not there is a coincidence between the modulation frequency and any one of the resonance modes of the PA cell, it is called a resonant or a non-resonant cell. A non-resonant PA cell is one so designed that it has no optical or acoustic resonances that influence the operation of the device in a notable manner in the region of modulation frequency employed [24]. The fig.3.3. shows the longitudinal modes in a cylindrical cavity for non-resonant and resonant operations. Processes like molecular relaxation times can be measured effectively by employing the non-resonant mode of the PA cell and determining the phase lag of the PA signal with respect to the modulation frequency [24].

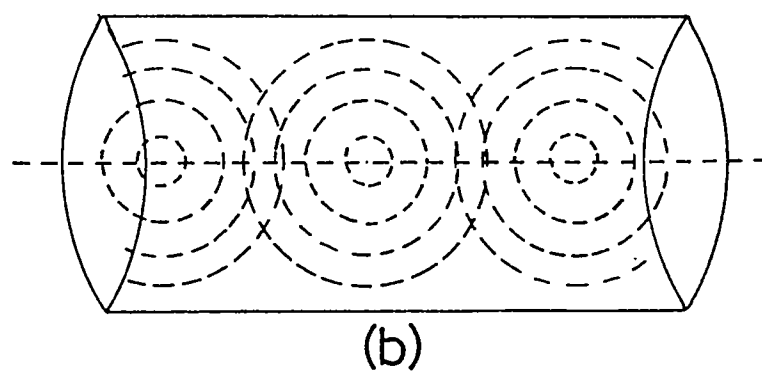
$$\phi_j = \tan^{-1}(\omega\tau_t) - \tan^{-1} \left(\omega \left[\tau_c^{-1} + \tau_r^{-1} \right]^{-1} \right) \quad \dots \dots \quad (3.02)$$

ϕ is the phase lag, ω the modulation frequency, τ_c the collisional relaxation time and τ_r the radiational relaxation time.

An acoustically resonant mode of operation will considerably complicate this equation and thus make the analysis difficult. Such PA cells have been used extensively for PA studies in solids and thin films. The major disadvantage of non-resonant cells is that their sensitivity is limited by a relatively large background continuum signal resulting from window and wall absorptions since the PA signal is same across the whole cell volume. In the case of pulsed PA studies, the detection being in the time domain, the resonance characteristics of the cell may be conveniently ignored. Since the off-resonance PA responsivity of the cell is small as compared to that near resonance, it is best if the cell volume of the non-resonant cell



(a)



(b)

Fig.3.3. The longitudinal modes of resonance of a cylindrical cavity in the (a) Resonant and (b) Non-resonant modes

(1-10cc), its cross section area and the modulation frequency (<100Hz) are kept a minimum so as to compensate for the loss of sensitivity in the off-resonance mode. Also, since the PA signal varies as $1/V_o$ (V_o the volume of the cavity), it is desirable that the cavity volume be kept a minimum. It is advantageous in the sense that only small quantities of sample gas are then required. If, the sample gas is absorbed by the cell walls, then a cell having large volume to surface area ratio has to be used thus sacrificing the sensitivity. For such applications, the resonant mode operation compensates for the loss of sensitivity due to increased cell volume.

In resonant operation, the acoustic energy is channeled into a highly symmetric mode. In addition to the potential increase in the sensitivity obtained at resonance, it would be expected that the radiation absorbed at the walls of the resonator chamber would couple only weakly to the standing wave and therefore produce a lower background noise than the same absorption in a non-resonant cell [25]. By switching to resonant operation of the PA cell, there is,

1. an increase in the signal-to-background (SBR) ratio
2. some increase in the sensitivity and,
3. an enhancement of signal-to-noise (SNR) ratio (here the noise will include the pre-amplifier noise).

The increase in the SBR makes sense until the background absorption coefficient α_b is decreased to the level of the minimum detectable absorption α_{min} , whose threshold depends on the electronic noise. These two conditions can be represented as,

$$\frac{(\text{SNR})_R}{(\text{SNR})_{NR}} = \frac{\bar{Q}(\omega_r) R_{nr}^2 \left(1 + \omega_{nr}^2 \tau_{nr}^2 \right)^{1/2} \left[U_N^2(\omega_{nr}) \right]^{1/2}}{R_r^2 \omega_r \tau_{nr} \left[U_N^2(\omega_r) \right]^{1/2}} \geq 1$$

and,

$$\alpha_b \leq \alpha_{\min} \quad \dots \dots \dots (3.03)$$

where, τ_{nr} is the thermal relaxation time of the heated gas on to the cell walls, and $\bar{Q}(\omega_r)$ characterizes the degree of increase in the PA signal at resonance frequency ω_r as compared to an equivalent resonant spectrophone of the same dimensions but free of resonance properties.

The term $\left[U_N^2(\omega) \right]^{1/2}$ is the spectral distribution of the noise. The essence of the above equations is that the sensitivity loss due to an increase in the volume of the resonant PA cell is compensated for, by an increase in the PA signal at resonance frequency [26]. Optimized resonant cells with high Q factors are used to determine accurately the thermo-physical and kinetic quantities [27-31]. Most applications of PA for trace analysis and pollution monitoring employ this method of operation with less optimized resonant cells of moderate Q factors. In general, the first order radial mode tends to have a lower resonance frequency than the first order axial resonance for cells of less than 10cm length, thus in many cases of resonant PA cell applications, the first order radial mode is used [32,33]. The other advantage of resonant operation being that the sample gas can be flowed through the cell without compromising on the sensitivity by placing the gas inlet and outlet where the standing acoustic wave has a node [1]. Existing wall absorptions can thus be saturated allowing accurate absorptivity or gas concentration

measurements [24]. The gas turbulence noise which might result from the flowing gas can be eliminated by using buffer volumes (volume of buffer space \gg cavity volume) on either sides of the cavity where the gas inlet and outlets are placed [34,35]. For comparison of resonant and non-resonant cells, the ratio of the PA signal due to the gas and that due to the windows are taken into account. Let p_g and p_w be the PA signals due to the gas and window. For a non-resonant cell,

$$p_g = \frac{(\gamma-1)I_0\alpha_g L}{i \omega V_0} \quad \dots \dots \dots (3.04)$$

$$p_w = \frac{(\gamma-1)I_0\alpha_w L_w A}{i \omega V_0} \quad \dots \dots \dots (3.05)$$

where, $\gamma = C_p/C_v$ α_g and α_w the absorption strengths of the sample and the window respectively, I_0 the incident laser intensity, L and L_w the lengths of the cavity and the window and V_0 is the volume of the cavity. The heat transport ratio A_h , depending on which a part of the signal generated at the windows is transmitted through the gas to the microphone is given by,

$$A_h = \left(\frac{k_w C_w}{k_g C_g} \right)^{1/2} \quad \dots \dots \dots (3.06)$$

Where, k_w and k_g are the thermal conductivities of the window and the gas, and C_w and C_g the specific heats of the window and the gas respectively. Thus, the ratio of these signals is,

$$\left[\frac{P_g}{P_w} \right]_{NR} = -\frac{\alpha L}{\alpha_w L_w A} \quad \dots \dots (3.07)$$

In the case of resonant operation,

$$P_g \propto \frac{\alpha \sqrt{L}}{R_o} \left\{ 1 - \left(\frac{R_o}{R_b} \right)^2 \right\} \quad \dots \dots (3.08)$$

$$\text{and } P_w \propto \alpha_w L_w A \frac{R_o}{R_b^2} \frac{1}{\sqrt{L}} \quad \dots \dots (3.09)$$

Where, R_o , R_b , L and L_b are the radius of the cavity, radius of the buffer volume, length of the cavity and the buffer volume respectively. The buffer volumes are such that they have a volume \gg than that of the cavity and the cavity opens out into these buffers on either sides. For $R_b \rightarrow \infty$, the gas absorption signal P_g becomes equal to the open cell resonator value and is proportional to $\frac{L^{1/2}}{R_o}$ thus,

$$\left[\frac{P_g}{P_w} \right]_{Res} \propto \frac{\alpha}{\alpha_w L_w A} \left(\frac{R_b}{R_o} \right)^2 L \quad \dots \dots (3.10)$$

so long as $L_b = 1/2 L$ with $L_b \gg R_o$. The ratio between the P_g and P_w for resonant and non-resonant cases show that we can limit the length of the cell for resonant case and still decrease the window absorption signal by an increase in the buffer diameter.

Typically, the ratio between p_g and p_w in the case of resonant operation was found to be almost 16 times that of a non-resonant cell of identical dimensions [35].

ii. Other Types Of PA Cells

As mentioned earlier, different configurations of the PA cell have evolved in the process of investigations of different properties of gases using PAS. The characteristics of three commonly used gas phase PA cell geometries are briefly discussed. In the first kind, (fig.3.4.a) an arbitrary 'T' shaped non-resonant detector with a volume V_n in the middle of which a tube of volume V_t , is attached and a microphone placed at the far end of it. The Q factor of such a cell, must be such that,

$$Q(\omega) > 1 + \frac{V_t}{V_n} \quad \dots\dots(3.11)$$

for maximum responsivity. Flowing gas cannot be used here and this kind of cell has low Q and τ_t the thermal relaxation time.

a. Helmholtz Resonator

By attaching another tube so that it forms two resonators coupled by a tube, these problems can be overcome. Such a configuration is the Helmholtz resonator [36-42] as shown in fig.3.4.b. Two volumes V_1 and V_2 are coupled by a tube of cross-sectional area A_c and length l_c . The gas in the channel acts as a plunger that can move along the channel. As it moves to V_1 , it rarefies the gas in V_1 and compresses the gas in V_2 , thereby experiencing a restoring force proportional to its displacement along the channel. The retarding thermo-viscous losses are also present here. The resonance frequency is given by [43],

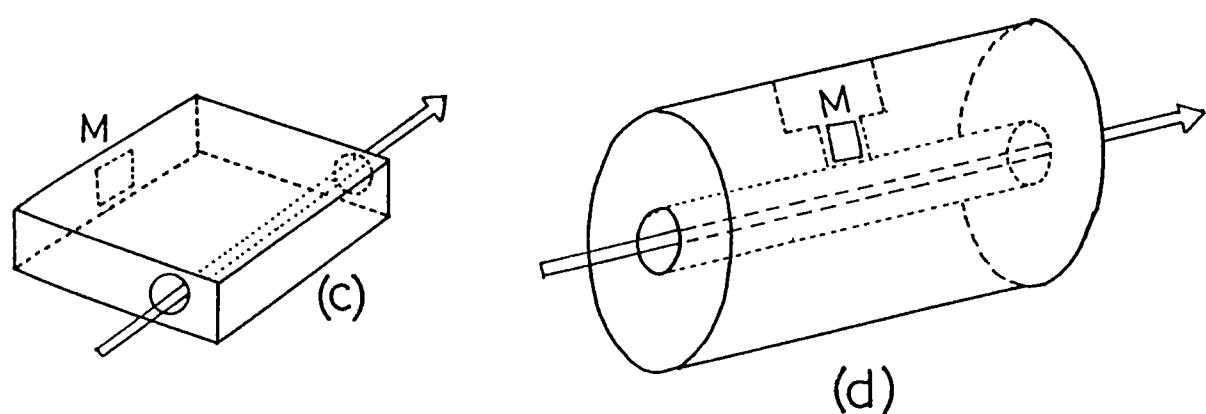
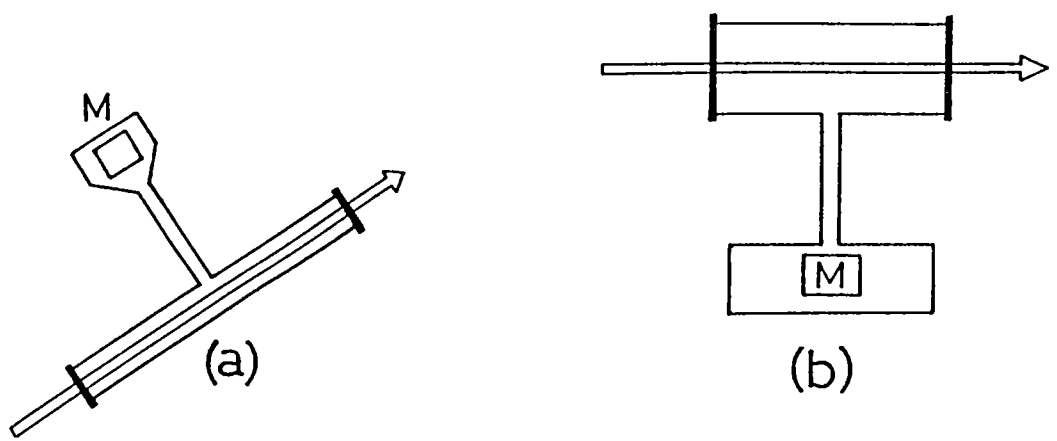


Fig.3.4. Different geometries of PA cell commonly used for gas phase studies (a) The 'T' geometry PA cell (b) Helmholtz resonator (c) Rectangular geometry (d) Cylindrical cell (M - microphone)

$$\omega_H = c \left[\frac{A_c}{I_c V_r} \right] \quad \dots \dots \dots (3.12)$$

$$\text{where, } V_r = \frac{V_1 V_2}{V_1 + V_2} \quad \dots \dots \dots (3.13)$$

The Q factor of such a configuration is,

$$Q_H = \frac{\rho A}{8\pi\eta} \left\{ \omega_H^2 - \left(\frac{4\pi\eta}{\rho A} \right)^2 \right\} \quad \dots \dots \dots (3.14)$$

The advantage of such a configuration is that the resonance frequency can be varied by simply changing the dimensions of the coupling tube. The Helmholtz resonator PA cell has been used for gas phase as well as high resolution pulsed PA spectroscopy of rare earths [37].

The second kind of PA cell is shown in fig.3.4.c. It has a large volume, rectangular cross section, and can be used for flowing gas studies. The τ_t can be made to be of the same magnitude as that of a non-resonant cell because of its limited height. It has higher Q and τ_t . Patel and Kerl [44] built such a rectangular waveguide (U band) PA cell on which a number of miniature electret microphones were attached. The microphone outputs were summed to get the net PA signal. This type of PA cell is useful when the laser source has a planar output such as a semiconductor laser. It was used to study the effect of low temperature, electric and magnetic fields on the PA signal.

b. Open Cavity Cylindrical PA Cell

The third type, (fig.3.4.d.) which has a cylindrical cross

section, is the most popular configuration of the resonant PA cell. It can have large volume to surface area, and resonant frequencies obtainable in the kilohertz regions which are accessible by mechanical modulators. It is easier to build a low-noise pressure transducer in this frequency region rather than in the Hertz region. Many modifications to this basic cylindrical cavity structure have been made for specific applications. The disadvantage, common to all resonant PA cells is the variation of the resonance frequency with temperature and the pressure and composition of the sample gas [31,45,46]. High Q factor (~ few hundreds) have been obtained for the radial resonant modes [32,33]. In certain cases, high Q factors (~ 10^3) have also been reported [47,48]. PA signals from cells with fixed volumes can be enhanced by using the multi-pass technique, wherein, the input radiation is made to reflect back and forth inside the PA cell many times [49]. The magnitude of ultimate gain in a multi-pass PA cell to that of a single pass cell is,

$$\frac{G^x}{G^1} \approx \frac{1}{1-R_m \exp(-\alpha L)} \quad \dots \dots \dots (3.15)$$

where, R_m is the mirror reflection coefficient and x the number of passes and α the absorption coefficient of the sample [50,51]. Typical values of N are 20-60. Assuming that the coherence length of the laser is much smaller than the PA detector dimensions, the equivalent total mean radiation power in the cavity is just the sum of the mean power in every separate beam. Such cells have been used for PA Raman studies (PARS) [50,8,52]. Geometries other than cylindrical have also been used [52], in which the laser is directed transverse to a cylindrical sample cell. This configuration allows the excitation of a lower longitudinal resonance frequency, and with the placement of the microphone along the longitudinal axis, allows for a more effective coupling of the acoustic mode energy into the microphone

diaphragm.

c. Optically Resonant Cell : Intra-cavity Operation

The pressure amplitude in a PA detector is proportional to the incident power or energy. A method to increase this is to place the PA cell inside an optical resonator. The optical resonator can be characterized by a quality factor $Q > 1$. The magnitude of this parameter is dependent on the electromagnetic losses of the resonator. These losses originate from the resonator walls and molecular absorptions [35]. To get a detector with linear response, the wall losses should not dominate. The value of Q is a function of the resonator geometry and the radiation frequency which means that the resonator has to be tuned when the radiation frequency is changed. An optical resonator is useful when the molecular absorption strength is so small that, (i) a resonator quality factor > 1 determined by the resonator wall absorption is attainable, (ii) A measurable PA signal with single pass detection cannot be obtained with the available radiation source. The PA signal being proportional to the laser power within the saturation limit, the more the power available, the better will be the signal for the weaker absorption. Since the power of the laser beam inside the optical resonator can be almost 400 times the extra-cavity power, if such a PA cell is placed in inside the cavity of a laser with an amplifying medium, then the radiation power substantially increases and the PA signal strength also increases correspondingly. The intra-cavity laser power P_{ic} is,

$$P_{ic} = \frac{2}{T_o} P_{ex} \quad \dots \dots \quad (3.16)$$

where, P_{ic} and P_{ex} are the intra and extra cavity laser powers and T_o the transmittance of the output coupler of the laser cavity. Here, the quantity $2/T_o$ is the Quality factor of the laser cavity [53]. The factor 2 arises in the case of a standing

wave resonator since the beam makes two passes through the PA cell for each incidence on the output coupler. For a ring laser, the factor of 2 does not arise. Quartz Brewster windows can be used for the PA cell to reduce losses in the cavity. In experiments involving ion lasers, care must be taken that the UV spontaneous emission of the plasma is filtered out, since, the cross sections for UV electronic transitions can be over billion times stronger than the weak phenomena like overtone absorption and thus it can present a large background signal in these cases. Such a configuration is employed to detect weak overtone absorptions, and also trace analysis of samples in vapour phase [54-61]. For these cases, it must be assumed that the detector losses is very much smaller as compared to the optical losses in the laser cavity ie, the molecular absorption process is not the major loss mechanism. Intracavity operation thus eliminate the need for a multi-pass optical arrangement, but the intra cavity arrangement needs extremely precise and highly stable optical alignment.

d. PA Cell For Pulsed Studies

Since pulsed lasers have high photon fluxes, the cell design should be different from that of cw PA cell in order to minimize the unwanted signals. The low repetition rate of pulsed lasers prevents any benefit from being derived from the use of the acoustic cell resonances and thus the non-resonant mode of operation is usually employed. However, by using a pulsed laser operating at a repetition rate which is a sub harmonic of the cell's resonance so that the lowest radial mode of the cell is excited, the resonance characteristics of the cell can be utilized advantageously [62,63]. So long as the pulse duration is short compared to the period of the resonant acoustic oscillations, the signal amplitude decays as $\exp(-M/2Q)$, where, Q is the quality factor and M the integral number of acoustic oscillations between the laser pulses. Since M increases as the laser repetition rate

decreases, for a typical 10Hz repetition rate, cells of relatively high Q ($> 10^3$) have to be used [53]. Another factor that influences the PA cell is the need to optimally monitor the ballistic acoustic wave generated by the sample absorption. The absorption of the light at the windows itself produces signals, which must travel one half of the cavity length to reach the microphone placed half way between the ends of the cavity, and will arrive typically $15L \mu\text{secs}$ after the absorption occurs (in air) at the window. These can be temporally isolated and can be reduced by using good quality, low absorption windows. Scattered light from the windows can strike the cell walls near the microphone and produce a signal which may be temporally close to the sample signal. This can be avoided by using clean windows and by using transparent cell wall material with an highly absorbing coating on the outside. The scattered light is transmitted by the cell walls but absorbed on the outside. The heat produced there will not generate any acoustic pulse that might carry to the microphone. To collect the largest possible fraction of the PA signal, the microphone is to be placed as close to the focal region of the laser beam as possible but however, the focused laser should not fall on the microphone since it will cause extensive noise and damage.

e. Spatial Resolution In PA Cells

In the case of pulsed PAS, the gated integration detection technique allows PA signals from different regions of the PA cavity to be detected by time selection. The spatial resolution here means the minimum volume of a local zone in the PA cell from which the PA signal can be extracted and detected. The value of the ultimate spatial resolution

$$L_{sp} = V_s \tau_R \sqrt{1 + (h/z)^2} \quad \dots\dots(3.17)$$

where, h is the distance between the microphone and the optical axis of the cell, z the co-ordinate along the optical axis in the cell taken from the center of the cell and τ_R the total time resolution of the PA system, which depends on (i) the laser pulse duration t_p , (ii) time constant of the acoustic detector (iii) the time of the non-radiative relaxation of the excited levels τ_n and (iv) the mutual geometry of the cell, microphone and the laser beam. The spatial resolution of the PA cell is impeded due to reasons such as the overlap of equal amplitude signals from different regions of the cell or when the leading edge of the PA signal is increased due to long t_p or τ_n . In these cases, the spatial resolution can be obtained by using spatial localization of the zone under investigation by introducing acoustic baffles and buffer volumes [64]. These elements effectively attenuate the PA signals propagating to the microphone from the end zones, and the excitation of the resonant vibrations in the buffer volumes increases the delay of the PA signals. The 'T' shaped geometry for the resonator has the highest spatial resolution with the longitudinal mode excited in the lateral appendix (fig.3.4.a.). Since in most of the PA cells, the PA signals are averaged over the cell volume during the detection time, the means of increasing spatial resolution essentially depends on the type of operation of the laser.

f. Differential PA Cell

In PA measurements involving cw sources and weak absorptions, it is necessary that the noise level be kept a minimum. One such method for noise reduction is the differential operation of the PA system. The three different ways of differential operation are as follows. In one type, two separate, identical cells are used. One contains the sample gas and the buffer while the other contains only the buffer gas. The excitation source passes

through both the cells and the difference in the PA signals eliminates the acoustic noise due to ambient conditions, window and cell wall absorptions, and to an extend the electrical noise seen by the two cells [65-67]. In another kind, the identical sample and reference cells are placed inside a common enclosure containing the sample gas. The sample and buffer are in both the cells under identical conditions. The excitation beam passes through and excites the sample in only one of the cells. The difference between the signals from the two gives a noise-free signal due to the sample [35]. This kind of cell design has been followed in the cw PA experiments performed as a part of this thesis work. Yet another method is the differential absorption technique which is often employed in laser detection and ranging (LIDAR). In this, the PA cell containing the sample is irradiated with two wavelengths λ_1 and λ_2 modulated at frequencies f_1 and f_2 respectively. The net PA signal is sent through a band-pass filter and analyzed by two different lock-in amplifiers L_1 and L_2 locked to f_1 and f_2 respectively. L_1 rejects the signal due to λ_2 modulated at f_2 and vice versa. Then the output of L_1 is proportional to absorption of λ_1 and that of L_2 to the absorption of λ_2 by the sample. These outputs are then fed to a differential amplifier, the output of which is then proportional to the product of the concentrations of molecules and the difference in the absorption cross section of the sample at λ_1 and λ_2 . The window heating, external sound etc. contribute to the common-mode input signals of the differential amplifier and are thus eliminated [68].

g. Specialized PA Cells

Many different designs of the PA cell have been used for different applications. High temperature cells for PAS need special design due to the very fact that the microphone is to be shielded from the high temperatures of the sample. A high temperature PA cell

for studies of samples of low vapour pressure has been described by Jalink and Bicanic [69]. The PA cell is based on the principle of a heat pipe oven. The microphone is placed near to the windows where the standing acoustic wave (second longitudinal mode of resonance is used) has a maximum. In this way, the microphone is placed away from the heated part of the cell. Moreover, there exists a boundary between the region containing the sample vapour plus the buffer gas and the volume filled by the buffer gas. This boundary isolates the microphone and the windows from contamination. The common problem in high temperature is that conventional miniature microphones cannot withstand high temperatures and normal shielding of the microphone reduces its sensitivity drastically. To overcome this, an high temperature PA cell for gas phase studies (maximum 450° C) with a unique gas flow designed to isolate the multiple microphones from the high gas temperatures without compromising on the sensitivity has been reported [70].

Window-less PA cells have been used as a solution to the lack of perfect windows specially in the IR region [71]. Such cells can be used for low absorption measurements and where continuous monitoring and flowing gas measurements are required. It has been shown that the openings in the resonant acoustic cavity can be used without greatly reducing the Q factor [71]. In such a cell, there are no windows, but in the cavity openings, acoustic filters are placed. These filters should ensure that the external noise does not enter the chamber. Also, they should allow for slow gas flow and show low acoustic admittance from internal direction. Window-less non-resonant differential operation of PA system allows for flow through measurements with total elimination of window signals by window-less operation and the ambient acoustic noise by differential operation [72] in a manner independent of the laser mode control and focusing. Less

than 10ppbV levels of trace gas were detected with this cell. The major advantage of such a system is that it can be used for direct environmental trace gas analysis and for agricultural applications. The major disadvantage of such a cell is that it can operate only at atmospheric pressures for the obvious reason that it does not have windows. For highly corrosive gases, normal metal PA cell and the microphone cannot be used. For this a solid quartz PA cell with a thin quartz membrane sintered on to one end of the PA cell acting as the acoustic transducer has been used for studies in gases like ICl [73].

3.3. Detection Of The PA Signal

The four main kinds of detectors being employed to detect the signal induced by non-radiative de-excitations,

- i. Acoustic detectors,
- ii. Refractive index gradient detectors,
- iii. Thermal detectors
- iv. Other exotic detectors

3.3.1. Acoustic Detectors

Photoacoustic spectroscopy generally uses this kind of detection. The pressure disturbance following absorption of radiation by the sample is detected by an appropriate and sensitive acoustic detector like microphone or the piezo-electric detector.

i. The Microphone

The conventional condenser microphone basically works on the principle of capacitance variations due to the sound waves. It has two parallel plates, where one plate is rigid and the other

acts like a diaphragm. The dielectric material between the plates is air. When acoustic waves are directed towards it, the diaphragm follows the vibrations of the sound, thereby altering the capacitance of the microphone, which leads to a voltage change that is detected by a high input impedance amplifier. The microphone signal increases with the bias voltage applied across the microphone [74]. These microphones have a generally flat response up to $\sim 15\text{kHz}$, which is ideal for PA studies, have low distortion and little response to mechanical vibrations. They respond well to pulsed pressure impulses, thus making them suitable for pulsed PA studies also. Brue & Kjaer model 4145 is one of the widely used condenser microphone having a sensitivity of $\sim 40\text{mV/pascal}$ in combination with a pre-amplifier. The electret microphone [75-78] works in the same principle as the condenser microphone, but with the difference that the capacitance is provided by an electret, which is a thin foil of material with a permanent electrical polarization and high dielectric constant. One side of the electret foil is metallized and the insulating side is placed on a fixed back plate. The impinging sound waves on the metallized side causes a change in the polarization characteristics of the electret material which in turn provides a small voltage between the metallized front electret and the back plate. The large capacitance/unit area possible in electrets enable them to be made into highly sensitive and miniature microphones. These microphones do not need the biasing voltage due to the permanent electrical polarization of the electret. Owing to the small capacitance of such microphones, the output impedance is high (specially at low frequencies) and thus necessitates the use of high input impedance amplifiers. Some commercial miniature electret microphones (Knowles Electronics model BT1759 and BT1753) have built-in FET pre-amplifiers and thus bias voltage has to be supplied. These microphones have a sensitivity of $\sim 10\text{mV/pascal}$ and can be effectively matched to a

low input impedance amplifier. The microphone detection is generally used for gas phase studies. Microphones do not couple very well with the acoustic signals in condensed samples. To overcome this, a gas column is used to transfer the acoustic disturbance from the sample surface to the microphone.

ii. Piezo-electric Detectors

Since only 10^{-4} of the acoustic pressure amplitude generated at the surface of a condensed matter sample is transmitted to the sample-gas interface and finally the diaphragm, microphones are not ideally suited for this application. To overcome this problem, a piezo-electric detector is attached directly to the solid or liquid sample. The pressure variations striking the piezo-electric element give rise to a voltage which follows the PA pulse. Piezo-electric detectors such as lead zirconate titanate (PZT), lithium niobate, quartz crystal etc. are used. The different kinds of piezo-electric devices and their applications to acoustic transducers are reviewed by Mason *et al* [79] and Juarez [80]. The sensitivity of a piezo-electric device and its frequency response is depended on its dimensions. For a typical transducer element of diameter and thickness of the order of a few mm, the sensitivity is $\sim 0.003\text{mV/pascal}$ as compared to the $5\text{-}10\text{mV/pascal}$ for a miniature electret microphone. The transducer is usually enclosed in a steel chamber to offer protection from electromagnetic pickup, corrosion and absorption of stray light [81]. The sample is then placed in tight contact with the transducer so that a better acoustic impedance matching between the detector and the sample is possible and can thus detect high frequency signals associated with the sample [4,82,83]. For corrosive environments, microphones protected with thin sapphire or metallic films have been used. Here, the microphone senses the movements of the film which follows the pressure fluctuations in the cell. This technique compromises on

the sensitivity since the sound waves do not fall directly on the microphone [73]. The new kind of piezo-electric transducers are the film transducers. They are made of highly insulating polymeric films poled in a strong electric field at elevated temperatures or by electron bombardment so that they become electrically polarized and thus exhibit piezo-electric effect. Films like polyvinylidene fluoride (PVF_2), teflon, mylar etc. are the commonly used films. Due to their very small thickness, they are more sensitive and does not have the 'ringing' effect. They have high rise times ($\sim 2\text{nsec}$) and their high flexibility helps in innovative transducer designs and better acoustic coupling with the sample [84].

iii. Refractive Index (RI) Gradient Detectors

When the sample temperature is altered due to the non-radiative relaxation process resulting from the absorption of radiation, the radial density and the refractive index profiles also reproduce the shape of the exciting light beam. The RI distortion acts as a lens to a weak probe beam sent through the sample collinear or normal to the direction of the pump beam. Heating of the sample leads to a RI minimum at the axis and thus forming a diverging thermal lens in the sample. The deflection of the probe beam is monitored by a position sensitive detector, which essentially consists of a pin-hole, knife edge, or an optical fiber, coupled to a photo diode or a photo multiplier tube. The temperature variations in the sample depending on the absorption manifests itself in the amount of deflection in the probe beam. Thermal lens technique, is usually applied only to liquids where microphone detection is difficult. This has been effectively used by many workers to detect weak overtone absorption in liquids using cw dye lasers [85-87]. Another variation of this

technique, called photothermal deflection technique (PTD) is employed for studies in solids and fluids. Here, the probe beam grazes the surface of the sample on which the pump beam is incident (Fig.3.5.). The resulting temperature variations create a RI gradient in the gas above the sample surface, which deflect the probe beam. This technique has been used for various kinds of investigations like surface studies, gas flow detection, trace analysis etc. [88-93]. The advantage of this technique is that remote analysis of corrosive or hot samples into which a microphone cannot be introduced can be done. Only the pump and probe beams need to be in contact with the sample while the detection equipment can be placed elsewhere. For weakly absorbing gases, PA technique has more detection sensitivity over thermal lens and photothermal techniques. Different detection methods have been used in this technique [94]. Compared to PA technique which can be termed as an 'ultrasensitive' technique, the PTD technique is not as sensitive since macroscopic heat generation is required to enable the probe beam to be deflected and thus detected. Thus PTD technique is less sensitive than the PA technique when it comes to detection of microscopic effects [95]. Nevertheless, this technique has been effectively applied to different studies in both condensed matter and gaseous samples [88,96].

iv. Thermal Detectors

Here, the temperature variations are directly measured by a sensitive thermistors placed in contact or in the vicinity of the surface of a strongly absorbing species. This technique eliminates problems due to external acoustic noise and uses relatively simple apparatus [97]. Superconducting bolometers have been used to measure the temperature changes in the irradiated low temperature solid. It has a fast response

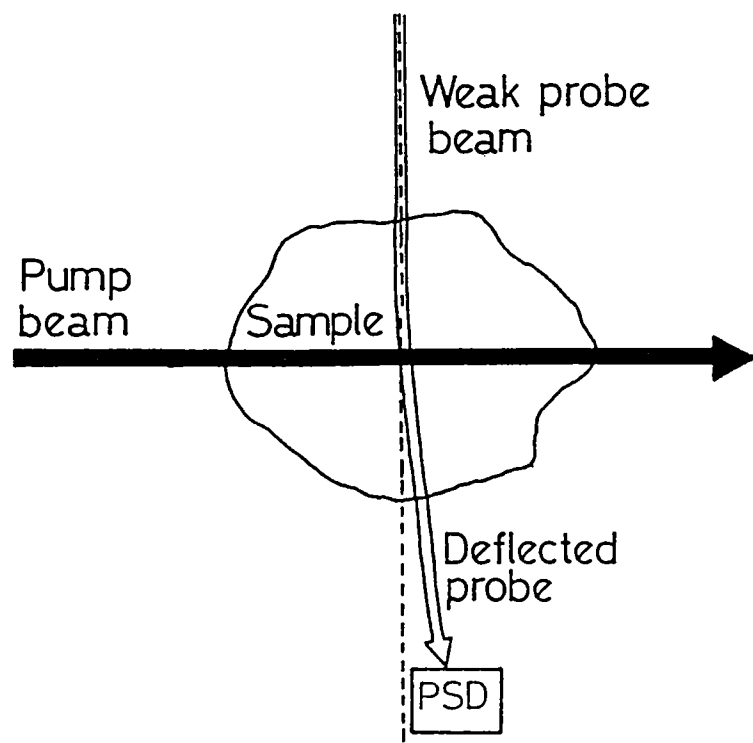


Fig.3.5. The detection scheme for refractive index gradient (PTD) technique (PSD – position sensitive detector)

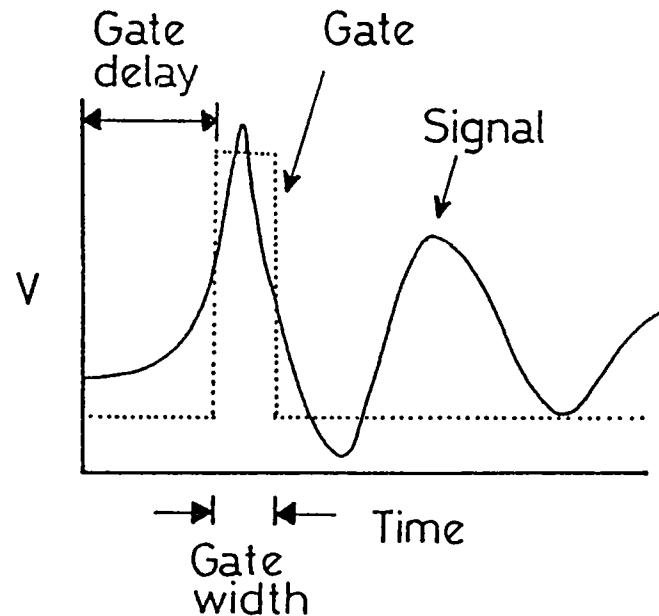


Fig.3.6. The box-car measurement technique showing the gate delay, gate width and the signal being measured

(>100kHz) and can be used to study relaxation dynamics in the lattice [98]. This technique can be used only for strongly absorbing samples and is relatively less efficient than acoustic detection.

v. Other Exotic Detectors

Several other kinds of detectors, which indirectly measure the pressure fluctuations in the sample have evolved. These techniques have been generally used where direct microphone detection is not possible. In the place of the microphone, a reflecting film or a pellicle is placed, which follows the pressure fluctuations in the chamber (as in a Golay cell), and can be measured by reflecting a probe beam off the film or pellicle [99-102]. A Fabry-Perot interferometer constructed with a pellicle beam splitter has also been used to detect the pressure variations [103]. A fibre-optic interferometer acoustic detector replacing the conventional microphone in a PA cell was used to detect NO₂ in the 50ppbV concentration region [104].

3.4. Detection Electronics

The detection electronics in PA studies, especially for low level signal detection should be capable of low-noise, low-distortion, and high-gain operation in frequency region of interest. Also, appropriate electronics have to be used depending on whether the PA detection is by pulsed or cw techniques.

3.4.1. Pre-amplifiers

In the case of weakly absorbing samples, the corresponding PA signal is also weak and this is required to be appropriately amplified before being processed. Ordinary condenser microphones

have a high output impedance and thus, a high input impedance pre-amplifier using FET is necessary. High gain pre-amps are commercially available, and can also be built using FET or low noise integrated circuits like NE536, AD50K, TL071 etc. Pulse amplifiers of high frequency bandwidth is required for amplifying pulsed PA signals from piezo-electric transducers. The typical noise level of the microphone is $\sim 4\text{nV}/\sqrt{\text{Hz}}$ and since the noise in the PA signal is also amplified, a trade-off between the signal to noise ratio (SNR) and the amplifier gain is required for optimum PA signal detection. It has to be noted that, even with the best available electronic circuitry, the amplifier noise exceeds the noise generated by transducer itself [105] resulting in a detection sensitivity far below the theoretical limits determined by the displacement of the microphone diaphragm [99,106]. Several circuits for microphone and piezo-electric transducer pre-amplifiers have been described [83,107-109]. The use of op-amps with low temperature coefficient and feedback substantially reduces gain drift with temperature in comparison to pre-amplifiers with FET or transistors as the input stage. Commercial electret microphones (Knowles BT1753 and BT1759) have built-in FET pre-amplifiers which makes it easy to couple them to moderately low input impedance of the amplifiers. Differential pre amplifiers, coupled to differential PA cells help in eliminating the signals due to window absorption, ambient noise etc. It must be noted that the frequency response of the microphone-preamplifier system should be flat within the modulation frequency range being used.

3.4.2. Signal Detection, Recovery And Processing : Pulsed And CW Detection

Depending on the type of excitation source, different methods of signal processing techniques have to be chosen. Usually, PA experiments are done using either pulsed or cw light sources. In

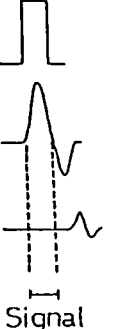
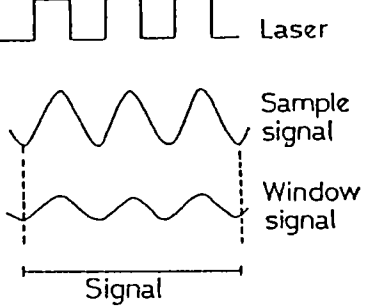
the case of pulsed sources, which usually have high peak intensity (up to 10^9 watts and above) and short duration (msec to femtosec), the PA signal is also pulsed and follows the excitation. In such a case, the PA signal is detected in the time domain using the gated integrator and signal averaging techniques.

Signal recovery is a vital part in obtaining noise-free output, the instruments for which will always be indispensable so long as experiments are being attempted with progressively smaller amounts of samples, weaker absorptions, smaller concentrations and fainter excitations. Most experiments today use electronic signal recovery and processing in one way or the other. Then and only it is possible to detect and analyze weak signals that are otherwise buried in noise and electro-magnetic interference. Pulsed signals arising due to pulsed excitation can be recovered and processed by the gated integration and averaging (Boxcar technique) technique whereas, for cw sources, modulation and phase sensitive detection technique (lock-in technique) are generally employed in the case of PA studies. The basic differences between the pulsed and cw mode of PA detection techniques is given in Table 3.1.

i. Pulsed PA Detection : Gated Integration Technique

In some cases, it might be essential to recover a part or the whole of an output signal pulse so that the signal can be analyzed. To recover such a signal buried in noise, some form of averaging process is required and for that, some type of multipoint averager or a Fourier transform analyzer is required. Signals of such transient nature, triggered by repetitive pulses from the excitation source can be analyzed in this fashion. The pulsed PA signal has in it, the signals due to the sample, window absorptions, scattering etc. So, it is necessary to detect only

Table.3.1. Some of the main differences between the pulsed and cw PA techniques

PULSED PAS	CW PAS
 <p>Laser Sample signal Window signal Signal</p>	 <p>Laser Sample signal Window signal Signal</p>
<p>Uses pulsed light source Signal detection in the time domain Resonant cell not essential Uses gated integration and signal averaging technique Acoustic noise is small during the small signal detection time More sensitive due to higher peak powers of pulsed source Signal averaging over large number of pulses required to compensate pulse-to-pulse instability of source Piezo-electric transducers usually used for condensed samples</p>	<p>Uses modulated cw source Signal detection in the frequency domain Resonant cell needed for PA signal enhancement and noise reduction Uses phase-sensitive (PSD) detection technique Noise elimination requires alternate techniques - may reduce PA signal More suited for intra-cavity operation Ratioing and differential operation of cell required for increasing S/N ratio and reducing variations due to laser power instability Microphones are generally used for all kinds of samples</p>

that part of the signal corresponding to the sample. This is achieved by the box-car integrator, which essentially is an instrument used to recover complex repetitive signals hidden in noise [110]. It has a frequency response which is ideal for the recovery of such waveforms, consisting, in the case of a waveform which repeats at regular intervals, a series of peaks at every Fourier component of the waveform plus a response extending from zero up to the cut off frequency $1/2\pi T_{\text{eff}}$ (where, T_{eff} is the effective time constant) of the equivalent low pass filter used in the Boxcar integrator. The response is zero at all other frequencies. The bandwidth of every peak in the same can be set by the C-R filter. The usual practical box-car has a C-R low pass filter which is connected to the voltage waveform to be measured for a short interval T_s once during each cycle of the complex waveform cycle. Since the time constant τ_r of the low pass filter is chosen to be \gg than T_s , it requires many repetitions of the sampling time T_s for the voltage on the capacitor of the C-R filter to approach the final value ie, the average value of the complex waveform plus noise during the time T_s . It is this averaging process that is responsible for the enhancement of the SNR provided by the box-car averager. If now, the sampling interval T_s is slowly scanned across the complex waveform, the entire waveform will appear at the output of the low pass filter provided, $T_s \gg 1/f_h$, where, f_h is the highest harmonic of significance in the waveform being measured and all the peaks of the frequency response up to f_h are of equal height. The complex waveform will then be faithfully reproduced if the scanning is done sufficiently slowly.

$$\text{Here, } T_{\text{eff}} = CR/r \quad \dots\dots(3.18)$$

$$\text{Where, } r = T_s / T_g \quad \dots\dots(3.19)$$

T_g is the time between successive openings of the gate. The bandwidth of each peak in the frequency response is $1/\pi T_{eff}$ ie, $r/\pi CR$. By fixing the delay and the gate width so that the voltage from the part of the PA signal pulse being measured is due to the sample, it is possible to temporally separate out the PA signal due to the sample from other unwanted signals contained in the PA signal pulse [109,111], thus improving the SNR of the detection. Since the pulsed PA signal is very strong due to the high peak powers of the laser, and since it also has a definite time delay with respect to the laser pulse, short detection times thus allows for better discrimination between the signal due to the sample and that due to windows, scattering, ringing effects, ambient noise etc. The pulsed PA signal, and the gate delay and width of the box-car are shown in fig.3.6.

ii. CW PA Detection : Phase Sensitive Detection Technique

Generally, in experiments using d.c. or static excitation (cw), the output signal appears in the form of a slowly varying d.c. proportional to the experimental parameter of interest. Severe measurement problems will occur when the signal voltage falls to a level comparable to the error voltages due to offsets and drifts in the transducer and its related electronics [112], as seen by fig.3.7.a. If the d.c. signal is 'chopped', ie, the cw radiation is modulated, then this output voltage now appears as a chopped voltage with the amplitude of the d.c. signal, superposed on the noise, as seen in fig.3.7.b. This signal, on passing through a high pass filter, removes the low frequency noise as seen by fig.7.c, but the residual high frequency noise is passed through this filter and it appears with the a.c. signal. This can be further refined by differential measurement procedure, in which, the mean voltage difference between successive cycles of modulation is measured and then averaged over a number of

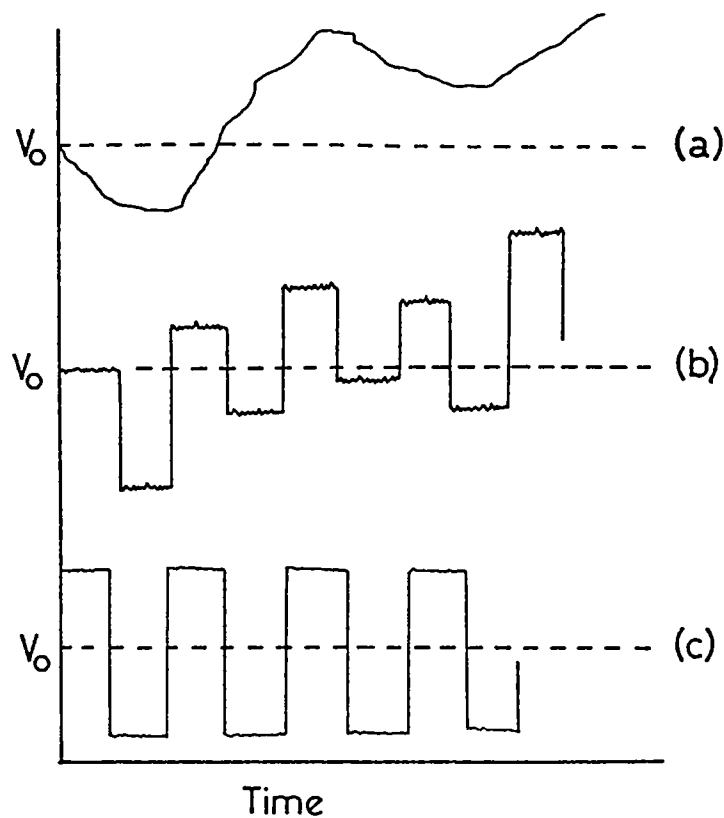


Fig.3.7. Detection of a cw signal (a) The d.c.signal + drift & noise (b) The chopped signal + noise (c) The a.c signal after passing through a high pass filter

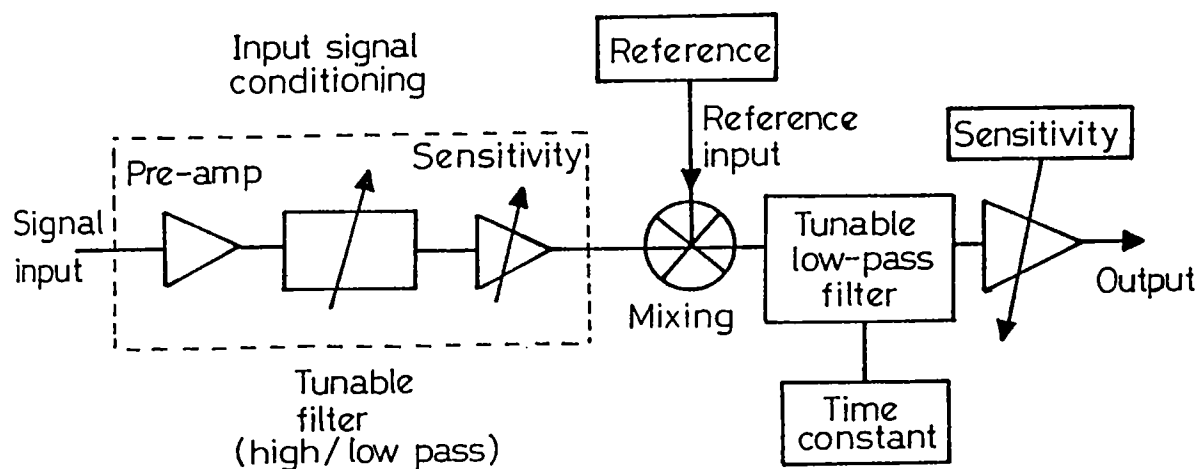


Fig.3.8. Schematic diagram of the basic lock-in amplifier

modulation cycles. Better elimination of noise is achieved by increasing time and the number of modulation cycles involved in averaging. The phase sensitive detector (PSD) [113] measures this difference voltage of interest automatically by using a synchronous reference voltage derived from the modulation source. This allows for the use of long averaging times for better SNR and is capable of operating with signals well below the background noise level. In other amplitude demodulation techniques such as the envelope detector, there is no fundamental distinction between the signal and the noise, whereas the PSD is engineered to respond specifically to the information bearing signal. Also, the PSD is responsive to both the amplitude and the phase difference of the signal and the derived reference. This finds a very important application of PAS to studies such as molecular relaxation times etc. The lock-in amplifier, responds only to the modulation frequency at which the signal also appears. So other noises, which appear at different frequencies are eliminated. The basic lock-in amplifier (LIA) is shown in fig.3.8. The signal conditioning part at the input amplifies the signal, and together with the mains frequency notch filter and the high pass filter, with cut-off at frequency f_L removes the low frequency noises. The mixing section has the inputs from the signal and the reference. The PSD forms the third part. It has a tunable low pass filter with a cut-off at frequency f_H which eliminated the high frequency noise and thus provides a flat response for the frequency region of the signal only. Other than these, the commercial LIA has various kinds of input filters, pre-amplifiers etc to suit specific applications. Figure 3.9.a. shows the spectrum of fundamental noise and fig.3.9.b., the amplitude spectrum of the common interference noise encountered with the signal. Figure 3.9.c. shows the amplitude response characteristics of the notch filter, high pass and the low pass filter indicating how the noise is removed. The low pass filter

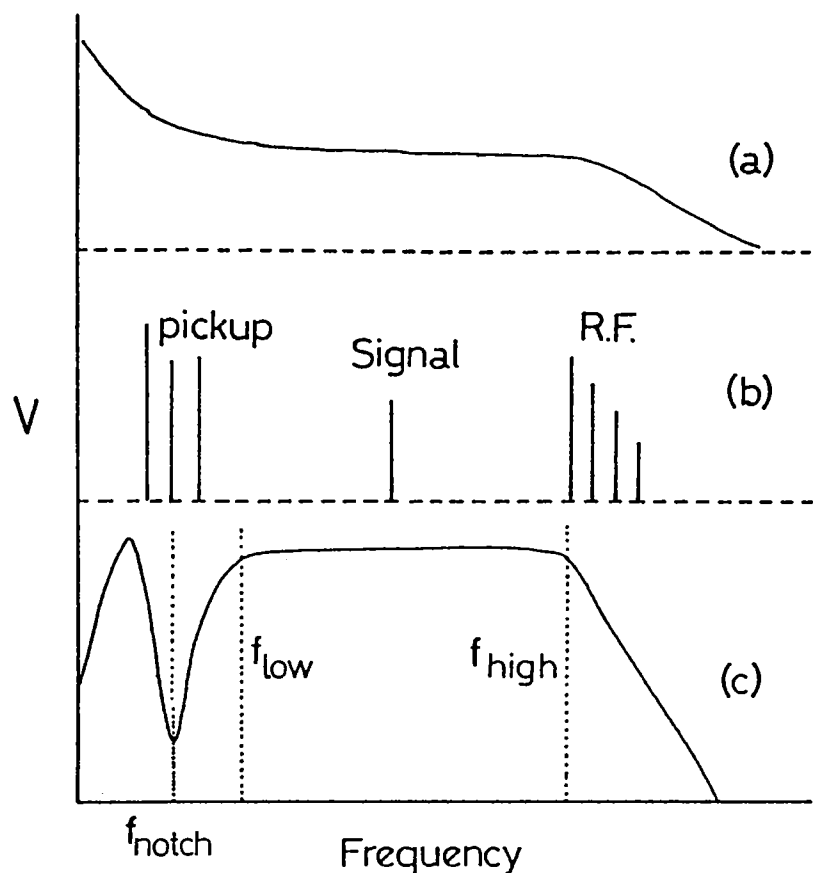


Fig.3.9. The various signals at the LIA input (a) Spectrum of the fundamental noise (b) common interference noise and signal (c) The bandpasses of the high pass, low pass and the notch filters of the LIA

is usually based on either a single or dual R-C filter giving a roll-off of either 6dB or 12dB per octave beyond the cut-off. The bandwidths are usually controlled by the time constant of the R-C. In most cases, it is best to have the lowest possible value of the time constant so that the LIA is not too sluggish in response. For optimum detection of the PA signal, an effective compromise between the time constant, sensitivity and the selection of the phase and the input filters are required so as to have a good SNR. Modern LIAs can be effectively linked to computers, thus making control, data acquisition and processing easier.

3.4.3. Noise In PA Signal

Noise has always been a serious limitation to the detection of weak PA signals. After a certain limit, it becomes difficult to distinguish the noise from the PA signal. The common types of noises encountered in PA signals are as follows, of which, some of the important ones are discussed.

- i. Background acoustic
- ii. Electronic
- iii. Brownian motion of the gas
- iv. Microphone noises and,
- v. Thermal and mechanical noises.

i. Acoustic Noises

Any PA signal not relevant to the absorption of the radiation by the sample can be grouped as the background signal and needs to be eliminated. Irrespective of its origin, the background signal is usually expressed in the form of an equivalent background absorption α_b . This value characterizes such absorption in the

medium at which a useful PA signal equal to the background signal arises. Thus α_b determines the ultimate sensitivity of the PA system. Experimentally, α_b is either determined in the PA cell away from the sample or with the sample replaced by a non-absorbing standard sample. The acoustic noises originate from different sources ie, from the ambient acoustic noise, building vibrations and the vibrations of the mechanical chopper, window absorption and due to the absorption of light scattered at the windows. Generally, the background noise in a PA cell can arise due to ;

1. Misalignment of the laser beam into the cavity and subsequent interaction of the radiation with the walls,
2. Diffraction and scattering at the input elements like diaphragm, mountings, edge of the chopper blades etc,
3. Fresnel diffraction in the windows,
4. The presence of foreign impurities with absorption bands coinciding with that of the laser frequency,
5. Hot absorption bands of different gases and multiphoton effects,
6. Weak absorption at forbidden transitions and continuum absorption.

The noise due to ambient acoustic noise, building vibrations and other mechanical vibrations can be eliminated by proper acoustic shielding of the PA cell and also by using compensation techniques such as a differential operation of the PA cell in which the signals due to these and also to the windows can be subtracted from the total signal since these noises are independent of wavelength. The absorption of light at the windows produces a signal which carries to the microphone. In the case of pulsed PAS, this can be isolated temporally, but for cw PAS, it appears in the same frequency regime as the signal. By using clean and

low absorbing windows and placing the windows far from the microphone can reduce this noise. Normalization of the PA signal for variations in the laser power also increases the SNR. Window-less operation also is possible, but only for operation at atmospheric pressure. Wavelength or Stark modulation of the absorption has a high noise rejection capability. For PA studies in flowing gases, the turbulence of the flowing gas also produces a noise. In non-resonant operation, where the modulation frequency is low and the PA signal having an inverse frequency dependence [114], some of the practical difficulties encountered are that (i) the gas inlets and outlets act as pneumatic short circuits at low frequencies, thus decreasing sensitivity, and the PA studies have to be done under sealed-off conditions thus limiting continuous monitoring of gases [34]. (ii) The power spectrum of the external as well as the noise induced by the flowing sample has a $1/f$ behavior. These can be reduced by operating the PA cell in its resonant mode and by placing the gas inlets and the windows at the nodes of the standing acoustic wave in the resonant cell. The coupling of the energy to the resonant acoustic modes from either the windows or the sample gas absorption would be quite different thus making it possible to reduce these noise. Higher modulation frequencies (\sim kHz) are used with resonant cells and microphones have lower noise in this region, and also the acoustic wave amplification at resonance overcomes the inverse frequency dependence, thus considerably reducing the noise problems. Moreover, the use of longitudinal modes of the resonance of an open tube resonator has a higher immunity to window absorptions, which is more prominent in multi-pass operations. Brewster windows can also be used to reduce window absorption and scattering noises, but the basic symmetry of a cylindrical resonator is then altered. The light scattered from the windows might strike the walls near the microphone thus producing a noise, which might be temporally close

to the signal in the case of pulsed PAS. This can be eliminated by box-car techniques and also by making the cell walls transparent and by using an absorbing layer on the outside. The scattered radiation is then transmitted by the walls and is absorbed on the outside. The signal generated there is not carried to the microphone. Baffle plates having circular aperture can be placed between the windows and the main part of the PA cavity to reduce the window absorption noise. This has a disadvantage that it drastically reduces the Q factor of the cell [115]. By keeping the cell walls highly polished, the resulting PA signal from it will be weakened, as long as the thermal mass of the cell walls is low. The signal output being inversely proportional to cell volume, the cell volume should be kept a minimum, but not too small that the signal due to the sample suffers appreciable dissipation to the walls and windows before reaching the microphone. Since the PA signal (S) is given by,

$$S \propto \frac{(k P)^{1/2}}{T} \quad \dots\dots(3.20)$$

where k , P and T are the gas thermal conductivity, pressure and temperature of the gas respectively, by introducing at higher pressures, a known gas having higher k and operating the PA system at lower temperatures, higher SNR can be obtained.

ii. Electronic Noise

The electronic noise is mainly due to the microphone, its related electronics and the pick-up due to the cables. The three general kinds of electronic noise are (i) series voltage noise (ii) shunt current noise and (iii) Resistor Johnson noise. The amplifier voltage noise is frequency independent. The thermal or Johnson noise is generated by the random motion of electrons in the resistive material at a finite temperature. The current or shot

noise are caused by discrete charge carriers when current flows through electronic devices. The Johnson and the current noise both decreases with increase in frequency. Generally, these noises occupy a frequency range far in excess of the signal frequencies of interest ie, $\sim 10^4$ to 10^8 Hz [112]. Johnson and current noise prevails at low frequencies while voltage noise dominates at higher frequencies. The cable pickup, 'hum' ripple and the saturated transformer pick-up noises all occur in the 10-200Hz region. All these noises can together be called the electronic noise. This noise level depends critically on the choice of components and layout for the system. The available miniature electret microphones have a typically broad band 1-5kHz noise of $5\mu V$ for a microphone area of 0.2cm^2 . The integration of the signal over a 10 sec time interval yields an effective bandwidth of $\sim 0.02\text{Hz}$ and a microphone noise level of 10nV . Such microphones have built-in FET pre-amplifiers, which are the main contributors to this noise. High quality commercial pre-amplifiers having noise factors $\sim 10\text{nV}/\sqrt{\text{Hz}}$, corresponding to a noise level of 3nV for a 10 sec integration time are available. By careful designing of the PA setup and the related electronics, the total noise level (including window and scattering noise) can be brought down to $10\text{-}20\text{nV}$ [25].

iii. Brownian Motion Noise

The thermal fluctuations can excite the acoustic normal modes in a cell, and thus fundamentally limit the PA sensitivity. The j^{th} normal mode excited by the Brownian motion of the gas is given by [116],

$$|A_j(\omega)|^2 = \frac{4\rho_0 c_0^2 kT}{\left\{ 1 - \left(\frac{\omega^2}{\omega_j^2} \right)^2 - \left(\frac{i\omega}{\omega_j Q_j} \right)^2 \right\} V_0 \omega_j Q_j} \quad \dots \dots \dots (3.21)$$

k = Boltzmann's constant, ρ_0 is the density and c_0 the velocity of sound in the medium.

for $\omega \ll \omega_j$,

$$|A_j(\omega)|^2 = \frac{4\rho_0 c_0^2 kT}{\omega_j Q_j V_0} \quad \dots \dots \dots (3.22)$$

The Brownian motion noise is very small and does not contribute as much to the total noise as the other sources.

iv. Microphone Noise

A condenser microphone employs a metal or a metallized foil or diaphragm mounted under a large radial tension. Acoustic pressure acting on one side of it causes motion, resulting in the change of the electrical capacitance between the diaphragm and the fixed plate. The motion of the diaphragm can be described in terms of the normal modes of vibrations in a thin plate supported around its perimeter. Only the lowest order mode of this vibration causes any appreciable change in the capacitance, ie, the mode that causes the diaphragm to bend outward in a circular shape [36].

When the microphone is connected to the input of an high input impedance amplifier, the output voltage (V_s) will be [117],

$$V_s = \frac{i(\gamma-1)V_b}{\omega \gamma P_0 \pi r_0^2 d} \left(\frac{V_m}{V_0 + V_m} \right) \alpha WL \quad \dots \dots \dots (3.23)$$

In addition to this signal generated by the light, there is also the noise generated by the Brownian motion. When the PA cell is small, the effective restoring force of the microphone is altered, since the movement of the diaphragm is also hindered by the compression of the gas in the cell itself. Thus, the Brownian motion signal noise is,

$$|V_{sn}(\omega)|^2 = \frac{4\rho_0 c_0^2 kT}{\omega_m^Q m v_m \left(1 + \frac{v_m}{v_0} \right)^2} \quad \dots \dots \dots (3.24)$$

The signal to noise ratio (SNR) is therefore,

$$\frac{(s/n)^2}{|V_{sn}(\omega)|^2} = \frac{|V_s(\omega)|^2}{|V_{sn}(\omega)|^2} = \frac{(\gamma-1)^2}{4kT\omega^2} \left(\frac{L\pi r_0^2}{v_0} \right)^2 \left(\frac{\omega_m Q_m}{\chi} \right) \alpha^2 \omega^2 \quad \dots \dots \dots (3.25)$$

The factor $(\gamma-1)^2$ can be increased to some extend by using mono atomic gases like helium. The SNR can also be improved by using the PA cell at lower temperatures.

The factor $\left(\frac{L\pi r_0^2}{v_0} \right)^2$ can be regarded as a coupling coefficient between the microphone and the PA cavity. This increases if the microphone diameter is increased and smaller cross-sectional area of the cell is used.

The SNR increases with frequency ω provided $\omega > 1/\tau_0$. At lower frequencies, the $1/f$ noise of the pre-amplifier predominates.

3.5. Scaling Laws For PA Cells

The performance of a PA system can be predicted to some extend. These help in comparison of the resonant and non-resonant operations of the PA cell.

Let R be the responsivity of the system. It is the measure of the electrical signal produced by the microphone for an unit amount of incident power absorbed by the sample. In both resonant and non-resonant operations, the electrical signal is proportional to the product of the area, sensitivity of the microphone, the incident power P_0 and the fraction of the incident power absorbed per unit length of the sample chamber. For small attenuations of the excitation beam per pass, the fractional absorption/unit length is,

$$A_a = \sigma C_f N \quad \dots \dots \dots (3.26)$$

σ is the absorption cross-section

C_f is the fractional concentration of the sample

N the total gas density (molecules/cc) at STP

The signal,

$$S = R P_0 A_a \quad \dots \dots \dots (3.27)$$

The system sensitivity is defined as the system response for a unity SNR. A convenient parameter (A_e) for the assessment of sensitivity of a PA system in the presence of electrical noise can be obtained from the total electric noise V_e by,

$$A_e = \frac{V_e}{R P_0} \quad (\text{cm}^{-1}) \quad \dots \dots \dots (3.28)$$

Unity SNR is obtained when $A_e = A_a$

It is difficult to establish scaling laws for the background signal arising from the window absorptions and scattering. If the scattering occurring was uniform along the length of the cavity, then the induced signal would act in the same way as a residual concentration of the absorbing sample and therefore, the parameter A_b due to the background signal V_b (window absorption + scattering) is,

$$A_b = \frac{V_b}{R P_0} \quad (\text{cm}^{-1}) \quad \dots\dots(3.29)$$

and would be independent of the length of the cavity. In the case of window heating alone, the value of A_b will be inversely proportional to the length of the cavity with R and P constant. Although A_b would be expected to vary with chamber geometry and optical configuration, it is nevertheless, a convenient parameter for comparing resonant and non-resonant modes. It has been shown that the performance parameters for a PA cell in both resonant and non-resonant modes indicate that the responsivity for resonant systems is ~ 14 times non-resonant one [25], other conditions remaining the same.

The dynamic range and sensitivity may be calculated directly from these parameters. For an absorption cross-section σ , the SNR of unity corresponds to a fractional concentration at atmospheric pressure of,

$$C_f(A_c) = \frac{A_c}{\sigma N} \quad \dots\dots(3.30)$$

The background signal, in terms of residual concentration is,

$$C(A_b) = \frac{A_b}{\sigma N} \quad \dots \dots \dots (3.31)$$

Although $C(A_c)$ is inversely proportional to P , and can be reduced by powerful excitation sources, but so long as saturation of the PA signal does not take place. $C(A_b)$ should be independent of power.

The upper limit of concentration, C_{max} for which the PA signal is linearly proportional to the concentration is determined by the absorption of the excitation beam. If, for example, a 2% linearity is demanded, then the product of A_e and the effective path length L_{eff} must be less than 0.02, or,

$$C_{max} = \frac{0.02}{\sigma N L_{eff}} \quad \dots \dots \dots (3.32)$$

Since the most stringent limit to the linear dynamic range is the background signal, all efforts must be done to bring them down to the minimum possible.

For pulsed sources, it must be noted that the laser power is not sufficient enough to deplete the ground state population of the absorbing molecule. The number of photons/Joule of the incident energy is $5.05 \times 10^{18} \lambda^{18}$, where, λ is the wavelength of optical radiation in microns. The fractional depletion of the measured species, assuming that all the molecules of the species are initially in the ground state of the absorption transition,

$$\Gamma = 5.05 \times 10^{18} \frac{\lambda \sigma E}{A} \quad \dots \dots \dots (3.33)$$

where, E is the total energy per pulse (Joules) and A the area of cross-section of the beam.

3.5.1. Noise Equivalent Power (NEP)

The NEP is the input heat, the response which is equal to the noise intensity. It can also be calculated from the pressure response (R_p) of the PA signal and the pressure fluctuations at resonance (N_p) [34].

$$R_p = \frac{Q}{\omega_r V_o} \quad \dots \dots \dots (3.34)$$

and,

$$N_p = \left[\frac{4kTB\rho c_o}{\pi R_o^2} \right]^{1/2} \left[\frac{4R_o}{d_h} \right]^{1/2} \quad \dots \dots \dots (3.35)$$

where, ω_r is the cell resonance frequency, R_o the cell radius, B the resonance bandwidth, ρ the density, c_o the velocity of sound in the sample gas and, d_h the gas thermal diffusion length. Thus the NEP is,

$$\text{NEP} = \frac{N_p}{R_p} = 2 \left[\frac{4kT^2 B k_h A'}{d_h} \right]^{1/2} \quad \dots \dots \dots (3.36)$$

For a non-resonant closed PA cell of radius R_o and length L , the equivalent trace gas concentration C_{eq} induced by total absorption of radiation at window surface is [34],

$$C_{eq} = \left(\frac{2}{\alpha L} \right) \left(\frac{k_1 C_2}{k_2 C_1} \right)^{1/2} \quad \dots \dots \dots (3.37)$$

where, k_2 = Specific heat conductivity of air
 k_1 = Specific heat conductivity of absorbing window
 C_1 = Specific heat capacity of absorbing window
 C_2 = Specific heat capacity of air

3.6. Conclusions

The various aspects of the instrumentation involved in the PA studies have been discussed. Different systems and sub-systems like the light source, PA cell, signal processing etc that make up the PA experimental setup are discussed in detail. The acoustic and electronic noise encountered in PA experiments are also briefly given. The scaling laws for PA cells are also discussed. Several of the parameters described above in connection with the PA instrumentation have great relevance in the context of gas phase PA studies.

3.7. References

- [1] Tam A C, "Ultrasensitive Spectroscopy" Ed. Kilger D S, (Academic Press, New York), 1983, Chapter 1
- [2] Rockley M G, *Chem.Phys.Lett.*, 68, 455, (1979)
- [3] Royce B S H et al, *Ultrasonic.Symp.Proc.*, p.62, (1980)
- [4] Farrow M M et al, *Appl.Opt.*, 17, 1093, (1978)
- [5] Gelbwachs J A, "Optoacoustic Spectroscopy And Detection" Ed. Y H Pao, (Academic press New York), 1977, p 79
- [6] Keely P L, "Optoacoustic Spectroscopy And Detection" Ed. Pao Y H, (Academic press New York), 1977, p 113
- [7] Claspy P C, Ha C and Pao Y H, *Appl.Opt.*, 16, 2972, (1972)
- [8] Siebert D R, West G A and Barret J J, *Appl.Opt.*, 19, 53, (1980)
- [9] Patel C K N, *Science*, 202, 157, (1978)

- [10] Viappiana C and Rivera G, *Meas.Sci.&.Tech.*, 1, 1257, (1990)
- [11] Kawabata Y *et al*, *Anal.Chem.*, 55, 1419, (1983)
- [12] Castleden S L *et al*, *Anal.Chem.*, 53, 2228, (1981)
- [13] Lehmann W *et al*, *Anal.Chem.*, 49, 549, (1977)
- [14] Moses E I and Tang C L, *Opt.Lett.*, 1, 115, (1977)
- [15] Kreuzer L B and Patel C K N, *Science*, 173, 45, (1971)
- [16] Kavaya M J *et al*, *Appl.Opt.*, 18, 2602, (1979)
- [17] Bechthold P S, "Photoacoustic Effect" Ed. E Luscher *et al*, (Friedr.Vieweg & Sohn, Wiesbaden) p 375, 1984
- [18] Morse P M and Ingard K V, "Theoretical Acoustics" (McGraw-Hill, New York, 1968)
- [19] Karbach A, and Hess P, *J.Chem.Phys.*, 83, 1075, (1988)
- [20] Karbach A and Hess P, *J.Chem.Phys.*, 84, 2945, (1986)
- [21] Gerlach G and Amer N M, *Appl.Phys.*, 23, 319, (1980)
- [22] Adams K M, *Appl.Opt.*, 27, 4052, (1988)
- [23] Fiedler M and Hess P, *Topics In Current Physics Vol.46: Photoacoustics, Photothermal and Photochemical Processes in Gases* Ed:Hess P, (Springer, Heidelberg), p89, (1989)
- [24] Rosengren L G, *Appl.Opt.*, 14, 1960, (1975)
- [25] Dewey C F, *Opt.Engg.*, 14, 483, (1978)
- [26] Zarov V P and Letokhov V S, "Laser Optoacoustic Spectroscopy" Springer Series in Optical Sciences,Vol.37, (Springer-Verlag, Berlin, 1985)
- [27] Moldover M R *et al*, *Phys.Rev.Lett*, 60, 249, (1988)
- [28] Avramides E and Hunter T F, *Mol.Phys.*, 48, 1331, (1983)
- [29] Parker J G and Ritke D N, *J.Chem.Phys.*, 59, 3713, (1973)
- [30] Bass H E and H X Yan, *J.Acoust.Soc.Am.*, 74, 1817, (1983)
- [31] Fiedler M and Hess P, *J.Chem.Phys.*, 93, 8693, (1990)
- [32] Goldan P D and Goto K, *J.Appl.Phys.*, 45, 4350, (1974)
- [33] Max E and Rosengren L G, *Opt.Comm.*, 11, 422, (1974)
- [34] Kritchman E *et al*, *J.Opt.Soc.Am.*, 68, 1257, (1978)
- [35] F J M Harren, PhD Thesis "The PA Effect Refined and Applied to Biological Problems" Katholieke University, The Netherlands, p 71, (1988)
- [36] Rosencwaig A, "Photoacoustics and Photoacoustic Spectroscopy" (Wiley Interscience, New York), (1983)

- [37] Shaw R W, *Appl.Phys.Lett.*, **35**, 253, (1979)
- [38] McClenney W A *et al*, *Appl.Opt.*, **20**, 650, (1981)
- [39] Busse G and Herboeck H, *Appl.Opt.*, **18**, 3959, (1979)
- [20] Nordhaus O and Pelzl J, *Appl.Phys.*, **25**, 221, (1981)
- [41] Ferneilus N C and Hass T W, *Appl.Opt.*, **17**, 3348, (1978)
- [42] Ferneilus N C, *Appl.Opt.*, **18**, 1784, (1979)
- [43] Lord Rayleigh, "Theory of sound" Vol.II, (Dover, New York, 1945), p 189-192
- [44] Patel C K N and Kerl R J, *Appl.Phys.Lett.*, **30**, 578, (1977)
- [45] Karbach A *et al*, *Chem.Phys.*, **82**, 427, (1983)
- [46] Dewey C F *et al*, *Appl.Phys.Lett.*, **23**, 633, (1973)
- [47] Thomas L J *et al*, *Appl.Phys.Lett.*, **32**, 736, (1978)
- [48] Nodov E, *Appl.Opt.*, **17**, 1110, (1978)
- [49] Aoki T, Katayama M, *Jap.J.Appl.Phys.*, **10**, 1303, (1971)
- [50] Koch K P and Lahmann W, *Appl.Phys.Lett.*, **32**, 289, (1978)
- [51] Kamm R D, *J.Appl.Phys.*, **47**, 3550, (1976)
- [52] Ioli N, Violino P, and Meucci M, *J.Phys.:E*, **12**, 168, (1979)
- [53] West G A *et al*, *Rev.Sci.Instr.*, **54**, 797, (1983)
- [54] Roper J, Neubrand A and Hess P, *J.Appl.Phys.*, **64**, 2838, (1988)
- [55] Stella G *et al*, *Chem.Phys.Lett.*, **39**, 146, (1976)
- [56] Reddy K V *et al*, *J.Chem.Phys.*, **76**, 2814, (1982)
- [57] Harren F J M *et al*, *Appl.Phys.:B*, **50**, 137, (1990)
- [58] Davidsson J *et al*, *J.Phys.Chem.*, **94**, 4069, (1990)
- [59] Gelfand J *et al*, *Chem.Phys.Lett.*, **65**, 201, (1979)
- [60] K V Reddy, *J.Mol.Spect.*, **82**, 127, (1980)
- [61] Wong J S and Moore C B, "Lasers and Applications", Editors :Guimaraes W O M *et al.*, (Springer, Berlin, 1981), p157
- [62] Dewey C F and Flint H R, "Technical Digest to the Topical Meeting on Photoacoustic Spectroscopy" Optical Society of America, 1-3 August, Ames, Iowa, USA, 1979
- [63] Efthimiades D and Burt J A, *Appl.Opt.*, **24**, 2450, (1985)
- [64] Zarov V P, "Optoacoustic Methods of Laser Spectroscopy", (Nauka-Novosibirsk, 1982), p126
- [65] Poizat O and Atkinson G H, *Anal.Chem.*, **54**, 1485, (1982)
- [66] Cahen D *et al*, *Rev.Sci.Instrum.*, **49**, 1206, (1978)

- [67] M W Sigrist, Brenegger S and Meyer P L, *Topics in current Physics Vol.46: "Photoacoustics, Photothermal and Photochemical Processes In Gases"* Ed:Hess P, (Springer, Heidelberg, 1989), p190,
- [68] Hoshimiya T, *Jap.J.Appl.Phys.*, 22, 203, (1983)
- [69] Jalink H and Bicanic D, *Appl.Phys.Lett.*, 55, 1507, (1989)
- [70] Hammerich M, Sorensen L V, Olafsson A and Henningsen J, Conference proceedings of the " 7th Topical International Meeting on Photoacoustic and Photothermal Phenomena", paper # O IX/5, p405, The Netherlands, 1991
- [71] Miklos A and Lorinez A, *Appl.Phys.:B*, 48, 213, (1989)
- [72] Tilden S B and Denton M B, *Appl.Spectos.*, 39, 1022, (1986)
- [73] Marinero E E and Stuke M, *Rev.Sci.Instrum.*, 50, 241, (1979)
- [74] P M Morse "Vibrations and Sound", (McGraw-Hill, New York, 1936)
- [75] Sessler G M and West J E, *J.Acost.Soc.Am.*, 34, 1787, (1962)
- [76] Sessler G M and West J E, *J.Acost.Soc.Am.*, 35, 1354, (1963)
- [77] Sessler G M and West J E, *J.Acost.Soc.Am.*, 40, 1433, (1966)
- [78] Sessler G M and West J E, *J.Acost.Soc.Am.*, 53, 1589, (1973)
- [79] Mason W P and Thruston R N, "Physical Acoustics" vol.14, (Academic Press, New York, 1979)
- [80] Juarez J A G, *J.Phys.E:Sci.Instrum.*, 22, 804, (1989)
- [81] Tam A C and Patel C K N, *Opt.Lett.*, 5, 27, (1980)
- [82] Patel C K N and Tam A C, *Appl.Phys.Lett.*, 34, 467, (1979)
- [83] Tam A C, *Rev.Mod.Phys.*, 53, 517, (1981)
- [84] A C Tam, *Rev.Mod.Phys.*, 58, 381, (1986)
- [85] Leite R C C et al, *Appl.Phys.Lett.*, 5, 141, (1964)
- [86] Solimini D, *Appl.Opt.*, 5, 1931, (1966)
- [87] Whinnery J R, *Acc.Chem.Res.*, 7, 225, (1974)
- [88] Sell J A, "Photothermal Investigations of Solids and Fluids" (Academic Press, New York, 1988), p 213
- [89] Higashi T et al, *Anal.Chem.*, 56, 2010, (1984)
- [90] Banish R M et al, *J.Appl.Phys.*, 64, 2907, (1988)
- [91] Chen G and Yeung E S, *Anal.Chem.*, 60, 864, (1988)
- [92] Ventzek P L G et al, *J.Appl.Phys.*, 70, 587, (1991)
- [93] Zapka W and Tam A C, *Appl.Phys.Lett.*, 40, 310, (1982)

- [94] Rose A, Vyas R and Gupta R, *Appl.Opt.*, **24**, 4626, (1986)
- [95] A C Tam, Conference proceedings of the " 7th Topical International Meeting on Photoacoustic and Photothermal Phenomena", paper # P IX/14A, p.365, The Netherlands, 1991
- [96] Tam A C, "Photothermal Investigations of Solids and Fluids" Ed. J A Sell, (Academic Press New York), 1988, chapt 1.
- [97] Brilmyer G H et al, *Anal.Chem.*, **49**, 2057, (1977)
- [98] Parker H et al, *Chem.Phys.*, **23**, 117, (1977)
- [99] Choi J G et al, *J.Appl.Phys.*, **52**, 6016, (1981)
- [100] De Paula M H et al, *J.Appl.Phys.*, **64**, 3722, (1988)
- [101] Miles R B et al, *J.Appl.Phys.*, **51**, 4543, (1980)
- [102] Tam A C et al, *Appl.Opt.*, **21**, 69, (1982)
- [103] Park S M and Diebold G J, *Rev.Sci.Inst.*, **58**, 772, (1987)
- [104] Munir Q and Weber H D, *Opt.Comm.*, **52**, 269, (1984)
- [105] Goldan P and Goto K, *J.Appl.Phys.*, **45**, 4350, (1974)
- [106] Smith R A, Jones F E and Charmar R P, "The Detection and Measurement of Infra-Red Radiation" (Oxford University, London, 1968)
- [107] Voigtman E et al, *Anal.Chem.*, **53**, 1442, (1981)
- [108] Beitz J V et al, *Rev.Sci.Inst.*, **61**, 1395, (1990)
- [109] Chakrapani G, et al, *Rev.Sci.Inst.*, **58**, 1871, (1987)
- [110] Malmstadt H V et al, "Electronic Measurement for Scientists" (Benjamin, London, 1974)
- [111] Williams P and Lam H W, *J.Phys.E:Sci.Instrum.*, **18**, 23, (1985)
- [112] Meade M L, "Lock-in Amplifiers : Principles and Applications", (Peter Peregrinus Ltd, London, 1983)
- [113] Dicke R H, *Rev.Sci.Instr.*, **17**, 268, (1946)
- [114] Kreuzer L B, *J.Appl.Phys.*, **42**, 2934, (1971)
- [115] Dewey C F, "Optoacoustic Spectroscopy and Detection", Ed. Y H Pao, (Academic Press, New York, 1977), p 47
- [116] Kittel C "Elementary Statistical Physics II" (Wiley, New York, 1958)
- [117] Olson H F, "Elements of Acoustic Engineering" (Van Nostrand-Reinhold, Princeton, 1947), pp. 220-224

3.8. Symbols and Notations

A	Laser beam cross sectional area
A_h	Heat transport ratio
A'	Longitudinal tube wall area
A_a	Fractional absorption/unit length
A_e	Sensitivity of PA system with noise
A_b	Sensitivity of PA system with background signal
A_c	Cross section area of coupling tube
$A_j(\omega)$	Amplitude of j^{th} mode
α_b	Background absorption coefficient
α_{\min}	Minimum detectable absorption
$\alpha_{mn}^{n\text{th}}$	n^{th} zero solution of the derivative of the m^{th} Bessel function
α_g, α_w	Absorption strengths of sample gas and window
B	Resonance bandwidth
C_f	Fractional concentration
C_1, C_2	Specific heat capacity of window, air
C_g, C_w	Specific heats of sample gas and window
C_{eq}	Equivalent trace gas concentration
C_{\max}	Upper limit of concentration
C	Capacitance
c_0	Velocity of sound in the gas filling the cavity
d	Microphone capacitance spacing
d_h	Gas thermal diffusution length
E	Total energy/pulse
f_{kmn}	Frequencies of resonance in a cylindrical cavity
f_1, f_2	Different modulation frequencies
f_h	Highest harmonic of significance in the measured waveform
F	Damping force
ϕ	Phase lag
Γ	Fractional depletion of measured species

γ	Ratio of specific heats
h	Distance between microphone and the optical axis of the cavity
I_0	Incident light intensity
k	Gas thermal conductivity
k	Boltzmann constant
k_h	Gas specific heat conductivity
k_1, k_2	Specific conductivity of window, air
k, m, n	The longitudinal, azimuthal and radial mode numbers
k_g, k_w	Thermal conductivities of sample gas and window
λ_1, λ_2	Different wavelengths
L_1, L_2	Different lock-in-amplifiers
L_w	Thickness of window
L_b	Length of the buffer volume
L_{sp}	Ultimate spatial resolution
L_{eff}	Effective path length
l_c	Length of the coupling tube
m	Mass of the diaphragm
η	Viscosity
N	Total gas density at STP
NEP	Noise equivalent power
N_p	Pressure fluctuations at resonance
P_{ic}	Intra-cavity power
P_{ex}	Extra-cavity power
p_g, p_w	PA signals due to sample gas and absorbing window
P	Gas pressure
P_0	Incident power
Q_j	Q factor of the j^{th} mode
Q_H	Quality factor of the Helmholtz resonator
$\bar{Q}(\omega_r)$	Characterizes the degree of PA signal increase at resonance
Q_m, Q'_m	Actual and effective Q factor of microphone
r_0	Radius of the microphone diaphragm

R	Resistance
R_m	Reflection coefficient of mirror
R	Responsivity of the PA system
R_o	Radius of the cavity
R_b	Radius of the buffer volume
R_p	Pressure response
ρ_o	Density
SNR	Signal-to-noise ratio
S	PA signal
σ	Absorption cross section
T_g	Time between sucessive openings of the gate
T_o	Transmittance of the output coupler
T	Gas temperature
T_{eff}	Effective time constant
τ_r	Time constant of the low-pass filter
τ_t	Total relaxation time
τ_R	Total time resolution of the PA system
t_p	Laser pulse duration
τ_n	Non-radiative relaxation time
T_s	Sampling time
τ_c, τ_r	Collisional and radiative relaxation times
τ_{nr}	Thermal relaxation time
τ_o	Damping time
V_o	Volume of the cavity
V_1, V_2	Volumes of the two resonating cavities
V_m	Microphone equivalent volume
V_e	Total electric noise
V_s	Output voltage of the microphone
V_b	Microphone bias voltage
V_b	Background signal
V_{sn}	Brownian motion signal noise
W	Laser power
ω_m	Resonance frequency of microphone

ω_H Resonance frequency of Helmholtz resonator
 ω Modulation frequency
 ω_0 Resonance frequency
 x Number of reflection passes
 χ Restoring force

CHAPTER IV

EXPERIMENTAL DETAILS OF GAS PHASE PHOTOACOUSTICS

ABSTRACT

This CHAPTER DETAILS THE VARIOUS SYSTEMS AND SUBSYSTEMS EMPLOYED IN THE EXPERIMENTAL SETUP FOR BOTH PULSED AND CW GAS PHASE PA STUDIES. THE DESIGN, FABRICATION AND THE CHARACTERISTICS OF THE THREE KINDS OF PA CELLS USED IN THESE STUDIES ARE DESCRIBED. THE ACOUSTIC RESONANCE CHARACTERISTICS OF THE DUAL CAVITY DIFFERENTIAL CELL ARE ALSO GIVEN.

CHAPTER IV

EXPERIMENTAL DETAILS OF GAS PHASE PHOTOACOUSTICS

4.1 Introduction

As discussed in Chapter III, a typical PA system requires a light source, a modulator if the source is cw, the appropriate PA cell and the detection electronics. For any kind of PA studies, it must be ensured that the experimental setup is appropriate to the kind of study and to the result sought. This means that the light source, type of PA cell and the signal processing technique also vary with the sample to be studied. Optimization of the PA setup is essential before any actual measurement is performed. This can be achieved only by trial and error methods. For proper detection and processing of the PA signal, it must be taken care that the noise interference (both acoustic as well as electrical) be kept at the minimum possible level. The light source must also be as stable as possible and the PA cell well isolated acoustically from the ambient acoustic noise sources.

The major difference between the pulsed and cw PA detection is in the fact that the former is detected in the time domain while the latter is in the frequency domain. This fact requires that different type of detection techniques have to be used in the respective cases. Nevertheless, the basic principle of PA generation in both the cases remains the same. Most of the noise in the case of the pulsed PA signal can be effectively

removed by the gated integration technique, but greater care must be taken to increase the SNR in the case of cw PA detection, which is in the frequency domain, and hence the signal and the noises appear in the same domain. As a result, it is difficult to isolate the weak PA signal from the noise as compared to the pulsed technique even though the phase sensitive detection technique does eliminate a major part of the noise.

4.2 Pulsed PA Experimental Setup

The schematic diagram of the pulsed PA experimental setup to study gas phase samples is shown in fig.4.1. The laser source for these experiments is a pulsed tunable dye laser pumped by a Q-switched Nd:YAG laser capable of providing a second harmonic output (532 nm). The laser energy is monitored by energy meters. The PA cell is a simple single cavity cell used in its non-resonant mode. The pre-amplifier is used to amplify the weak PA signals detected by the microphone. The detected PA pulse is processed using a fast gated integrator and a box-car averager. An oscilloscope is used to monitor the PA and the laser pulses. The averaged PA signal is ratioed with respect to the laser energy so as to get a normalized PA spectrum. A chart recorder is used to record the spectrum.

Increase in the SNR without compromising on the PA signal can be obtained only by trial and error. One has to try out different combinations of laser pulse rate, gate width, the number of pulses over which averaging is performed, the wavelength scanning speed of the dye laser and of course, the input and output filters of the box-car and the sensitivity controls of the gated integrator, signal processor and the chart recorder to obtain an optimum combination which provides good SNR as well as reasonably fast and faithful response to the varying PA signal.

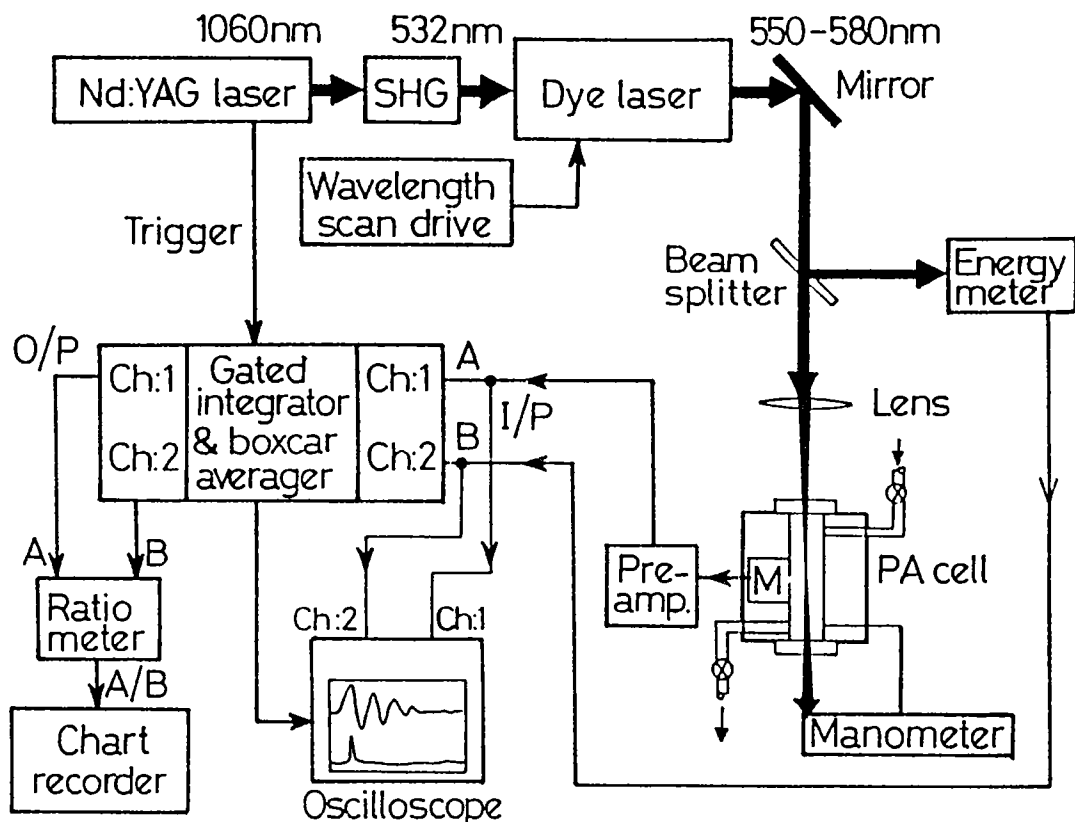


Fig.4.1. Schematic diagram of the pulsed PA experimental setup

4.2.1. The Pulsed Laser

The pulsed pump laser used here is an electro-optically Q-switched Nd:YAG laser having a fundamental output of $1.06\mu\text{m}$ (Quanta Ray DCR 11). The diffraction coupled resonator delivers a 'doughnut' shaped beam profile (fig.4.2.) at energies of the order of 275mJ at $\sim 10\text{nsec}$ pulse width with a power stability of $\pm 4\%$ [3]. The laser is capable of pulsing at a rate of 1-16 pulses/sec. It has a second harmonic generator (KD^{*}P crystal) which can be placed in the path of the fundamental beam to provide the second harmonic output at 532 nm at less than 10 nsec pulse width with a conversion efficiency of approximately 50%. Figure 4.2. shows the schematic of the Nd:YAG laser. Higher order harmonics at 355nm and 266nm can be obtained by introducing the appropriate crystals in the beam path. The laser beam has a typical linewidth of $< 1\text{cm}^{-1}$ and a beam divergence of $< 0.5\text{mrad}$. The laser provides trigger outputs to synchronize the oscilloscope, energy meter, box-car averager etc.

4.2.2. The Pulsed Dye Laser

To obtain continuously varying wavelengths, a tunable laser has to be employed. In this case a pulsed dye laser (Quanta Ray PDL 2) is used. The schematic of this laser is shown in fig.4.3. It is pumped by the second harmonic output at 532nm of the above mentioned Nd:YAG laser. The dichroic mirror assembly separates the remaining $1.06\mu\text{m}$ part from the 532nm beam. One half of this beam is used to pump the Rhodamine 590 (in methanol) dye in the side pumped oscillator part of the laser and the other to excite the dye in the end pumped amplifier part of the tunable laser. In the case of certain other dyes, a pre-amplifier has to be introduced in the oscillator part of the laser.

Wavelength tuning is performed by the stepper motor

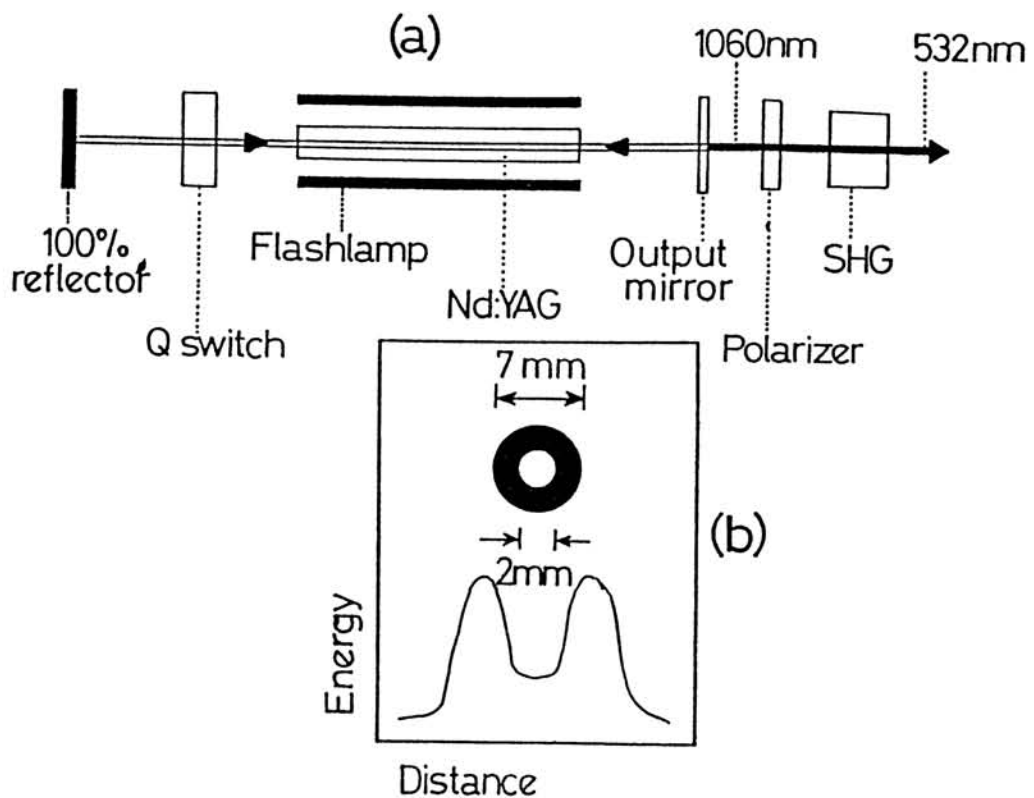


Fig.4.2. Schematic diagram of the (a) Nd:YAG laser (b) Beam profile of the Nd:YAG laser

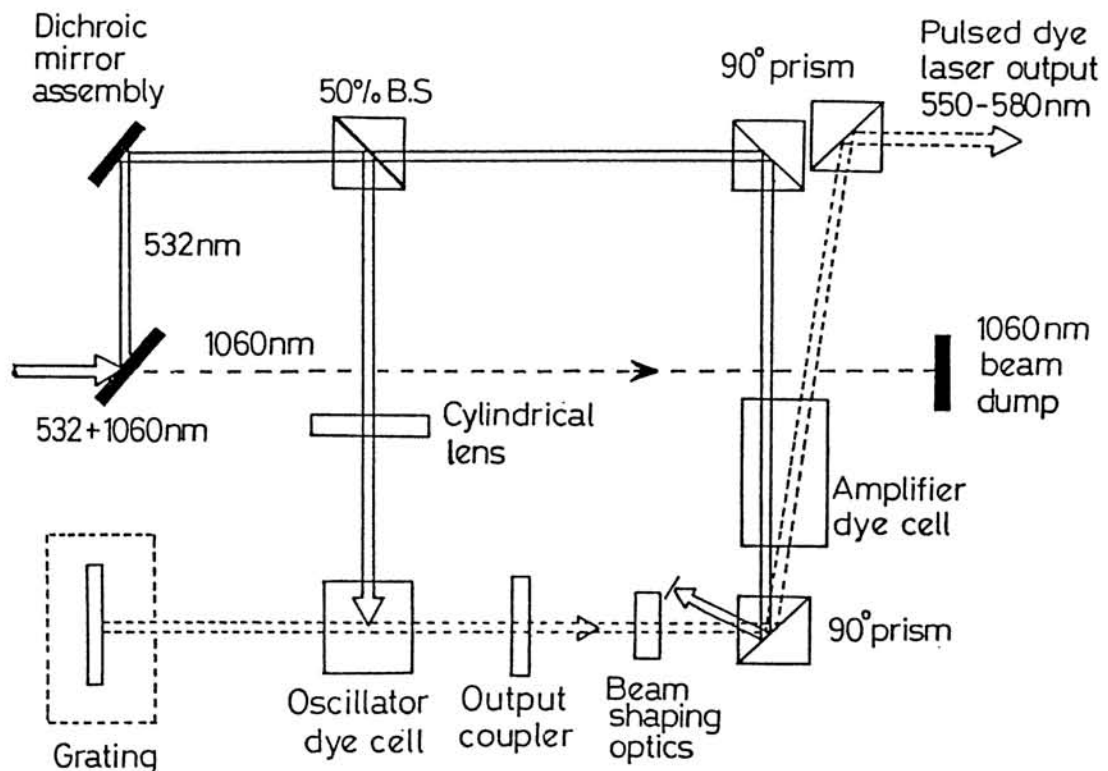


Fig.4.3. Schematic diagram of the pulsed dye laser

attached to the grating element in the oscillator part, which is placed in a vacuum enclosure to enable pressure tuning of the cavity. The stepper motor can vary the wavelength at a minimum of 0.04nm/step. In this configuration, this dye laser can provide a continuous wavelength output from \sim 540 to 580 nm peaking at \sim 564nm [4]. The wavelength reading is obtained from a factory calibrated readout provided on the dye laser assembly. The wavelength readings were checked often using a monochromator. Peak powers of the order of several megawatts can be obtained and this is ideal to probe the non-linear effects in the samples.

4.2.3. The Laser Energy Monitors

It is quite important to measure accurately as far as possible the laser energy that is made to be incident on the sample in the PA cell, specially for experiments involving non-linear effects since they have a strong power dependence. In these experiments, two kinds of laser energy/power meters have been used. For $1.06\mu\text{m}$ measurements, an on-line energy meter is utilized (Delta Developments). This is placed in the path of the beam from which a small part is sampled and detected by a photodiode and the calibrated energy is displayed. This has the advantage for single shot measurements since the actual energy of the laser pulse used can be obtained. It also provides a signal pulse proportional to the laser energy and this is used for normalizing the PA signal since the pulse-to-pulse energy variation, specially at lower laser energies vary from 5 to 10%. For measuring dye laser outputs, a part of the beam is reflected off and measured using a calorimetric power meter (Scientech model 362 or a Coherent-Labmaster with the appropriate measuring head). Usually, the energy readings are taken in the main beam path before or after the experimental data has been recorded.

4.2.4. The Pulsed PA Cell

The PA cell used for pulsed PA studies is a closed, non-resonant one made of aluminum with a cavity diameter of 6mm and a length of 11cm (fig.4.4.). The miniature electret microphone (Knowles BT 1759) is placed in a side chamber drilled perpendicular to the direction of propagation of the laser beam. The microphone is coupled to the cell cavity by means of a small hole of 1mm diameter. The cell cavity is sealed by quartz windows of thickness 3mm and diameter 2.5cm, which are held in place by aluminum flanges and neoprene 'O' rings. Gas inlet and outlets are provided and the needle valves attached to them control the gas flow in and out of the cell. The cell can be thus operated at low as well as high pressures up to 1 atmosphere. A rotary pump is used to evacuate the PA cell before a gas fill at the required pressure. The focused laser beam traverses along the longitudinal axis of the cavity in such a way that the beam waist is smallest in the vicinity of the microphone. Care must be taken to avoid the laser beam from scattering and striking the walls of the chamber since this will produce typical high amplitude signals which are not characteristic of the sample. By monitoring the PA signal on an oscilloscope while aligning the laser beam through the cell it is possible to avoid these spurious signals. Also, the focused laser beam should not fall on the quartz windows since they are likely to get damaged in the process. The whole PA cell was mounted on a stand which again, is placed on vibration damping materials to reduce the ambient vibrations. Since in the case of pulsed PA detection, the different noises can be effectively isolated temporally from the sample signal, and due to the higher PA signal levels obtained by high peak power pulsed lasers, it is not necessary that the resonance characteristics of the PA cell be used for improving the SNR. Since the windows are placed close to the chamber and the gas

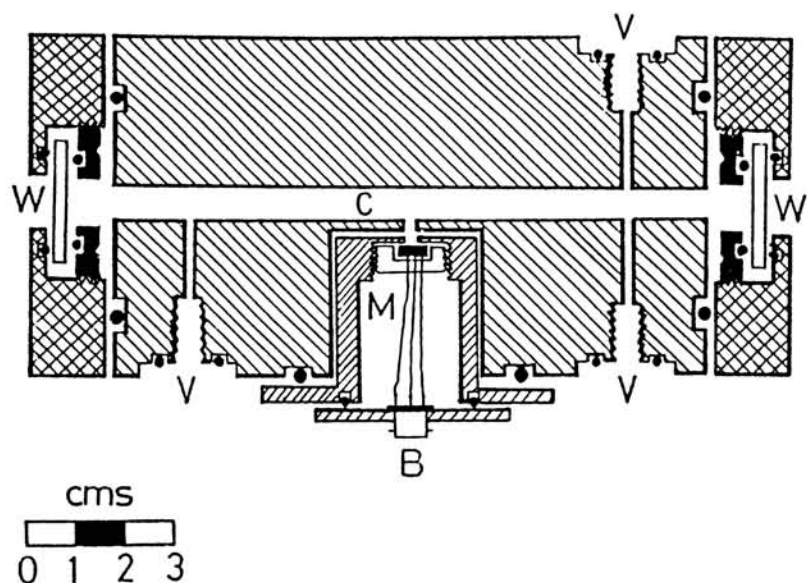


Fig.4.4. Schematic of the single cavity PA cell used for pulsed PA studies. C - cavity, V - gas inlet/outlet ports
M - microphone chamber, W - window, B - connector

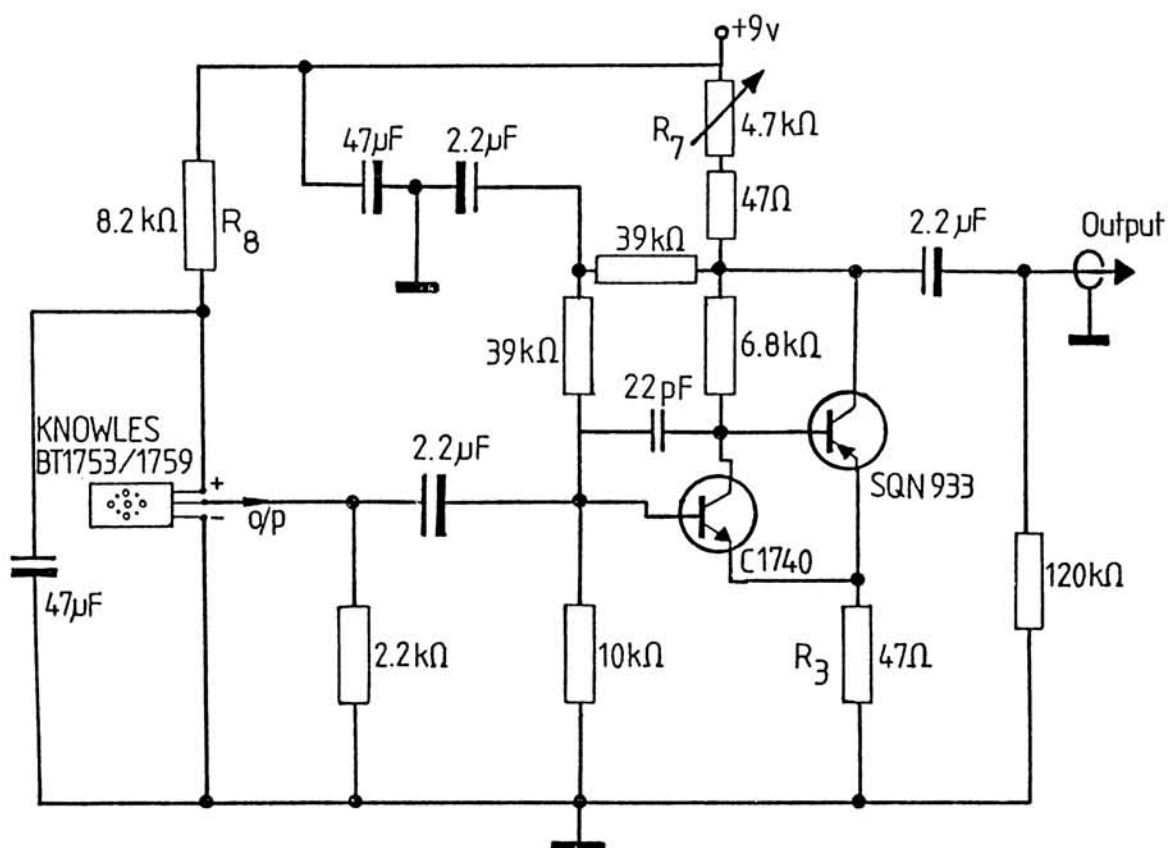


Fig.4.5. The circuit diagram of the electret microphone pre-amplifier

inlets, it is required that the windows are cleaned frequently so as to avoid damage due to the laser beam specially while using samples like formaldehyde, which tend to polymerize into a white powder on the windows and the cell walls while nitrogen dioxide gets adsorbed on to the cell walls and to the epoxy sealings in the cell. This makes it necessary for the cell to be frequently cleaned thoroughly. Also, the microphone, being exposed to these samples, tends to deteriorate in sensitivity due to contamination and thus needs to be changed as and when required.

4.2.5. The Microphone Pre-Amplifier

The signals detected by the electret microphone are usually very weak. Since the typical capacitance variations that are generated in the electret is of the order of a few pico-farads, its impedance at audio frequency is very high and thus its output needs to be fed to circuit with a high input impedance which is usually a FET source-follower buffer stage built into the microphone capsule. This acts as an impedance transformer with typical output impedances of a few hundred ohms. The bias voltage needed for the microphone is to be supplied externally. The electret microphone pre-amplifier used here is a two stage transistor amplifier having high gain and low noise. Fig.4.5. shows the circuit diagram of this pre-amplifier. The microphone bias (1 to 9v dc for BT1759) is provided by the voltage dropped at R_8 and is decoupled by the $2.2\mu F$ capacitor. R_1 is the load for the FET buffer. The amplifier is a two stage circuit consisting of low noise transistors SQN 933 and C1740. Its input impedance is $\sim 8k\Omega$ and the gain determined by the ratio of $R_7:R_3$. The potentiometer in series with R_7 provides continuous gain up to 100 from unity. The gain is adjusted so that the PA signal is not saturated or clipped. The circuit consumes 1.5mA of current and is powered by a 9v battery to avoid ripple. For higher frequency operations, R_7 can be decreased which reduces the output impedance

of the pre-amplifier and thus larger cable lengths can be driven without attenuation at higher frequencies. The output of the microphone is typically 5-7mV/Pascal ($1 \text{ Pascal} = 1\text{N/m}^2 = 10\mu\text{bar}$). To put this figure into proper context, it may be noted that the threshold of audibility (0dB) is taken as occurring at a sound pressure of $0.0002\mu\text{bar}$ and the threshold of pain, 120dB higher at $200\mu\text{bar}$. The microphone hence begins to overload at about 105dB, so the maximum voltage that can be expected in normal use is about 20mV or a corresponding 2V at the pre-amplifier output for a gain of 40dB. The frequency response of the pre-amplifier is flat within 3dB from less than 100Hz to about 17kHz which is ideal for PA detection. The pre-amplifier is placed very close to the microphone to reduce the cable length and the subsequent pick-up noise.

4.2.6. The Box-car Averager

The box-car averager is used to process repeated pulsed signals that are generated in an experiment. The box-car used here is a Stanford Research Systems SR250 module [5]. It essentially has a fast gated integrator and an averager. Triggered by the pulse from the laser, the gate provides an adjustable delay from a few nano seconds to 100 msecs before the gate (width adjustable from 2nsec to 15msec) is generated. The signal at the gate is integrated by the fast gated integrator and is normalized by the gate width to provide a voltage proportional to the part of the input signal pulse level at the gate. The sensitivity control of the box-car averager provides further amplification of the signal. The two channels of the SR250 module processes both the PA signal and the pulse corresponding to the laser energy from the energy meter. These signals are then averaged over the desired number of pulses depending on the required SNR. Typically, the signals are averaged over 30 pulses. Averaging over larger number of pulses does increase the SNR, but makes the system very sluggish

in response to fast variations in the PA signal. The gated and averaged signals from both the channels are then ratioed by the SR235 analog signal processor module. This process annuls the variations in the signal introduced by pulse-to-pulse energy variations and due to the dye laser output energy profile over the wavelength of interest. It also has an output time constant control, which can further increase the SNR. The measured signal amplitudes can be displayed on the SR275 display module of the box-car.

4.2.7. The Chart Recorder

The ratioed signal from the output of the SR235 signal processing module of the box-car is fed to a analog-digital x-y chart recorder (Rikadenki RY-102A) to obtain the normalized PA spectrum of the sample. The recorder has sensitivity controls and thus further amplification of the signal can be done if required. The linear ramp voltage for the x axis movement of the chart recorder is provided by the gate scanner module (SR200) of the box-car.

4.2.8. The Digital Storage Oscilloscope

A digital storage oscilloscope (DSO) (200MHz, Iwatsu DS 8621) is used to monitor the PA signal pulse and the intensity of the laser pulse. This oscilloscope has signal averaging facility and can replace the gated integrator and the box-car averager for point-to-point measurements of PA data. The pulse shapes can be digitally stored and plotted. The DSO is also required while setting the gate width and delay of the gated integrator. The signals from the PA cell, the energy meter and the gate signals from the box-car averager are all monitored on the DSO, which is triggered by the trigger pulse from the laser. The DSO has facilities to capture and store the pulse shapes for later analysis and to obtain a hardcopy using a plotter/printer.

4.2.9. The Gas Pressure Monitor

The gas pressure in the PA cell is monitored by a mercury manometer as well as a high pressure digital pirani gauge (Vacuum Techniques VT-DHP-11), which is capable of pressure measurements from atmosphere to $\sim 10^{-3}$ mbar with good resolution in the high pressure regions which is not possible in the case of the mercury manometer. The resolution of the mercury manometer below 7mbar is very small and thus the pirani gauge is used. This gauge is provided with relay control outputs to control gas filling solenoid valves.

4.3. The CW PA Experimental Setup

The schematic diagram of the cw PA experimental setup is shown in fig.4.6. Here, the pulsed laser is replaced by a continuous wave laser and thus the need for a mechanical chopper for modulation arises. The phase detection or lock-in detection technique is used in place of the gated integration and averaging technique. The rest of the experimental details remain more or less the same as the pulsed technique. More effort is involved in this case to ensure good SNR.

4.3.1. The CW Laser Source

The laser source used here is a 12 watt argon ion laser (Spectra Physics model 171) capable of providing either discrete lines of wavelength 514.5, 496.5, 488, 476.5 nm etc. or a multiline output containing all the lasing wavelengths. The wavelength of some of the prominent lines and their relative output powers when the laser is operated at 12 watts multi-line mode are shown in fig.4.7. The discrete lines can be obtained by tuning the prism which is placed in the cavity. The laser output has a gaussian profile and has a frequency stability of 60MHz/ °C and a stability

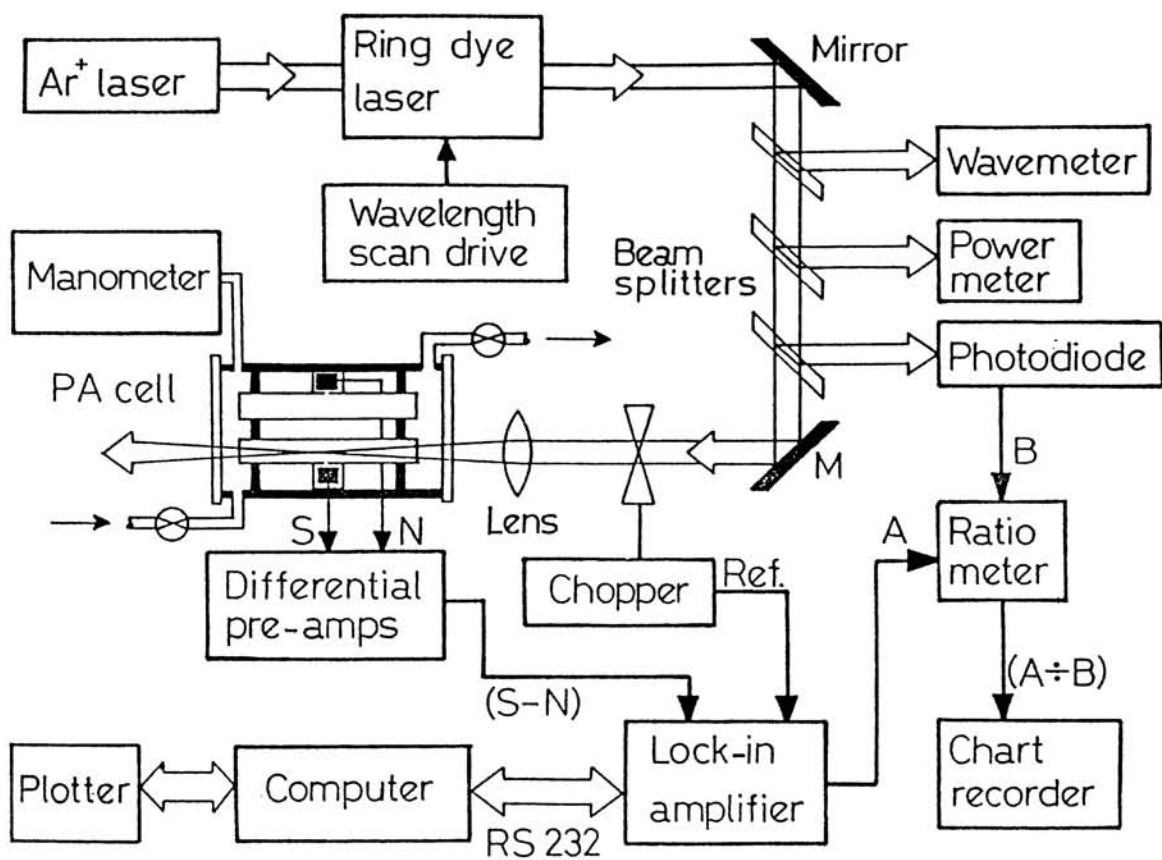


Fig.4.6. The schematic diagram of the cw PA experimental setup

of $\pm 0.5\%$ when used in the light control mode [6]. The laser is also capable of providing UV output (351.1 - 363.8 nm, multiline), but with different optics and with much less efficiency.

4.3.2. The Ring Dye Laser

The dye laser used is the ring dye laser (Spectra Physics 380-D), which is pumped by the 514.5nm or the multiline output of the argon ion laser. The dye used is the rhodamine 6G in ethylene glycol and provides a tuning range of 570 to 620nm. The traditional single frequency dye lasers operate with a standing wave inside the cavity. Since the maxima and minima of the standing wave are stationary, the dye molecules located at the minima of the intra-cavity radiation field are not stimulated by the feedback radiation as a result of which, the gain at these points can be much higher than that in the gain-saturated region. This 'spatial hole burning' frequently causes the gain in these regions to be high enough to sustain simultaneous lasing at different wavelengths corresponding to a mode whose maxima match the unused gain regions. This severely limits the output power of a standing wave dye laser. To avoid this, a travelling wave, figure-of-eight shaped optical cavity is employed in the 'ring' dye laser. The travelling wave ring laser can produce an order-of-magnitude more single frequency power than a standing wave dye laser under the same conditions and is also capable of receiving higher input pump powers. The schematic diagram of the ring dye laser used is shown in fig.4.8. The unidirectionality in the cavity is obtained by a Faraday rotator and a quarter wave plate. The plate thicknesses are designed such that for light propagating in the correct direction, optical rotations cancel while rotations add for opposite propagation directions. Since light propagates around the cavity continuously, all the dye molecules receive feedback radiation and thus spatial hole burning does not occur. The coarse tuning element in the ring laser

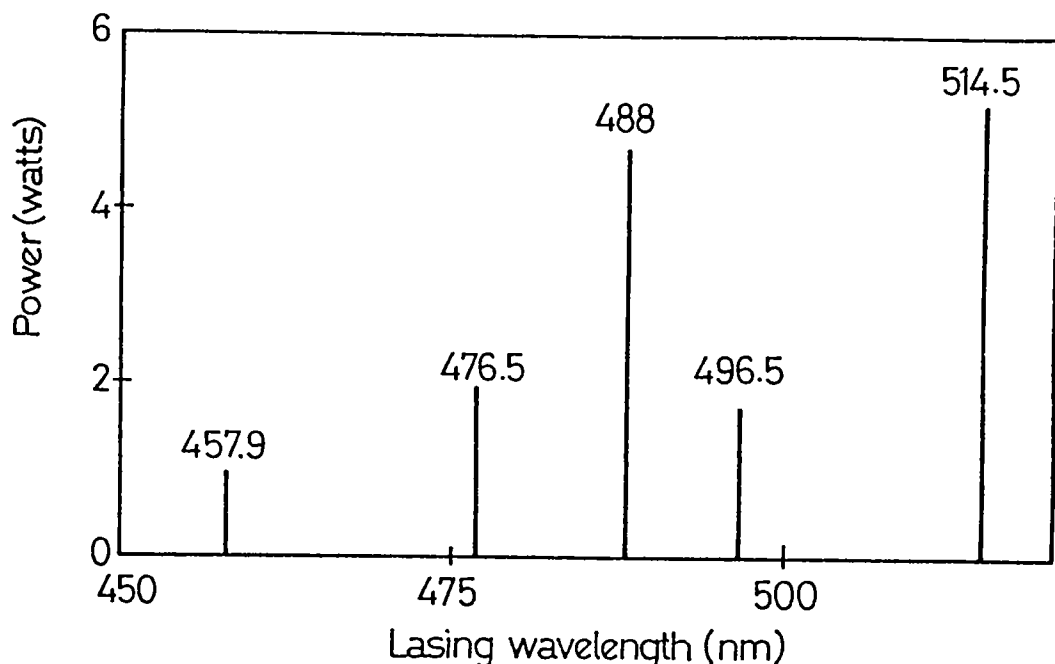


Fig.4.7. The relative powers of the lasing wavelengths of the argon ion laser (12watts, multi-line operation)

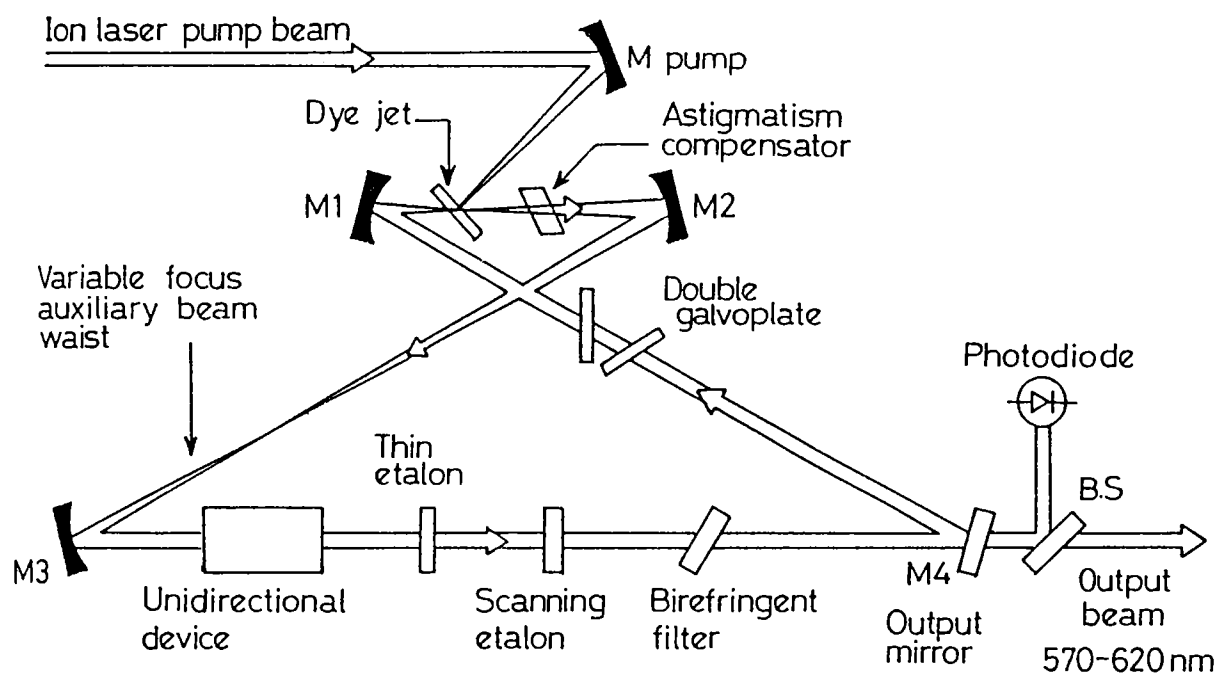


Fig.4.8. The schematic diagram of the ring dye laser

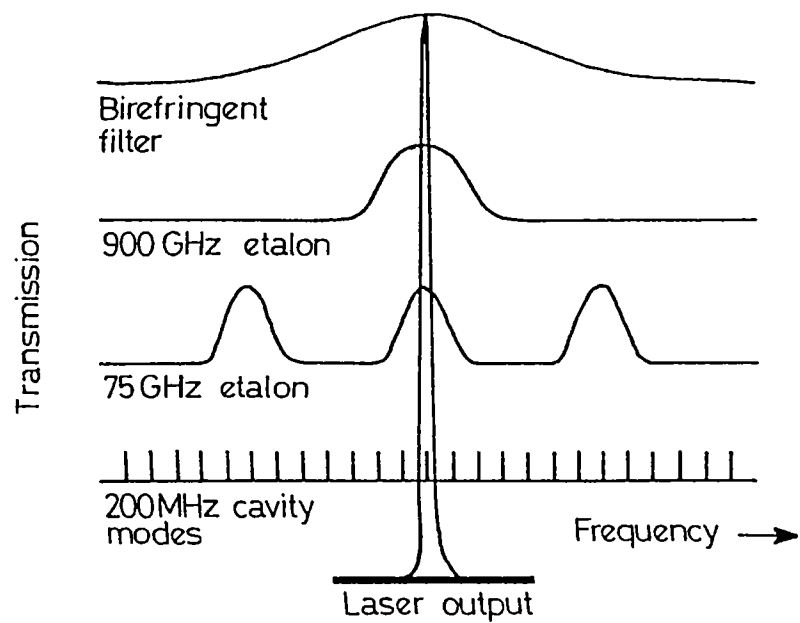


Fig.4.9. The band-passes of the various tuning elements in the ring dye laser cavity

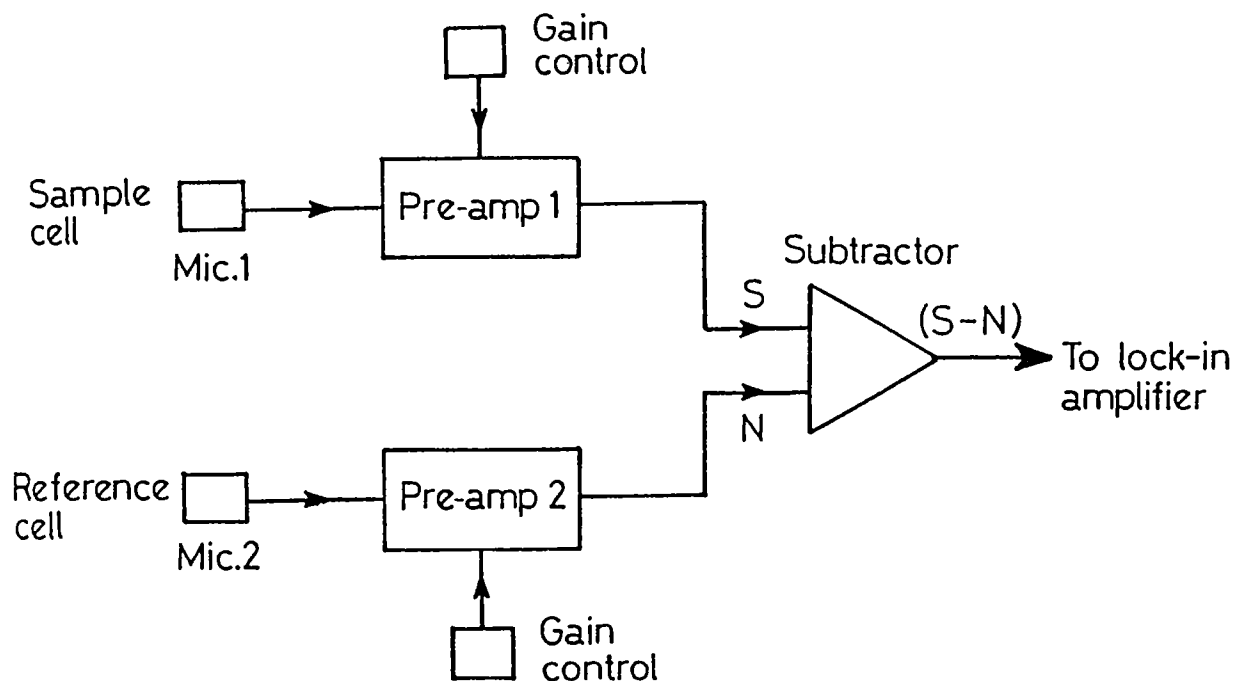


Fig.4.10. The detection scheme in the differential PA technique

cavity is a birefringent filter placed in the beam path. It is a standard one element filter made of quartz crystal, cut with the optical axis in the plane of the plate and inserted at Brewster angle with the laser beam in the cavity. When the plate is rotated, the extraordinary index of refraction is changed as seen by the laser beam. This change results in a rotation of the plane of polarization of the intra-cavity laser beam. Because of the large number of Brewster surfaces inside the cavity, the wavelength whose rotation corresponds to an integral multiple of two sees the minimum loss and is therefore sustained as the lasing wavelength. This coarse tuning is performed by a piezo-electric element driven by an inchworm translator (Burleigh CE-1000). A variable speed control allows fine movement of the inchworm translator from $0.01\mu\text{m/sec}$ to $\geq 2\text{mm/sec}$ and thus the birefringent filter can be tuned very precisely across the wavelength region. The finer tuning elements in the cavity are, the fine etalon (FSR = 900GHz), and the scanning etalon (FSR = 75GHz). The band-passes of the various tuning elements in the ring dye laser cavity are shown in fig.4.9. The laser is also capable of single frequency stabilized operation with cavity tuning (10/30GHz) for high resolution studies [7].

4.3.3. The Optical Modulator

The mechanical chopper (EG&G, model 192) is used to square-wave modulate the laser beam in the cw PA studies. The chopper has a frequency stability of $\pm 0.2\%$ per hour after a one hour warmup [8]. By using different slotted wheels, a frequency range from 5Hz to 5.5kHz is possible. The modulation frequency output is provided as reference to lock-in amplifiers. While operating in the higher frequency regions, the acoustic noise and vibrations produced by the chopper requires that it be isolated acoustically from the PA setup.

4.3.4. Wavelength Monitoring

The dye laser output wavelength is monitored by a wavemeter (Burleigh WA-20VI). It is essentially a scanning Michelson interferometer coupled to a fringe counting system. The wavelength to be measured is fed into the device and is made to interfere with a reference wavelength inside the device. A part of the reference beam is provided outside for alignment of the sample beam (of unknown λ) into the system. The fringes are counted and the wavelength automatically calculated and displayed. The inputs from the reference and the input channels are gated to form a train of pulses. The unknown input wavelength is calculated as [9],

$$\lambda = \left(\frac{N_o}{N} \right) \lambda_o \quad \dots\dots(4.1)$$

Where, λ is the input wavelength, λ_o the wavelength of the reference (He-Ne laser, $0.6329917\mu\text{m}$), N_o the number of reference pulses (632991), and N the number of sample pulses. The pulses from the reference channel are then counted and compared to that obtained due to the reference channel of known wavelength, and the wavelength is calculated from Eqn.4.1 and is displayed as wavelength or wavenumber with a resolution of 0.01nm (0.1cm^{-1}) in the low resolution mode and 0.001nm (0.01cm^{-1}) in the high resolution mode. Only a very low power (0.1mW) of the sample laser beam through the 2mm input aperture is required for accurate wavelength measurements and thus the required laser power can be tapped from the main beam with only negligible loss.

4.3.5. The Microphone Pre-Amplifier

Two different kinds of microphone pre amplifiers have been used in these studies. One is made of two separate transistor electret

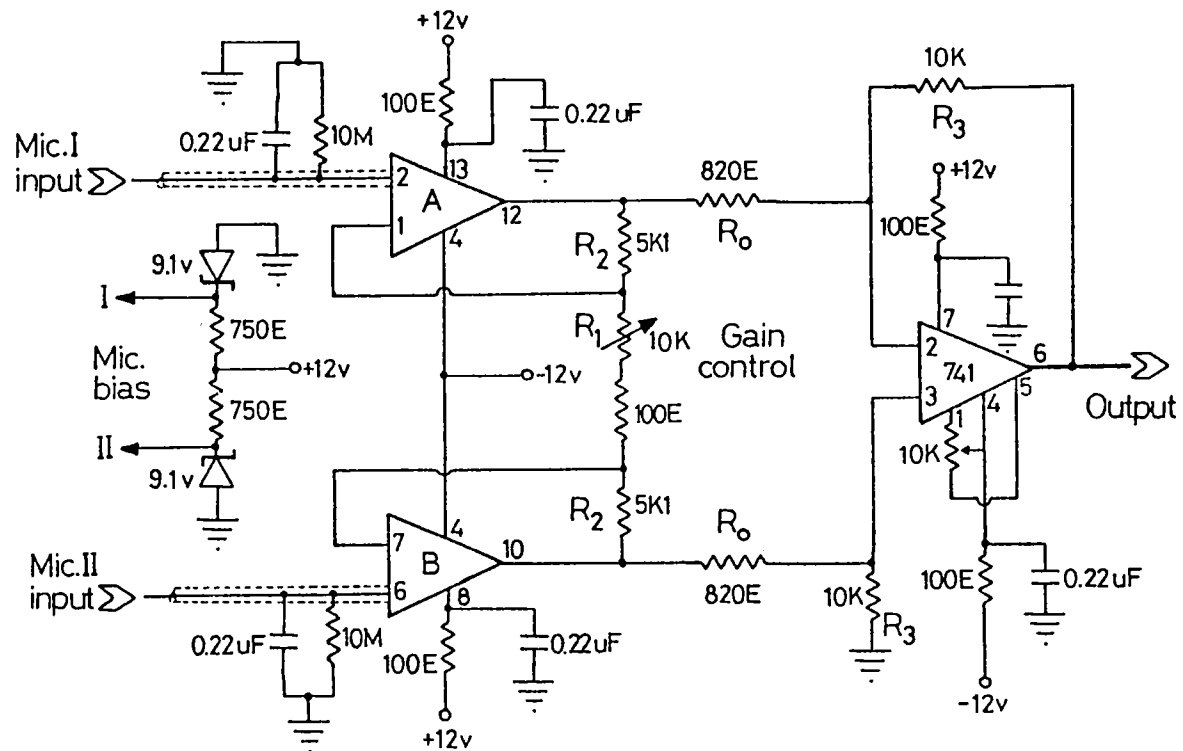
microphone pre-amplifiers and their output subtracted and the other is made from dual op-amps available in the market. Though the IC based pre-amp offered a higher gain, it suffered on account of noise as compared to the transistorized pre-amp.

i. Electret Microphone Pre-Amplifier

The PA signals from the two microphones are amplified appropriately using identical low noise amplifiers. The block diagram of the differential PA signal detection scheme is shown in fig.4.10. The two pre-amplifiers are identical to that used in the pulsed PA case (fig.4.5.). In this case, the gains of the two identical pre-amps are required to be matched before the microphone signals from the two PA cavities are amplified due to the fact that it is not possible to obtain microphones and pre-amplifiers having identical characteristics. The pre-amp has also a differential or single ended input option for the operation with lock-in amplifiers having single ended input. Since the lock-in amplifier used in these studies has a differential input, the two amplified microphone signals are directly fed to the differential inputs of the lock-in amplifier.

ii. IC Based Differential Pre-Amplifier

A single integrated circuit differential pre-amplifier was designed and constructed for this purpose in addition to the above mentioned type of pre amplifier since the previously mentioned pre-amplifier has a limiting gain of about ~ 50 . The circuit diagram of the differential pre-amplifier is given in fig.4.11. The differential section of the pre-amplifier consists of a low noise, dual op-amp (747) used in the differential mode into which the inputs from the two microphones from the PA cell are fed. The net gain of the pre-amplifier depends on the values of the resistances in the gain control section of the pre-amplifier as,



A,B : 1/2 747

Fig.4.11. The circuit diagram of the differential microphone pre-amplifier

$$\text{Net Gain} = \left(S_s - S_r \right) \left(1 + \frac{2R_2}{R_1} \right) \left(\frac{R_3}{R_o} \right) \quad \dots \dots (4.2)$$

Where, S_s and S_r are the signals from the sample and reference microphones of the PA cell. The resistances in the gain control section of the pre-amp are all of 1% tolerance to enable optimum balancing of the two sections. The differential output is further amplified by a single low noise op-amp to the required gain level. The pre-amp is powered by a 12v regulated dual power supply. For lower pre-amp noise levels, commercially, pin-to-pin compatible op-amps can replace the existing ones used in the present pre-amp. The maximum gain of this pre-amp is $\sim 55\text{dB}$.

4.3.6. The Lock-In Amplifier

The lock-in amplifier (LIA) used for these cw PA studies is a heterodyning LIA (EG&G model 5208). The input signals at the reference frequency are mixed with an internally developed local oscillator output derived from the reference signal. The resulting sum and difference signals are applied to a quasi-resonance filter to remove the upper side-band. The difference signal is then processed as the information signal. This allows for the use of narrow band fixed frequency filters while still allowing operations over a wide frequency range. The differential inputs of this LIA has a common mode rejection ratio (CMRR) 120dB maximum from 60Hz to 1kHz with a 6dB/octave roll-off above 1kHz. The internal noise is $\sim 5\text{nV}/\text{Hz}^{1/2}$ at 1kHz [10]. Different input filters in the LIA, depending on the noise level can be chosen to further refine the signal. The system has auto-operations on settings, range, offset, normalization etc. which enable easier initial setting of the instrument. The system also has an internal ratio facility which, in the case of PA experiments is used to normalize the output against the power

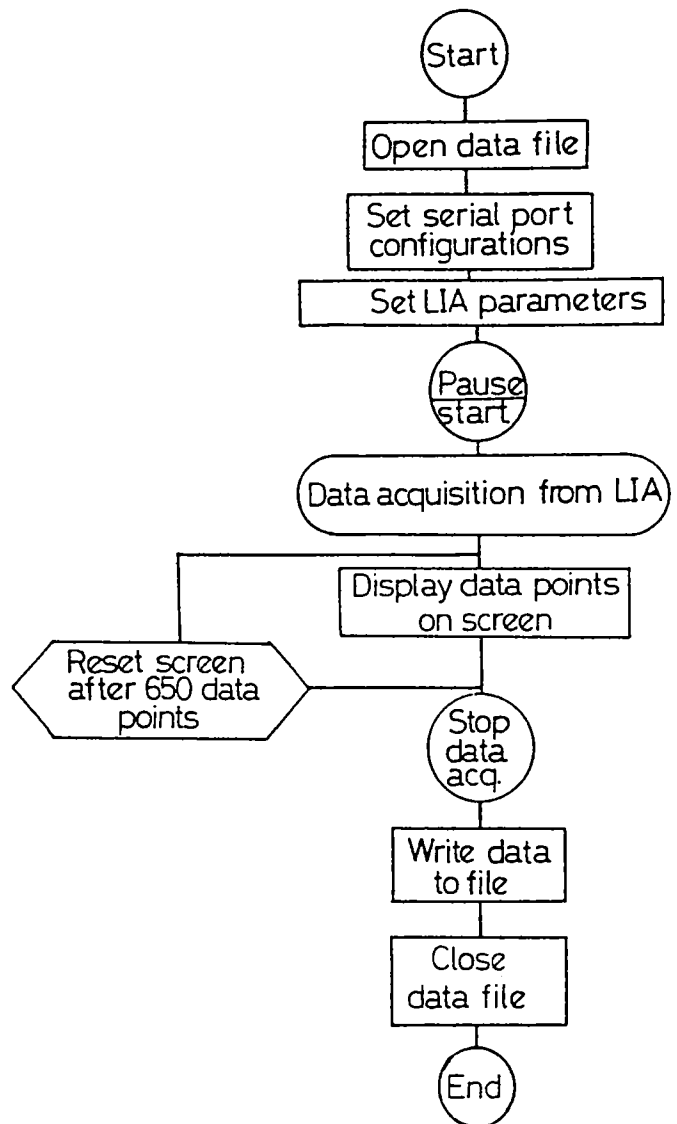


Fig.4.12. The flow chart for the programme for LIA control and data acquisition process

fluctuations in the laser beam in time and also while tuning across the wavelength range. An output time constant control is provided to reduce the signal noise further to an acceptable level. A good compromise between the choice of input filters, amplification (sensitivity) and time constant has to be made for good results. All these functions can be controlled remotely using a computer and the resulting data can also be acquired by it via the conventional RS-232-C serial or IEEE-488 parallel interfaces. A program in BASIC language was developed and used to control the front panel of the LIA using the RS-232 serial interfaces of the LIA and the computer (PC-AT286, 10MHz) and to acquire the data. The algorithm for the LIA control and data acquisition is shown in fig.4.12. The LIA returns the data to the computer in the form of in-phase, quadrature (out-of phase) signal amplitude, magnitude of the signal (square root of the sum of the squares of the in-phase and quadrature parts of the signal) and log of the magnitude of the signal , depending on the command function sent to the LIA by the computer. The acquired data is temporarily displayed on the computer screen and is also simultaneously stored for further processing, which is done by standard scientific graphics softwares capable of curve fitting and smoothing operations. The processed data in the form of graphs or spectra are obtained via a dot matrix printer or a pen-plotter (HP-7475A).

4.4. Design And Characteristics Of The Dual Cavity PA Cell

Due to the more unwanted consequences of the background noise in cw PA measurements as compared to the pulsed measurements, the design of the PA cell for the former should incorporate adequate changes so as to assist in signal enhancement and background noise suppression. Dynamic differentiation of signal and noise is the best approach to adopt in this context. Thus a dual cavity PA

cell to operate in the differential mode was designed and fabricated.

4.4.1. The Dual Cavity Differential PA Cell

In the case of cw PA detection, the acoustical noise is a major problem. The normal single cavity PA cell is not sufficient to suppress the spurious noise. For this, a dual cavity, open resonator PA cell has been designed and fabricated. The basic principle of the differential PA cell is that there should be two identical PA cavities in a common enclosure containing the sample gas under identical conditions. The excitation source passes through only one of the cavities. The difference between the outputs from the two cavities will give a relatively noise free signal since the external and other acoustic noises form the common mode input signals of the differential amplifier and are thus canceled, as seen from the fig.4.10.

The schematic diagram of the PA cell assembly is shown in fig.4.13. The system mainly consists of two stainless steel tubes (10cm long with 6mm diameter) which form the two open resonators (C) of the PA cell [1,2]. The inner surface of these tubes are polished to reduce absorption of the incident laser by the walls. These are supported by teflon spacers (T). A miniature electret microphone (M) (Knowles BT 1759), acoustically sealed using epoxy in a teflon holder is mounted centrally on to the side of each of the tubes and the cavity is connected to the microphone chamber by a hole of ~ 1mm diameter. The microphones used were assumed to be identical in characteristics for this purpose. The two tubes are about 5mm apart and their microphones are well isolated acoustically from each other and the surroundings. The pair of tubes are placed centrally in a larger aluminum cylinder (A) of length 20cm and wall thickness ~ 3cm such that each of the tubes opens into a bigger volume of diameter ~

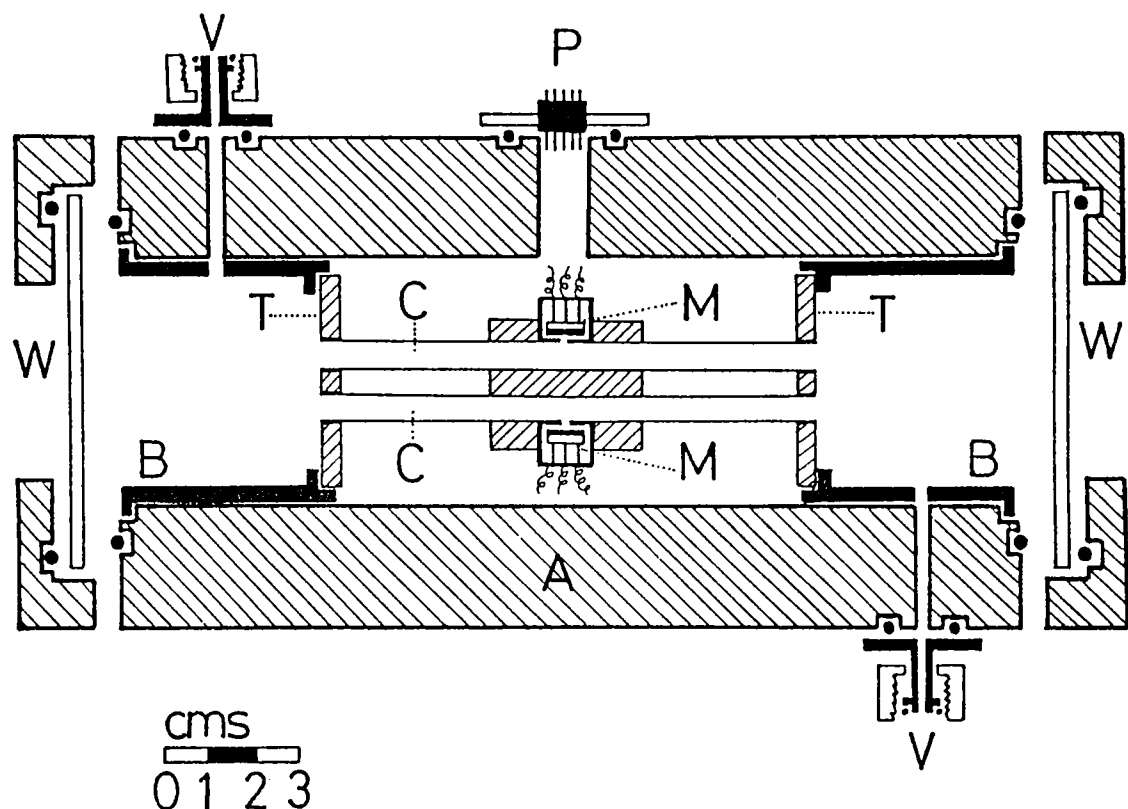


Fig.4.13. The schematic of the dual cavity differential PA cell
 A - aluminium cylinder, B - Buffer ring, C - cavity
 V - gas inlet/outlet ports, M - Microphone
 T - Teflon spacers, P - microphone connector

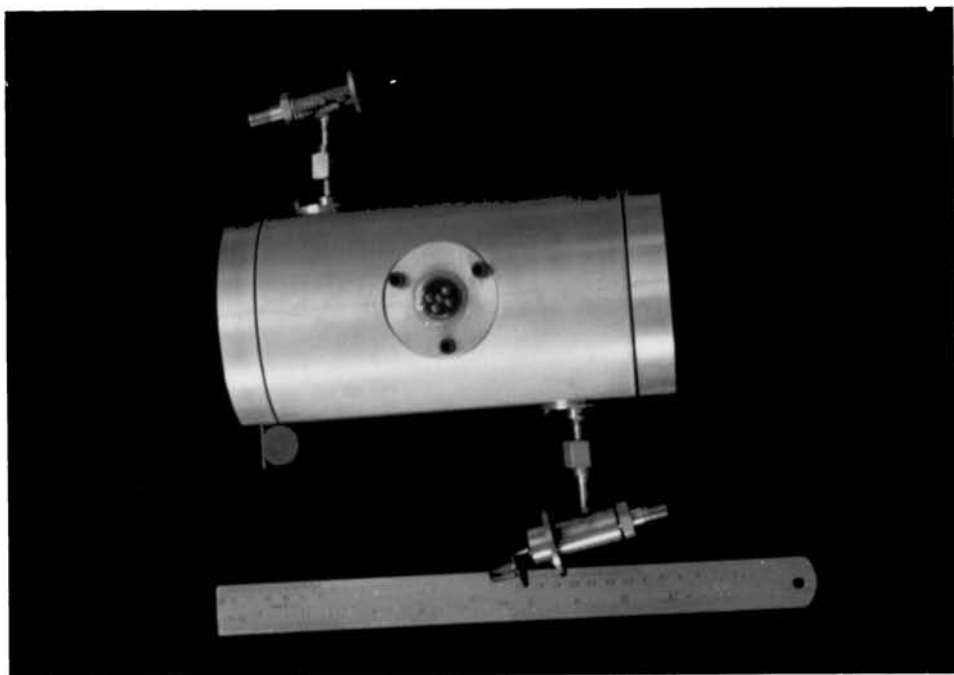


Fig.4.13.a. The photograph of the dual cavity PA cell showing the gas valves, microphone connector and the window attachments

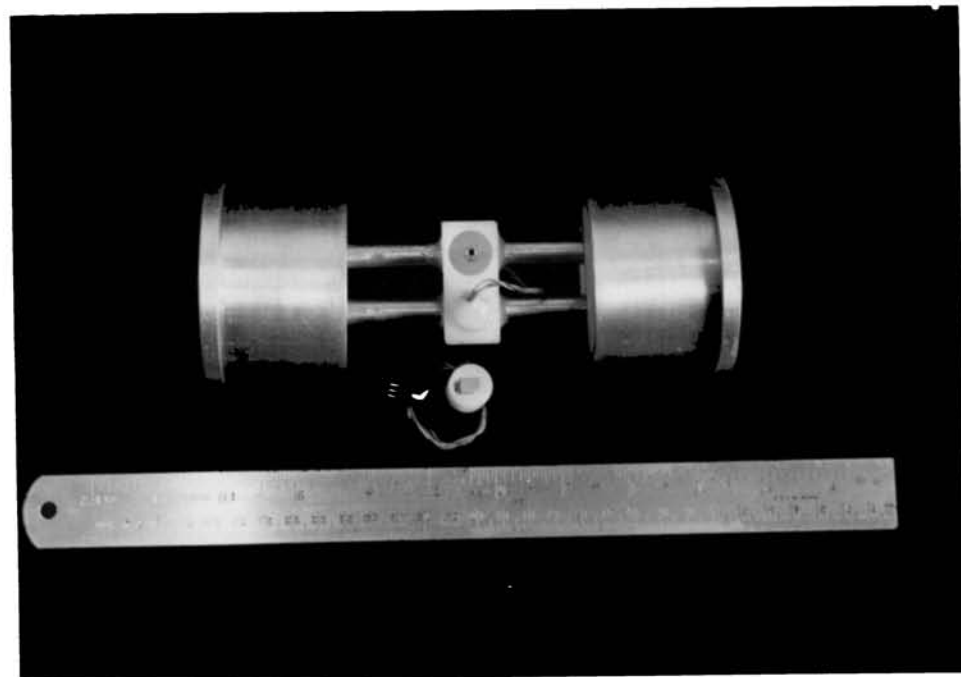


Fig.4.13.b. The photograph showing the PA cavities, buffer volumes and the microphone mountings

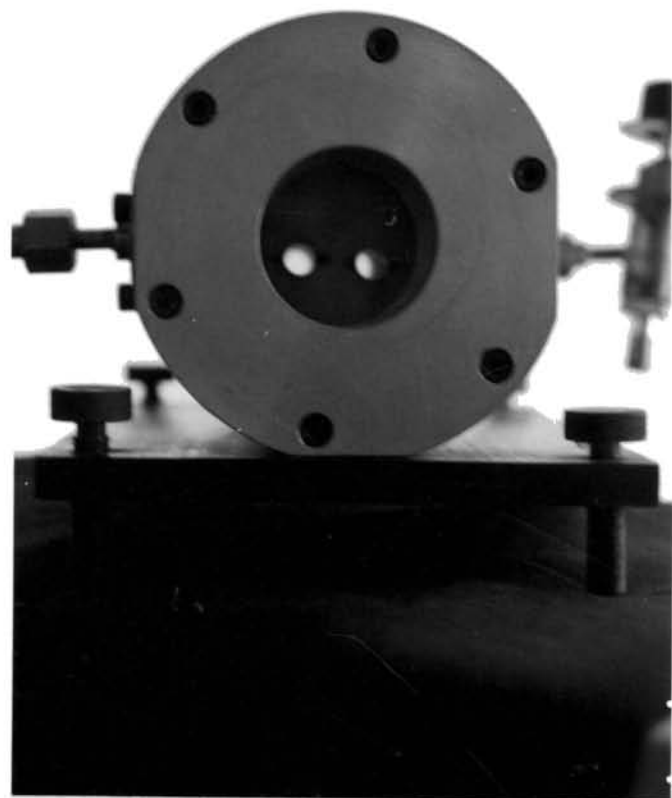


Fig.4.13.c. The photograph of the cross section of the PA cell showing the two cavities

6cm and length 5 cm on either side. The volume of this "buffer" space is much larger than that of the cavities formed by the stainless steel tubes. The buffer volume helps in isolating the window absorption signals from the microphones and reduces the gas flow induced turbulence and the resulting pressure fluctuation when the PA cell is used in the continuous flow mode. The buffer volume can be varied by varying the diameter of the sleeve ring (B) inserted on either side of the aluminum cylinder. The cell has connecting ports (V) for inlet and outlet valves to control the gas flow. Good quality needle valves were designed and fabricated for these purpose. The windows (W) are of good quality optical glass and all the fixtures are "O" ring sealed so that the cell can be operated under low gas pressures which is essential for trace gas analysis. The microphone connections are taken out through a 5 pin vacuum feed-through connector (P) sealed with epoxy on to the larger aluminum cylinder (A). The cell is mounted on a heavy metal plate supported by vibration absorbing material.

4.4.2. Characteristics Of The PA Cell

Some of the characteristics of the PA cell have been obtained from experimental data, the most important of them being the acoustic resonance characteristics which are quite important in cw PA measurements where the mode of operation of the PA cell depends very much on its acoustic resonances.

i. Acoustic Resonance

Since the acoustic characteristics of the PA cavity play a very important role in the enhancement of the PA signal, suppression of acoustic noise and in increasing of the SNR of the PA system, it is necessary to study these resonance characteristics of the PA cell cavity in some detail. Since the PA cavity is an open

cylinder enclosed in a larger enclosure, for all practical purposes, the PA cavity can be assumed to be an open cylindrical tube. The theoretical aspects of the modes of acoustic resonance possible in such a configuration are dealt with in the earlier chapter on PA instrumentation. In our case, only the longitudinal resonance modes are taken into consideration since in the present configuration, the axial or azimuthal mode excitations, having much higher resonance frequencies being difficult to generate using the present setup which uses a mechanical modulator. For the longitudinal mode, the resonance frequency basically depends on the length of the cavity and on the density and viscosity of the sample gas contained in it. The acoustic resonance characteristics of the PA cell were determined with air at atmospheric pressure as sample. A simple loudspeaker was kept close to one of the windows of the cell and the frequency tuned from 400 to 5000Hz and the microphone output was obtained and normalized against the amplitude of the audio signal being applied (fig.4.14). Fig.4.15 shows the frequency response of the PA cell excited by an acoustic signal from a signal generator and with air at atmospheric pressure as the medium. The fundamental and the first harmonic of the resonance frequency are clearly seen with slight variations induced by the influence of other aspects like the buffer volume, vacuum ports and the teflon spacers in the cell cavity which tend to distort the resonance profiles. Sub-resonances below the fundamental resonance frequency are also seen, but are generally weaker than the f_{001} fundamental resonance mode. As mentioned in the previous chapter, though many different modes of resonances can be excited in this frequency region only a few are observed due to the symmetry and the other previously mentioned conditions. The fig.4.16. shows the various f_{00k} modes of resonance and their frequencies possible for a cell of the above dimensions.

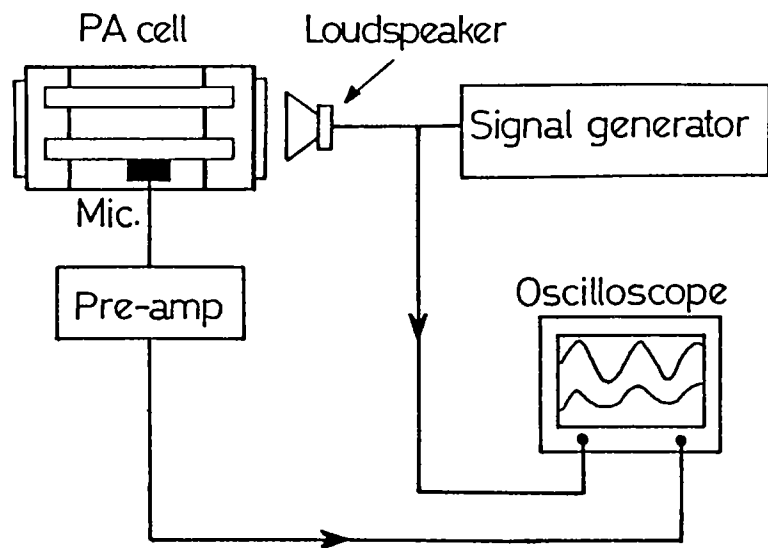


Fig.4.14. The experimental setup for the measurement of the acoustic response of the PA cell

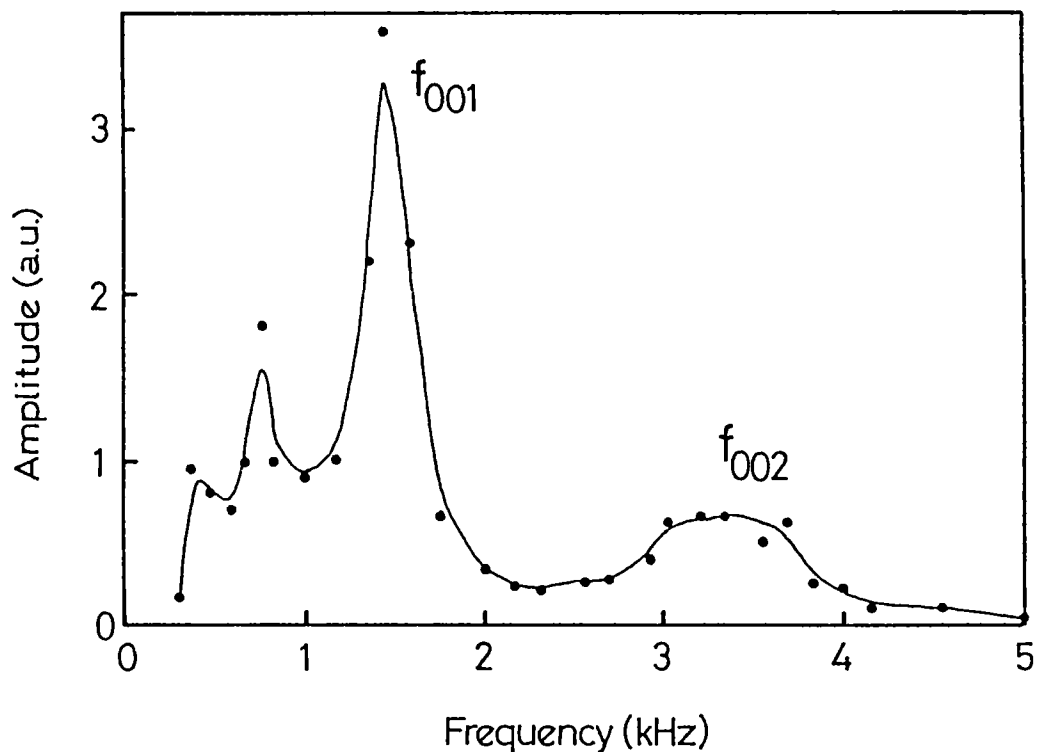


Fig.4.15. The acoustic response of the PA cell under excitation with an acoustic source

ii. Frequency Response Of PA Signal

The frequency response of the photoacoustic signal from the PA cell was obtained using Nitrogen dioxide (NO_x) as the sample gas and a 6mW He-Ne laser (632nm) as the excitation source. The experimental setup for the resonance characteristics measurement is shown in fig.4.17. The modulation frequency is tuned across the frequency range 800 to 2000Hz and the amplitude and phase of the PA signal are recorded. A typical modulation frequency response of the amplitude and phase of the PA signal are shown in fig.4.18. As the frequency tunes across one of the acoustic resonances of the PA cavity, there is a many-fold enhancement of the PA signal amplitude and an abrupt change of quadrant in the phase angle as seen in the plot. The amplitude of the PA signal increases as the chopping frequency ω approaches the resonance frequency ω_0 of the cell. It is maximum at $\omega = \omega_0$ and decreases as ω increases further and is constant till another acoustic resonance mode is encountered. The phase of the signal also correspondingly varies till resonance is achieved, when it abruptly changes quadrant after which, it again continues to vary. The cell is said to be a resonant cell if the experiments using the cell are performed with the modulation frequency made to coincide with any one of these resonance frequencies. The cell resonance information is thus available through both the amplitude and the phase of the PA signal.

It is interesting to note how the resonance characteristics of the PA cell varies with the pressure of an highly absorbing sample gas in the cavity. This was done by using the NO_x gas samples at different pressures. For high concentration gas samples ($\sim 98\% \text{NO}_2$ in $\sim 90\% \text{NO}_x$:air mixture synthesized in the laboratory), it was seen that the fundamental resonance frequency (f_{001}) varies from $\sim 1.25\text{kHz}$ to $\sim 1.05\text{kHz}$ as

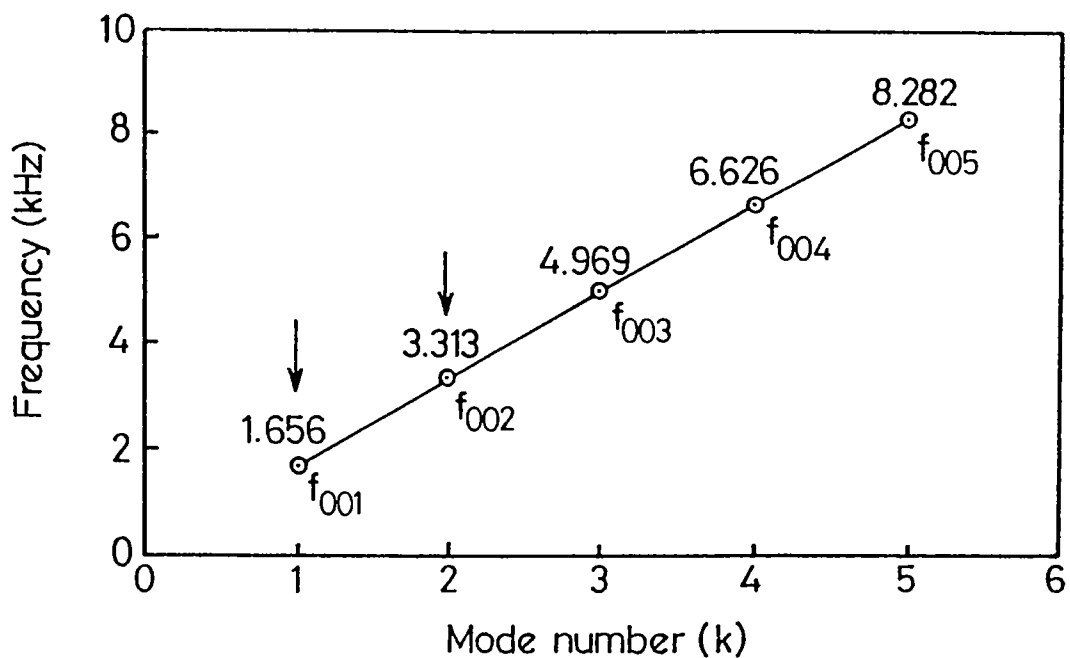


Fig.4.16. The graph showing the different modes of the f_{00k} resonance theoretically possible and their respective frequencies for the PA cell

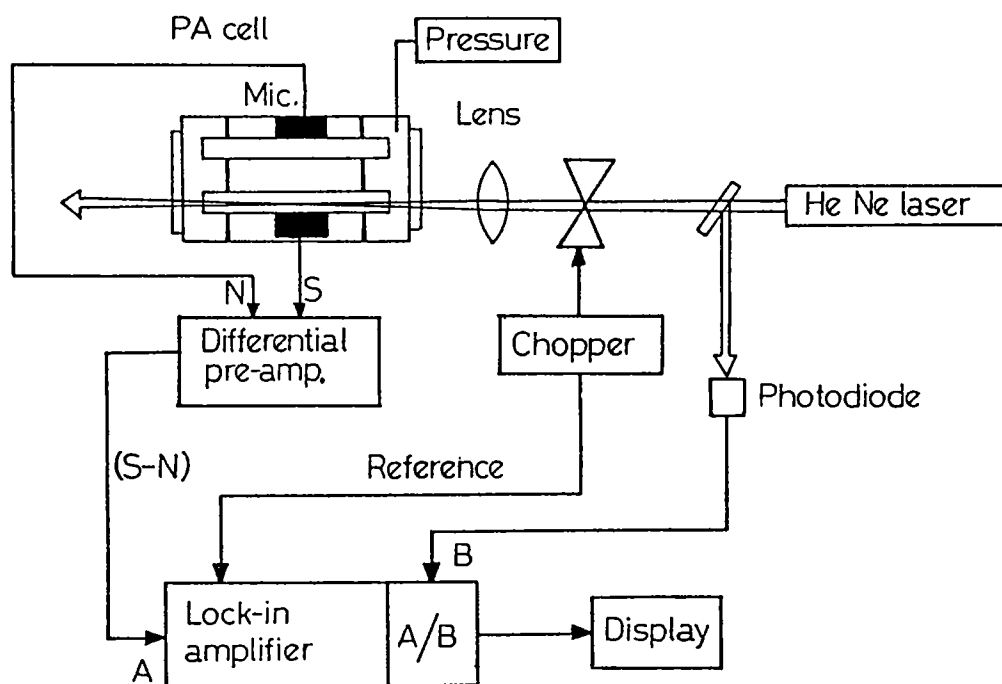


Fig.4.17. The experimental setup for the measurement of the frequency response of the PA signal from the cell

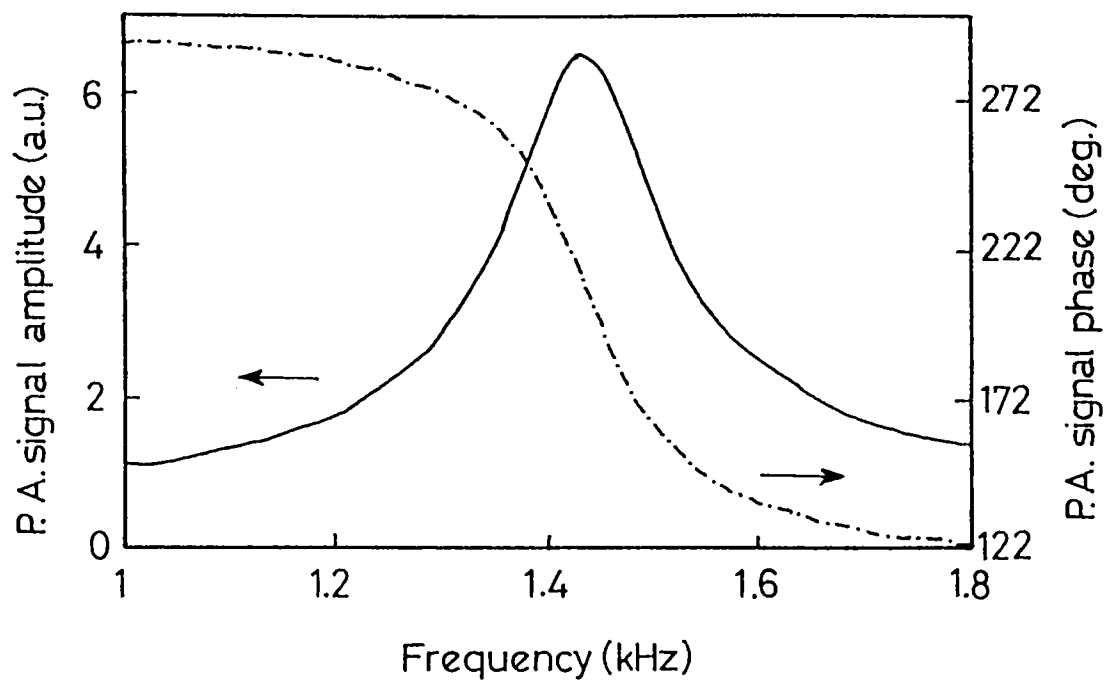


Fig.4.18. The typical modulation frequency response of the amplitude and phase of the PA signal from the PA cell with NO_x gas as the sample

the total gas pressure is increased from 25 to 300 Torr. This is clearly visualized in the 3-D representation of the amplitude and phase response of the PA signal at different pressures (fig.4.19.a&b). This variation of the resonance frequency reflects both in the amplitude as well as the phase of the PA signal as the modulation frequency is tuned across the resonance as seen in fig.4.20. The decrease in the PA signal is also observed as pressure is increased due to possible saturation of the PA signal at sufficiently high pressures. Similar resonance frequency shift observations have been reported for the axial resonances of the PA cell using $\text{CH}_4:\text{Xe}$ mixtures [11,12] and in the $\text{N}_2\text{O}_4 \rightleftharpoons \text{NO}_2$ reaction dynamics [13]. This variation can be understood as a speed-of-sound anomaly caused by the variation due to the $\text{N}_2\text{O}_4 \rightleftharpoons \text{NO}_2$ reaction in the velocity term c_0 of the equation for the frequency of the cell ie,

$$f_{kmn} = \frac{\pi c_0}{2} \left\{ \left(\frac{k}{L} \right)^2 + \left(\frac{\alpha_{mn}}{R_0} \right)^2 \right\}^{1/2} \quad \dots \dots (4.3)$$

(Where the various quantities are defined under Eqn.3.01.). Under ideal conditions,

$$f_{kmn} = f_0 = \frac{1}{2L} \sqrt{\frac{\gamma P}{\rho}} = \frac{c_0}{2L} \quad \dots \dots (4.4)$$

$$\text{where, } c_0 = \sqrt{\frac{\gamma P}{\rho}}$$

where, γ the compressibility of the gas and has a value 1.4 and 1.33 for diatomic and triatomic gases respectively, P the gas pressure, and ρ the density of gas in the cell. The subsequent variation of the acoustic velocity (c_0) in the cell with gas pressure is given in fig.4.21. The low concentration NO_x mixture

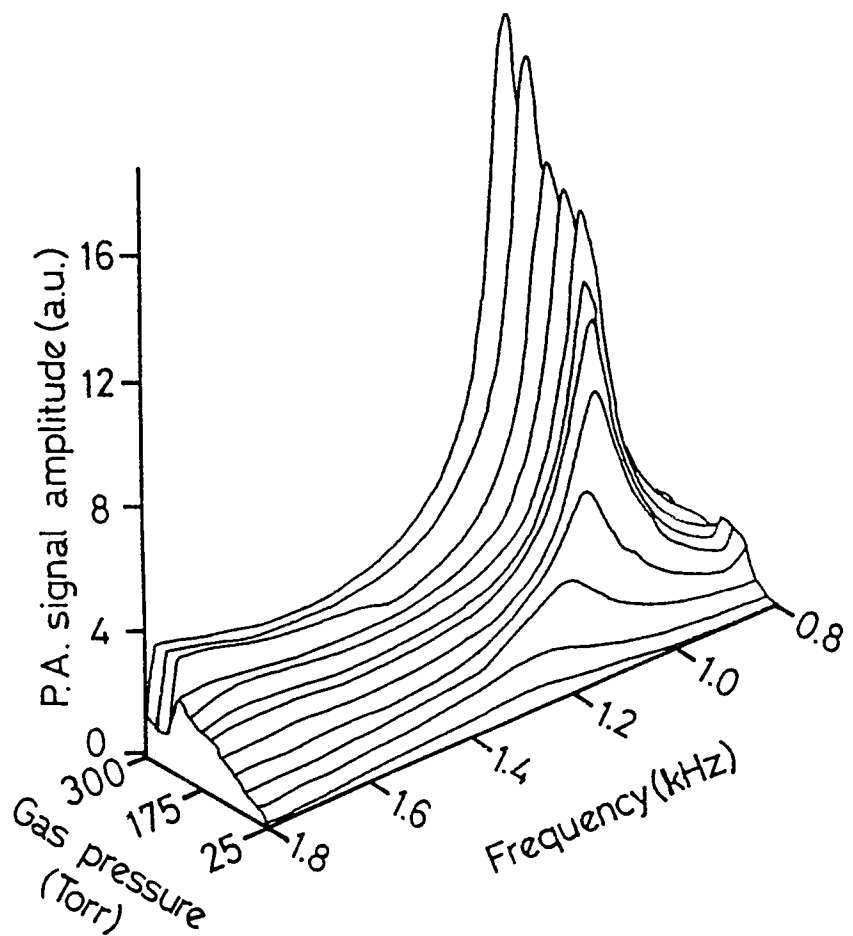


fig.4.19a. The 3-D representation of the variation of the frequency response of the PA signal amplitude for high concentration NO_x sample

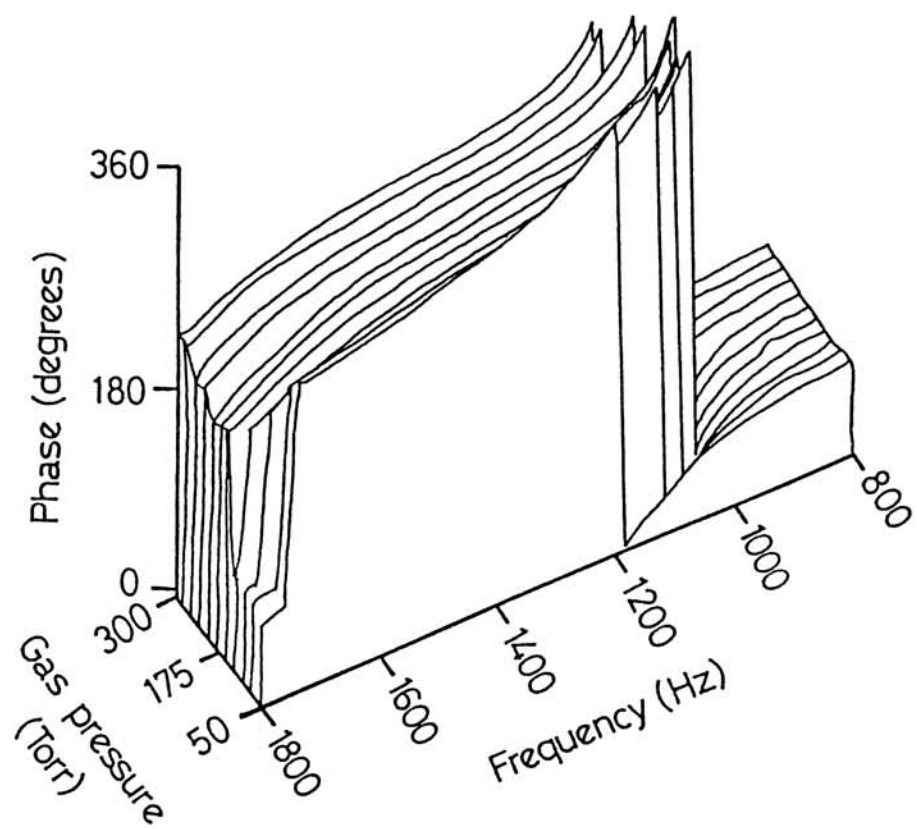


Fig.4.19b. The 3-D representation of the variation of the frequency response of the phase of the PA signal with gas pressure for high concentration NO_x sample

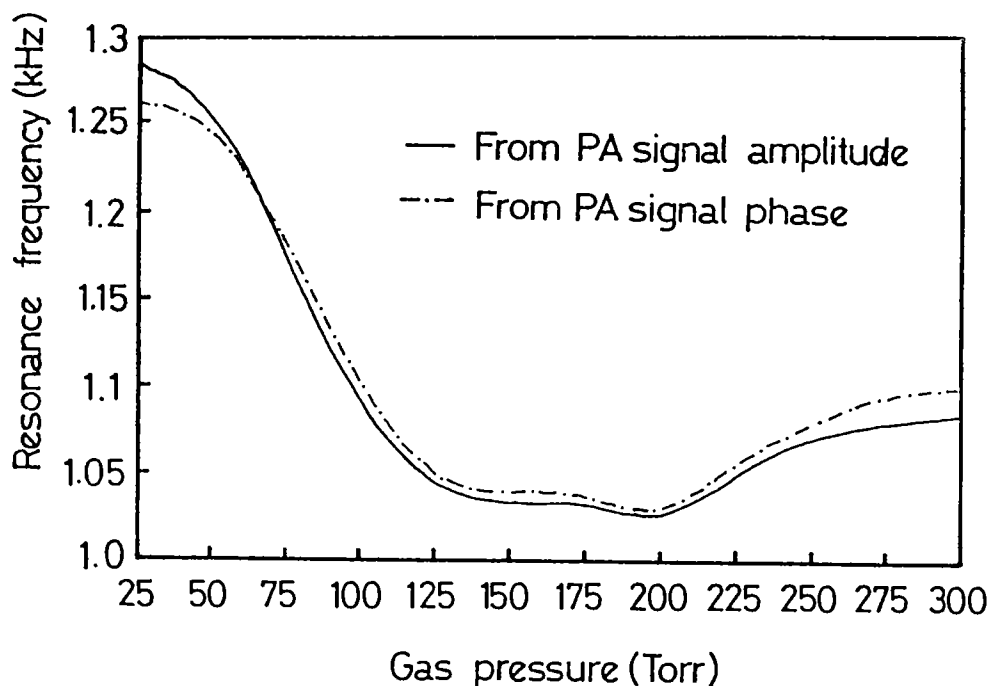


Fig.4.20. The variation of the resonance frequency of the PA cell with gas pressure obtained from the amplitude and phase of the PA signal using high concentration NO_x

does not induce noticeable variation in the acoustic velocity. It is seen that, for high concentration NO_x samples, this variation of the acoustic velocity c_o assumes a polynomial variation with the gas pressure as,

$$c_o = \alpha_0 P^0 + \alpha_1 P^1 + \alpha_2 P^2 + \alpha_3 P^4 \quad \dots \dots (4.5)$$

where, the coefficients $\alpha_0 = 322.355$, $\alpha_1 = -1.7372$,

$$\alpha_2 = 8.1253 \times 10^{-3} \text{ and } \alpha_3 = -1.1665 \times 10^{-5}$$

The experimental data compares well with the values obtained from the polynomial fit of the variation of c_o with gas pressure as seen from the plot (Fig.4.21.a).

The boundary layer effect, virial shift and relaxation dispersion produce shifts of the resonance frequency. The surface losses are due to the interaction of the standing wave with the internal resonator surface. The dissipation processes due to the thermal and viscosity gives rise to the thickness of the zones d_h and d_v where the energy exchange between the gas and the resonator walls occurs due to the thermal conductivity k and the viscosity respectively as mentioned in chapter 2. The Q factor for the surface losses in the cell can be calculated as,

$$Q_{\text{sur}}^{-1} = L^{-1} \left[d_v + (\gamma-1)d_h (1+L/R_o) \right] \quad \dots \dots (4.6)$$

The dissipation due to d_h and d_v at the surface change the sound velocity and consequently the resonance frequency. The corresponding shift decreases with increasing pressure and is given by [12],

$$\delta\omega_{\text{sur}} = -1/2 Q_{\text{sur}}^{-1} \omega_o = -1/2 K_1 P^{-1/2} \omega_o \quad \dots \dots (4.7)$$

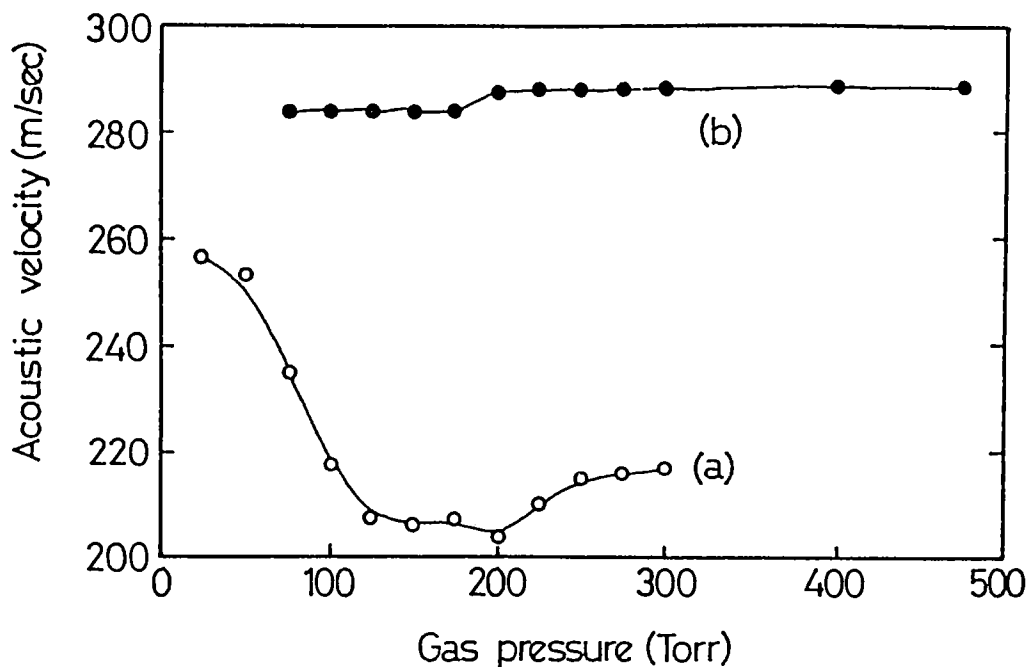


Fig.4.21. The variation of the acoustic velocity in the gas filling the PA cell using (a) high concentration and (b) low concentration NO_x samples

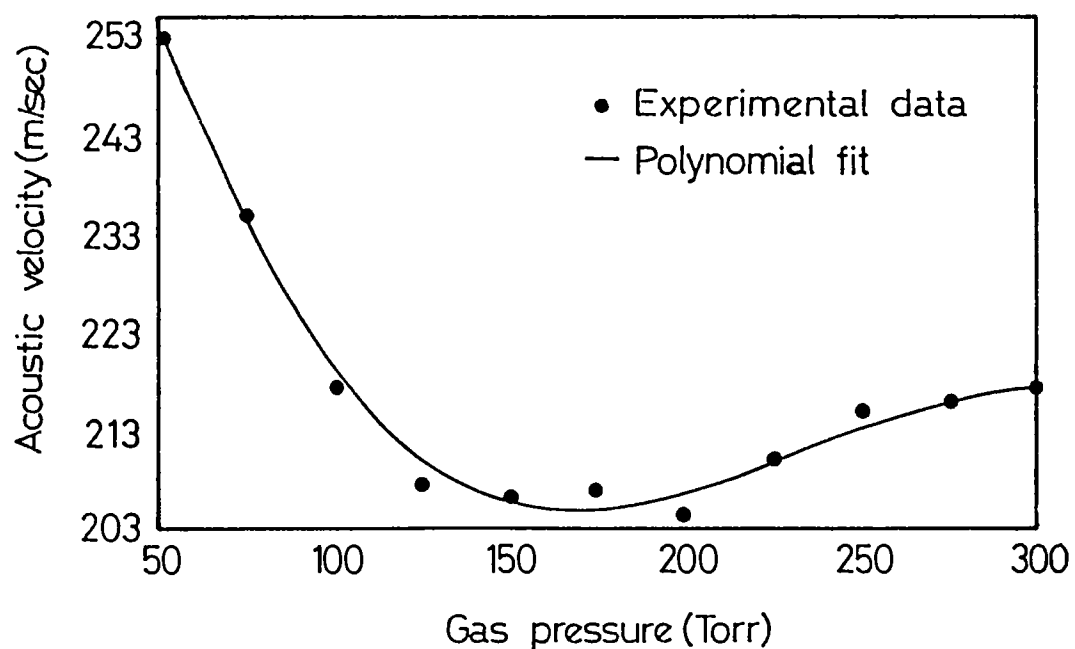


Fig.4.21(a) The variation of the acoustic velocity in the PA cell containing high concentration NO_x and the exponential fit of the experimental data.

where K_1 is a constant. At high pressure, intermolecular forces cause deviation from ideal gas laws normally employed to calculate the resonant frequencies of the cavity. This leads to a variation of the sound velocity and a shift of the resonance frequency. The real gas correction increases with pressure and can be determined as [14,15]

$$\delta\omega_{vir} = \frac{P \omega_0}{R T} \left(B + \frac{RT}{C_v} \frac{dB}{dT} + \frac{(RT)^2}{2C_v C_p} \frac{d^2B}{dT^2} \right) = K_2 P \omega_0 \quad \dots \dots \dots (4.8)$$

Where, R is the universal gas constant, P the gas pressure, B the second virial coefficient and K_2 is a constant. The frequency dispersion due to the vibrational relaxation [16-18] has to be also considered and this frequency shift is due to the dispersion of sound velocity in the ω, P region where the relaxation processes occur. If molecular relaxations are absent, then the frequency of the cylindrical cavity and the corresponding velocity of the sound waves in the gas filling the cavity can be determined as in Eqn.4.3 and 4.4 under ideal conditions. In the case of a molecular relaxation process occurring, the sound velocity is complex and can be represented by [16],

$$c(\omega, P) = \left[\gamma(\omega, P) \frac{P}{\rho} \right]^{1/2} \quad \dots \dots \dots (4.9)$$

where, $\gamma(\omega, P)$ is the effective heat capacity ratio for the sound wave at frequency ω and pressure P . For the corresponding heat capacity at constant volume,

$$C_v(\omega, P) = C_{tr} + C_{rot} + \frac{C_{vib}}{1+2\pi i(\omega/P)P\tau} \quad \dots \dots \dots (4.10)$$

where C_{tr} , C_{rot} and C_{vib} are the contributions of the translational, rotational and vibrational degrees of freedom to the heat capacity

respectively, and $P\tau$ is the product of the pressure and the relaxation time. At low sound frequencies (high pressure), the effective heat capacity is equal to the static value, whereas at high sound frequencies (low pressure), the contributions of the vibrational heat capacity will be zero. At intermediate ω, P values, the effective heat capacity varies between these two extreme values. For the corresponding shift of the resonance frequency we can get, from Eqn.4.3, the relationship

$$\frac{\omega(\omega, P)}{\omega_0} = \frac{c(\omega, P)}{c_0} = \left[\frac{\gamma(\omega, P)}{\gamma} \right]^{1/2} \quad \dots \dots (4.11)$$

The real part of the complex equation describes the relaxational dispersion of the resonance frequency [14] as,

$$\omega(\omega, P) = \left[\operatorname{Re} \left(\frac{\gamma(\omega, P)}{\gamma} \right)^{1/2} \right] \omega_0 \quad \dots \dots (4.12)$$

The equation finally employed for calculation of the resonance frequency as a function of ω and P is obtained by adding the shifts due to the surface losses (Eqn.4.7.) and the virial shift (Eqn.4.8.) to the frequency dispersion equation given above arising from the fact that a finite time is required for energy exchange between different degrees of freedom so that,

$$\omega(\omega, P) = \left[\operatorname{Re} \left[\frac{C_p(\omega, P) C_v}{C_v(\omega, P) C_p} \right]^{1/2} - \frac{K_1}{2 P^{1/2}} + K_2 P \right] \omega_0 \quad \dots \dots (4.13)$$

The halfwidth of the resonance peak also is affected by the gas pressure. In this case, three broadening effects are to be considered *i.e.*, damping by surface losses, Stokes-Krichhoff losses

and damping due to the relaxation process. As found in the frequency shift, the broadening caused by the boundary-layer effects increases with decreasing pressure. The contribution of the surface losses to the bandwidth $\Delta\omega$ can be derived from Eqn.4.3. as [14],

$$\Delta\omega_{\text{sur}} = Q_{\text{sur}}^{-1} \omega_0 = K_1 P^{-1/2} \omega_0 \quad \dots \dots \dots (4.14)$$

At low pressure, the volumetric losses make a small contribution to the half width of resonance. The following expression is thus obtained for the Q factor of these processes [19],

$$Q_{\text{vol}}^{-1} = \left[\frac{2\pi\omega}{\gamma P} \right] \left[\frac{4}{3} \eta + (\gamma-1) \frac{kM}{C_p} \right] \quad \dots \dots \dots (4.15)$$

M being the molecular mass, η the viscosity of the gas and k the gas thermal conductivity. Thus the contribution of the free space viscous and thermal dissipation (Stokes-Krichhoff's losses) to the bandwidth of resonance peak is,

$$\Delta\omega_{\text{vol}} = Q_{\text{vol}}^{-1} \omega_0 = (K_3/P) \omega_0 \quad \dots \dots \dots (4.16)$$

where, K_3 is a constant. As in the previous case, if relaxation processes occurs in the investigated ω, P region, these energy exchange processes make a significant contribution to the broadening of the resonance peak. The corresponding value of the $\Delta\omega$ can be determined from the imaginary part of the Eqn.4.11. as [14],

$$\Delta\omega_{\text{rel}}(\omega, P) = \left[2 \text{Im} \left(\frac{\gamma(\omega/P)}{\gamma} \right)^{1/2} \right] \omega_0 \quad \dots \dots \dots (4.17)$$

As for the resonance frequency, the final half width of the resonance peak can be represented by summing all the damping

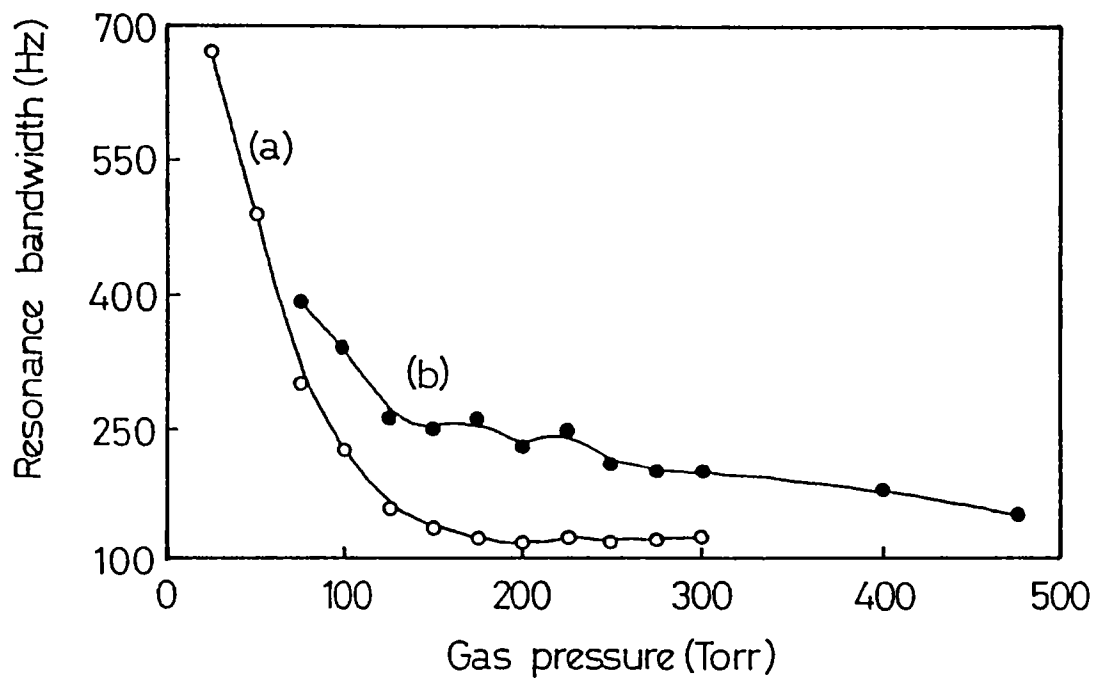


Fig.4.22. The graphical representation of the variation of the resonance bandwidth for (a) high concentration and (b) low concentration NO_x samples

effects to get,

$$\Delta\omega(\omega/P) = A \left[2 \operatorname{Im} \left[\frac{C_p(\omega/P) C_v}{C_v(\omega/P) C_p} \right]^{1/2} + \frac{C_1}{P^{1/2}} + \frac{C_3}{P} \right] \omega_0 \quad \dots\dots(4.18)$$

Here, the factor A takes care of additional broadening effects that have not been considered such as those due to scattering at windows and other obstructions in the cavity [12]. Fig.4.22. shows the variation of the resonance bandwidth with gas pressure for high and low concentration NO_x samples.

Similar studies were done with a lower concentration NO_x samples ($\sim 98\% \text{NO}_2$ in $\sim 4\% \text{NO}_x$:air mixture obtained from the Fertilizers and Chemicals Travancore Ltd, (FACT), Eloor, Cochin). It was seen that for these low concentration samples no marked shift in the resonance frequency was observed with increase in gas pressure, though the resonance bandwidth variation was observed. This is represented in fig.4.23. There was also no indication of any frequency shift from the phase of the PA signal in this case. The resonance effect was probably not observed in the low concentration samples since the gas density in those samples was obviously not sufficient to produce detectable changes in the velocity of sound in the gas.

iii. Relaxing Heat Capacity Of The Sample Gas

The variation of the resonance frequency (fig.4.20) with gas pressure is similar to the above mentioned ultrasonic dispersion curve. The frequency change depends on the change of heat capacity and is proportional to the resulting change in sound velocity. The relaxing heat capacity can thus be calculated from

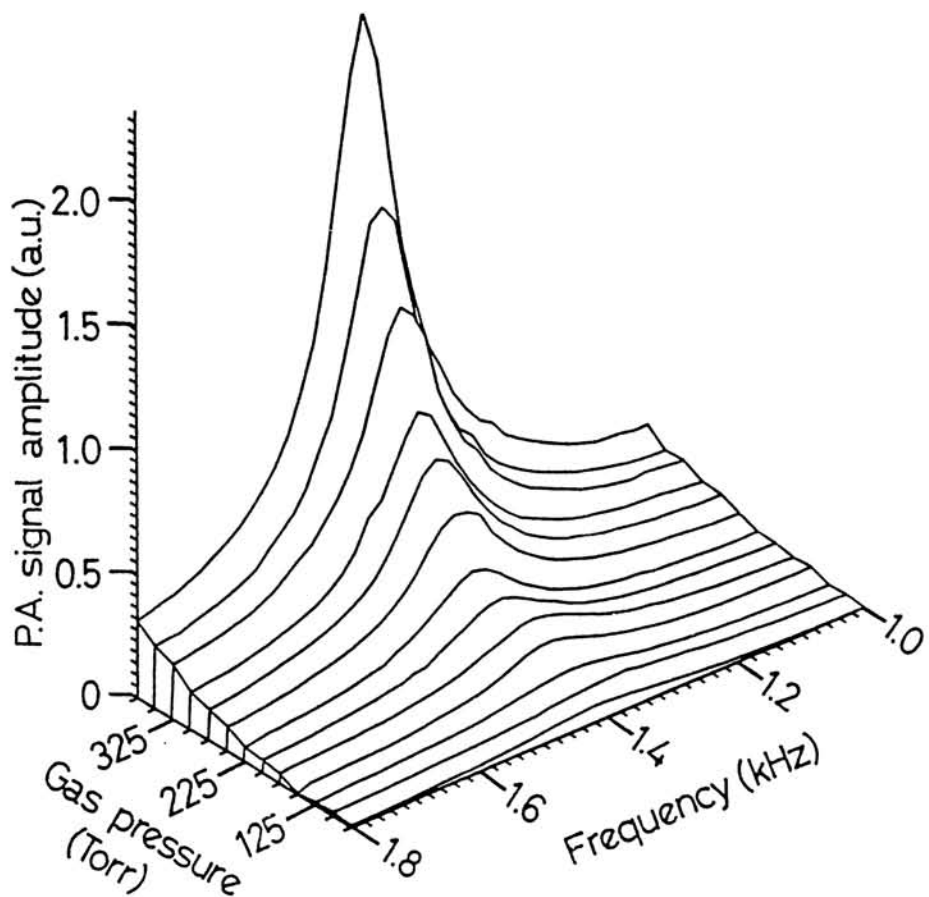


Fig.4.23. The 3-D representation of the variation of the frequency response of the PA amplitude with gas pressure for low concentration NO_x sample.

the width of the dispersion curve. The product of the frequency and pressure values at the point of inflection lead to the relaxation time of the gas as in the case of ultrasonic dispersion measurements. This method of calculating the relaxation time of the gas by frequency measurements rather than by velocity measurements is more accurate as demonstrated by Frank and Hess in mixtures of CH_4 and Xe [11]. From fig.4.20., this quantity can be calculated for the NO_x gas mixture used in these studies. The pressure and the frequency at the point of inflection are 125 Torr and 1037.5 Hz respectively and the relaxation time of the high concentration NO_x gas mixture was found to be,
 $P_T = 0.12 \mu\text{sec}$ Torr.

iv. Quality Factor (Q) And PA Cell Constant (F)

As mentioned earlier, the Q factor of the cell is dependent on the dissipative processes in the cavity. The Q factor of the cell can be easily evaluated by studying the acoustic resonance of the PA cell. From the experimental data, the Q factor can be evaluated by experimentally determining the resonance frequency (ω_0) and the bandwidth ($\Delta\omega$) around that resonance as,

$$Q(\omega_0) = \frac{\omega_0}{\Delta\omega} \quad \dots\dots(4.19)$$

Since both ω_0 and $\Delta\omega$ are dependent on the gas pressure, the type of variation of the Q factor with the gas pressure is obvious as seen in fig.4.24. The Q factor increases with pressure first and then decreases for high pressures. Similar observations, however unexplained, have been reported by Fiegel et al [21], where the Q factor of the PA cell, monitored using the $14549.99\text{cm}^{-1} R_1 R_{11}$ line in the B-band of molecular oxygen increases up to a pressure of 400 torr and then decreases. Both high and low concentration NO_2 gas samples gave similar results, even though the resonance

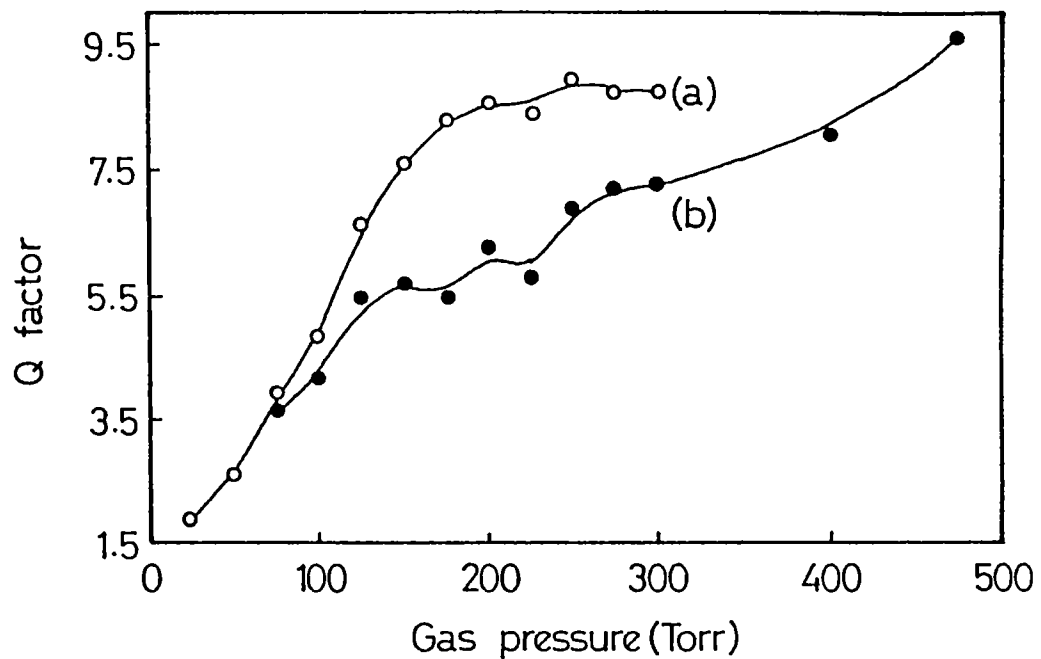


Fig.4.24. The variation of the Q factor of the PA cell using (a) high concentration (b) low concentration NO_x samples

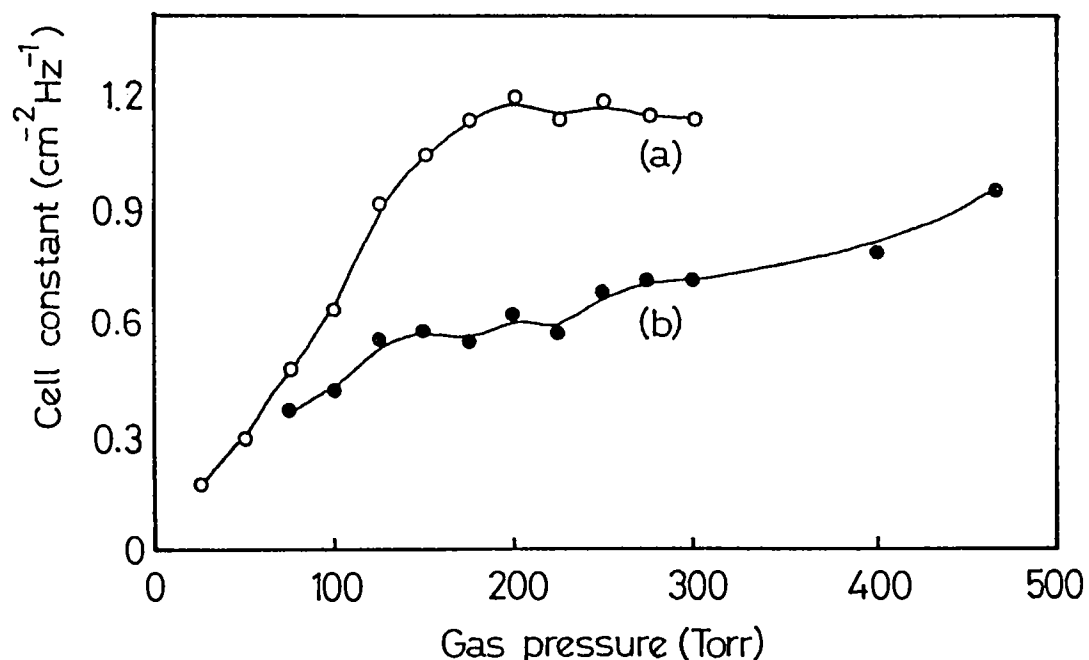


Fig.4.25. The variation of the cell constant $F(\omega_0)$ of the PA cell using (a) high concentration (b) low concentration NO_x samples

frequency shift was observed only for high concentration sample.

From the transmission line theory [1,20] for the acoustic wave propagation in a cylindrical cavity, a cell constant F , independent of the laser power (W) and the absorption coefficient (α) can be defined at resonance frequency $p = F(\omega = \omega_0) \alpha W$, where p is the pressure response of the cell, α is the absorption coefficient at one atmosphere pressure of the sample gas at the wavelength of laser radiation used, W the laser power and ω_0 the resonance frequency. For a given cell geometry the cell constant,

$$F(\omega_0) = \frac{(\gamma-1) L Q G}{\omega_0 V_0} \quad \dots \dots \dots (4.20)$$

putting $V_0 = \pi R_0^2 L$ and $Q = \omega_0 / \Delta\omega$, R_0 being the radius of the cavity and $\Delta\omega$ the resonance bandwidth. The cell constant can thus be experimentally evaluated as,

$$F(\omega_0) = \frac{(\gamma-1) G}{\pi R_0^2 \Delta\omega} \quad \dots \dots \dots (4.21)$$

where, γ is the ratio of specific heats, (approximated to 1.33 for triatomic gases), Q the quality factor, V_0 the volume of the resonator and G is a geometrical factor of order 1. In effect, the cell constant is proportional to γ and is inversely proportional to the resonance bandwidth $\Delta\omega$. This can be seen in fig.4.25. which shows the variation of the cell constant with the gas pressure.

v. Pressure Response Of PA Cell (R_p)

The pressure response to the input modulated power can be defined as $\Delta p / \Delta q$, where, Δp is the periodic pressure signal induced by the

periodic absorbed power Δq . From transmission line theory, this quantity can be evaluated as [2],

$$R_p = \frac{Q_r}{\omega_0 V_0} \quad \dots \dots \dots (4.22)$$

where ω_0 is the resonance frequency and Q_r the quality factor of a particular resonance mode. At resonance the pressure response has an inverse resonance frequency variation, and again, we can see that the R_p has an inverse $\Delta\omega$ variation as seen in fig.4.26.

vi. Gas Thermal Diffusion Length (d_h)

In the PA cavity, the thermal expansion of the gas is adiabatic. Near the walls of the cavity, it changes into isothermal expansion since the walls in the practical PA cell are at ambient temperature which is constant in time and does not follow gas periodic temperature variations [2]. Apart from a narrow region near the cell walls kept at constant temperature, the gas temperature tends to follow the pressure signal. Therefore a pressure signal generated upon the external walls induces a large temperature gradient, inducing gas flow from outside. This heat flow occurs in a region of width which is equal to the gas thermal diffusion length d_h and its rate being approximately equal to,

$$W_h \cong k_h (A/d_h) \Delta T \quad \dots \dots \dots (4.23)$$

where, T is the ambient gas temperature, A the total cell surface area, k the gas specific heat conductivity and ΔT the temperature difference produced upon the range d_h near the walls. For an open longitudinal PA cell of the kind used in these studies, the quantity d_h can be evaluated as [2],

$$d_h = \frac{\pi R_0}{Q} \quad \dots \dots \dots (4.24)$$

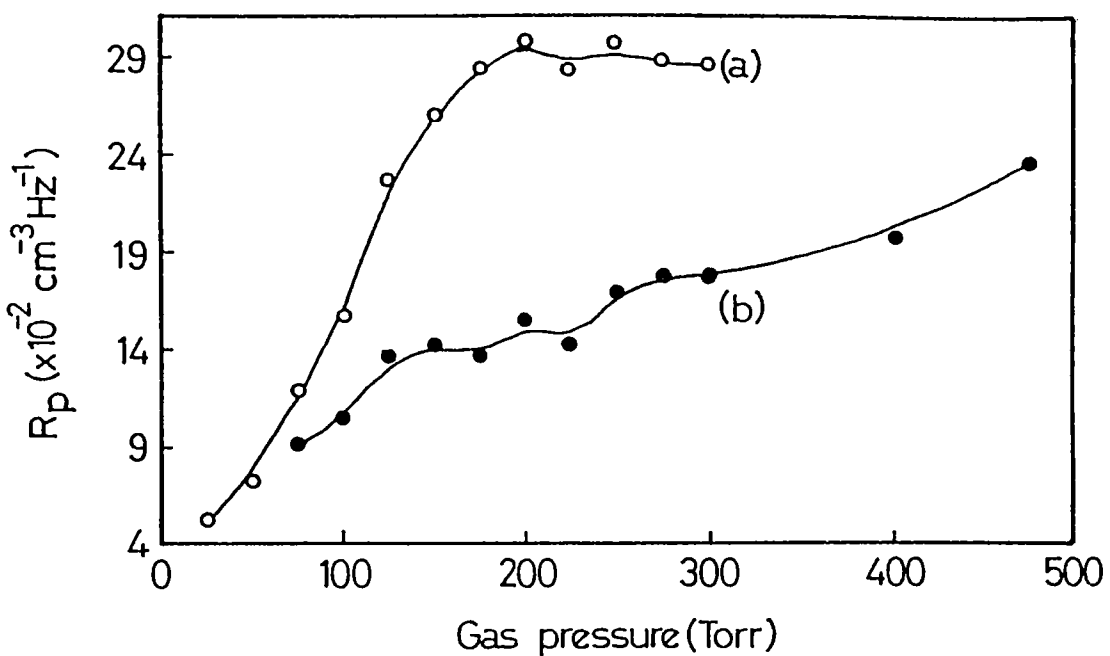


Fig.4.26. The variation of the pressure response of the PA cell using (a) high concentration (b) low concentration NO_x samples

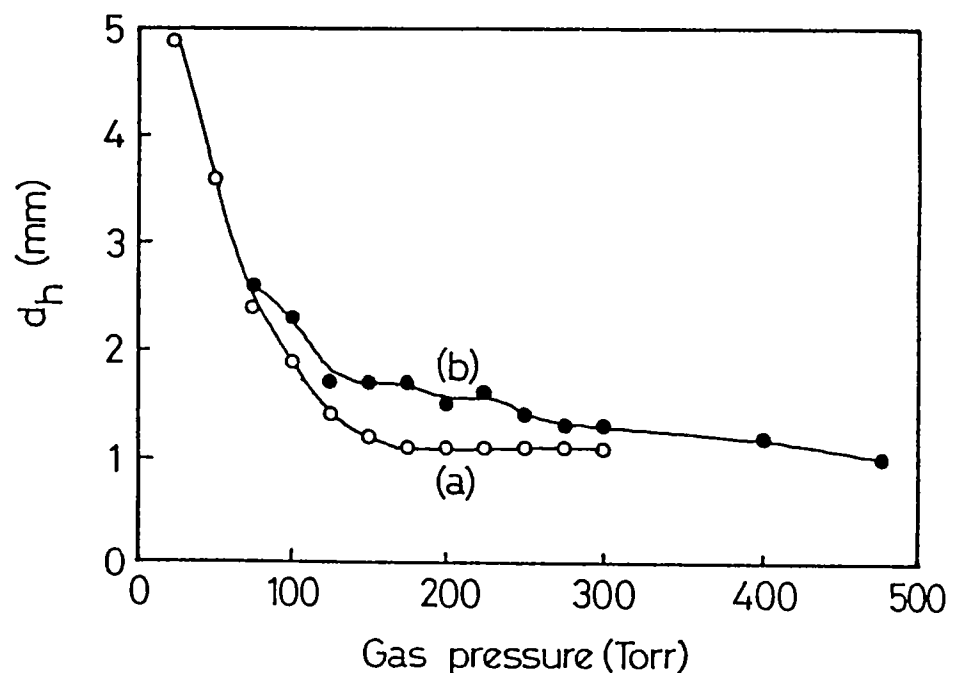


Fig.4.27. The variation of the gas thermal diffusion length of the PA cell using (a) high concentration (b) low concentration NO_x samples

The variation of the gas thermal diffusion length with the gas pressure is given in fig.4.27. It can be seen that, as the gas pressure increases, this quantity decreases and is constant for pressures greater than 200 Torr for high concentration gas samples. Or, the PA signal is damped in a smaller distance as the gas pressure increases.

4.5. Conclusions

The different systems and subsystems in the experimental arrangements for the pulsed and cw PA studies have been detailed. The design and characteristics of the pulsed and dual cavity differential PA cell as well as the pre-amplifiers have also been discussed. Some of the characteristics of the dual cavity PA cell, using both high and low concentration NO_x samples have been determined.

4.6. References

- [1] Harren F J M, PhD thesis "*The PA Effect Refined and Applied to Biological Problems*" Katholieke University, The Netherlands, (1988)
- [2] Kritchman E, et al, *J.Opt.Soc.Am.*, **68**, 1257, 1978
- [3] Quanta Ray model DCR11 Nd:YAG laser instruction manual
- [4] Quanta Ray model PDL-II pulsed dye laser instruction manual
- [5] Stanford Research Systems box-car averager instruction manual
- [6] Spectra Physics model 171 argon ion laser instruction manual
- [7] Spectra Physics model 380 ring dye lasers and accessories instruction manual
- [8] EG&G model 192 mechanical chopper instruction manual
- [9] Burleigh model WA20VI wavemeter instruction manual
- [10] EG&G model 5208 lock-in amplifier instruction manual
- [11] Frank K and Hess P, *Chem.Phys.Lett.*, **68**, 540, (1979)

- 12] Karbach A, Roper J and Hess P, *Chem.Phys.*, **82**, 427, (1983)
 13] Fiedler M and Hess P, *J.Chem.Phys.*, **93**, 8693, (1990)
 14] Johnson R H, et al, *Appl.Opt.*, **21**, 81, (1982)
 15] Richardson E G, "Ultrasonic Physics, 2nd Edition", (Elsevier, Amsterdam, 1962)
 16] Matheson A J, "Molecular Acoustics", (Wiley-Interscience, New York, 1971)
 17] Herzfeld K F and Litowitz T A, "Absorption and Dispersion of Ultrasonic Waves", (Academic Press, New York, 1959)
 18] Cottrell T L and McCoubrey J C, "Molecular Energy Transfer in Gases", (Butterworths, London, 1961)
 19] Morse P M and Ingard K V, "Theoretical Acoustics" (McGraw-Hill, New York 1968)
 20] Bernegger S and Sigrist M W, *Appl.Phys.B*, **44**, 125, (1987)
 21] Fiegel R P, Hays P B and Wright W M, *Appl.Opt.*, **28**, 1401, (1989)

4.7. Symbols and Notations

	Total surface area of the cavity
$\alpha_0 - \alpha_3$	Coefficients of the polynomial
	Second virial coefficient
	Capacitance
c_0	Velocity of sound in the gas contained in the cell
h_v^d	Gas thermal and viscous diffusion lengths
ω	Resonance frequency shift
	PA cell constant
SR	Free spectral range
	Geometric factor for the cell
k_{mn}	Resonance frequency of cell
	Ratio of specific heats
(ω, P)	Effective heat capacity
	Gas specific conductivity
$K_1 K_2 K_3$	Constants

L	Cavity length
λ, λ_0	Unknown and reference wavelengths
N, N ₀	Number of sample and reference pulses
P	Gas pressure
ρ	Density of gas
Q	Quality factor of the PA cell
R	Resistance
R	Universal gas constant
R ₀	Cavity radius
R _p	Pressure response at resonance
S _s , S _r	Signals from sample and reference cells
SNR	Signal to noise ratio
T	Ambient temperature
ΔT	Temperature difference
τ	Relaxation time
V ₀	Volume of the cell
ω, ω_0	Modulation and resonance frequency
$\Delta\omega$	Resonance bandwidth

CHAPTER V

PULSED PHOTOACOUSTIC STUDIES OF FORMALDEHYDE VAPOUR

ABSTRACT

THIS CHAPTER DEALS WITH THE DETECTION AND ANALYSIS OF THE PAS OF FORMALDEHYDE VAPOUR IN THE VISIBLE REGION USING THE TWO PHOTON ABSORPTION (TPA) PROCESS. THE ENVIRONMENTAL ASPECTS OF FORMALDEHYDE WITH REFERENCE TO ATMOSPHERIC POLLUTION AND ITS DETECTION USING THE TPA PROCESSES ARE BRIEFLY DESCRIBED. THE RECORDED PA SPECTRUM IS ANALYZED ON THE BASIS OF THE OPA AND TPA ABSORPTION PROCESSES OCCURRING IN THE SAMPLE. AN ATTEMPT HAS BEEN MADE TO APPLY THIS TECHNIQUES TO A FEW OTHER SAMPLES.

CHAPTER V

PULSED PHOTOACOUSTIC STUDIES IN FORMALDEHYDE VAPOUR

5.1. Introduction

As discussed in the previous chapters, PA technique is an effective tool to investigate the spectroscopy of atoms, molecules as well as condensed matter. The high sensitivity of the technique helps in studying very weak processes like overtone absorption, multi photon absorptions, forbidden transitions, trace detection etc in the absorbing species. The present chapter deals with the PA effect investigated using pulsed dye laser.

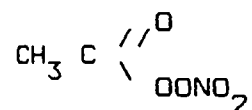
Formaldehyde (HCHO) is a very commonly used organic compound and finds applications different areas like preservation, pest control and synthesis of plastics and resins. It is a colorless soluble gas at room temperature having a boiling point of -21°C . The very high reactivity of this gas even with itself makes it very difficult to isolate and to handle it in its pure form. It is thus commercially available as an aqueous solution (37-50% by weight of HCHO). The high chemical reactivity of this simplest form of the aldehyde group finds applications as an important intermediate in the manufacturing of resins, dyes, plastics pharmaceuticals etc.

Apart from these applications, HCHO is considered as one of the primary atmospheric pollutant, and thus the PA method of detection and spectroscopic analysis of HCHO vapour have considerable significance from the point of view of pollution

monitoring. Formaldehyde is an intermediate in low temperature combustion systems [1] and incomplete burning of fuel in internal combustion engines makes it an important primary air pollutant [2]. Furthermore, it is an oxidation product of hydrocarbons in photochemically active atmospheres, either by OH radical attack or in the case of terminal olefins by direct oxidation by ozone [3,4]. The organic acids together with other carbonyl compounds (aldehydes and ketones) in the atmosphere are produced in olefin-ozone reactions and are also formed in free radical oxidation during degradation of hydrocarbons [21]. Apart from being an eye irritant, and as such undesirable, HCHO may contribute to the initiation of atmospheric chain reactions by its photodissociation (at 113.9 nm) in the UV which occurs at a rate of 0.4/h in average sunlight [5,6]. Though the quantum yield of photodissociation is unity, the ratio and the wavelength dependence of the primary processes yielding,



respectively is still not very clear [7-9]. Recent data on the band dissociation energy of HCHO indicate that the formation of free radicals by photodissociation is confined to excitation wavelengths less than 324nm [10,11]. The photolysis of HCHO in parts, leads to the formation of H atoms and formyl radicals as mentioned above and it is seen that species such as H, CH_3 , CHO etc are highly reactive and can initiate, or participate in highly complex reaction sequences leading to a variety of products. This has been particularly observed in urban atmospheres where the NO and NO_2 concentrations are higher [55] resulting in their reaction with reactive hydrocarbons (RHC), producing important pollutants like the PAN (peroxyacetyl nitrate) having a structure,



To evaluate the formation of free radicals in the atmosphere, which is the main cause of pollution by HCHO, it is necessary to perform real-time measurements of HCHO concentrations in the atmosphere and also in simulated laboratory conditions. The rather scant data on HCHO concentration measurements both in laboratory and atmospheric conditions have been mainly obtained by calorimetric and other wet chemical techniques such as the Schiff's test [12-14].

5.2. Detection of Formaldehyde

High concentrations of formaldehyde have been determined in automobile exhausts and oil smoke by laser Raman technique using nitrogen laser at 333.1 nm, but no absolute concentration measurements were possible due to the interference of C₂H₄ in this wavelength region [15]. Differential absorption technique was used to determine HCHO concentrations in laboratory conditions using a Zeeman tuned Xenon laser in the 3.5μm wavelength region [16]. Fluorescence is another technique that has been effectively used to detect low concentrations of HCHO in air. A flashlamp pumped dye laser operating in the 320-350nm region was used to excite the fluorescence in the HCHO sample. The fluorescence intensity was found to be linear up to 10 ppm of HCHO. A detection limit of 5ppmV of HCHO in air at atmospheric pressure was achieved [5]. The sharp near-UV absorption regions in HCHO have been investigated by different techniques by early workers, though these studies were basically limited to the spectroscopic aspect of HCHO molecule rather than for trace detection and analysis. The many-fold advantages of photoacoustics can be effectively applied to detect organic pollutants without much difficulty. Pulsed PA technique using UV lasers is preferred for detection since this technique can detect still lower concentration than the cw technique without compromising on

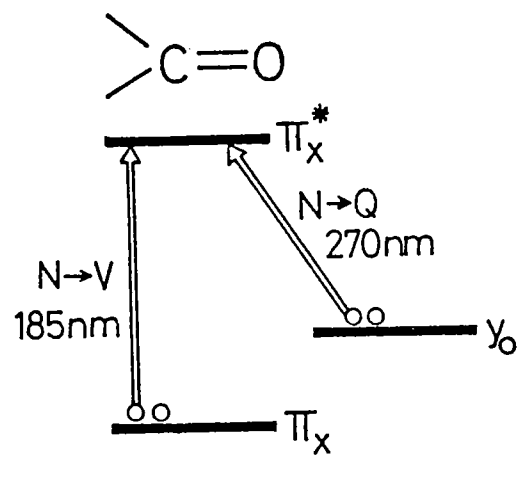
the sensitivity of the system. Atmospheric organic acid pollutants like acetic acid (CH_3COOH) and formic acid (HCOOH) have been detected by pulsed PAS technique using frequency doubled visible lasers to obtain UV output in the 220nm region [17]. Similar PA studies using UV lasers have been employed to determine trace quantities of sulfur dioxide also [18,19]. The Earlier reported work on detection of HCHO by PAS was carried out using a frequency doubled pulsed dye laser at 303.59nm. A detection limit of 50ppmV was obtained under laboratory conditions [20]. Most of the experiments in PA detection of organic species use either UV lasers ($< 350\text{nm}$) or IR ($> 1.5\mu\text{m}$) as the excitation due to the strong absorption in the UV-blue and IR regions exhibited by the carbonyl species. In the visible region, these compounds do not have strong absorption and even if absorption takes place, it is very weak and the absorption is due to phenomena like two photon absorption (TPA), overtone absorption etc. Using powerful pulsed lasers or by using intracavity detection, these weak phenomena occurring in organic compounds can be detected. TPA is a better tool for detection of such samples since the TPA signal is proportional to the square of the incident light intensity and thus can be easily detected as long as the requirements for TPA to occur are satisfied.

5.3. Absorption Spectrum of Formaldehyde

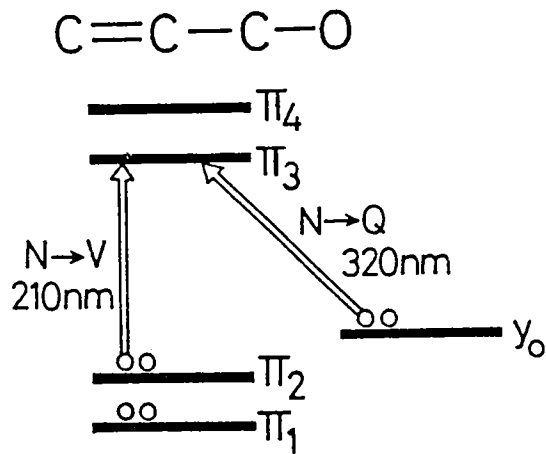
As is well known, most short chain organic molecules do not exhibit strong absorption in the visible region. Formaldehyde has strong absorption in the UV and blue regions (180 to 350nm) [27,28] and in the NIR regions ($> 1250\text{nm}$). The detailed analysis and interpretation of the the absorption bands in HCHO were first accomplished by Dieke and Kistiakowsky, who gave the interpretation of the electronic absorption spectrum of this polyatomic molecule in some of the main UV absorption bands lying

in the 353 to 326nm region [29]. HCHO absorbs weakly in the 270nm region and strongly in the 185nm region. The first of these bands is assumed to be due to the symmetry forbidden N \rightarrow Q transition $\sigma^2 \pi_x^2 y_o^2 \rightarrow \sigma^2 \pi_x^2 y_o^2 \pi_x^*$ [41]. This assignment is supported by an analysis of the rotational structure of the band which indicates that the transition moment lies in the plane of the molecule so that the transition cannot involve both the Π_x and Π_x^* [29]. The energy level for the carbonyl and conjugated carbonyl group are given in fig.5.1. Formaldehyde decomposes at 290nm as HCHO \rightarrow CO + H₂ [42]. Apparently the energy is absorbed by the carbonyl group and then passed on to a C-H bond. The absorption at 185nm is assumed to be due to the N \rightarrow Q transition $\sigma^2 \pi_x^2 y_o^2 \rightarrow \sigma^2 \pi_x^2 y_o^2 \sigma^*$ which is similar to the long wavelength transition found in singly bonded basic groups. It is also probably overlapped by the N \rightarrow V transition $\sigma^2 \pi_x^2 y_o^2 \rightarrow \sigma^2 \pi_x^2 y_o^2 \pi_x^*$ [43]. The N \rightarrow V transition occurs from a bonding orbital in the ground state of a molecule to a higher energy orbital formed from the same atomic orbitals. For transitions between π orbitals, these are often called $\pi \rightarrow \pi$ transitions. The N \rightarrow Q transition occurs from a non-bonding orbital localized on an atom to an anti-bonding orbital, or other higher energy orbitals. For transitions to π orbitals, these are often called n \rightarrow π transitions [43].

The normal absorption spectrum of HCHO solution recorded using a UV-VIS-NIR spectrophotometer (Hitachi U3410) in the wavelength region 185 to 2500nm is given in fig.5.2. It is seen that the sample has high absorption bands in the UV as well as IR regions with weak absorptions bands in the visible (fig.5.3.) and NIR regions. The UV absorption in HCHO is due to electronic absorption while that in the visible, NIR and IR due to the combinations of the various vibrational modes frequencies of the planar HCHO molecule. The six normal modes of vibration (v_1 to



(a)

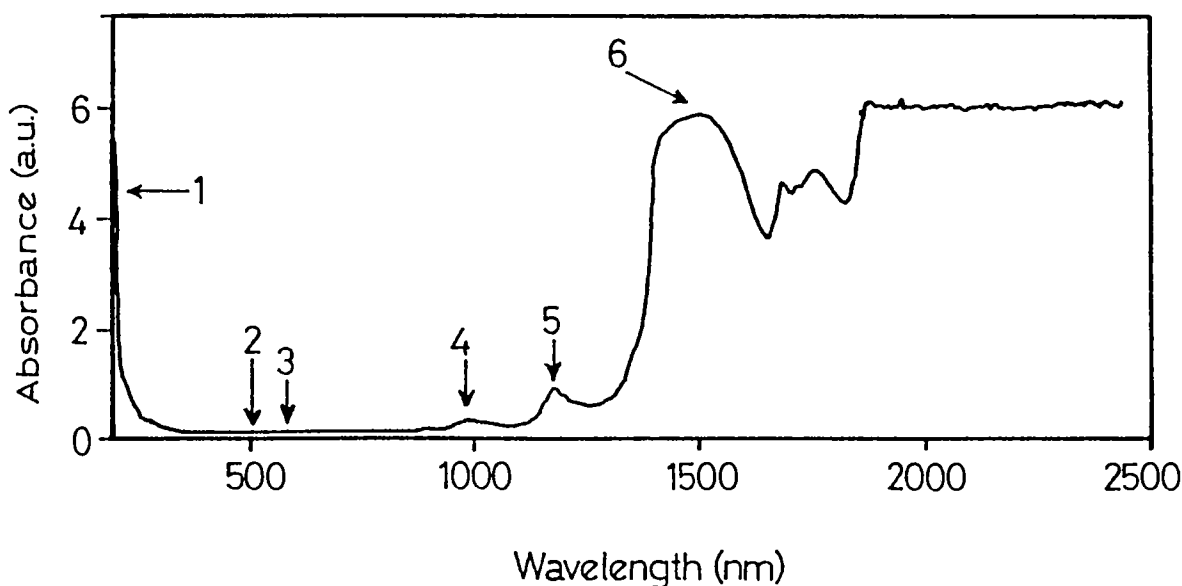


(b)

Carbonyl group

Conjugated carbonyl group

fig.5.1. The energy levels for the (a) carbonyl and (b) conjugated carbonyl groups



g.5.2. The UV-VIS-NIR absorption spectrum of HCHO showing the various combination absorption bands

able.5.1. The band positions, probable assignments and the relative absorbance values for formaldehyde absorption in the UV-VIS-NIR region

PEAK No.	BAND POSITION (cm ⁻¹)	PROBABLE ASSIGNMENT	RELATIVE ABSORBANCE (a.u.)
1	UV band	A ₂ ² → B ₂ ¹	5.5
2	19268	5v ₁ + 2v ₅	0.097
3	17715	5v ₁ + 3v ₆	0.006
4	10101	3v ₁ + 2v ₄	0.36
5	8421	3v ₁	0.85
6	6666	(3v ₁ + v ₆) ₂	5.8

v_6) of the planar HCHO molecule and their ground and excited state fundamental frequencies are represented in fig.5.4. The various band positions, probable assignments and their relative absorbance are given in Table 5.1. It is evident from the above table that the absorbance decreases with increasing involvement of higher vibrational modes in the combination band formation.

5.4. Two Photon Absorption (TPA) Process

Two photon absorption processes is one of the most well studied of the different optical non-linear phenomena. PA effect has been effectively used to detect this processes in samples using moderately powered pulsed and cw lasers. This process allows one to detect and analyze samples having strong UV absorption by using tunable laser in the visible region.

5.4.1. Introduction

As the name suggests, TPA occurs essentially due to simultaneous absorption of two photons of similar or different frequency. The process can be thought of as a kind of modulation phenomenon where the effect of the electromagnetic fields of one of the absorbed photons modulates the energy spectrum of the sample in such a way that a second photon can be absorbed while the modulation lasts [30]. In one photon absorption (OPA) processes, only "allowed dipole transitions" can be studied. In gases, the "forbidden" transitions are too weak to be observed by OPA. One then is limited to the exploration of a small subset of energy eigen states of the sample namely, those belonging to a particular symmetry group of the system. The allowed transitions in TPA cover a much larger range of symmetry types often those which are inaccessible by OPA. Further, in gases and liquids, polarization studies are not possible by OPA due to the averaging out of the polarization effects. On the other hand, TPA in solids, liquids

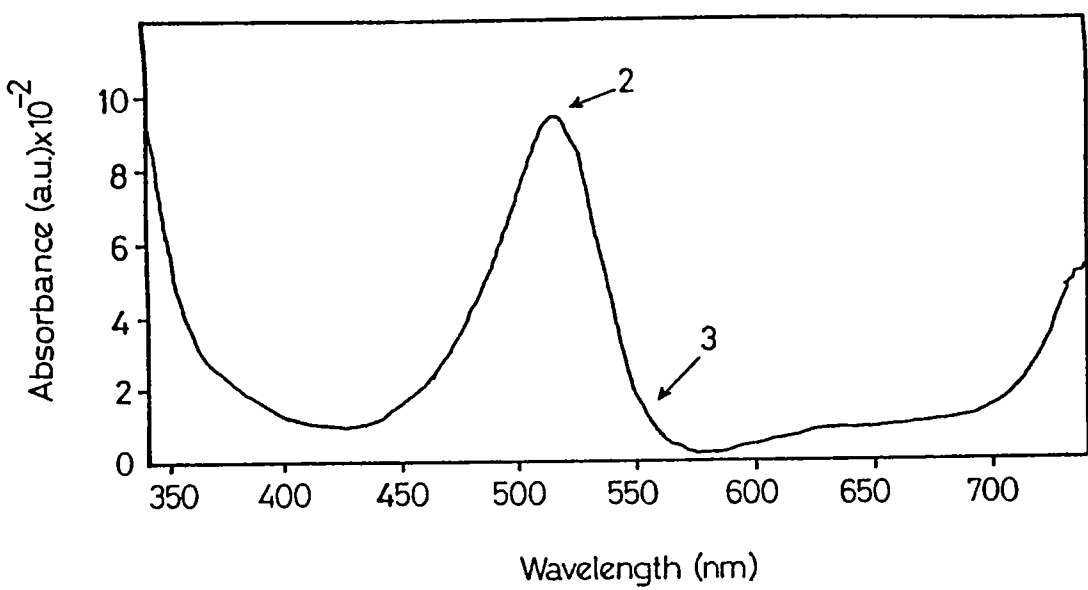


Fig.5.3. The weak $5\nu_1 + 2\nu_5$ combination band recorded with higher sensitivity in the wavelength region of $\sim 519\text{nm}$ using a UV-VIS-NIR spectrophotometer

Vibration frequency modes (cm^{-1})	ν_1	ν_2	ν_3	ν_4	ν_5	ν_6
$X^1\text{A}_1$	2766.4	1746.1	1500.6	1167.3	2843.4	1251.2
${}^1\text{A}''$	2847.0	1173.0	887.0	124.6	2968.0	904.0

Fig.5.4. The various conventional and normal modes of vibration in planar HCHO molecule and their ground and excited state fundamental frequencies

and gases can almost uniquely identify the symmetry of the eigen states of the molecules/atoms of the sample provided the right experimental technique is utilized to detect the TPA. The main characteristics of TPA are,

1. The initial and final states should have the same parity, ie, a transition that is forbidden for one photon absorption process is allowed in the TPA process.
2. The probability of TPA is proportional to the fourth power of the electric field ie, to the square of the intensity.
3. The final state may have an excitation energy in the UV region while the incident radiation has an energy in the blue-VIS region. Thus if a sample has absorption in the 280nm region, and the parity conditions are satisfied, then the TPA can be induced by using an excitation source of approximately twice the wavelength ie, 560nm.
4. It is also possible to eliminate the momentum transfer between the electromagnetic field associated with the excitation source and the atom or molecule, thus eliminating Doppler broadening.

The first two characteristics make it possible to reach different states that cannot be reached from the same initial state in an OPA process while the last characteristic assures that highly excited states can be investigated with high spectral resolution [31].

A similar kind of process, though not to be confused with TPA is the two-step process in which one photon populates the energy state of the matter originally in ground state and the second photon then makes the final transition to the higher energy level. In two-step process, the existence of a stationary excited state is mandatory while it is not so in the case of TPA, where the two photons are absorbed simultaneously.

Since the TPA cross section is very small, very high intensities of the excitation source and sensitive detection techniques are required to detect this phenomena. TPA has been detected by various techniques such as the pump-probe technique where the transmission of the probe beam is monitored as the pump is tuned across the TPA profile of the sample, by monitoring phenomena associated with the sample such as fluorescence, photo-decomposition, stimulated emission, non-radiative de-excitation etc. Though the theoretical prediction of TPA was put forward in 1931 by Geoppert-Meyer [32], the first experimental demonstration of TPA and its application to spectroscopy had to wait till the advent of high power lasers [33-35]. Since then, TPA has been applied extensively to spectroscopy of solids, liquids and gases using various detection techniques [36,37]. Doppler-free technique was coupled with TPA process to study the samples under high spectroscopic resolution [38,39]. TPA was detected using photoacoustics in CH_3I and CH_3D vapours using excitation source in the wavelength region 396 to 403nm and this was used to develop a two photon photoacoustic spectrometer by Wilder and Findley [40].

5.4.2. Brief Theory of TPA Process

Since the PA detection of HCHO is essentially due to the TPA process, a brief description of the optical non-linear processes and the TPA process are described below.

i. Non-Linear Optical Process

A dielectric medium when placed in an electric field is polarized, if the medium does not have a transition at the frequency of the field. each constituent molecule acts as a dipole, with a dipole moment p_i and the dipole moment vector per unit volume is [44],

$$\bar{P} = \sum_i \bar{p}_i \quad \dots \dots \dots \quad (5.1)$$

here the summation is over the dipoles in the unit volume. The orienting effect of the external field on the molecular dipoles depends on both the properties of the medium as well as the field strength. Thus,

$$\bar{P} = \epsilon_0 \chi : \bar{E} \quad \dots \dots \dots \quad (5.2)$$

where χ , which is a second order tensor, is the polarizability or dielectric susceptibility of the medium, E the electric field associated with the light. This relation is valid for field strengths of conventional sources. The quantity χ is a constant, independent of E , its magnitude being a function of frequency. With sufficiently intense laser radiation, the above relation does not hold good and the components of p_i can be generalized to,

$$p_i = \epsilon_0 \left(\chi_{ij}^{(1)} E_j + \chi_{ijk}^{(2)} E_i E_j + \chi_{ijkl}^{(3)} E_i E_j E_k \dots \right) \quad \dots \dots \dots \quad (5.3)$$

where $\chi^{(1)} E$ is the same as in equation 2 and is responsible for the linear optical effects, while the coefficients $\chi^{(2)}, \chi^{(3)} \dots$ define the degree of non-linearity and are known as the non-linear optical susceptibilities. If the field is low, as in the case of low intensity light sources, only the first term in the above equation need be considered and it is seen that the P is linearly proportional to the intensity of light, or it deals with 'linear optics'. When the higher order terms are to be considered at high light intensities, the P is no longer linearly dependent on the intensity and thus represents the 'non-linear optics'.

The interaction of electromagnetic radiation with matter involves processes in which several photons can take part. An early example is provided by the Raman scattering process. In this, one photon is absorbed, another emitted and the difference in photon energy is taken up by a transition in the material system from an initial state $|j\rangle$ to a final state $|f\rangle$ [31]. The symbolic Hamiltonian describing this event is proportional to $a_1^\dagger c_i^\dagger c_f^\dagger$ where, a_1^\dagger represents an annihilation operator for photons in mode 1, a_2^\dagger represents the creation operator in mode 2, while the c_i^\dagger takes an electron out of state $|j\rangle$ and c_f^\dagger puts an electron in state $|f\rangle$. The closely related phenomenon of two photon absorption is described by a term in the Hamiltonian proportional to $a_1^\dagger a_2^\dagger c_i^\dagger c_f^\dagger$ [32]. The energy balance for the two photon process as compared to Raman scattering is shown in fig.5.5. In Raman scattering involves spontaneous emission of a Stokes-shifted photon, the intensity of scattered light at ω_2 is proportional to the intensity of light at ω_1 . The power absorbed in two photon absorption is however, proportional to square of the incident light intensity. Thus, though both these processes were known during the same period, the experimental demonstration of TPA had to wait till the advent of high intensity laser sources. Moreover, the frequency of the laser must be adjustable if the two photon transition occurs between sharp energy levels and no accidental coincidences between the laser frequency and the energy separations exist. Thus the TPA process could be applied to spectroscopy only with the advent of tunable high power lasers.

The rate of energy absorption by matter in the presence of electromagnetic field can be represented by ,

$$\left\langle \frac{d}{dt} \frac{\text{absorbed energy}}{\text{volume}} \right\rangle_{\text{time}} = \langle \vec{j} \cdot \vec{E} \rangle \quad \dots\dots(5.4)$$

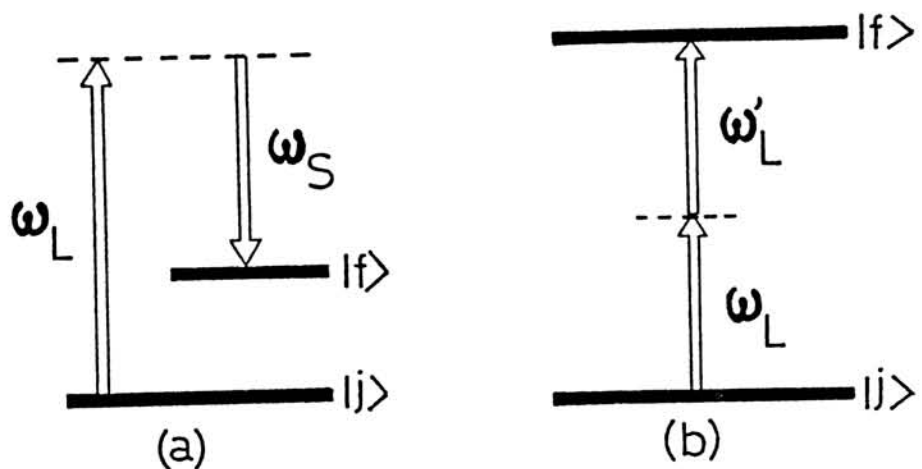


Fig.5.5. The comparison of the energy relations in (a) Raman scattering and (b) Two photon absorption processes

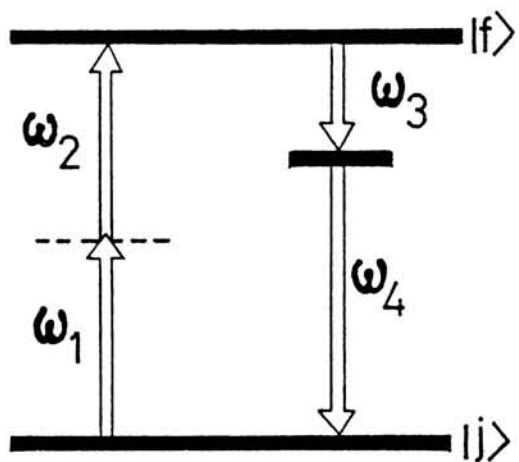


Fig.5.6. The representation of the energy relations in two photon absorption process

where, \bar{j} is the current density, \bar{E} the electric field associated with the electromagnetic field [30]. The absorption coefficient can be represented by,

$$\alpha = \frac{\left\langle \frac{d}{dt} \frac{\text{absorbed energy}}{\text{volume}} \right\rangle}{\text{Energy flux}} \quad \dots \dots \quad (5.5)$$

α can be expanded as $\alpha(I)$ to give,

$$\alpha = \alpha(I) = \alpha^{(1)} + \alpha^{(2)}I + \alpha^{(3)}I^2 + \dots \quad \dots \quad (5.6)$$

ii. Third Order Non-Linear Susceptibility and TPA

The absorption coefficient is related to the imaginary part of the optical susceptibility tensor. The second order $\chi^{(2)}$ term is responsible for phenomena like Second Harmonic Generation (SHG). The third order non-linear ($\chi^{(3)}$) susceptibility can cause various kinds of non-linear phenomena like Third Harmonic Generation (THG), TPA, Stimulated Raman Scattering (SRS) etc. Two photon absorption phenomenon occurs as a special case of this third order non-linear optical phenomena in which the total polarization can be represented as,

$$P_i^{(3)} = \chi_{ijkl}^{(3)} E_j^{\omega_1} E_k^{\omega_2} E_l^{\omega_3} \dots \quad \dots \quad (5.7)$$

such that $\omega_1 + \omega_2 + \omega_3 = \omega_4$

The χ^3 term causes the two photon absorption which can be obtained by putting $\omega_3 = -\omega_3$

$$\text{Since } E(-\omega_3) = E^*(\omega) = x_{ijk1}^{(3)} \epsilon_j \epsilon_k \epsilon_1^* \quad \dots \dots (5.8)$$

$$P_i = \chi_{ijkl}^{(3)} (-\omega_4; \omega_1, \omega_2, -\omega_3) E_j E_k E_l^* \quad \dots \dots \dots (5.9)$$

$$P^{(\omega_4)} e^{-i\omega_4 t} = \chi_{ijkl}^{(3)} (\omega_1, \omega_2, -\omega_3) E_j E_k E_l^* e^{-i(\omega_1 + \omega_2 - \omega_3)t} \quad \dots \dots \dots (5.10)$$

current density $\bar{j} = \frac{\partial P}{\partial t}$ $\dots \dots \dots (5.11)$

$$= -i\omega_4 P^{(\omega_4)} e^{-i\omega_4 t} = -i\omega_4 \chi_{ijkl}^{(3)} (\omega_1, \omega_2, -\omega_3) E_j E_k E_l^* e^{-i\omega_4 t} \quad \dots \dots \dots (5.12)$$

absorbed energy is equal to $E_l^* \cdot \bar{j}$ $\dots \dots \dots (5.13)$

$$E_l^* \cdot \bar{j} = -i\omega_4 \chi_{ijkl}^{(3)} E_j^* E_j E_k E_k^* \quad \dots \dots \dots (5.14)$$

TPA coefficient is related to the imaginary part of the third order non-linear susceptibility $\chi^{(3)}$ and is proportional to I^2 , where I , the intensity of the incident light is, given by,

$$I = \frac{c}{8\pi} |E|^2 \quad \dots \dots \dots (5.15)$$

TPA process is illustrated in fig.5.6. In this case, ω_1 and ω_2 may not be equal. When they are equal, then,

$$P_i \propto |E_j(\omega_1)|^4 \quad \dots \dots \dots (5.16)$$

Thus it can be seen that the TPA process is proportional to the square of the incident intensity. The excited atoms or molecules de-excite to the ground state via radiative transitions like fluorescence (ω_3 and ω_4) [Fig.2.b.] or by non-radiative paths, which can be detected by calorimetric techniques like the PA technique. From experimental data, the occurrence of TPA process can be verified by observing the absorption spectrum and the variation of the TPA signal with the laser intensity.

5.5. PA Detection of Formaldehyde

The experimental details and the results of the PA studies of the DPA and TPA studies in formaldehyde vapour are discussed below.

5.5.1. Experimental Details

The sample used in these studies is a 35% GR analytic grade solution of formaldehyde (E Merck India Ltd.). The sample was taken in a glass jar and connected to the PA cell via a needle valve. The cell was evacuated to rotary vacuum and the required pressure of the HCHO-air mixture in the sample jar was let into the PA cell which was then sealed off from the pump and the sample reservoir to reduce the noise that might be induced by a continuous gas flow through the cell [22]. The actual concentration of the HCHO in the mixture was not estimated due to the lack of other analytic techniques such as gas chromatography in the laboratory. All the pressures indicated in the following experimental data corresponds to the pressure of the HCHO-air mixture filled into the cell cavity. The sample reservoir was maintained at a temperature of about 50°C. For studies in the IR region, the fundamental 1.06 μ m output of the Nd:YAG laser was used and the frequency doubled 532nm was used to pump the dye laser for studies in the visible region giving the output from 540 to 580nm.

To avoid the formation and accumulation of the polymer of HCHO ie, paraformaldehyde (HCHO)_x (it is formed when HCHO solution is evaporated, upon standing or when subjected to low temperatures [12]) in the PA cell, which can lead to laser induced damage of the cell windows or degradation of the microphone, the cell is evacuated and flushed repeatedly with air as frequently as possible.

5.5.2. Pulsed PA Spectrum of Formaldehyde

The pulsed dye laser output is tuned over the wavelength range 560 to 580nm using the grating in the dye laser cavity. The PA signal is detected by the microphone and the amplitude of the first peak in the PA signal pulse thus obtained is processed by the gated integrator and the box-car averager. This signal is normalized with respect to the power spectrum of the dye laser output monitored by a laser power meter which records the power of the dye laser as its wavelength is scanned over the required range. The PA spectrum was recorded at various laser power levels and at different gas mixture pressures. The normalized PA spectrum of HCHO recorded at a peak laser power of 0.6MW is shown in fig.5.7. It shows a prominent peak at 564.5nm along with a number of comparatively weaker satellite bands on either side of it. The spectral profiles of the normalized, low resolution PA spectra of HCHO vapour was found to be different at different laser powers as seen in the figure.5.8. Since HCHO shows only a very weak absorption profile in the wavelength region being studied, and the evolution of the strong 564.5 nm band in the PA spectrum at sufficiently high laser powers can be an indication of the occurrence of some non-linear process in the sample. To confirm this, the variation of the PA signal with the laser power was investigated. The fig.5.9. shows the log-log plot of the laser power vs the PA signal amplitude at 564.5nm. As seen in

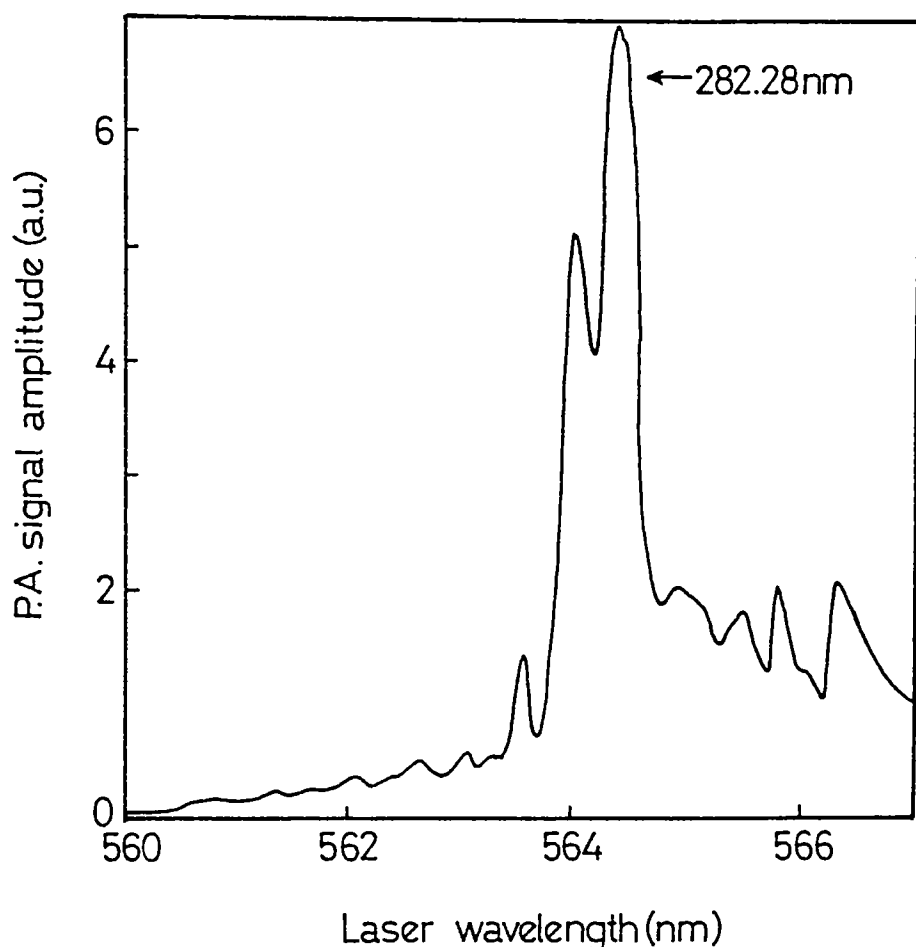


Fig.5.7. The normalized PA spectrum of HCHO vapour at a peak laser power of 0.6MW (Pressure \sim 100Torr)

In the figure, at lower laser powers, the slope of the plot is approximately unity indicating a one photon process (OPA) and at higher laser powers, the slope has a value of almost 2 and this indicates clearly the occurrence of a two photon process (TPA). The weak satellite bands also show the same behavior.

In order to confirm the occurrence of OPA, the liquid phase absorption spectrum of HCHO was recorded (fig.5.2.). Under considerably increased sensitivity, a weak absorption band in the 25 to 575 nm region was observed (fig.5.3.), which peaks at \approx 519nm. This band coincides with the most likely overtone combination $v_1^{5}v_6^3 = 5v_1 + 3v_6$, where the v_1 and v_6 are two of the six normal mode vibration frequencies of planar HCHO molecule as shown in fig.5.4. In gas phase, the peak will generally shift to the longer wavelength side due to the fact that the degree of freedom of the molecule is more restricted in the solution as compared to the vapour state. Thus the gas phase spectrum will also resolve the finer structures.

Formaldehyde, like most of the organic compounds does not exhibit any strong absorption in the visible region of the spectrum. Thus the OPA at lower laser powers has to be attributed to the excitation of the longer wavelength tail in the overtone combination band in the 519nm region. The TPA at higher laser powers can only be due to the transition between the ground and excited electronic states of HCHO as shown in fig.5.10.

Formaldehyde contains a carbonyl group with a characteristic weak absorption in the UV region due to the $n \rightarrow \pi^*$ transition ($f = 10^{-4}$ to 10^{-2}) [23]. The ground state of HCHO has a planar configuration with C_{2v} symmetry and is in the 1A_1 state. The excited state should be 1A_2 if the molecule is planar in the excited state also. However, the excited state happens to be nonplanar due to vibronic interaction but does not deviate too

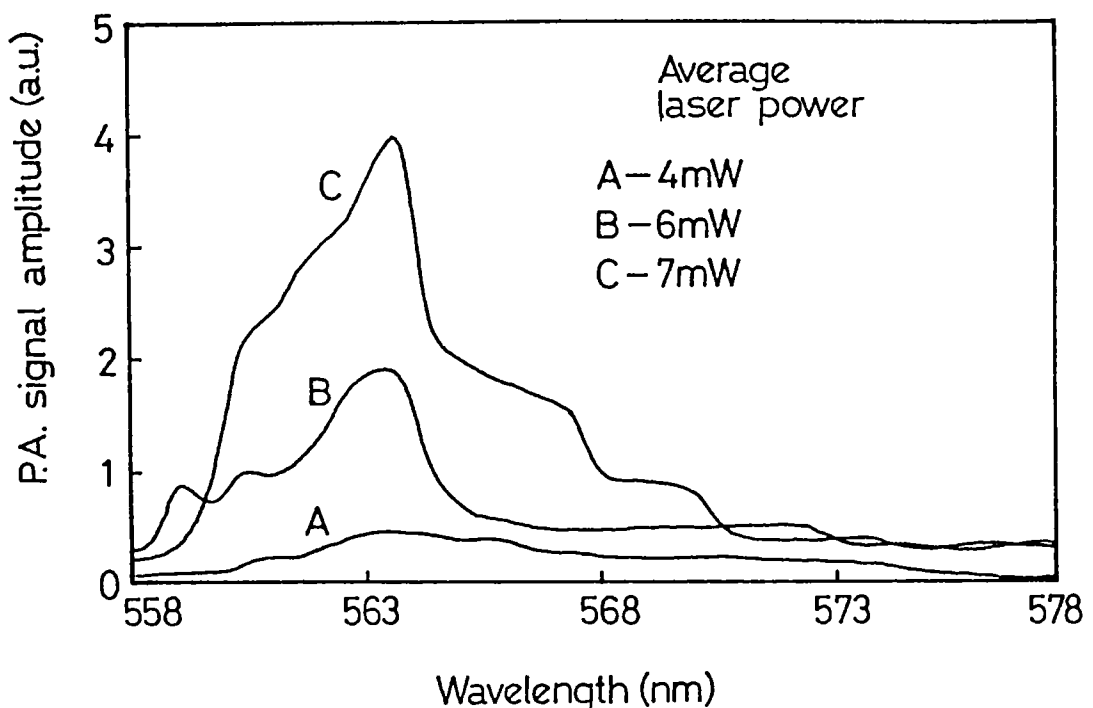


Fig.5.8. The PA spectral profile of HCHO vapour at different laser power levels (Pressure \sim 100 Torr)

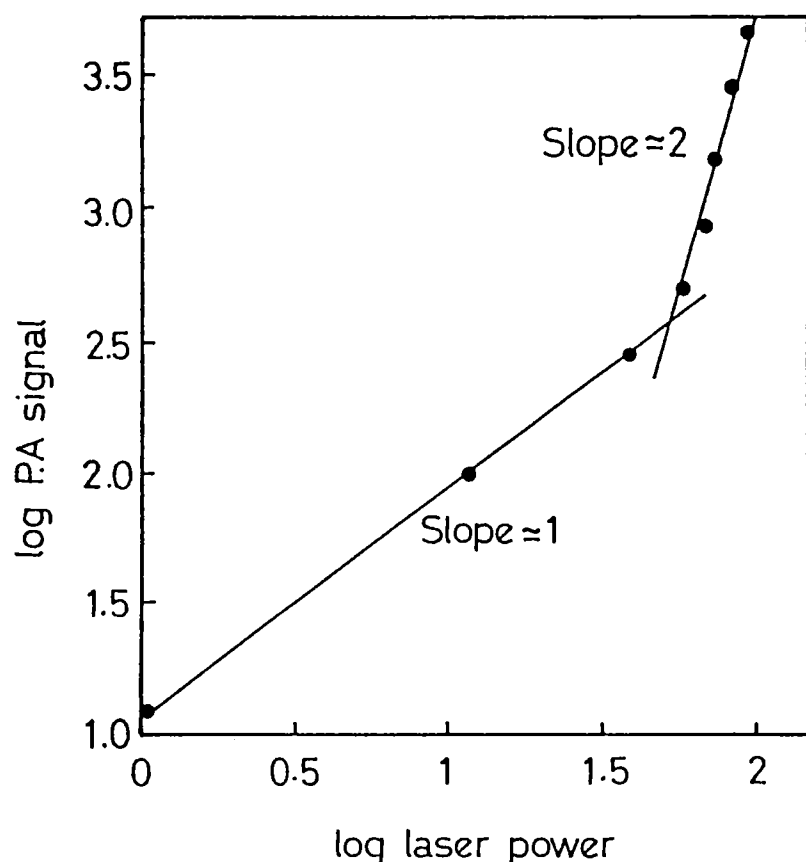


Fig.5.9. The log-log plot of the variation of the PA signal with laser power in the HCHO vapour at 564nm wavelength

much from planarity. This C_s symmetry gives an inversion doubling in the lowest vibrational levels with upper states $^1A''$. The lower inversion component behaves like A_2 and the upper like a B_2 vibronic level of a planar molecule in the A_2 electronic state [24,25]. Only $^1A_1 \rightarrow ^1B_2$ transition is allowed in OPA. The low oscillator strength (f) of the UV band in the OPA spectrum is due to the fact that the upper state is not far from planar structure. In TPA, however, the $^1A_1 \rightarrow ^1A_2$ transition can take place.

Thus the observed TPA is due to the $^1A_1 \rightarrow ^1A''(A_2)$ transition in the region 350 to 230 nm. The TPA at $\approx 560\text{nm}$ is due to one of the members of the 2^n4^1 progression [26], $(nv^1 + 1v^1)$ with $n = 6$. The satellite bands observed are typical sub band heads in an asymmetric top molecule like formaldehyde.

The variation of the PA signal with the gas pressure and average laser power at 564nm is shown in figures 5.11. and 5.12 respectively. The OPA and TPA processes are evident here too, but the PA signal saturates at higher gas pressures.

The absorption spectrum also shows a combination band in the 1100 to 900 nm wavelength region peaking at $\approx 990\text{nm}$ (fig.5.13.) which was investigated using pulsed PAS, the fundamental $1.06\mu\text{m}$ wavelength of the Nd:YAG laser being the excitation source. This band corresponds to the $3v_1 + 2v_4$ overtone combination and occurs in the vicinity of the laser excitation wavelength ie, $1.06\mu\text{m}$. Since the fundamental laser output of the Nd:YAG laser cannot be tuned, only the variations of the PA signal with laser power and the gas pressure were measured. The log-log plot of the PA signal and the laser power for the at $1.06\mu\text{m}$ is given in fig.5.14. In this case too, the occurrence of OPA (slope ~ 1) at lower laser powers and TPA (slope ~ 2) at higher laser powers have been observed. The variation of the PA signal with gas pressure also shows signal saturation at higher

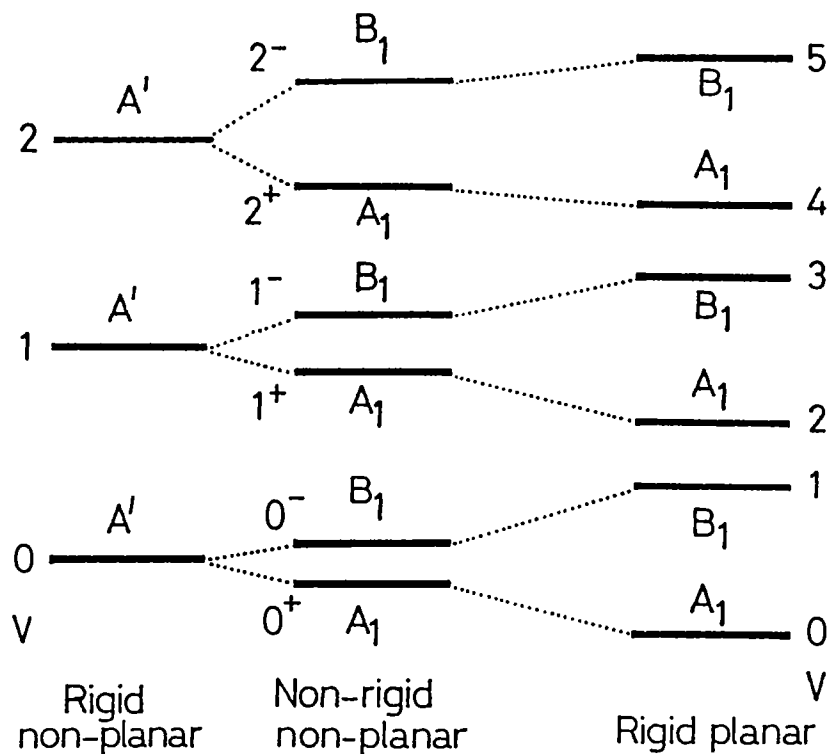


Fig.5.10. The energy levels of the non-rigid formaldehyde molecule

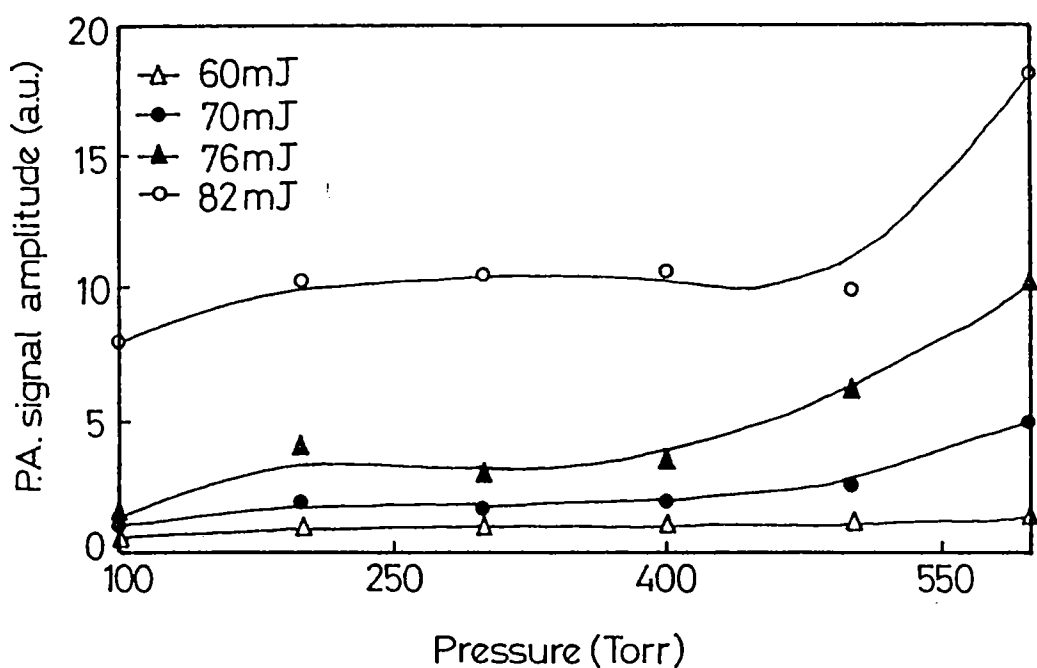


Fig.5.11. The variation of the PA signal with gas pressure of HCHO-air mixture at 564nm

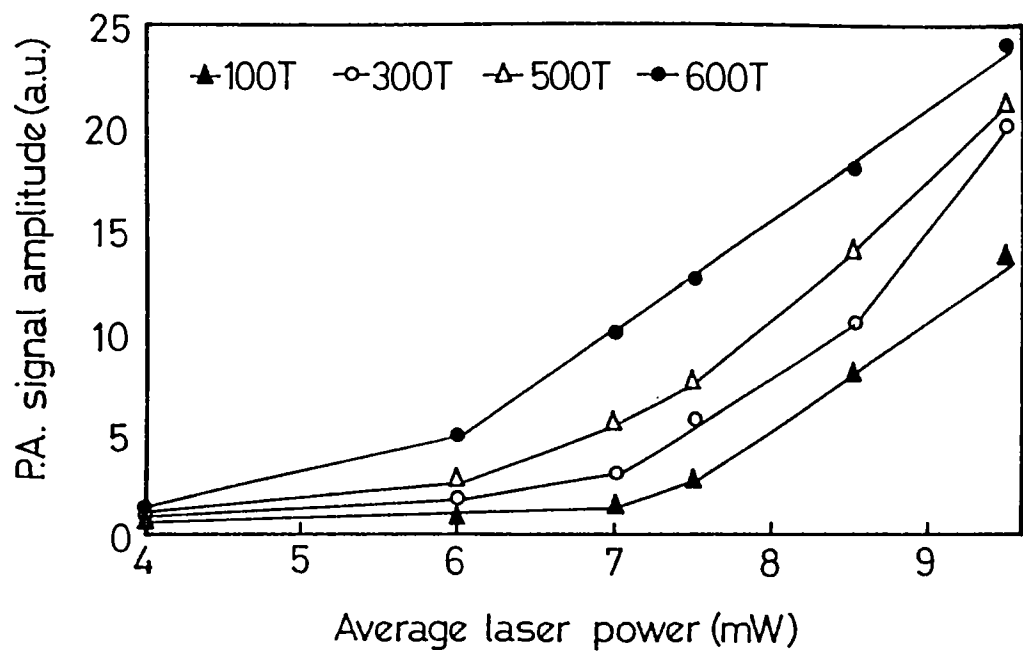


Fig.5.12. The variation of the PA signal in HCHO-air mixture with average laser power at 564nm

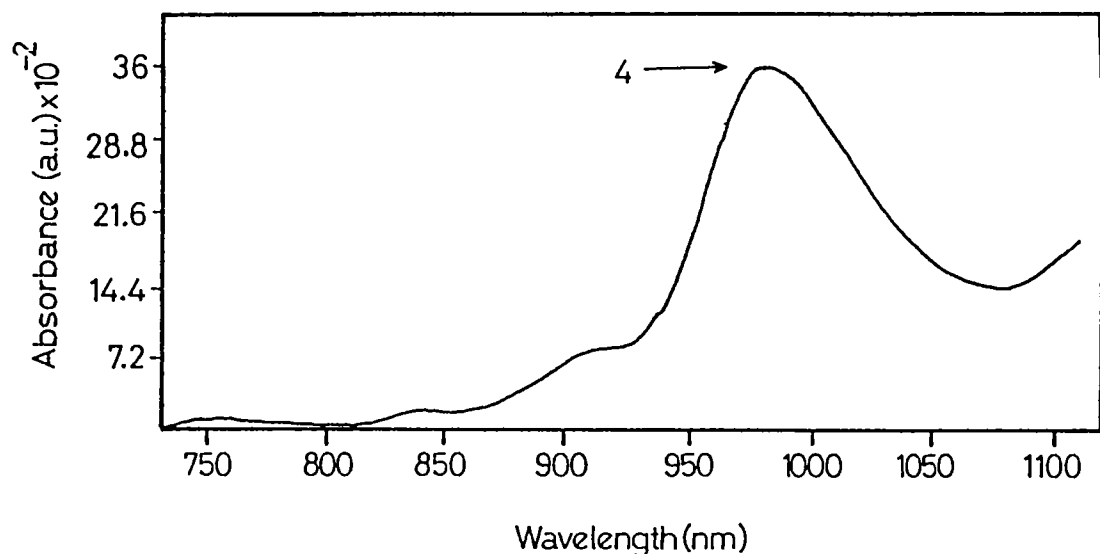


Fig.5.13. The overtone combination band ($3\nu_1 + 2\nu_4$) in the 990nm region in the absorption spectrum of formaldehyde

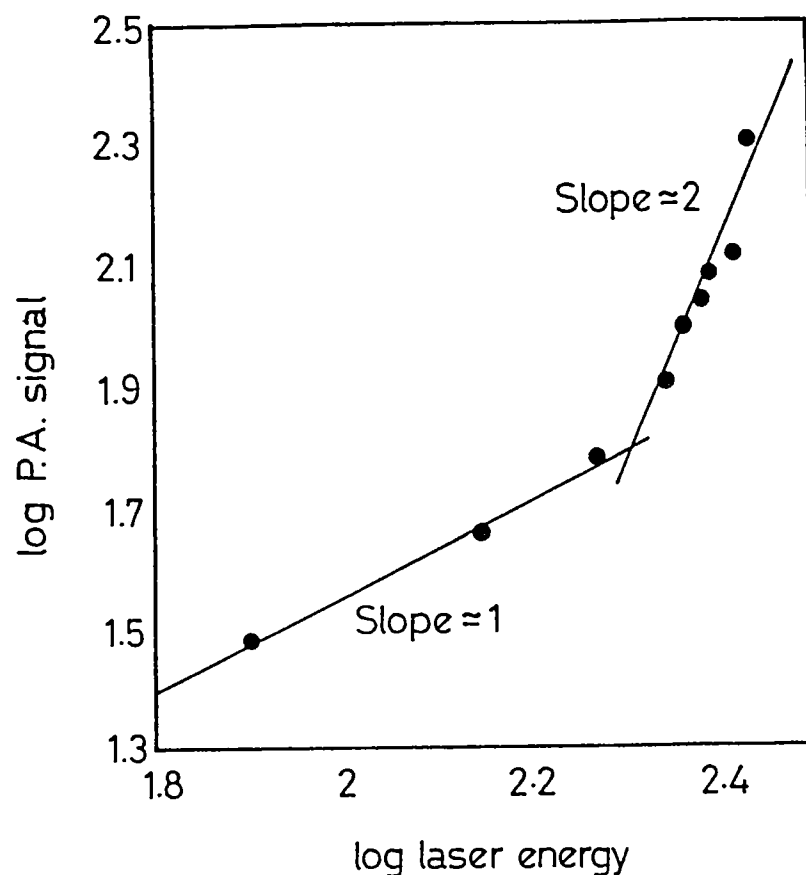


Fig.5.14. The log-log plot of the variation of the PA signal with the laser power at $1.06\mu\text{m}$ wavelength

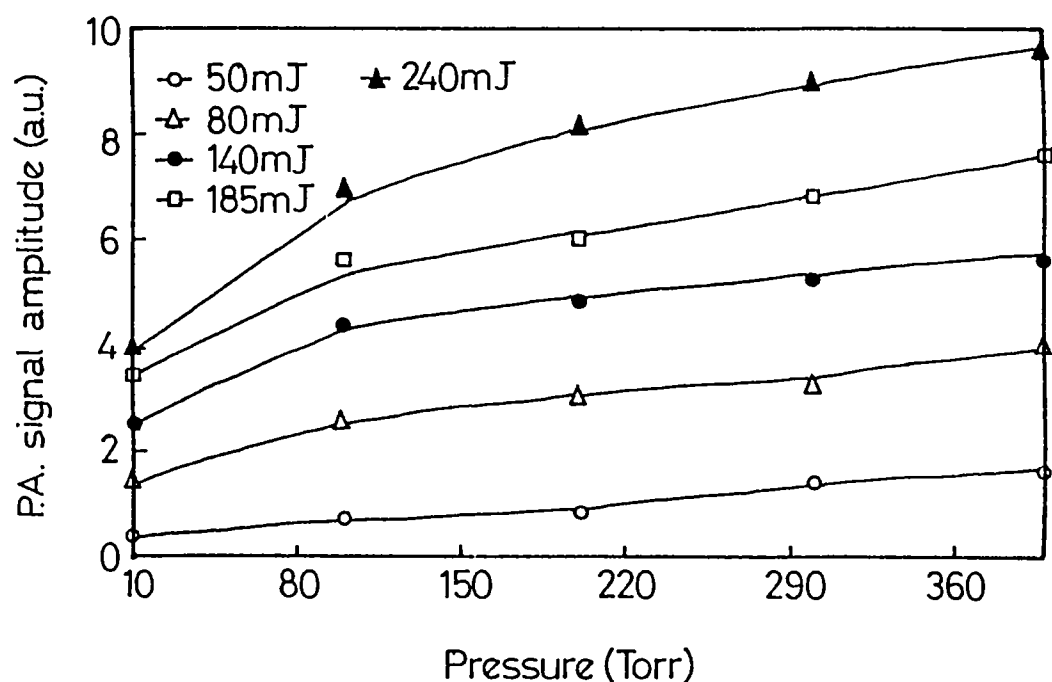


Fig.5.15. The variation of the PA signal with the HCHO-air mixture pressure at $1.06\mu\text{m}$ laser wavelength

as pressures as in the case of studies using the pulsed dye laser fig.5.15).

5.6. PA Investigations of TPA Processes in Other Samples

The technique of pulsed photoacoustics to detect possible multi photon process occurring in gases was extended to a few other samples like sulfur dioxide , methanol and acetone.

Sulfur dioxide has a very readily observed absorption band system [54] in the region of 300nm as seen in fig.5.16. With a relatively large absorption length, this absorption band extends from 400 to 200nm, being probably composed of two or more systems [28]. The main absorption band system of SO_2 extends from 320 to 260nm and is referred to as the $\tilde{\text{A}} \rightarrow \tilde{\text{B}}$ band system of the 300nm wavelength region. These bands are degraded towards the red and are fairly closely spaced up to 275nm (2nm spacing [49]), below which, the bands are diffuse and the lower wavelength end of the system consists of head-less bands [45,46]. The analysis of the SO_2 absorption spectrum shows many bands, with the following maxima of these bands being of interest in these investigations ie, 285.2, 283.23, 281.81, 281.55, and 279.7 nm, since the wavelength region available from the pulsed dye laser corresponds to the possible TPA wavelengths of these band heads.

Detection of SO_2 , specially using PA technique has always been of interest since it is one of the major pollutants in the atmosphere and is a product of almost any combustion process and in the fertilizer production process. Earlier workers have used the strong UV absorption of SO_2 to detect and analyze the sample using corresponding UV laser sources. Excimer lasers or pulsed dye lasers, extended in their wavelength to the UV region by using second harmonic generators have provided to be ideal tools for SO_2 detection [18,47], and detection limits of the order of ppbV

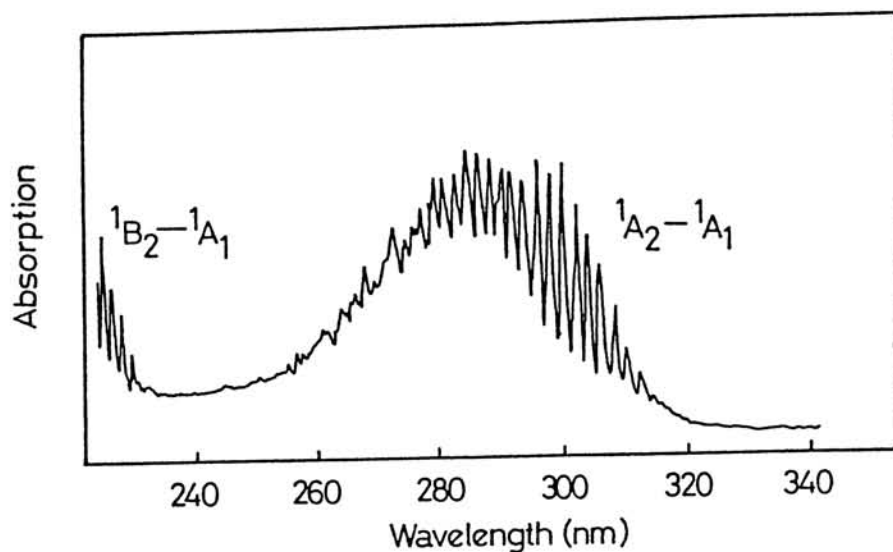


Fig.5.16. The low resolution absorption spectrum of SO_2 in the 300nm wavelength region [54]

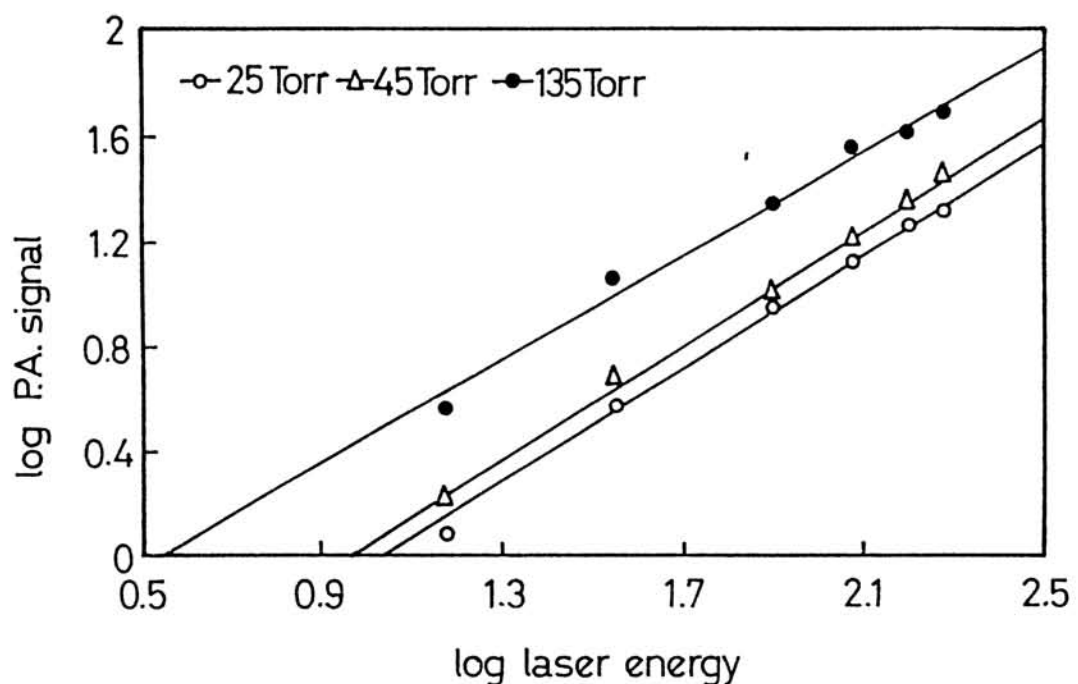


Fig.5.17. The variation of the PA signal with laser energy at $\sim 563\text{nm}$ laser wavelength for SO_2 sample

levels have been reported using a 10mJ/pulse 308nm excimer laser [18] and the UV tunable dye lasers. IR sources in the $9.024\mu\text{m}$ (CO_2 laser) [51-53] and 7.3 to $8.7\mu\text{m}$ wavelength region (Nernst glower) also have been used to detect and study the vibrational relaxation process in SO_2 [48]. Excimer lasers, probably combined with Raman conversion techniques can replace the dye lasers in the UV region used in these detection methods, but they lack the dye laser's broad tunability. Also, while several suitable wavelengths within 285-315nm are available, none is close to the 300nm region where the SO_2 absorption is maximum. The advantage of using wavelengths greater than 300nm for SO_2 detection is that for atmospheric measurements of SO_2 , the wavelengths below 300nm can cause interference by ozone absorption and also reduces the absolute absorption cross section, specially for high concentration SO_2 measurements [49].

The present investigations in SO_2 was to look into the possibility of detecting the sample using the 560-580nm visible output from the pulsed dye laser by possible TPA processes in the sample. SO_2 was generated in the laboratory by the action of concentrated HCl acid on sodium metabisulphite ($\text{Na}_2\text{S}_2\text{O}_5$), and the evolving SO_2 gas was dried by passing through concentrated H_2SO_4 and the gas collected in an evacuated stainless steel jar. The remaining process of gas filling into the PA cell is identical to that for HCHO experiments. Here, no buffer gas was used and the pressure indicated is the total pressure of the sample alone. Though a strong PA signal exists, no PA spectrum was obtained as the dye laser was tuned across the wavelength region, for any combination of gas pressure and laser energy investigated. To check for the possibility of a TPA process, the variation of PA signal with the laser energy at the wavelengths corresponding to the 281nm absorption band maxima of SO_2 at various gas pressures were monitored (fig.5.17). It was seen that the variation does

not indicate any TPA process in the sample. The measured variation of the PA signal, which obviously cannot be due to a direct absorption or by combination bands by SO_2 in this wavelength region, is probably due to a pressure independent enhancement of the background PA signal with the laser energy, since the order of magnitude of the PA signal does not vary considerably as the gas pressure is varied from 25 to 135Torr.

The absence of TPA process could be due to the non-compliance of the conditions that are essential for the occurrence of TPA process. Also, the possibility of reaction of the occluded water vapour in the aluminium cell with the SO_2 gas, thus decreasing the amount of SO_2 available in the cell and the consequent absence of the PA spectra cannot be ruled out. Further, detailed investigations are required to understand these results.

Similar studies in vapours of methanol and acetone also failed to show any TPA process occurring in them, though they have strong UV absorptions. Studies of these samples in liquid phase also proved likewise.

5.7. Conclusions

The importance of detection of formaldehyde and its effect on the atmosphere are discussed. The PA effect has been applied to detect formaldehyde in the visible region by two photon absorption process. This could not be applied to some other samples of interest having possible TPA absorption processes.

5.8. References

- [1] Fish A, *Angen.Chem.*, **80**, 53, (1968)
- [2] Hurn R W, "Air Pollution : Mobile Combustion Sources", Ed. Stern A C, (Academic, New York, 1986) vol.3., p. 55
- [3] Levy H, *Planet Space Sci.*, **20**, 919, (1972)
- [4] Niki H, Daby E E and Wienstock B, "Mechanisms of Smog Reactions", Advances in Chemistry series 113, (Am.Chem.Soc., Washington DC, 1972)
- [5] Becker K H, et al, *Appl.Opt.*, **14**, 310, (1975)
- [6] Calvert J G, et al, *Science*, **175**, 751, (1971)
- [7] McQuigg R D, Calvert J G, *J.Am.Chem.Soc.*, **91**, 1590, (1969)
- [8] Sperling H P and Toby S, *Can.J.Chem.*, **51**, 471, (1973)
- [9] Thomas S G and Guillory W A, *J.Phys.Chem.*, **77**, 2469, (1974)
- [10] Warneck P, *Z.Naturforsch.*, **26a**, 2047, (1971)
- [11] Warneck P, *Z.Naturforsch.*, **29a**, 350, (1974)
- [12] Scientific Encyclopedia (Van-Norstrand, Princeton, New Jersey, 1958) p.689
- [13] Altshuller A P "Air Pollution : Organic Gaseous Pollutants", Ed. Stern A C, (Academic, New York, 1986) vol.3., p. 115
- [14] References on photochemical air pollution in Japan, compiled by Air Quality Bureau, EPA, Japan (May, 1973)
- [15] Inaba H and Kobayasi T, *Opto.Electron.*, **4**, 101, (1972)
- [16] Linford G J, *Appl.Opt.*, **12**, 1130, (1973)
- [17] Cvijin P V, et al, *Appl.Spect.*, **42**, 770, (1988)
- [18] Cvijin P V et al, *Anal.Chem.*, **59**, 300, (1987)
- [19] Gilmore D A and Atkinson G H, proceedings of the "Fourth International Topical Meeting on Photoacoustics, Thermal and Related Sciences", Canada, (1985), paper # MC7
- [20] Boutonnat M et al, *Topics in current Physics, Vol.46: Photoacoustic and Photothermal Phenomena* Ed: Hess P, (Springer-Verlag, Heidelberg) 1989, p.137
- [21] Brocco D and Tappa R, *J.Chromatogr.*, **367**, 240, (1986)
- [22] Krutchman E, et al, *J.Opt.Soc.Am.*, **68**, 1257, (1978)

- [23] Herzberg G, *Molecular Spectra And Molecular Structure III, Electronic Spectra And Electronic Structure Of Polyatomic Molecules*, (Van Nostrand, England, 1967) p 519
- [24] Walsh A D, *J.Chem.Soc.*, p.2306, (1953)
- [25] Brand J C D, *J.Chem.Soc.*, p.858, (1956)
- [26] Job V V, *et al*, *J.Mol.Spectrosc.*, 30, 365, (1969)
- [27] Henri V and Schou, *Z.Phys.*, 49, 774, (1928)
- [28] Pearse R W B and Gaydon A G, "The Identification of Molecular Spectra", (Chapman & Hall, London, 1965), p. 107
- [29] Dieke G H and Kistiakowsky G B, *Phys.Rev.*, 45, 4, (1934)
- [30] H Mahr, in "Quantum Electronics, Vol.I, part A", "Two Photon Spectroscopy", ed. Rabin H and Tang C L, (Academic, New York, 1975) p.285
- [31] Bloembergen N and Levenson M D, "Doppler free Two Photon Absorption Spectroscopy", in "Topics in Applied Physics, Vol.13", Ed. Shimoda K, (Springer-Verlag, Berlin, 1976); p.55
- [32] Geoppert-Meyer M, *Ann.Phys.*, 9, 273, (1931)
- [33] Kaiser W and Garrett C G B, *Phys.Rev.Lett.*, 7, 229, (1961)
- [34] Hopfield J J and Thomas D G, *Phys.Rev.*, 132, 563, (1963)
- [35] Hopfield J J and Warlock J M, *Phys.Rev.*, 137, A1455, (1965)
- [36] Bredikhin V I *et al*, *Sov.Phys.USP.*, 16, 229, (1973)
- [37] Warlock J M in "Laser Handbook", "Two Photon Spectroscopy", Ed. Areechi F T *et al*, 1972
- [38] Cagnac B, *et al*, *J.Phys.(Paris)*, 34, 845, (1973)
- [39] Levenson M D and Bloembergen N, *Phys.Rev.Lett.*, 32, 645, (1974)
- [40] Wilder J A and Findley G L, *Rev.Sci.Instrum.*, 58, 968, (1987)
- [41] Mulliken R S, *J.Chem.Phys.*, 3, 564, (1935)
- [42] Worrish R W G *et al*, *Trans.Faraday.Soc.*, 30, 108, (1934)
- [43] Matsen F A "Electronic Spectra in Visible and UV, Part.2", in "Chemical Applications of Spectroscopy", Edited by West W, (Interscience Publishers, New York, 1956) p. 660.
- [44] Laud B B, "Lasers and Non-linear Optics", (Wiley Eastern Ltd., New Delhi, 1985, chapter 13, p.163
- [45] Clements J H, *Phys.Rev.*, 47, 224, (1935)
- [46] Price W C and Simpson D M, *Proc.Royal.Soc.*, 165, 272, (1938)
- [47] Koch K P and Lahmann W, *Appl.Phys.Lett.*, 32, 289, (1978)

- [48] Slobodskaya P V and Rityn E N, *Opt.Spectrosc.*, 47, 591, (1979)
- [49] Brassington D J, *Appl.Opt.*, 20, 3774, (1981)
- [50] Adrian R S, Brassington D J, Sutton S and Varey R H, *Opt.Quantum.Electron.*, 11, 253 , (1979)
- [51] Duley W W, "Laser Processing and Analysis of Materials", (Plenum Press, New York, 1983), p.408
- [52] Menzies R T and Shumate M S, *Science*, 184, 570, (1974)
- [53] Menzies R T, *Appl.Phy.Lett.*, 22, 592, (1973)
- [54] Hamada Y and Merer A J, *Can.J.Phys.*, 53, 2555, (1975)
- [55] Pitts J N, "Combustion Generated Air Pollution", Edited by Starkman E S, (Plenum Press, New York, 1971) p.67

5.9. Symbols and Notations

- α Absorption coefficient
- a_1 Annihilation operator
- a_2^\dagger Creation operator
- c Velocity of light
- ϵ_0 Dielectric constant in vacuum
- \vec{E} Electric field associated with the light
- \vec{j} Current density
- I Intensity of light
- \vec{p} Dipole moment vector/unit volume
- p_i Dipole moment
- ω Frequency of light
- $v_1 - v_6$ Vibrational modes of HCHO molecule
- χ Polarisibility

CHAPTER VI

PHOTOACOUSTIC STUDIES IN NITROGEN DIOXIDE

ABSTRACT

APTER VI DEALS WITH THE RESULTS OF THE PULSED AND CW PAS STUDIES
E IN GAS PHASE NITROGEN DIOXIDE. THE ROLE OF NO₂ IN
OSPHERIC POLLUTION AND THE IMPORTANCE OF ITS DETECTION ARE
TIONED. AN ATTEMPT HAS BEEN MADE TO OBTAIN THE PA SIGNATURE
CTRA OF NO₂ IN THE VISIBLE REGION USING BOTH PULSED AND CW DYE
ERS IN THE 560-570 AND 570-600NM RESPECTIVELY. THE ABSORPTION
RACTERISTICS AND THE VARIATION OF THE PA SIGNAL USING THE HIGH
LOW CONCENTRATION NO_x SAMPLES WITH THE GAS PRESSURE AND LASER
ER ARE GIVEN. THE NOISE LEVEL AND THE MINIMUM DETECTABLE
NAL ARE ALSO CALCULATED. DUE TO THE EXTREME COMPLEXITY OF THE
BLE SPECTRUM OF NO₂, A COMPLETE ANALYSIS OF THE SAME HAS BEEN
IND TO BE VERY DIFFICULT.

CHAPTER VI

PHOTOACOUSTIC STUDIES ON NITROGEN DIOXIDE

6.1. Introduction

Structurally speaking, NO_2 is a very simple, non-linear triatomic molecule. However, from a spectroscopic point of view, it has a wide and varied physical and chemical properties and it yields a very complex absorption spectrum stretching from the UV into the IR regions due to its coloured nature. Pure NO_2 is highly reactive and toxic and it combines with ambient oxygen to form a mixture of various oxides of nitrogen (its dimerization to nitrogen tetroxide, N_2O_4 is a classic example of chemical equilibrium), is deeply coloured making it highly absorbing in the visible region, and is apparently a chief chemical agent in the atmospheric pollution process. Its affinity to water is the main cause for formation of acid rain. The chief source of atmospheric oxides of nitrogen are from high temperature combustion sources. It has been proved that the oxidation process in the oxides of nitrogen-hydrocarbon-sunlight system is the main cause of photochemical air pollution and it is found to be a major component of smog formation [1]. NO and NO_2 are present in pollution free atmospheres at nominal concentrations of 0.2ppb and 0.5 to 4ppb respectively. It is seen that their residence times in the atmosphere is about 4 and 3 days respectively [5]. Effects like colouration of the atmosphere,

photochemical reactions, hazards to vegetation and animals and other health effects are the pronounced results of NO_2 pollution. The effect of atmospheric pollutants on plants and animals has been studied by many workers in the past [6]. Exposure of plants to concentration levels of $\sim 10\text{ppm}$ of NO_2 has been found to reduce their growth by over 35% [7]. For humans, it was seen that the airway resistance of the lungs increases with moderate exposures to NO_x . Higher levels of concentrations can also be fatal. It was also reported that the illness rates were higher in environments having NO_2 concentrations exceeding 0.06ppm [8]. The acute symptoms from these high concentrations that prevail in urban atmospheres are similar for SO_2 exposure also.

The inter-relationships between the various oxides of nitrogen viz, NO , N_2O , NO_2 , NO_3 , N_2O_4 etc. symbolized by NO_x are complex, particularly in the presence of light, oxygen, ozone and organic matter. It is however evident that among these oxides, only NO_2 is both present in significant amounts and has a strong absorption of sunlight, the energy source required for the initiation of photochemical air pollution. Furthermore, it photodissociates to give highly reactive fragments of oxygen atoms capable of initiating the thermal reactions responsible for the overt physiological manifestation of smog such as eye irritation and plant damage. While the importance of NO_2 in air pollution was recognized years ago, until recently, the basic information covering the details of its photochemistry in both the mm Hg pressure range and the ppm concentration ranges was relatively scarce [2,3].

6.2. Sources of Atmospheric NO_2

NO_x is generated by many man-made processes such as, fuel oil combustion, solid fuel combustion, incineration, agricultural

burning and even, to an extend, by household fires. Though some of these may look insignificant, they have a cumulative effect on the net NO_x levels. Among these, the major producer of NO_x is the automobile exhaust of which NO and NO_2 are the main constituents. NO is formed during the high temperature combustion and is subsequently oxidized to NO_2 by a relatively slower reaction which takes place only in the exhaust streams with large concentrations of NO and excess of oxygen. Generally, it is seen that 99% of the NO_x in auto exhaust is NO [9], and in Diesel engines, 37% of the NO_x is found to be NO_2 [10].

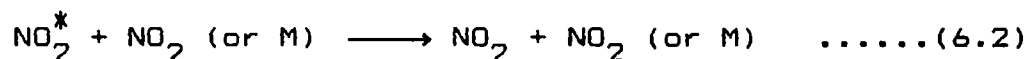
6.3. Photochemistry Of NO_2 In The Visible Region

The vapour phase photochemistry of NO_2 in the visible region of the solar spectrum ($> 435.8\text{nm}$) is a good example of the mechanism consisting only of photophysical processes. In this region, irradiation of either pure NO_2 or of NO_2 in air with hydrocarbons added does not lead to permanent chemical changes in the system. This is particularly pertinent to air pollution since a large fraction of the sunlight absorbed by NO_2 falls in the region of $\lambda \geq 435.8\text{nm}$ [4] as seen in the fig.6.1. In this region, several mechanisms occur which can be represented as follows ;

1. Absorption : The first reaction to occur is the photochemical dissociation of NO_2 by the 300-400nm UV photon



2. Collisional de-activation



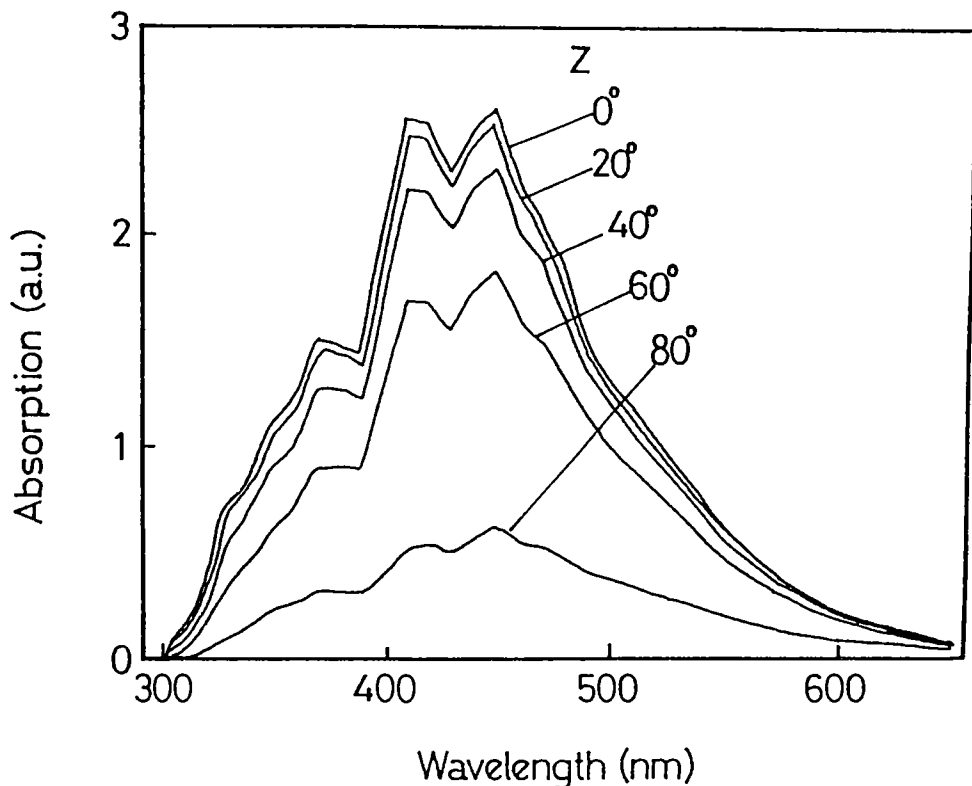


Fig.6.1. The absorption of sunlight by NO_2 at different incidence angles (z) of the sun [4]

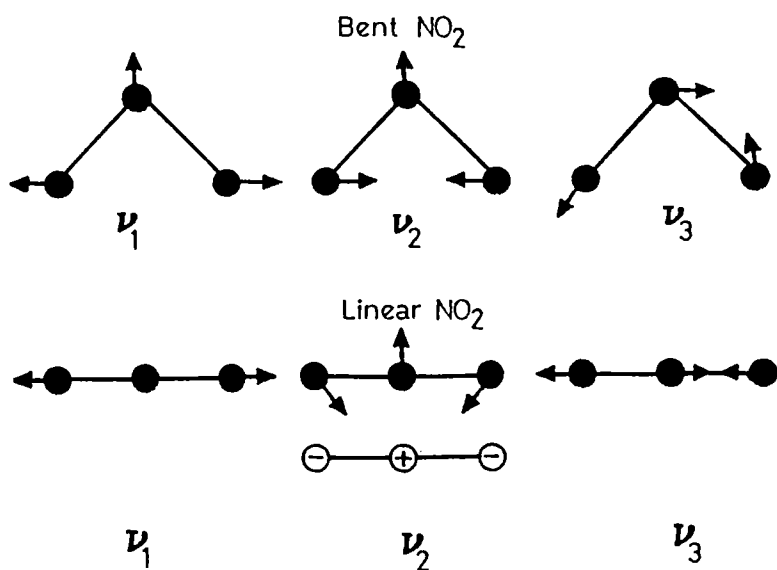


Fig.6.2. The various vibrational modes of bent and linear NO_2 molecule

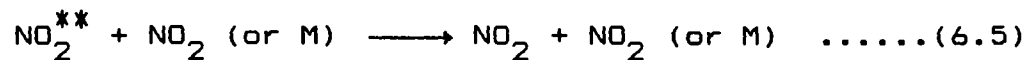
3. Fluorescence



4. Resonance Transfer (Intersystem crossing)



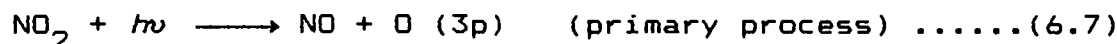
5. Collisional de-activation



6. Fluorescence



Step 4 is a resonance transfer from a higher excited electronic state to a lower one. It is a general type of process highly important in the photoactivated system. The specimens M in steps 2 and 5 is a third body which may take up the electronic excitation energy of NO_2^* or NO_2^{**} and convert it into thermal energy without chemical change and can be any molecule in air. The direct photodissociation of NO_2 in the 300nm region into nitric oxide (NO) and highly reactive oxygen atoms in their ground electronic state (3p) takes place as,



In the far UV, the oxygen atom formed is in the first excited state $\text{O}({}^1\text{D})$. It is important to note that there is significant difference in the reactivity of the oxygen atoms in the ground state triplet (3p) and the singlet excited state (${}^1\text{D}$). The atomic oxygen produced in this process is highly reactive which

ombines through collisions with molecular oxygen present in abundance to give ozone and NO in the case of traces of NO_2 as,



The ozone produced in the above reaction (8) is relatively stable to thermal decomposition and exist long enough to form or be a precursor to many of the host of compounds that characterize a typical photochemical 'smog' [13]. The ozone reacts very rapidly with NO originally produced in the primary process to yield,



In these cases also, M is the third body which must be present to siphon away the energy formed in the highly exothermic reaction process, otherwise, the hot O_3 molecule would immediately disintegrate into O and O_2 [11]. The rates of these reactions will depend on the intensity of the UV radiation and thus the altitude of the sun and the atmospheric UV absorption. The reactions 6.9 and 6.10 play a vital role in the ozone layer depletion. The high altitude aircrafts flying in the stratosphere ($\sim 18\text{ kms}$) release NO as exhaust, which reacts with the ozone present there. The NO is not consumed in these reactions and thus there is a net depletion of the ozone and the atomic oxygen in the upper atmosphere, thus contributing to create the 'ozone hole' [12].

6.4. Detection Of Nitrogen Dioxide

There are many methods to estimate the NO_x or NO_2 concentrations in trace amounts [34], and a few commonly used ones are described

ere. Various estimation techniques for NO_2 have evolved over the years and they include photometric (absorption, fluorescence etc), calorimetric, adsorption and chemiluminiscence.

The most common and easiest method to estimate NO_2 is by photometric methods, though it is not very sensitive. The NO present in the NO_x is completely converted to NO_2 by bubbling it through potassium permanganate solution [30]. The NO_2 is then bubbled through the Greiss-Ilosvay reagent as modified by Saltzman [31]. The intensity of the pink color of the reagent is indicative of the concentration of NO_2 . High concentrations of NO_2 can be directly measured by monitoring the absorption of a particular wavelength of visible light in comparison to a standard sample. Another commonly used technique for NO_x determination is the phenoldisulfonic acid method, which measures the total combined nitrogen oxides or compounds (except nitrous oxide) whether it be HNO_3 , NO_2 , NO, any organic nitrogen compound or an inorganic nitrate [32]. A NO_2 detector based on the chemiluminiscent reaction between NO_2 and 'luminol' (5-amino-2,3-dihydro-1,4-phthalan-zinedione) in alkaline solution capable of detecting both NO and NO_2 in the sub ppb region has been reported [27,28,8]. The total NO_2 in NO_x can also be determined by oxidizing all the NO to NO_2 and then bubbling it through water. NO_2 is easily absorbed by water and the estimation of the acid content in the resulting solution can give a rough estimation of the NO_2 concentration. Adsorption of NO_2 on substances like silica gel have been used to determine NO_2 concentrations though it is not efficient at low concentrations [33]. The gas chromatography technique is yet another method to determine NO_2 concentrations accurately. This method does not have a large dynamic range and moreover, each test sample requires a standard reference sample of comparable concentrations to obtain the results and is thus inconvenient. The differential

absorption technique was employed to determine remotely in ppm concentration, the NO₂ distribution over a chemical factory using a tunable dye laser and a LIDAR setup [35].

6.4.1. Calorimetric Detection Techniques For NO₂

The two mainly used calorimetric techniques for NO₂ detection are the photoacoustic and the photothermal deflection (Thermal lens) techniques. The various advantages of these techniques for trace analysis and pollution monitoring of NO₂ over other conventional techniques are listed in chapter 1.

i. Thermal Lens Technique

The thermal lens technique (PTD technique) has also been used by several workers to detect the NO₂ species. Tran and Franko used the dual wavelength, differential thermal lens technique to detect 300ppb of NO₂ for a 30mW multiline argon laser pump source. Essentially, in the thermal lens technique, the deflection of a weak probe beam due to the refractive index gradient produced by the absorption of the stronger pump beam by the sample is monitored and this technique is also a calorimetric technique like the PA detection technique. Higashi et al [23] used this technique to detect 5ppb of NO₂ using the 488nm line of the argon ion laser since it gave the largest signal due to its large output power and large molar absorptivity ($\epsilon = 60$). Pulsed thermal lens was used to detect the atmospheric traces of NO₂ using an excimer pumped dye laser and a trace detection limit of 4ppb was obtained [24,25,26].

ii. PA Detection Of NO₂

The major advantage of the PA detection scheme, as mentioned in earlier chapters, is its *in situ* monitoring capability. Though other gases have been extensively detected and studied in detail using the PA technique, not many workers have used this technique to actually study this gas. The first reported study of NO₂ using PA detection technique was by Harshbarger and Robin who used a white light source-monochromator setup to record the visible PA spectrum of NO₂. It was observed that The PA spectrum follows the absorption spectrum up to the neighbourhood 400nm at which point the absorption peaks and then begins to decrease slowly, whereas the heat amplitude suffers a dramatic reduction to about two-thirds of its peak intensity in the same wavelength region. It is at 400nm that the dissociation limit of NO₂ is reached (Equ.6.7). Even though the dissociation limit of NO₂ is 398.6nm, the fall-off in the PA signal begins at only 420nm [14,46]. The PA signal falls due to the fact that the absorbed energy finds an alternative decay route in the process of photodissociation. The use of high resolution dye laser for exciting the NO₂ reveals extensive fine structure in the PA spectrum, but in spite of this, there is still no sharp onset for the dissociation. Kreuzer *et al* used the CO₂ laser at powers of ~ 1watt to detect 0.1ppb of NO₂ in nitrogen buffer using the PA technique [15]. Agnus *et al* used the modulated cw dye laser to detect 10ppb of NO₂ [16] and Claspy *et al* used a 250mW pulsed dye laser to detect \approx 10ppb of the same using the PA detection technique [17]. Using a resonant PA cell, the PA spectrum in low resolution was observed in the 580-610nm region. Since the molar extinction coefficient of NO₂ in this region is less than 20, this technique has obvious applications for the analytical determination of not only NO₂, but of any gas having even an extremely weak absorption in the wavelength region

of the laser. A fibroptic sensor based resonant PA cell was used to detect traces of NO_2 [18]. A fibroptic interferometer, constructed in the Mach-Zehnder arrangement replaces the microphone in the cavity and a detection limit of $\sim 50\text{ppb}$ was obtained for a laser power of 500 mW using the argon ion laser. The continuous products of the photolysis of nitromethane and the subsequent formation of NO_2 was studied by PA techniques by Colles et al, in which they monitored the levels of NO_2 after a flash photolysis of nitromethane [19]. Poizat and Atkinson used the differential PA technique to detect NO_2 concentrations of the order of 2ppb, and a linear dependence of the PA signal on the NO_2 concentrations for over 6 orders of magnitude was obtained using the various wavelengths of a krypton ion laser [20]. PA detection technique using argon laser was used to monitor the evolution of NO_2 in the NO-O_3 reaction, which essentially are the critical components involved in the chemistry and physics of the troposphere and the stratosphere [21]. The concentration changes in NO and NO_2 agreed well with other detection techniques. NO_2 has been used frequently to calibrate PA systems due to its high absorption in the visible region. Since the NO_2 group exists in most of the organic explosives, PA detection can be effectively used to detect the explosive vapours by using a broad-band tunable laser to probe the absorption due to the asymmetric stretching near $6\mu\text{m}$ or the -O-N stretching mode near $11\mu\text{m}$, the specific location being determined by the basis molecule to which this group is attached [44]. The peak asymmetric stretch absorptions in $-\text{NO}_2$ group occur at 6.039 and $6.086\mu\text{m}$ in ethylene glycol dinitrate (EGDN), and at 5.97, 6.046 and $6.079\mu\text{m}$ in nitroglycerine (NG). The -O-N absorptions occur at 11.148, 11.628 and $11.877\mu\text{m}$ in EGDN and at 11.099 and $11.905\mu\text{m}$ in NG [45]. By looking for these signature absorptions, these molecules can be traced using PAS, but the effects of interfering species are more severe in this wavelength region.

PART A : Pulsed PAS

i. Brief Insight Into The Spectroscopy Of The NO₂ Molecule

Nitrogen dioxide is one of the few relatively stable gaseous molecules with an odd number of electrons. Furthermore, it is one of the few well known triatomic molecules that absorbs in the visible region. The whole spectrum of this molecule is extremely complex and its analysis has frustrated experimentalists and theoreticians ever since it was first observed by Brewster in 1834. The unusual complexity in the visible absorption spectrum of NO₂ is attributed to the following : the fine structure due to the spin S=1/2 of the unpaired electron, and the hyperfine structure due to the nuclear spin I=1 of the ¹⁴N atom, and the overlapping of the excited electronic states. The coupling between the four electronic states, each of which can interact with the other three states through various perturbation mechanisms also plays an important role in its highly irregular spectrum. The visible absorption spectrum of NO₂ is so dense (approximately 19000 lines in the 553-648nm region) that a very high resolution is necessary to separate single vibrational-rotational lines. Although partial analysis of some select bands have been performed on the basis of high resolution fluorescence and absorption measurements, wide range, very high resolution spectra are still necessary for a thorough understanding of the complete visible spectrum. The absorption lines of NO₂ in the visible region have been listed as an atlas in two books, both of which present absorption and fluorescence data in a very detailed manner [36,37]. Many workers [38,39,43,47,48] in the past have investigated the visible absorption, fluorescence, and Raman spectra of NO₂ in the past starting from Broida [43] in 1969 who

observed the fluorescence of NO_2 under argon ion laser excitation.

Triatomic molecules of the type YXY have three normal modes viz, v_1 the symmetric stretch, v_2 the bending vibration and v_3 the asymmetric stretch. The energy ordering of the vibrational modes is usually $v_3 \geq v_1 \gg v_2$. The various vibrational modes of the linear and bent NO_2 molecules are represented in fig.6.2. The direction of the arrows indicate the nuclear motion whereas the magnitude indicates the displacements. The centre of mass does not move for normal mode vibrations. The absorption in the visible region of NO_2 is due to the $^2\text{B}_2 \rightarrow ^2\text{A}_1$ transition as shown in fig.6.3. The $^2\text{B}_2$ state is obtained from the $^2\text{A}_1$ state by promotion of an electron from the 3b_2 to the 4a_1 orbital. It has been known from calculations that the $^2\text{B}_2$ state is expected to be more bent than one in the ground state. Thus, excitation to the $^2\text{B}_1$ state should make the molecule somewhat linear [37]. It is seen from the calculations of Gillispie *et al* that the $^2\text{B}_2$ to $^2\text{A}_1$ states may readily interact with each other, because of the potential surfaces are close to each other and hence are said to have favourable Franck-Condon overlap factors.

ii. Pulsed PA Spectrum Of NO_2

Here we describe the experimental procedure and the results of pulsed PA spectrum of NO_2 gas in the 560-580nm region of the visible spectrum. The experimental setup for the pulsed PAS of NO_x is as mentioned in Chapter 3. The advantage of using the visible wavelength for NO_x detection is that NO , which is a part of the NO_x species, does not have any interference in the visible region, whereas, it interferes in both the UV as well as the IR regions. The single cavity PA cell was used for these studies. The gas is filled into the cell at the required pressure (no

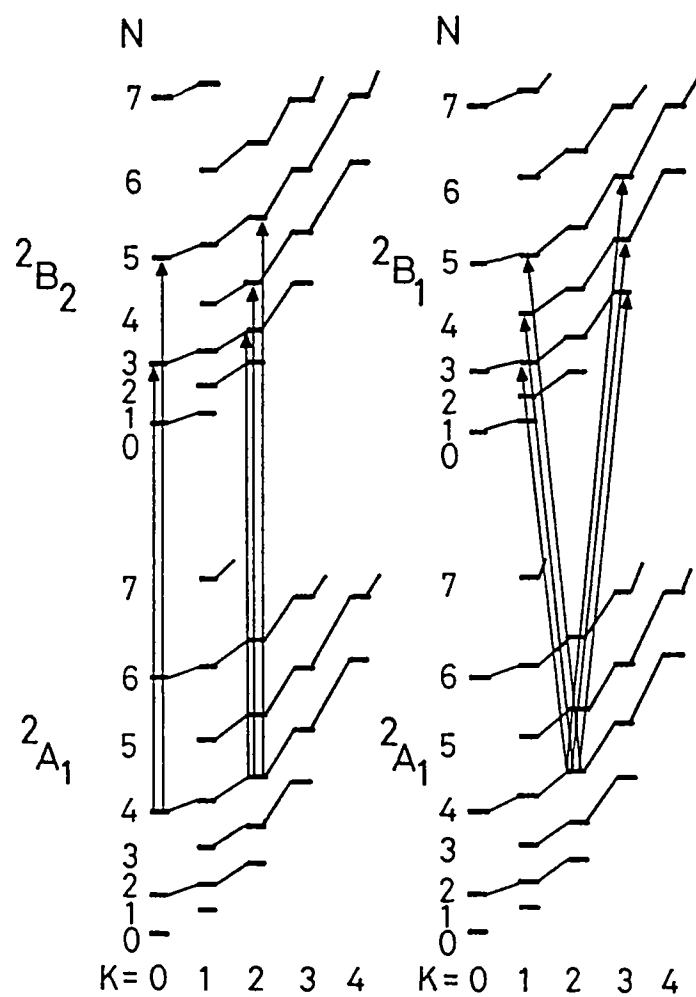


Fig.6.3. The schematic of the allowed NO_2 electronic transitions

buffer gas was used) and the pulsed dye laser is tuned across the wavelength. The spectrum observed is basically the $^2B_2 \rightarrow ^2A_1$ band system of NO_2 in the visible region. The energy profile of the dye laser is compensated by the ratioing technique. Figure 6.4. shows the normalized PA spectrum of high concentration NO_2 in the visible region. The UV-VIS-NIR absorption spectrum of NO_2 in this wavelength region (fig.6.4.) shows only a broadband structure peaking at 564 nm which corresponds to the peak output wavelength of the pulsed dye laser. From the above figure, it can be seen that at the wavelength where the absorption of NO_2 shows a maximum, the PA signal tends to show a dip, indicating the possibility of an alternate radiative path of de-excitation occurring at this wavelength, thus causing a decrease in the PA signal. This dip in the PA spectra can be used as a signature of the presence of NO_2 in trace analysis studies since this signature is clearly evident at all the pressure and laser energy ranges that were studied.

iii. Laser Energy And Pressure Variations Of The PA Signal

The PA spectrum at different laser energies is given in fig.6.5. The pressure variation of the PA spectrum is shown in fig.6.6. It can be seen that though the baseline of the PA signal increases with pressure, the spectrum is not resolved at low or high pressures. This is due to the pressure saturation of the PA signal induced by the increased collisional energy transfer in the sample which in turn reduces the energy available for the non-radiative de-excitation, thus reducing the PA signal. The collisional effects and the variation of the microphone response at high gas pressures could also induce such a pressure variation [29]. Pressures of less than 200 Torr was found to give well resolved spectra. The PA signal variation with gas pressure is represented in fig.6.7. The PA signal initially increases with

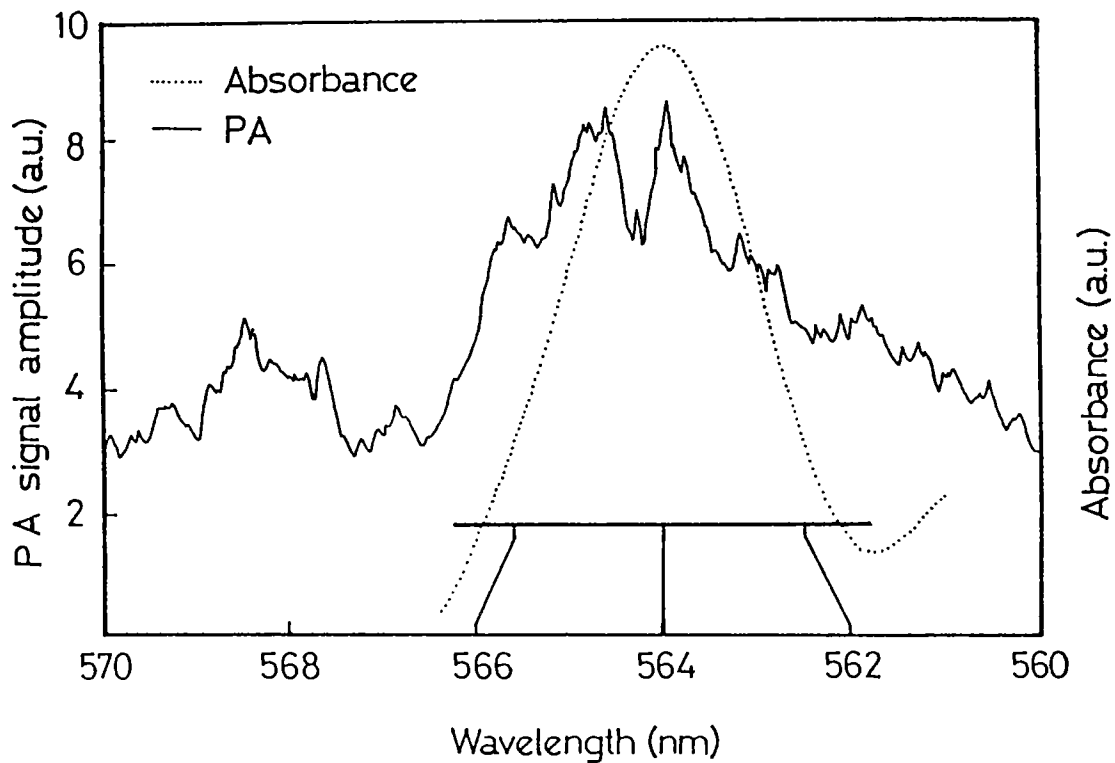


Fig.6.4. Normalized pulsed PA spectrum of NO_2 and the absorption spectrum recorded with a UV-VIS-NIR spectrophotometer in the same wavelength region. Pressure ~ 150 Torr, Laser energy $\sim 2.5\text{mJ/pulse}$

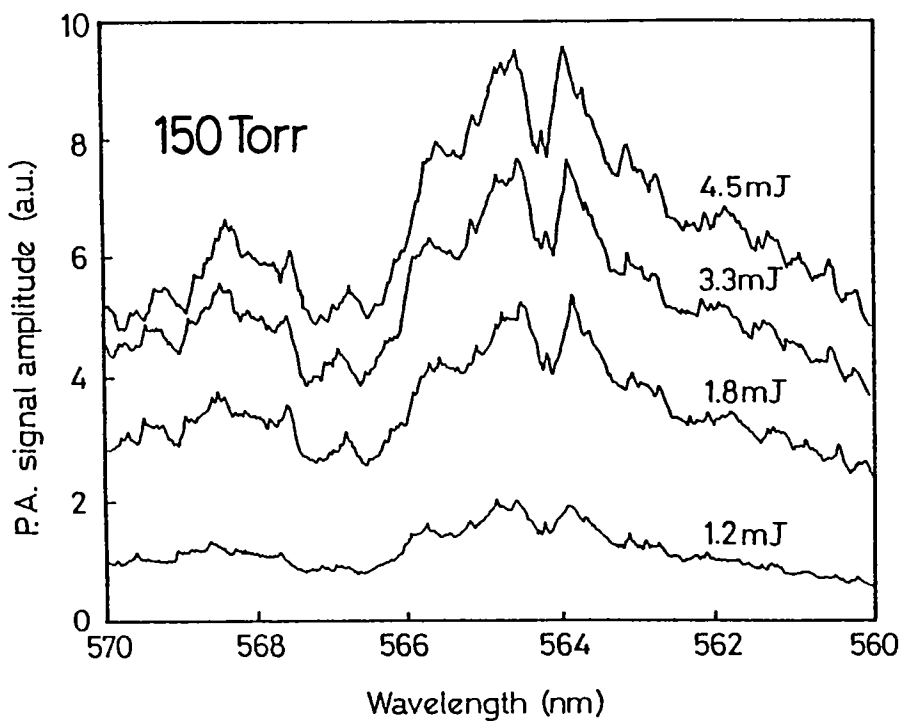


Fig.6.5. Pulsed PA spectrum of NO_2 at different laser energies

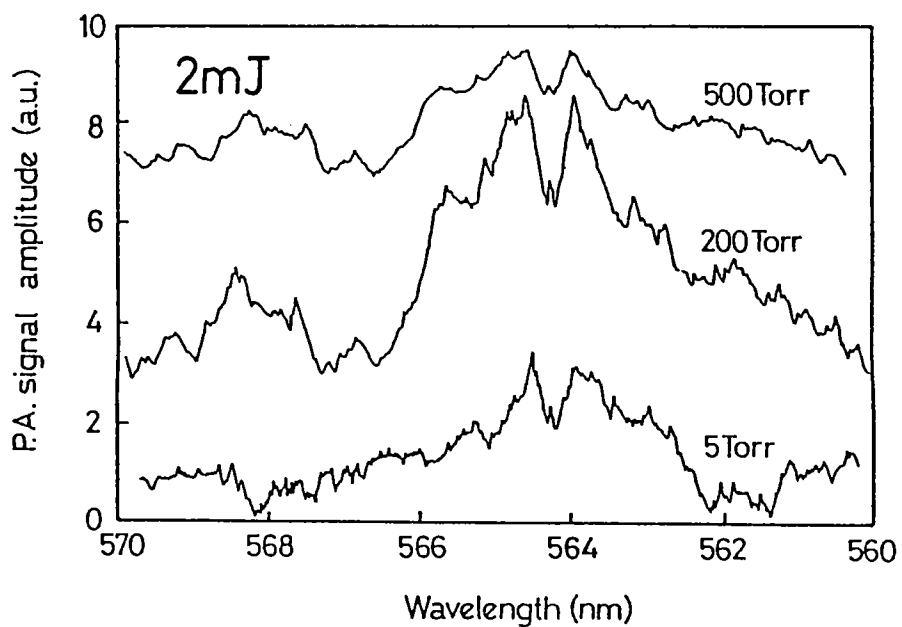


Fig.6.6. Pulsed PA spectrum of NO_2 at different gas pressures

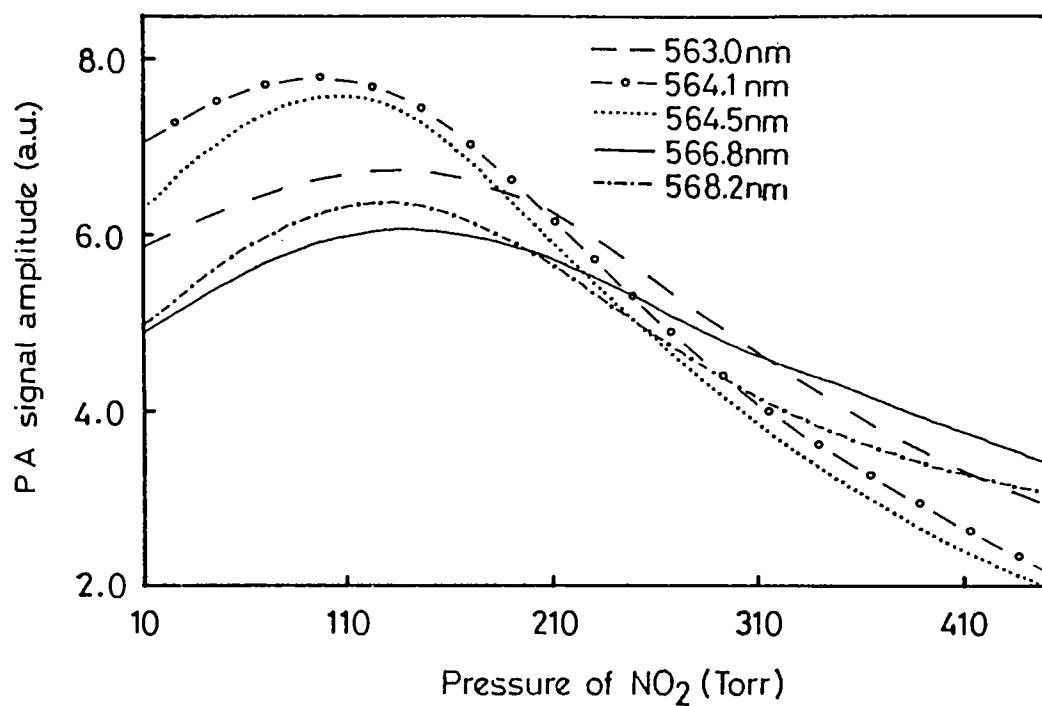


Fig.6.7. The variation of the PA signal with gas pressure at some of the spectral peak points (Laser energy $\sim 3.3\text{mJ/pulse}$)

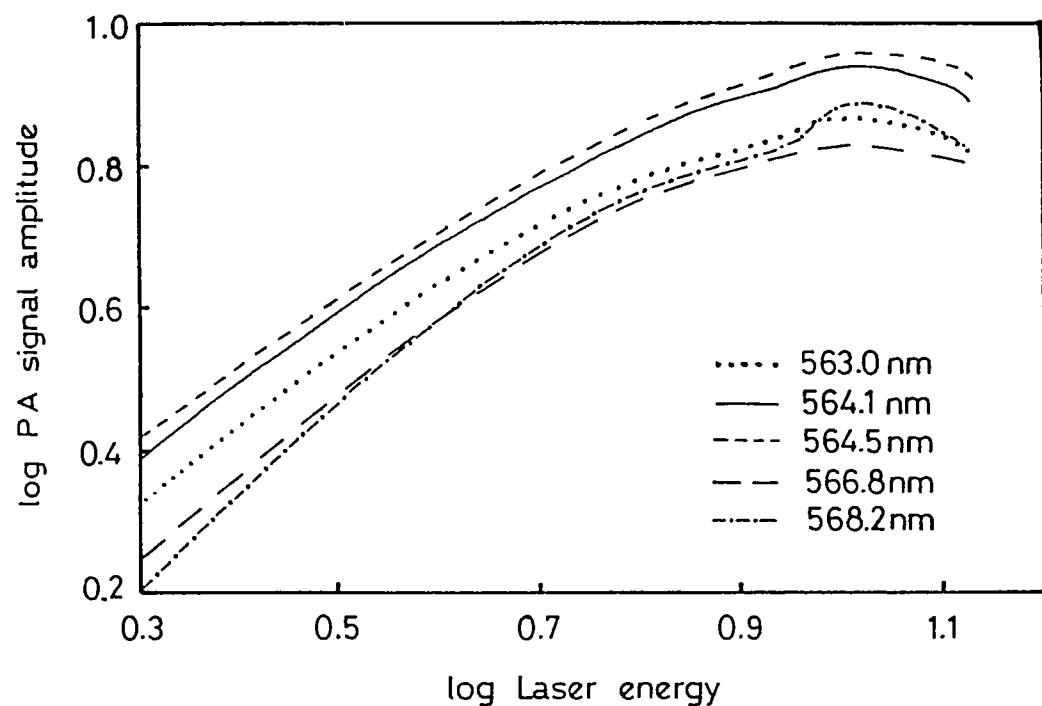


Fig.6.8. The variation of the PA signal with laser energy at some of the spectral peak points (Pressure ~ 100 Torr)

the pressure of the gas and then decreases with further increase in pressure. This is seen for all the peak positions at all the laser energies studied. The laser energy variation of the PA signal at few of the prominent peak positions is given in fig.6.8. The PA signal is linear up to a laser energy of 10mJ after which PA saturation, which is characterized by a decrease in the PA signal is observed. The decrease in PA signal is due to the $1/I_0$ dependence of the PA signal at high laser intensities (I_0) which is quite well predicted in the PA theory.

PART B : CW PAS

i. CW PAS Of NO₂

Since NO₂ has high absorption in the wavelength region of the argon ion laser, it is best suited for the detection of NO_x species. The absorption coefficient of NO₂ at different Argon ion laser wavelengths have been reported by Sakurai and Broida [43]. Fig.6.9. shows the absorption coefficient of NO₂ at some of the argon and krypton ion laser wavelengths [43]. The absorption coefficient was found to be linear with respect to the gas pressure in the region of pressure investigated. NO₂ exists in equilibrium with N₂O₄, the mole fraction of N₂O₄ at 1 Torr total pressure being less than 0.015. The radiative lifetime of the excited NO₂ was also estimated as 10^{-5} secs. To be able to apply this technique to trace analysis of the gas sample, it is essential to obtain not only the signature spectrum, but also the variation of the signal with the input laser power and the gas pressure, which determines the concentration of the gas. The following studies are all done in the regions of tens of Torr pressure (typically 25-300 Torr). The non-availability of standard certified gas samples and an alternate efficient method

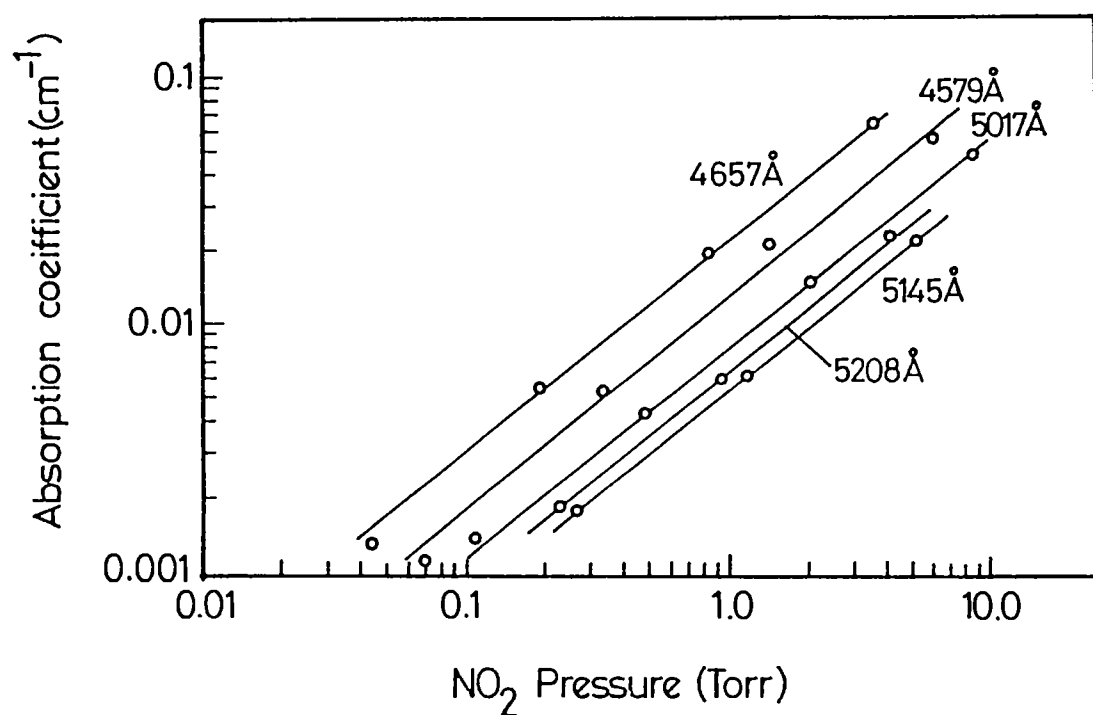


Fig.6.9. The variation of absorption coefficient of NO_2 with gas pressure for some of the lasing wavelengths of argon and krypton ion lasers [43]

to analyze the prepared gas samples, very low pressure studies on the gas samples have not been carried out. It has been reported however, that the PA signal is linear in the low pressure regions also. The PA signal response for different pressures of both low and high concentration NO_2 at different laser powers of the multiline output as well as the various discrete lasing lines of the argon ion laser, viz, 514.5, 496, 488, 476 and 458 nm was studied. In all the cases, the PA signal shows a linear variation with pressure and laser power for low pressures and moderate laser powers. In high concentration samples, this linearity ceases to exist (*i.e.*, saturation of the PA signal sets in) at lower laser powers and pressures as compared to the low concentration samples. The details of the results of these studies are described below.

ii. Laser Power Variations Of The PA Signal

The laser power variations of the PA signal for different pressures of high concentration NO_2 using the multiline output of the argon ion laser is shown in fig.6.10. The PA signal remains linear with the laser power up to $\sim 125\text{mW}$ after which the PA signal is saturated and it decreases with further increase in laser power. This is typically the kind of PA saturation mentioned earlier in Chapter 2. Similar studies on the low concentration NO_2 (fig.6.11.) show that the PA saturation occurs only at laser powers greater than 1watt. In both these cases, the variation of the PA signal with laser power in the low laser power region is linear. The variation of the PA signal with laser power of the different lasing wavelengths of the argon ion laser at a gas pressures 400 Torr of low concentration NO_2 are represented in fig.6.12.a. It can be seen that the absorption of NO_2 is maximum for the 496nm and minimum for the 488 and 514nm wavelengths. Within the laser power range employed, no PA

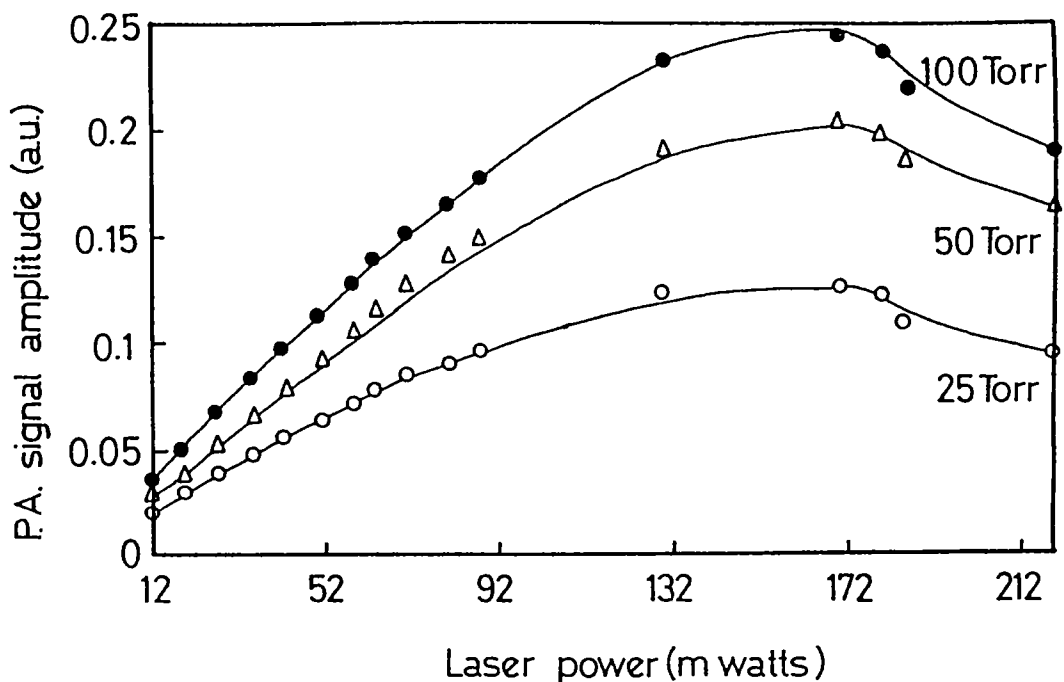


Fig.6.10. The variation of the PA signal with the power of the multiline output of the argon ion laser at different gas pressures of high concentration NO_2

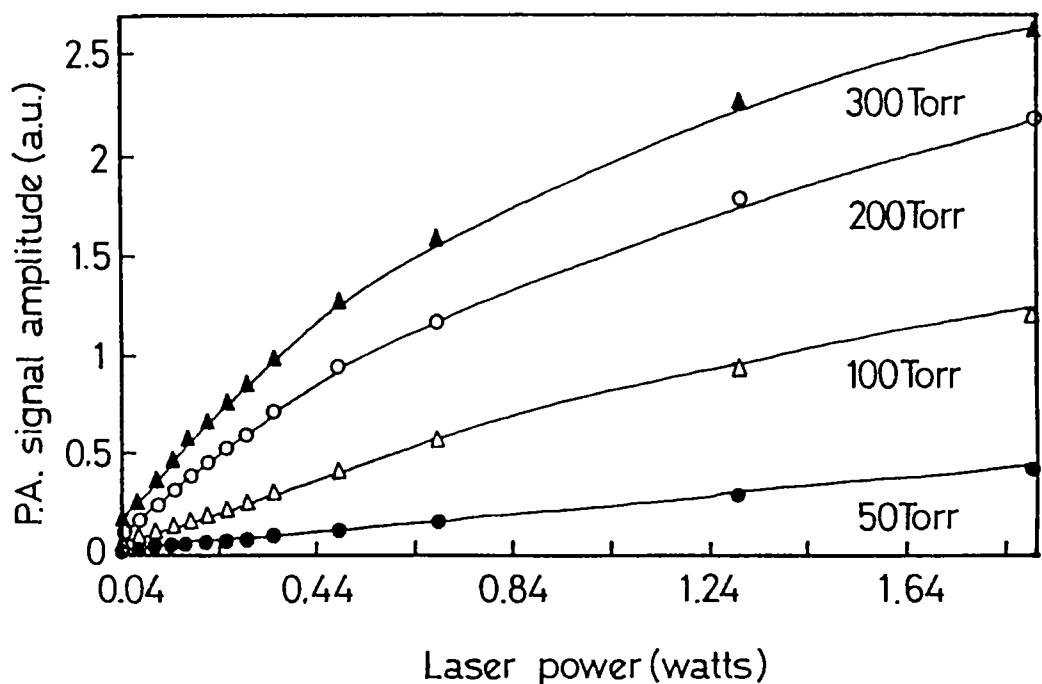


Fig.6.11. The variation of the PA signal with the power of the multiline output of the argon ion laser at different gas pressures of low concentration NO_2

saturation was observed. Similar observations were obtained for different gas pressures also.

iii. Gas Pressure Variations Of The PA Signal

Figure 6.12.b. shows the variation of PA signal with the gas pressure at different laser powers of the 514nm wavelength of the argon ion laser for low concentration NO_x . The saturation behaviour of the PA signal is clearly seen from this graph. Similar results were obtained for all the other lasing wavelengths of argon ion laser. The gas pressure variations of the PA signal for high and low concentration NO_2 at different laser powers of the argon multiline laser output are shown in fig.6.13. and fig.6.14. respectively. It is interesting to note that in the case of the low concentration NO_2 , the PA signal is linear up to the measured maximum gas pressure of 300 Torr while in the case of the high concentration NO_2 , there is a periodic variation of the PA signal with pressure as the pressure is increased. The PA signal peaks at a gas pressures of ~ 75 Torr, ~ 175 Torr, and 275 torr. One possible reason for such a behaviour of the PA signal could be that there can be altered equilibrium values in the $\text{NO}_2 \rightleftharpoons \text{N}_2\text{O}_4$ reaction rates which results in an enhanced concentration of N_2O_4 at gas pressures beyond 75, 175 and 275 torr resulting in a decreased absorption and thus the PA signal. Another possibility is the formation of dimers of NO_2 at higher concentrations. The existence of such dimer formation in NO_2 , formed by the bi-molecular collision between an electronically excited NO_2 and a ground state NO_2 molecule has been reported by Butler et al [47] resulting in the emission of continuum in the fluorescence spectrum.

Observations similar to (fig.6.7. and 6.13.) the variation of the PA signal with gas pressure were made in mixtures of CH_4

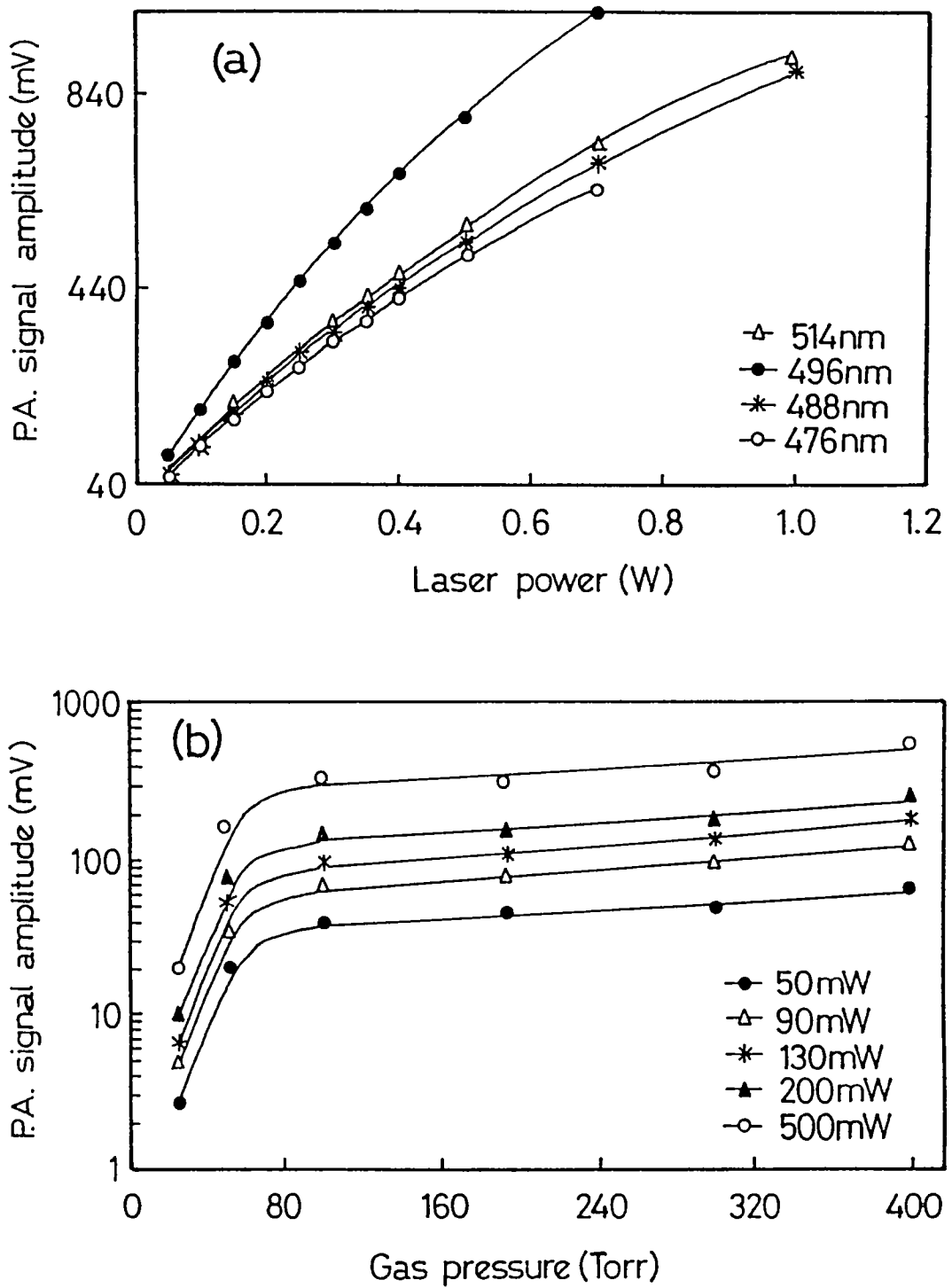


Fig.6.12. The variation of the PA signal with (a) power of the discreet lasing lines of argon ion laser and (b) gas pressure of low concentration NO_2 at 514nm wavelength

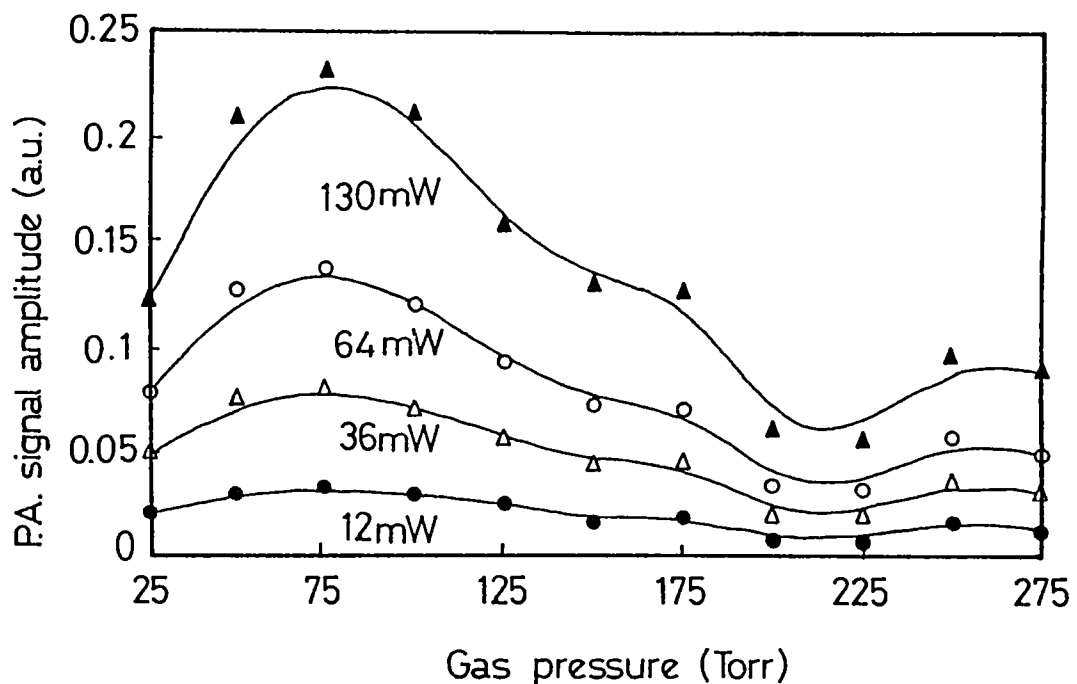


Fig.6.13. The variation of the PA signal with gas pressure for different laser powers of the multiline output of the argon ion laser for high concentration NO_2

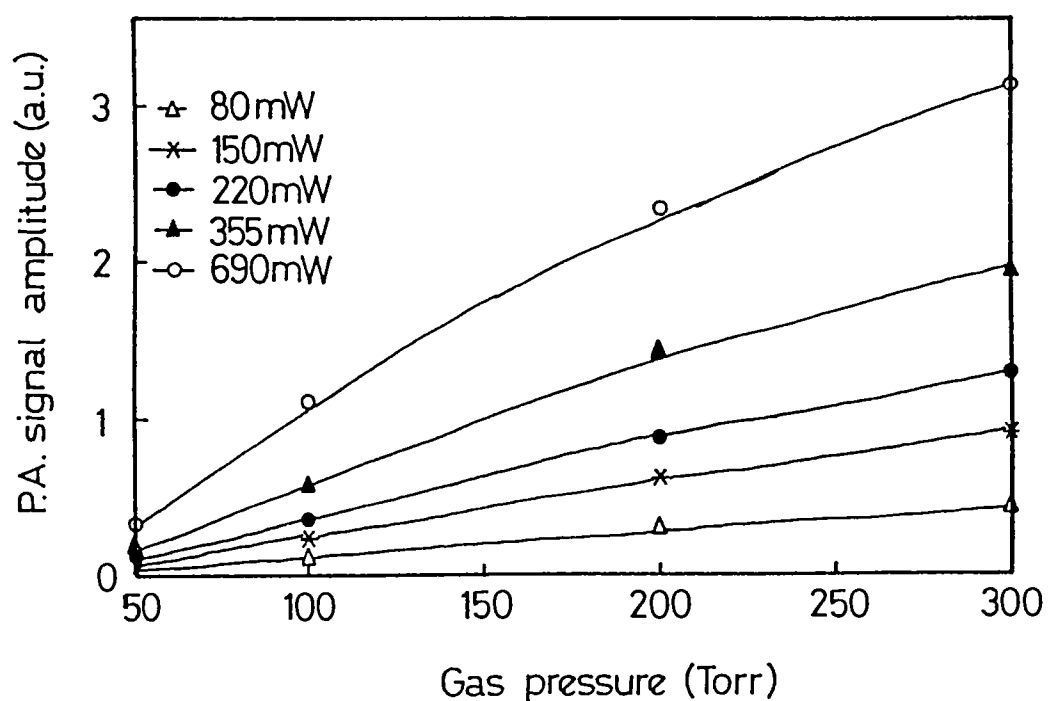


Fig.6.14. The variation of the PA signal with gas pressure for different laser powers of the multiline output of the argon ion laser for low concentration NO_2

and different buffer gases detected at the $3.39\mu\text{m}$ He-Ne laser wavelength by Wake and Amer [50,51] in the process of the study of the non-resonant and resonant PA signals with respect to pressure and buffer gas. Starting from the thermodynamic solid-gas theory of Kerr and Atwood [52], which provides a suitable starting point to analyze the PA signal strength in the case of a weakly absorbing gas confined to a cylindrical cavity excited by a radiation passing through the axis of the cavity, one may analyze these results. Taking the expression for the first harmonic lock-in amplifier output,

$$V = S(P_0, \gamma, T) \beta(P_0) \frac{I_0 P_0}{4\pi L k T} \left[\sum_m \frac{D_m \exp(i\theta_m)}{\left[1 + \left(\frac{\omega^2 a^4}{\alpha^2 \xi_m^4} \right)^{1/2} \right]} \right] \dots \quad (6.11)$$

Here, $S(P_0, \gamma, T)$ is the sensitivity of the microphone, and

$$\tan(\theta_m) = \left[\frac{\omega a^2}{\alpha \xi_m^2} \right]^{-1}$$

I_0/L is the laser power incident/unit length, $\beta(P_0)$ is the fraction of I_0/L absorbed, P_0 and T the equilibrium pressure and temperature of the gas, k and α the effective thermal conductivity and effective thermal diffusivity respectively, ξ_m is the m^{th} root of the 0^{th} order Bessel function $J_0(\xi) = 0$. D_m (b) the numerical coefficient that depends on b, the ratio of the Gaussian beam waist to the cell radius a. D_m is difficult to estimate for small values of b due to round-off errors and can be verified as,

$$\sum_m D_m(b) = 1 - b^2 + \frac{b^2 - (2b)^{-2}}{\exp(1/b^2)} \dots \quad (6.12)$$

The variation in the PA signal can be described on the basis of the above equation as,

- (a) The initial rise in the PA signal is due to a direct consequence of the increase in pressure P_o and a decreasing k .
- (b) The term $\left(\frac{\omega^2 a^4}{\alpha^2 \xi_1^4}\right)$ becomes greater than unity near the peak of each curve allowing the $1/P_o$ dependence to cancel the P_o factor and thus limits any further increase in the PA signal.
- (c) The high pressure fall in the PA signal is due to a decreasing power absorption, $\beta(P_o)$ and a decreasing microphone sensitivity at high pressures.

Wake and Amer [50], using different buffer gases showed that noble gases produce the largest PA signal. Those gases with large thermal diffusivities yield largest signals at high pressure than those with smaller diffusivities. A practical consequence of this behaviour is that if one were to optimize the SNR of the system, the following should be taken into account : the term $\left(\frac{\omega^2 a^4}{\alpha^2 \xi_m^2}\right)^{1/2}$ of Equ.6.11 must be kept of the order of unity or smaller for as high a pressure as possible. Since α is proportional to $k(P_o C_v)^{-1}$, C_v being the specific heat at constant pressure, the first term eventually drops out, the P_o and k dependence cancels out and the signal becomes proportional to $1/C_v$. Until this happens, however, the PAS signal rises with pressure. Ideally, then, one requires a buffer gas of small k and high α values. Both this factor and the high pressure dependence mentioned above point to as small a C_v as possible indicating the selection of a noble gas as buffer. One may also moderate the increase of $\left(\frac{\omega^2 a^4}{\alpha^2 \xi_m^2}\right)^{1/2}$ by varying other factors. One should use as low a modulation frequency as possible, although the $1/f$ noise of the electronics sets the limit

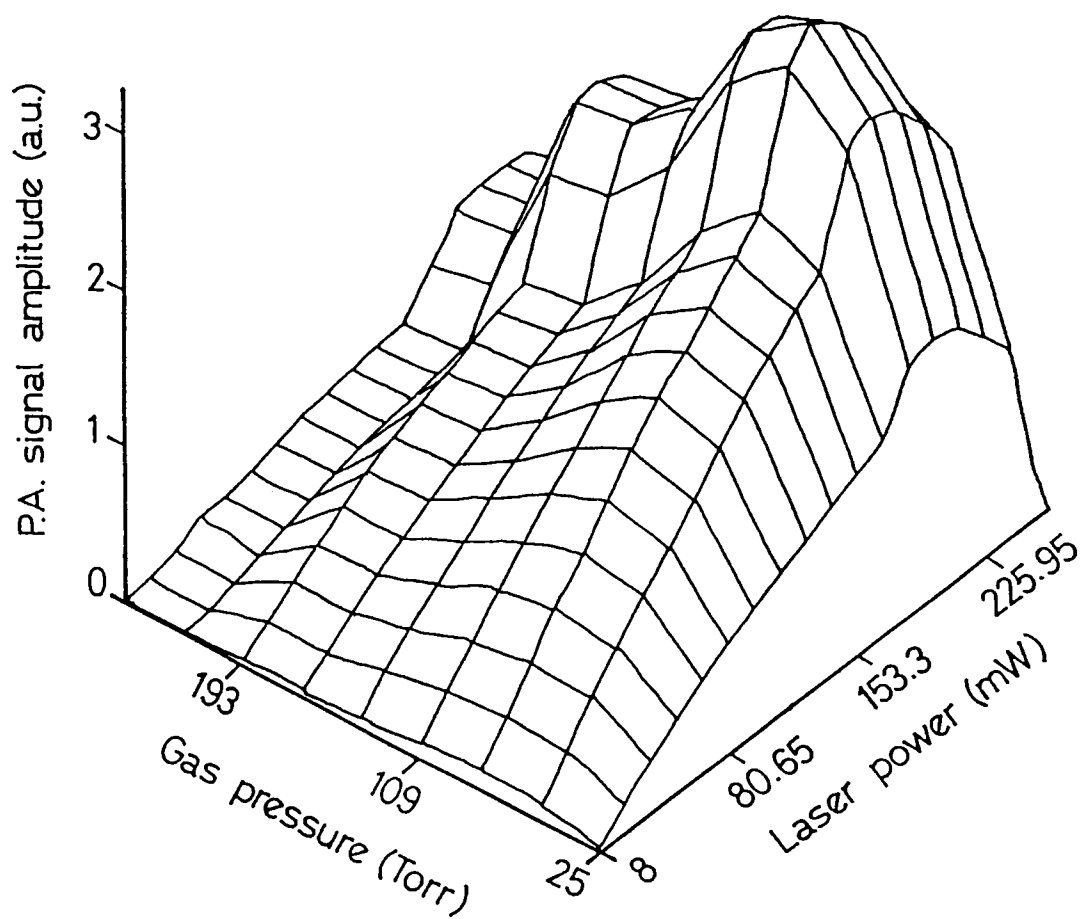


Fig.6.15. The 3-D representation of the laser power and gas pressure variation of the PA signal for high concentration NO_2 using the multiline output of the argon ion laser

of this approach. A reduction in the cell radius would benefit since this enters as a factor in the fourth power. Here too, a tradeoff exists as D_m falls with increasing b value. Also reducing the temperature enhances the signal as well as lowers the electrical noise to a limit [50]. In general, higher signal may be obtained with an absorber-buffer mixture than with any amount of the absorber alone.

The pressure and laser power variations of the high concentration NO_2 using the multiline output of the argon laser are summarized in the 3-D plot given in fig.6.15. From these data, the pressure corresponding to the lowest signal detectable can be calculated. This was done by monitoring the PA signal at a fixed laser power while the cell was being evacuated. The residual gas in the cell after the cell is pumped down can still give a signal which was detected to be $10\mu\text{V}$ at a laser power (multi-line output) of 35mW which corresponds to a pressure of $\sim 7 \times 10^{-3}$ Torr of high concentration NO_2 which means that detection limits of a few tens of ppb can easily be achieved in a gas mixture. Thus the potentiality of this technique for monitoring of NO_2 in the context of atmospheric pollutants is obvious.

iv. CW PA Spectrum Of NO_2

The absorption spectrum of NO_2 recorded using a UV-VIS-NIR spectrophotometer in the visible region of 570-600nm region is given in fig.6.16. The complex nature of the absorption of NO_2 is clearly evident from this spectrum. To record the PA spectrum of NO_2 , the ring dye laser is tuned across the wavelength region and the PA signals obtained from the differential PA cell is normalized against the variation in laser power across the dye laser output profile. The normalized PA spectrum of NO_2 is shown in fig.6.17. The spectrum, quite different from the absorption

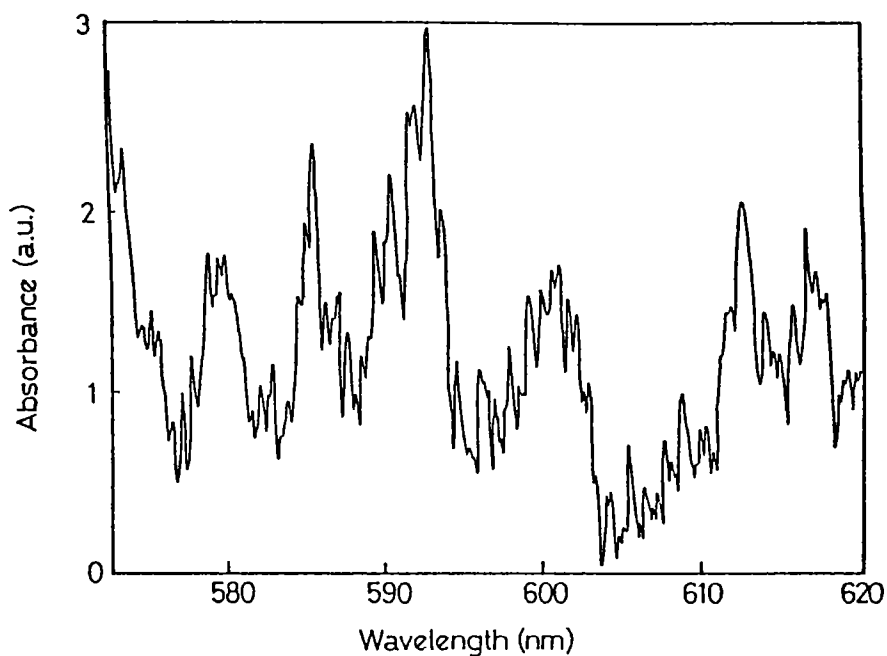


Fig.6.16. The absorption spectrum of NO_2 in the 570–620nm region recorded using a UV-VIS-NIR spectrophotometer

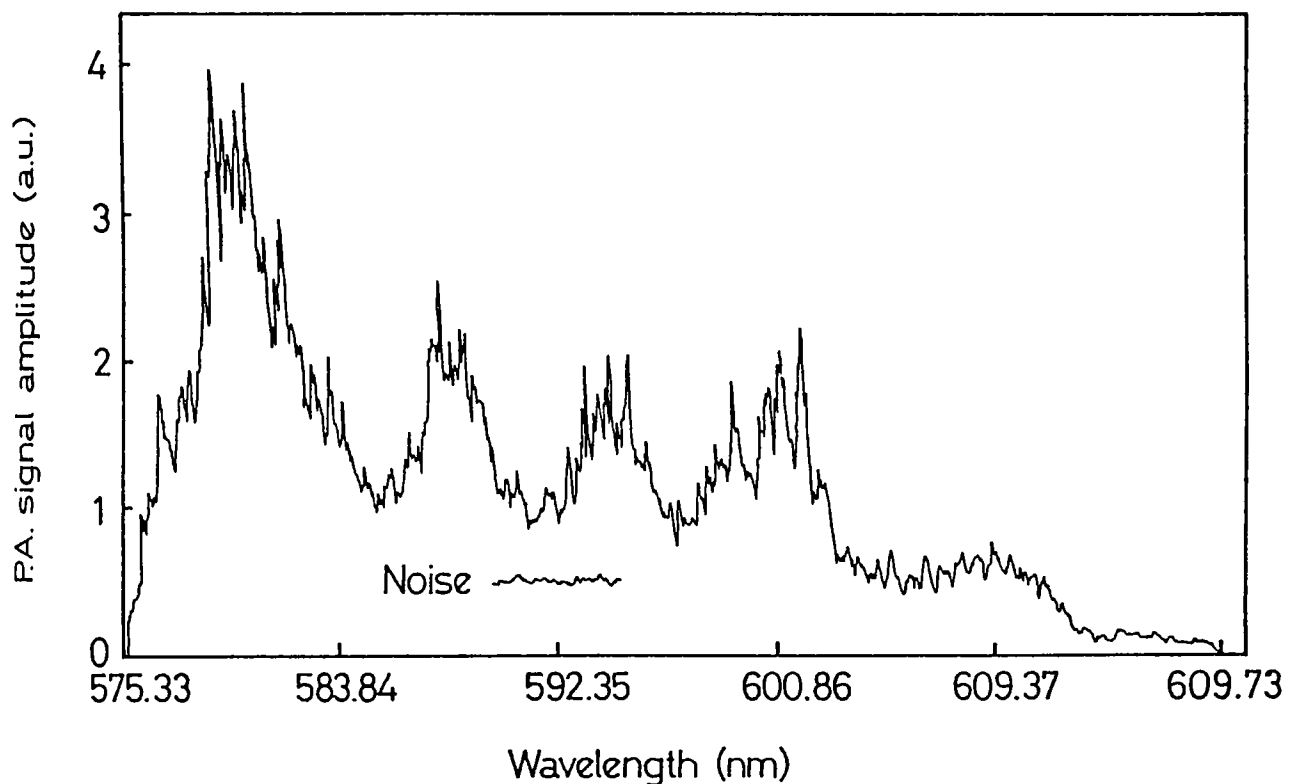


Fig.6.17. The normalized cw PA spectrum of high concentration NO_2 in the wavelength region 575–609nm (Pressure \sim 100 Torr, pre-amp gain \sim 40dB, Average laser power \sim 150mW)

spectrum obtained for the same wavelength region, shows four bands of the $^2B_2 \rightarrow ^2A_1$ band system of the visible region. Spectra with similar features of NO_2 in the visible region has been reported by many workers employing different detection techniques like absorption [37,39], fluorescence by supersonic beam technique [48], opto-galvanic detection technique [49], polarization spectroscopy [53,54,55] and by calorimetric techniques like PA and PTD methods. Most of the work other than absorption and fluorescence of NO_2 does not detail spectroscopy of the sample but has concentrated on the detection of the sample. The PA spectra of the different bands in the $^2B_2 \rightarrow ^2A_1$ transition in the wavelength region of the dye laser are given in the expanded from in fig.6.18.a,b,&c. The noise reduction capability of the dual cavity differential cell used for these studies is evident from the noise level indicated in the above spectra. The noise level was recorded by plotting the PA signal versus time at a particular wavelength. Typically, a total noise of 3.3mV in a signal of 700mV was observed at a wavelength of 568nm with the amplifier gain at 40dB, and 2.6mV at 588nm, where the total signal is \sim 400mV. The fine structure of all the bands is clearly resolved in the present PAS mainly due to the narrow linewidth of the ring dye laser (\approx 30GHz). Such resolved features have been detected for the first time in the case of NO_2 PA spectrum in the visible region.

6.5. Conclusions

The significance of studies on NO_2 specially in the context of atmospheric pollution and the detection of NO_2 by PA technique using both pulsed and cw dye lasers have been described. The signature spectrum of NO_2 in the 560-600nm has been established and the nature of variation of the PA signal with the gas pressure and laser energy/power has been determined. It is seen that the

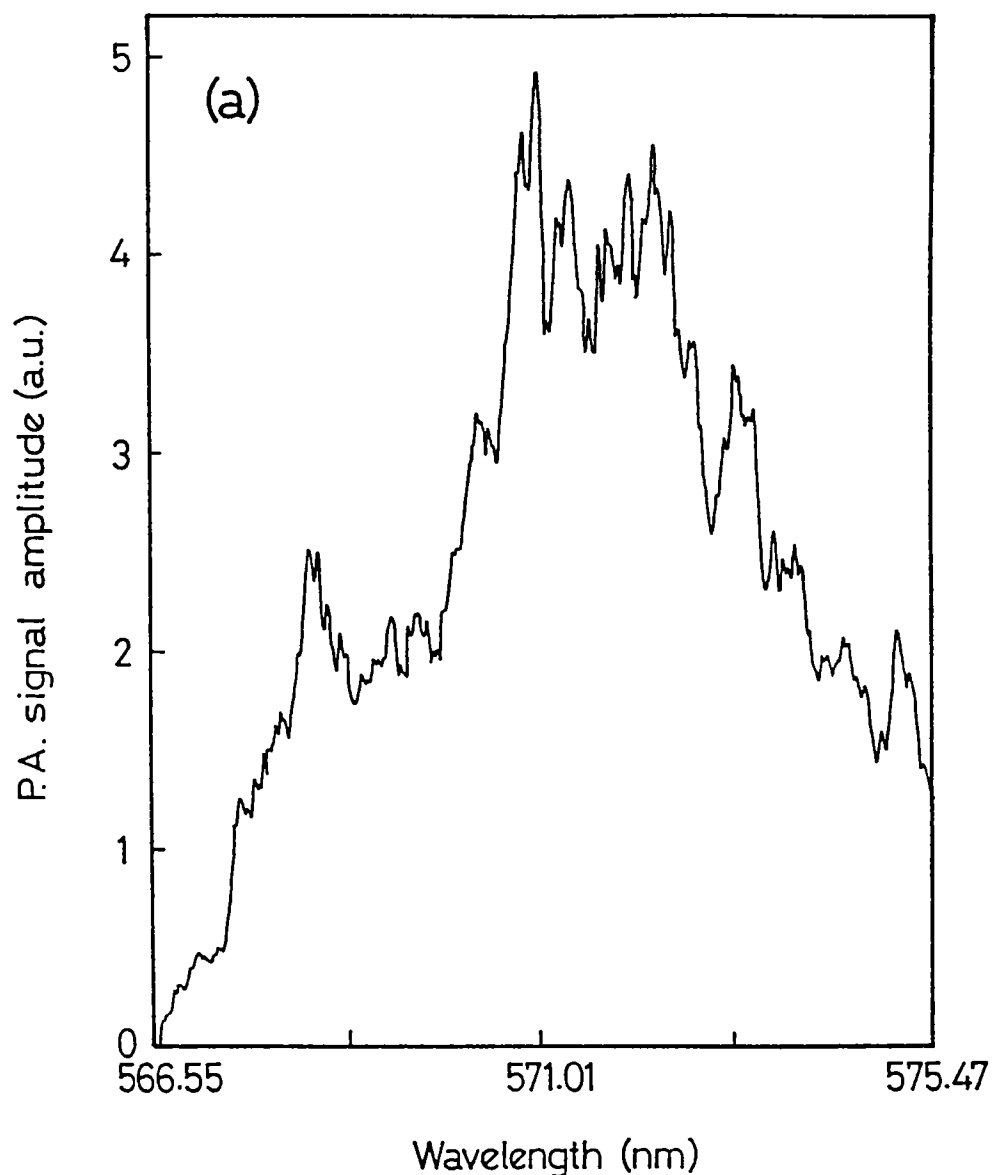


Fig.6.18(a) The cw PA spectrum of NO_2 in the (a) 566–575 nm wavelength region

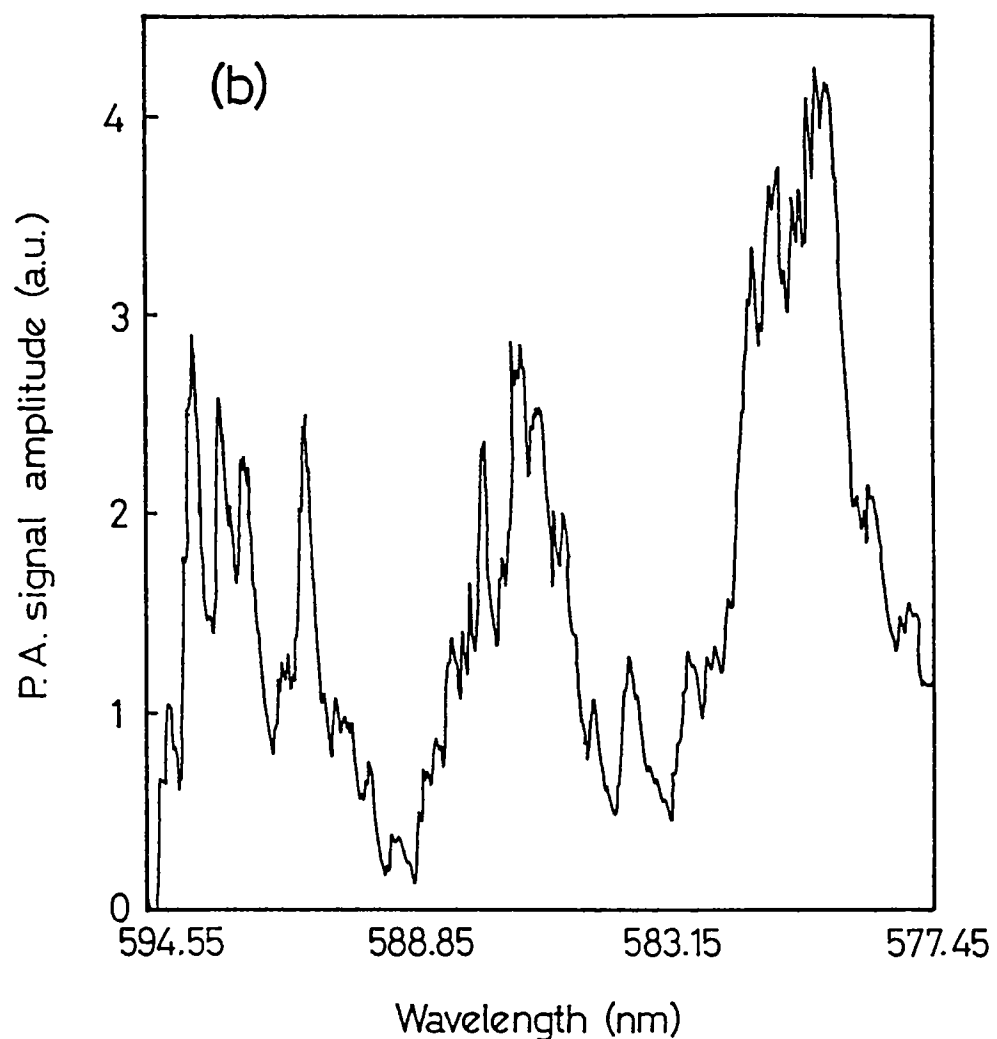


Fig.6.18(b) The cw PA spectrum of NO₂ in the (b) 577-594nm wavelength region

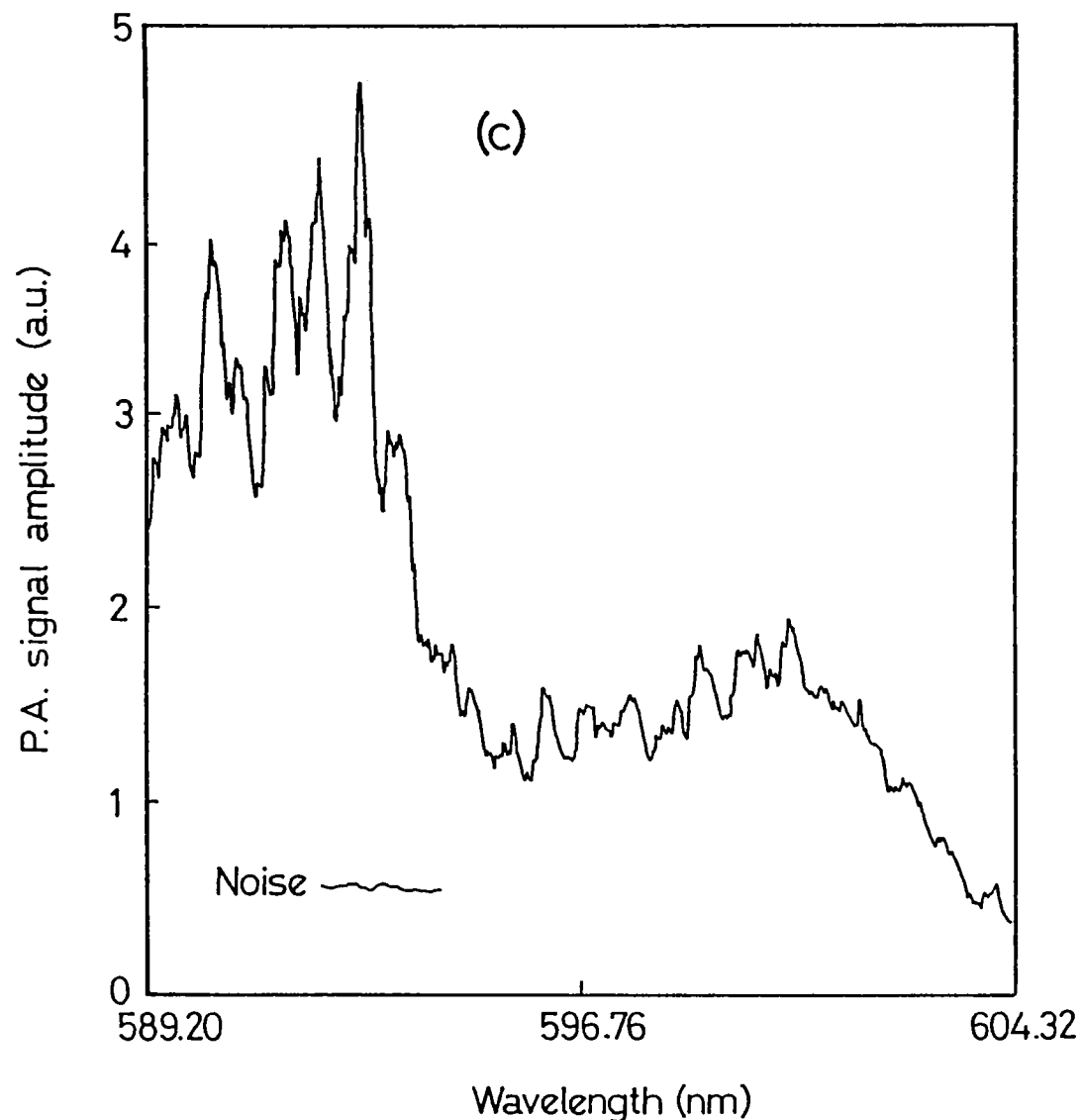


Fig.6.18(c) The cw PA spectrum of NO₂ in the (c) 589–604nm wavelength region

PA signal tends to saturate easily for high concentration samples. The differential PA detection technique employed here has a very low noise level as is evident from the spectra recorded.

6.6. References

- [1] Haagen-Smit A J and Wayne L G, in "Air Pollution, Volume I", Edited by Stern A C, (Academic Press, New York, 1968)
- [2] Schuck E A and Stephens E R, in "Oxides of Nitrogen" Advances in Environmental Sciences, Vol.1, Editors : Pitts J N and Metclaf L R, (Interscience, New York, 1969)
- [3] Pitts J N, Sharp J H and Chan S I, *J.Chem.Phys.*, 40, 3655, (1964)
- [4] Leighton P A, "Photochemistry of Air Pollution", (Academic Press, New York, 1961)
- [5] Robinson E and Robbins R C, *J.Air.Pollut.Control.Assoc.*, 20, 303, (1970)
- [6] Nadel J A "Combustion Generated Air Pollution", Editor : Starkman E S, (Plenum Press, New York, 1971), p.239
- [7] Darley E F, "Combustion Generated Air Pollution", Editor : Starkman E S, (Plenum Press, New York, 1971) p. 245
- [8] USEPA "Air Quality Criteria for Oxides of Nitrogen", National Air Pollution Control Administration, USA, Publication # AP-84, 1971
- [9] Campan R M and Neerman J C, *S.A.E.Trans.*, 75, 582, (1967)
- [10] Reckner L R, Scott W E and Biller W F, *A.P.I.Proc.*, 45(III), 133, (1965)
- [11] Dobbins R A, "Atmospheric Motion and Air Pollution", (Wiley-Interscience, New York, 1979), p.174
- [12] Johnson F S, *Aeronaut.& Astronaut.*, 11, 16, (1973)
- [13] Pitts J N et al, *Environ.Sci.Technol.*, 3, 241, (1969)
- [14] Harshbarger W R and Robin M H, *Acct.Chem.Res.*, 6, 329, (1973)
- [15] Keruzer L B, Kenyon N D and Patel C K N, *Science*, 177, 344, (1972)
- [16] Agnus A M, Marinero E E and Colles M J, *Opt.Comm.*, 14, 223, (1975)
- [17] Claspy P C, Ha C and Pao Y H, *Appl.Opt.*, 16, 2972, (1977)

- [18] Munir Q and Weber H P, *Opt.Comm.*, **52**, 269, (1984)
- [19] Colles M J, Agnus A M and Marinero E E, *Nature*, **262**, 681, (1976)
- [20] Poizat O and Atkinson G H, *Anal.Chem.*, **54**, 1485, (1982)
- [21] Fried A and Hodgeson J, *Anal.Chem.*, **54**, 278, (1982)
- [22] Tran C D and Franko M, *J.Phys.:E.*, **22**, 586, (1989)
- [23] Higashi T, Imasaka T and Ishibashi N, *Anal.Chem.*, **55**, 1907, (1983)
- [24] Mori K, Imasaka T and Ishibashi N, *Anal.Chem.*, **55**, 1075, (1983)
- [25] Imasaka T and Ishibashi N, "Thermal Lens Spectrophotometry for Trace Analysis", in the Proceedings of the First Korea-Japan Joint Symposium on Analytic Chemistry, Vol.I, p.47, (1985)
- [26] Imasaki T, Higashi T and Ishibashi N, *Anal.Chem.Acta.*, **245**, 191, (1991)
- [27] Wendel G J, et al, *Anal.Chem.*, **55**, 937, (1983)
- [28] Maeda Y, Aoki K and Munemori M, *Anal.Chem.*, **52**, 307, (1980)
- [29] Patel C K N and Kerl R J, *Appl.Phys.Lett.*, **30**, 578, (1977)
- [30] Thomas M D et al, *Anal.Chem.*, **28**, 1810, (1956)
- [31] Saltzman B E, *Anal.Chem.*, **26**, 1949, (1954)
- [32] Jacobs M B, "Chemical Analysis Series, Vol.I", (Interscience, New York, 1949), p354
- [33] Foster E G and Daniels F, *Ind.Engg.Chem.*, **43**, 986, (1951)
- [34] Faith W L and Atkisson A A, "Air Pollution IInd Ed." (Wiley-Interscience, New York, 1972)
- [35] Rothe K W, Brinkmann and Walther H, *Appl.Phys.*, **4**, 181, (1974)
- [36] Uehara K and Sasada H, "High Resolution Spectral Atlas of Nitrogen Dioxide - 659-597nm" Springer Series in Chemical Physics, **41**, (Springer-Verlag, Heidelberg, 1985)
- [37] Hsu D K, Monts D L and Zare R N, "Spectral Atlas of Nitrogen Dioxide - 553-648nm", (Academic Press, New York, 1978)
- [38] Abe K et al, *J.Mol.Spectrosc.*, **38**, 552, (1971)
- [39] Stevens C G et al, *Chem.Phys.lett.*, **18**, 465, (1972)
- [43] Sakurai K and Broida H P, *J.Chem.Phys.*, **50**, 2404, (1969)
- [44] Claspy P C, "Optoacoustic Spectroscopy and Detection", Edited by Pao Y H, (Academic Press, New York, 1977), chapter 6.

- [45] Pristera F et al, *Anal.Chem.*, 32, 495, (1960)
- [46] Robin M B, "Optoacoustic Spectroscopy and Detection", Edited by Pao Y H, (Academic Press, New York, 1977), chapter 7.
- [47] Butler S, Kahler C and Levy D H, *J.Chem.Phys.*, 62, 815, (1975)
- [48] Smalley R E, et al., *J.Chem.Phys.*, 61, 4363, (1974)
- [49] Feldman D, *Opt.Comm.*, 29, 67, (1979)
- [50] Wake D R and Amer N M, *Appl.Phys.Lett.*, 34, 379, (1979)
- [51] Thomas L J, Kelley M J and Amer N M, *Appl.Phys.Lett.*, 32, 736, (1978)
- [52] Kerr E L and Atwood J G, *Appl.Opt.*, 7, 915, (1968)
- [53] Brand J C D, Cross K J and Ernsting N P, *Chem.Phys.*, 59, 405, (1981)
- [54] Sugimoto N et al, *Chem.Phys.Lett.*, 106, 403, (1984)
- [55] Teets R et al, *Phys.Rev.Lett.*, 37, 683, (1976)

6.7. Symbols and Notations

- a radius of the PA cell
- α Effective thermal diffusivity
- b Ratio of the Gaussian beam waist and the cell radius
- C_v Specific heat at constant volume
- $D_m(b)$ Numerical coefficient dependent on b
- γ Ratio of specific heats
- I_0 Incident laser power
- k Effective thermal conductivity
- L Length of the cell
- ω Modulation frequency
- P_0 Gas pressure
- S Sensitivity of the microphone
- T Temperature
- v Normal vibrational modes of NO_2
- V First harmonic output of LIA
- ξ_m m^{th} root of the 0^{th} order Bessel fn. $J_n(\xi) = 0$

CHAPTER VII

PHOTOACOUSTIC STUDY OF LASER INDUCED DAMAGE THRESHOLD AND PLASMA PROCESSES

ABSTRACT

THE PROCESS OF LASER INDUCED DAMAGE AND ITS DETECTION USING THE PA TECHNIQUE ARE DESCRIBED. THE THRESHOLD ENERGY DENSITY FOR DAMAGE OF A VARIETY OF MATERIALS LIKE BULK POLYMERS, METALS AND THIN FILMS HAVE BEEN DETERMINED TO SHOW THE VERSATILITY OF THIS TECHNIQUE. IN-SITU PA MONITORING OF THE LASER ENERGY DURING LASER GENERATED PLASMA PROCESSES HAS ALSO BEEN DESCRIBED.

CHAPTER VII

PHOTOACOUSTIC STUDY OF LASER INDUCED DAMAGE THRESHOLD AND PLASMA PROCESSES

7.1 Laser Induced Damage Process : General Introduction

When a low power laser beam passes through a transparent material, no irreversible effect is observed, but at sufficiently high power or energy density, transient or permanent effects may be produced in the material. These effects include absorption and refractive index changes, removal of material from the surface, production of internal voids, melting vaporization and even violent shattering. This phenomenon of optical damage has always been a major limiting factor for the operation of high power lasers and their associated optical elements. There is a threshold value for the power density of laser beams for producing such irreversible damage effects in each material and this value is called the Laser damage Threshold (LDT) for the particular material. LDT values have great significance in connection with the studies on interaction of laser beam with materials. Ever since the output of laser systems has reached levels at which these effects are observed, there has been widespread interest in this area of research. The major part of the studies on LDT was done by workers in laboratories pursuing high power laser fusion experiments since it was they who first noticed the adverse effects of this phenomenon. The interest in Laser induced damage (LID) ranges from investigations of the mechanisms involved in this process and its practical applications to the improvement of the quality of laser optic elements by increasing their LDT.

Investigations on newer, more sensitive and dependable methods of determining this quantity are also important [1]. As the mechanism of LID is still not fully understood and moreover, since there are numerous parameters that finally determine the LDT of a material, a technique that can be applied to determine this quantity accurately for different kinds of samples has still not been evolved. Damage can occur either internally or at the surface of the target. The internal damage can occur due to particulate inclusions, small inhomogeneities, absorption or self-focusing in the material. The external damage is a more sensitive quantity and it depends, to a great extent on the surface finish, imperfections, impurities, inclusions or irregularities on the target surface [2]. Of the two, the surface damage is more serious since it occurs at a lower energy density, and it is often the surface of the target material that finds applications in laser reflection optics. The phenomenon of dielectric breakdown in bulk materials due to laser irradiation has not found much importance unlike surface damage mechanism due to the obvious applications of optical surfaces. The study of the bulk processes only helps in understanding the behavior of dielectrics because both the bulk and surface damage are often accompanied by plasma formation and so both of them involve, related, if not identical phenomena. It is seen that the power densities for surface damage is generally 0.3 to 0.5 times the bulk LDT values.

Laser damage threshold can be defined as the laser power or energy density at which physical damage to the surface occurs. Thus the determination of this quantity is a purely destructive testing process, though photoacoustic microscopy can, to an extent determine (non-destructively) the possible sites on the surface that might have a lower damage threshold. It is usually expressed in terms of the energy density or sometimes in terms of

the electric field associated with the laser beam. In general, it is seen that damage occurs to a given target under laser irradiation at a power level which is dependent on both the material parameters and the laser characteristics like wavelength, the temporal and spatial profile of the laser pulse etc. UV lasers have greater ionizing capability by virtue of their shorter wavelength as compared to the greater thermal energy of the IR lasers. Thus, a UV laser can cause greater damage to a surface than an IR laser of identical pulse shape, energy and width characteristics. Most of the mechanisms that result in damage to the target are dependent on the peak energy density though some are dependent on the total energy. In order to explain this phenomenon, various mechanisms have been proposed of which a few important ones are given in this chapter.

The actual measurement of the LDT involves three steps ie, to irradiate the sample at several laser energy densities, to measure the absolute characteristics of the laser pulse and finally to determine which of the laser pulses caused the damage to the target. Though the steps described are quite simple, the process of an absolute measurement of this quantity is beset with various problems. Some of these problems faced are discussed below [3].

7.1.1. Laser Beam Parameters

The questions that arise regarding the laser pulse parameters are the following ;

What parameters should be measured to determine the laser flux or intensity ? What is the relative or absolute accuracy of the measurements ? How large should be the size of the focal spot in order to measure practical laser damage threshold ? And, how many sites should be tested ?

Since the laser pulse energy varies with the pulse width and the beam profile, these parameters must also be measured accurately. Sophisticated instruments like the streak camera, videocon, recticon [4] or even pyroelectric or photodiode arrays are often required for these measurements. In such cases, the serious problem is that regardless of how the image is recorded, there is a background noise level which greatly complicates the interpretation of the low-intensity wings of the profile. This can be eliminated to an extent by placing an aperture, the diameter of which is approximately equal to the FWHM of the profile. For such a setup, with a laser of pulse width less than 1 nsec, the uncertainties in LDT measurements due to the laser energy, flux and intensity are ± 3 , $\pm 5-7$ and $\pm 10-15\%$ respectively. The absolute accuracy in the energy density measurements, however depends on the accuracy of the calorimeter used to determine the pulse energy, which, using commercial energy meters, can be measured with good precision within an error margin of $\leq 5\%$. Since it is the determination of the beam profile that involves serious problems, often, only the results of LDT measurements without shot-to-shot determination of the beam profile are reported. Obviously, the margin of experimental error is definitely enlarged in these cases. Even the ability to determine the laser flux within a 5% error does not imply that the LDT can be measured with the same degree of accuracy since uncertainties can be introduced by the large step-sizes in flux during the sequence of shots used for irradiation, or by indecision as to whether damage has actually occurred or not for a particular laser shot. The laser spot size must be big so as to ensure that the worst-case defects have been encountered. The morphology of laser damage in thin films show that damage occurs at isolated regions in the film, the exact nature of defects responsible for this being still unknown. The test area must be illuminated uniformly to within the desired precision of the LDT

measurement. Typically test areas > 5mm diameter are used. Since damage is a cumulative effect, multiple shots at the same site will lower the LDT. It is better to expose a new site to each shot under the assumption that the surface morphology is uniform within the measurement error. For testing of laser optics, it is needed to know as to how many shots the surface can endure before damage sets in. For such studies, multiple exposure is ideal, so long as the pulse-to-pulse stability of the shots is ensured. The work presented in this chapter has followed the method of "single-shot" laser damage threshold measurements. Moreover, there is no *a-priori* guarantee that different sites will respond alike to the same flux level. The total energy Q in terms of energy density $\epsilon(r)$ at the focal plane can be expressed as [5],

$$Q = \epsilon(r) \int_0^{\infty} 2\pi r dr \quad \dots \dots \dots (7.1)$$

$$\text{and for a Gaussian beam, } \epsilon_0 = \frac{2Q}{\pi r_0^2} \quad \dots \dots \dots (7.2)$$

where, ϵ_0 is the peak on-axis energy and r_0 the radius at which the intensity has fallen to $1/e^2$ of its original value. In terms of the peak on-axis intensity, the damage threshold,

$$I = \frac{2Q}{\pi r_0^2 \tau_L} \quad \dots \dots \dots (7.3)$$

The r.m.s. electric field associated with this intensity is,

$$E = 19.41 \left[\frac{I \text{ (W/cm}^2)}{\eta} \right]^{1/2} \quad \dots \dots \dots (7.4)$$

where τ_L is the laser pulse width, η is the refractive index of the material. The total energy Q is related to the incident energy on the focusing lens (Q_{in}) as,

$$Q = Q_{in} \tau_L T_S \quad \dots\dots(7.5)$$

T_L and T_S are the transmissions of the focusing lens and the sample respectively.

7.1.2. The Test Sample

The relevant questions regarding the test sample for LDT measurements are ;

What should be the surface finish of the sample ? How should the sample surface be cleaned before testing ? Will the use of detection techniques such as 'breath-fogging' during the experiments reduce the damage threshold ? Can a small 'witness' sample, identical to the actual larger optical element to be tested, be tested for LDT *in lieu* of testing the original sample ? And what should be the angle of the test sample with respect to the laser ?

Since dust or other minute inclusions at the focal sites reduce the LDT at those sites, careful cleaning of the sample surface with organic solvents helps, but for large diameter beams, this problem is not very critical as compared to focused beams. Scratches and residue on the surface as a result of cleaning can also cause lower LDT, and thus should be done carefully. The surface finish of the sample can be visually inspected using intense white light and, if the sample is not hygroscopic, by breath-fogging technique, which has been a time honored process of

checking surfaces. However, there have been indications of lowering of LDT by repeated breath-fogging and the resulting residue formation on the surface [6]. It is ideal to orient samples like polarizers, reflectors etc., relative to the beam as it would be in actual usage. The LDT of anti-reflection (AR) films have been found to be independent of whether the film is used as an entrance or exit surface. In the case of using a 'witness' sample (for example, a smaller, similar surface coated simultaneously with the actual bigger optical element to be tested) being used instead of the actual element to be tested, there is no guarantee that the witness sample is in every way identical to the actual one, since the damage process is dependent on various parameters. Thus this method cannot be a fool-proof method of testing a sample. Moreover, in AR coatings, the LDT was found to be highly dependent on the substrate material properties [7]. Since there is no guarantee that each point on the sample surface will have identical surface features, multiple irradiation of the sample surface can give an average value of the damage threshold.

7.1.3. Detection Technique

Many methods of detection of the LDT have been reported, none of which can be acclaimed as accurate and fool-proof for all kinds of samples. It is seen that the LDT measurements are influenced by many parameters relating to the experimental conditions like pulse width, repetition rate, beam diameter, beam focusing, temperature, laser frequency, optical pumping conditions etc, and to the sample conditions like material growth or preparation conditions, surface finish, presence of impurities etc. Some of the problems faced in the conventional LDT determination techniques are :

What is the practical definition of laser damage ? How does

one determine whether damage has occurred, and how certain is the determination ? Is there a single, fool-proof indicator of the damage occurrence that is usable with all types of test samples ? And do the LDT measured in the laboratory correlate with the levels at which the optical element actually operates ?

The different techniques used for detection of LDT are described below ;

(a) Emission of Spark/Light

Detection of sparks and light emission can be made by visual observation of the damage process in a dark room. A spark is defined to be a plasma heated sufficiently that it expands vigorously, sometimes audibly. Often, light emitted by a diffuse plasma appears as a glow rather than a spark. There is also the possibility that fluorescence emission can occur without occurrence of damage. The difficulty in detection may arise from the fact that light emission may not be seen either due to other visual distractions or due to the frequency range of the emission. Also the difficulty exists in distinguishing the actual source of light emission ie, if it is from the front or back surface or from the bulk. This technique only aids the detection of LDT rather than the actual determination and is not reliable for multi-layer AR films.

(b) Change in Scattering/Reflection

The visual detection of the variation of small-angle scattering or reflection/transmission of a probe beam from the site of irradiation can give indication regarding the damage process. This simple technique is remarkably successful in thin films if large beams are used so that many scatterers are produced in the near-threshold damage sites.

(c) Particulate Plumes

They are detected by focusing a light beam on to the damage site. The disadvantage in this technique is that very little material is ejected during damages occurring near to the threshold.

(d) Microscopy

Techniques such as scanning electron microscopy (SEM), bright field, dark field microscopy, Normarski microscopy [8] etc. are often used to detect the threshold. SEM technique, though effective in locating damages, is time consuming and destructive in nature. For thin film samples the Normarski microscopy is the most suited technique. This detects the change in optical scattering from the target induced by the microscopic film ruptures caused by the irradiation.

(e) Breath-fogging Technique

It is one of the easiest and time tested techniques to observe the occurrence of laser damage on non-hygroscopic bare surfaces. This technique, as the name indicates, functions so absolutely that other tests are redundant. To be most effective, the test must be performed soon after the irradiation is completed, since the breath-fogging pattern becomes less distinctive after several days. As mentioned earlier, it has been seen that repeated use of this technique leaves a residue which tends to decrease the LDT of the sample.

(f) Surface Potential Mapping Technique

Mapping of the surface potential on the target surface throws light on the post irradiation condition of the surface [9]. It is seen that the surface potential or the work function of the

target material varies as a function of position with respect to the site of laser irradiation. In dielectric materials, an accumulation of negative charges in an area ten times the diameter of the laser spot was observed. Only in the case of copper was the polarity of the surface charges positive. No potential change was observed for ripple formation on silicon surfaces. A Kelvin type non-contact probe, working on the principle of adjusting the d.c. voltage on the test capacitor formed by the sample surface and a reference electrode so as to null out the a.c. variations in the capacitance voltage caused by physically dithering the reference electrode, was raster scanned over the irradiation site with a resolution of ~ 1mm to obtain the surface potential mapping. Although no pre-damage changes in the surface potential were observed, all larger damage features had a surface potential changes associated with it. Damage types such as the pit formation have been detected successfully using this technique. It is seen that the post-damage surface potential decays over a time scale of hours to a fixed value approximately 1/4th of its initial value which corresponds to permanent damage. The interesting thing to note in this technique is that the absence of pre-damage potential changes indicate that this technique is relatively unaffected by the process of surface cleaning. The relatively large area of the surface potential distribution (4-6mm compared to a laser spot diameter of 0.3mm) with respect to the irradiation site suggests that the adjacent test sites should be sufficiently spaced out during measurement process.

7.2. Mechanisms of Laser Induced Damage

Of the many proposed mechanisms to explain the various aspects of the laser damage process, a few important ones are briefly mentioned below. Since most of these models require complicated parameters such as the material band structure and the electron

effective mass which are often not available for many dielectric materials, it is impossible to calculate the damage threshold due to each of the competing mechanisms. Thus the only practical way to determine the most appropriate model is to examine their predictive ability in describing the various damage thresholds with easily controlled experimental or sample variables such as the laser pulse width, energy, wavelength and sample (bulk and surface) properties.

The optical power levels for catastrophic damage to bulk materials (intrinsic damage level) is related to the thermal and electrical breakdown of an insulating material. Massive insulators have a.c. dielectric breakdown strengths (E_B) of 1-5 MV/cm, equivalent to optical power densities (P_D) of 50-1000 MW/mm², obeying the equation,

$$P_D = \frac{E_B^2}{Z'} = \frac{E_B^2 \eta}{Z_0} \quad \dots\dots(7.6)$$

Where, Z' and Z_0 are the impedances of the dielectric and free space respectively, and η the refractive index. It is interesting to note that the relation between P_D and E_B is independent of wavelength except through the refractive index η . Since the interaction can occur between several mechanisms and will modify the apparent power density distribution, these intrinsic quantities are rarely measured. In practice, the laser damage threshold of a material, in a particular set of experimental circumstances may be due to one or more of the many mechanisms involved. Some of these are given below :

7.2.1 Electron Avalanche

Electron avalanche is probabilistic in nature, since it results from the multiplication of an initially produced free electron.

There is always a non-zero probability of the damage, and this is dependent on the optical intensity. If p_1 and p_n are the probabilities of damage in the first and the n^{th} shot so that $p_1 \propto \exp(-K/E)$ where K is the constant determined by the sample properties and the experimental conditions and E is the electric field associated with the light wave, then [10],

$$p_n = p_1 \left(1 - p_1 \right)^{n-1} \quad \dots \dots \dots (7.7)$$

It is also relevant, to approach practical situations, by considering large areas. In this case, a number of free electrons may be produced instead of one as in the above treatment. If $p = p(E)$ is the probability for breakdown when one initial electron is present, then, $p'(E) = np(E)$ is the probability for breakdown when the area of the beam is increased and n initial electron are sampled. If $np(E) > 1$, then $p'(E)$ is taken as unity. The effect of this is to make the damage probability versus power density curve to have a steep rise, thereby making the LDT well defined. This mechanism does not explain satisfactorily the damage process if,

- i. the value of K is high,
- ii. a larger volume of material is involved than that which is small enough to reveal the probabilistic properties of damage
- iii. an experiment where intermediate power densities were missed or self-focusing always produced an intensity so that intermediate ranges were not studied, or if,
- iv. a material in which a non-avalanche process dominates the damage process.

7.2.2. Multiphoton Ionization

When the incident photon energy is approximately $1/3^{\text{rd}}$ that of the band-gap energy E_b of the solid, multiphoton absorption can take place and can contribute significantly to the breakdown process. Thus the LDT will decrease as the laser frequency is increased beyond an equivalent photon energy of $\sim \frac{1}{3} E_b$ [11]. The multiphoton ionization process is said to be the prime source of the supply of electrons to start the electron avalanche process [12-14].

The Keldysh model [15] for multiphoton ionization process is widely accepted among the various other models due to its comparatively easier numerical analysis and due to better correlation with experimental results [16,17]. For n-photon absorptions ($n > 3$), only this analysis gives comparable correlation between the calculated and experimental values. According to this analysis, the dependence of the optical energy/unit area on the laser pulse width τ_L reveals that if $E_b < \hbar\omega$, the breakdown process is independent of time. For very high order photon processes, $E_b \gg \hbar\omega$, and then the process is linearly time dependent. This also predicts a decrease in the breakdown field with increase in laser frequency. Multiphoton (two and three photon) processes have been shown to be the cause of laser damage in materials like CdTe, CdS and ZnSe under IR laser irradiation. The damage process has been detected using PA technique in conjunction with transmission techniques [18].

7.2.3. Conduction Electron Absorption

It is possible for an electron in the conduction band of a material to be accelerated by the laser field to a greater energy than the band-gap, thus leading to electron avalanche. For this

to occur, the lifetime of the electrons in the conduction band must be long enough and field strong enough to produce sufficient number of electrons with energy greater than the band-gap energy. It has been analyzed that the power density needed for damage to occur by this mechanism changes from being time-independent, for pulses longer than 10^{-7} sec to being inversely proportional to the pulse width τ_L for shorter pulses [19]. The threshold power density has a wavelength dependence ($P_D \propto \lambda^{-2}$) and a temperature dependence through the electron concentration.

7.2.4. Stimulated Brillouin Scattering

Stimulated Brillouin scattering results from an internal feedback mechanism which amplifies an acoustic wave and a secondary electromagnetic wave at the expense of the input laser beam [19]. At high power levels, damage occurs from the mechanical stresses associated with the acoustic wave. For long pulse lengths and cw lasers, a steady state scattering is reached and damage occurs at constant power density. For Q-switched lasers, the threshold power density is inversely proportional to τ_L .

7.2.5. Absorption by Inclusions

Many samples are likely to contain inclusions and impurities of atoms or clusters of foreign materials. Absorption at the wavelength of the input laser by inclusions, bubbles, sharp scratches etc. can lead to severe local heating and to damage due to the resultant thermal expansion or melting of the surrounding material. The damage threshold in this case may be related to [10],

1. The energy density required to produce a fracture stress in the host at the surface of the inclusion due to expansion of the heated outer shell with little heat being conducted into

the inclusion or the host lattice. This has a $\tau_L^{1/2}$ dependence and is relevant for very short pulses or for very large inclusions ($E_D \propto \tau_L^{1/2}$).

2. The energy density required to produce a fracture stress in the host due to the expansion of the inclusion. This is time independent and relates to the intermediate size of the inclusion for which $E_D \propto R$, R being the radius of the inclusion.
3. The energy density required to produce a fracture stress due to the thermal mismatch between the inclusion and the host lattice (both being heated by conduction) and holds good for long pulses or very small inclusions ($E_D \propto \tau_L/R$).

7.2.6. Bulk Absorption

Bulk absorption can occur due to the presence of impurities, color centers, conduction electrons or by the lattice, and can cause laser damage by the heating and the consequent fracture of the region surrounding the laser beam. This threshold is dependent on both the pulse length and the area heated ($E_D \propto \tau_L/a_0^2$, where a_0 is the beam radius). The proportionalities are dependent on the thermal properties of the material [19].

7.2.7. Self-Focusing

The self-focusing is a reduction of the laser beam diameter below the value predicted from the optical properties of the unirradiated material, and can result from any process which leads to an increase of the index of refraction with increasing light intensity and/or temperature [20]. The actual damage process will still be due to one of the above mentioned mechanisms, but

the damage occurs at a lower damage threshold owing to the substantial increase in energy density due to the additional focusing. Possible causes of self-focusing are, electrostriction, electronic distortion, molecular liberation and absorptive heating.

Electrostriction would occur in a dielectric material under laser irradiation as the net electrostriction force at any point is proportional to the square of the electric field. Thus a radially symmetric beam would lead to a radially symmetrical stress with an associated change in the refractive index leading to self-focusing.

Heating by absorption at the laser frequency will lead to thermal self-focusing if $d\eta/dT$ (η is refractive index and T the temperature) is positive. If it is negative, it can contribute to local increase in power density, but not self-focusing. The threshold power density for damage due to self-focusing is inversely proportional to the pulse length provided the latter is small compared to the acoustic interaction time.

The electronic distortions and molecular liberation processes dominate at very short pulse lengths whereas electrostriction dominates for Q-switched pulses and thermal self-focusing for free-lasing pulse trains.

7.3. Forms of Laser Induced Damage

As a result of the irradiation of the surface with laser pulse, any one or many of the above mentioned mechanisms can induce different kinds of damage to the test sample. Damage can occur on the front surface, inside the sample or on the rear surface of the test target. Some of the major types of laser induced damage observed are the bulk, surface and the inclusion damages. These

different kinds of damages exhibit different characteristics and occur at a range of threshold energy density for a given material. Scaling laws provide a general guide to the behavior of the damage threshold as the experimental conditions such as the pulse width (τ_L), spot size surface roughness etc. are changed. Departures from the expected scaling often indicates the onset of some new phenomena or the introduction of extrinsic factors. Relations such as the $\tau_L^{1/2}$ dependence of the damage threshold, are widely applicable to surface damage occurring due to very short pulses. For longer pulse widths (greater than a few 100 psec), extrinsic factors may enter the scene, which cause a departure from this scaling law. Finally, these scaling laws are empirical and lack full theoretical justification. Nevertheless, they provide a useful guide for exploratory damage studies to new conditions and provide a test of consistency for measured LDT values.

7.3.1. Surface Damage

The measured surface-damage thresholds for samples in air are apparently higher for the front than for the rear surface. At the front surface, the plasma that is formed at the threshold occurs in air and protects the sample by absorption of the incident power. At the rear surface, the plasma occurs inside the material, thus increasing the absorbed power density in the material and causing more catastrophic damage. Sparks are usually visible and these provide some kind of visual indication of the onset of surface damage.

The surface-damage threshold is highly sensitive to the degree of polish, type of polish, surface cleanliness and subsequent treatment. The surface-damage threshold increases with the quality of the surface polishing. The scratches on the surface should be less than $1/100^{\text{th}}$ of the wavelength of the laser

light for maximum surface-damage threshold [21]. 'Soft' materials may have apparently a flawless surface, but still contain a badly disturbed or polycrystalline surface layer. Chemical polishing and ion-beam cleaning of the surfaces does improve the quality and thus the LDT of the surface [22].

In the surface of the damaged layer, another interesting form of damage *i.e.*, the formation of ripple patterns have been observed. Melting of a surface by laser radiation typically leaves its trace in the form of permanent ripples or corrugations. It is seen that the ripple formation occurs due to laser damage, laser annealing, etching etc. They appear close to the melting point or the damage threshold and appear in all materials ranging from metals to semiconductors to dielectrics irradiated with high power lasers of all wavelength ($10.6\mu\text{m}$ to UV) and pulse widths (psec to cw) [9,23]. The patterns are often unrelated to the beam profile and appear even if the incident beam is smooth. Many forms of such patterns like ripples, streaks etc have been reported all of which have not been fully understood as yet. Explaining a particular pattern needs to answer at least two questions, (which may or may not be related) regarding (i) what is the source of the pattern and, (ii) by what physical mechanism is it imprinted on to the sample surface [24].

Of the many possibilities, it is often seen that the source of the pattern generation is light scattering from material imperfections or dust particles. The scattered radiation, being coherent with the incident beam, interferes with the latter to form patterns of modulated irradiance which now acts on the material. A point like scattering centre like a dust particle located in the ambient air at a distance z away from the sample surface makes a system of confocal ellipses (circles in the case of normal incidence) described by,

$$r_n = \frac{\eta \lambda \left[B_1 + \sqrt{1 + B_2 (1 - B_2^2)} \right]}{(1 - B_1^2)} \quad \dots \dots (7.8)$$

where $B_1 = \cos\phi \sin\theta$ and $B_2 = 2z/\eta\lambda\cos\theta$, θ being the beam incidence angle measured from the surface normal and ϕ the polar angle in the sample surface measured in the plane of incidence. η is the refractive index, λ the wavelength of the laser, and r_n is the distance from the vertical passing through the scatterer to the n^{th} fringe. In the case of linear rather than a point-like scatterer, such as scratches on the surface, fringes parallel to the scatterer are produced and usually have a spacing of $\lambda/(1 \pm \sin\theta)$ [25]. However, these patterns are often more complex than that simple geometric optics would indicate. The efficiency of interference in a particular direction depends on the state of polarization of the incident beam. The formation of fringes with spacings of $\lambda/\cos\theta$ running parallel to the polarization direction of a p-polarized incident beam was observed on nominally smooth surfaces [26]. It is seen that the spacing of the ripple formed is related to the wavelength of the incident radiation. It is proportional to λ_0 , the vacuum wavelength of radiation in the case of metals and small band-gap semiconductors. If the scattered wave propagates inside the material rather than in air, one would expect the fringe spacing to scale with λ/η , (where η is the refractive index of the sample material for wide band-gap dielectrics) rather than λ . Fringes with such spacings were observed in transparent dielectrics [27]. Though these patterns differ in spacing, they all run in a direction normal to the applied optical field [9]. A generalized treatment of interference of scattered waves in terms of nonradiative "radiative remnants" propagating along the surface of the material

was proposed by Sipe *et al* [28,29].

Surface deformations are the most common and efficient scatterers but "latent" patterns, such as lateral variations in the lattice temperature or in free-carrier density [30] seem to result in the same scattering even on geometrically smooth surfaces. Stimulated scattering at surface polariton waves [28,31] have been observed in molten Germanium [32] and quartz [33]. Whatever the origin, the scattered fields from different scattering features interact and diffract at the ripples forming secondary ripples. Since the resulting pattern contains Fourier components at several spatial frequencies, once a fringe pattern has been implanted physically on the surface, it can perpetuate itself coherently in subsequent, fully or partially overlapping laser shots [34]. This may explain the gradual build up of periodic damage pattern that is frequently observed during repeated irradiation by pulses too weak to cause any conspicuous damage individually [35]. Once the heavy damage has occurred, these surface patterns tend to deflect or scatter a large part of the incident light, thus enabling the detection of a reduced specular reflectance [36].

How are these modulated irradiance patterns physically transformed into a persistent variation of the surface geometry ? The basic sequence is that at laser damage threshold levels, the surface melts, undergoes deformation and finally after irradiation, resolidifies making the deformations permanent. The mechanism of deformation is dependent both on the absorbed fluence and the material properties [37]. The melt pattern actually formed would be random for a mathematically homogeneous beam, but even the slightest modulation of the irradiance by interference or other mechanisms will produce regularities in the pattern.

Also often related to surface rippling are the acoustic

phenomena. Pulsed melting of surface will cause an abrupt local increase in the density which acts as a strong source of acoustic waves [38]. Ripples result from the interference of the incident beam and the surface waves generated on the sample surface though the exact nature of these waves are not clearly known. Surface capillary waves frozen-in after irradiation have been related to surface ripples with wavelengths in the μm range and are unrelated to light scattering [39,40].

Another potential source for ripple formation in the melt regime is surface oxides which can stay solid on top of the melt layer and these tend to become wrinkled like the skin on milk [41]. At even high irradiance, the molten surface is shaped by evaporation [42]. On polished surfaces, strong evaporation results in extreme damage, manifested optically by diffuse rather than specular reflections [43].

A decrease in the surface damage with the ambient gas pressure has been observed in IR optical materials at $10.6\mu\text{m}$. It has been explained on the basis of the adsorbed water vapour assisted damage process on the surface. The condition for breakdown development in the water vapour region corresponds to the requirement that the rate of increase in of the energy of electrons in the field of laser radiation of intensity I must exceed the maximum rate of energy loss by electrons due to elastic collisions with neutral molecules [44], so that,

$$I > \frac{m^2 c \Delta}{2 \pi M e^2} \omega^2 \left(1 + \frac{v_e^2}{\omega^2} \right) \approx 2.65 \times 10^7 \left(1 + \frac{v_e^2}{\omega^2} \right)$$

.....(7.9)

Where, m , e are the mass and charge of the electron, Δ the ionization potential, M the mass of the molecule, ω the laser

frequency and c the velocity of sound. $v_e = \rho_v u_e \sigma/M$ is the frequency of free electron collision with neutral molecules, u_e mean electron velocity, σ the cross section of electron collision with molecules and ρ_v the vapor density. The dependence of the LDT on the vapour density is evident.

7.3.2. Impurity/Inclusion Damage

Low threshold levels for internal damage can be associated with identifiable singularities like dielectric inclusions, bubbles (voids), metal or metal oxide particles and misoriented crystallites. All these singularities have their own limited range of damage thresholds and the likely cause of the damage can be determined by repeated analysis of the values and appearance of the damage.

Since the focal point of the lens is unlikely to coincide with an inclusion, some variation in the damage threshold values are to be expected, specially while using focused radiation. Also, it is possible to miss microscopic inclusions when performing single-shot experiments. It is therefore advisable to test the sample with a larger beam diameter or by multiple irradiation of adjacent areas to the test site and obtaining an average value. Voids or bubbles also lead to damage which occurs at higher power levels and this tends to have a greater catastrophic effect. Some materials get damaged more severely when the laser beam is in a certain crystal plane or when it has a certain polarization. The sample is more susceptible to damage by cleavage when the direction of the laser is parallel to the cleavage plane of the crystalline sample [1].

The most noticeable feature unique to the impurity/inclusion model is the prediction of an increase in the damage threshold with decrease in the film thickness due to the fact that

the inclusion size is limited by the thickness of the film [45]. Based on this theory, an approximate evaluation of the damage parameters can be made, so that, the radius at which the first damage occurs is given by, [46]

$$r_d = \frac{1}{2} \sqrt{\pi D_h \tau_L} \quad \dots \dots \dots (7.10)$$

where, k_m is the thermal conductivity of the host material and τ_L the laser pulse width. The damage threshold in terms of the electric field associated with the laser is,

$$E_{\text{dam}} = \sqrt{k_m C_m \rho_m \tau_L} \quad \dots \dots \dots (7.11)$$

Here, k_m C_m ρ_m are the thermal conductivity, specific heat and the density of the sample (host) material respectively. These relations not only show the square root dependence of the laser damage threshold on the laser pulse width, but also predicts that the LDT is proportional to the temperature at which damage occurs and varies as the square root of the product of the specific heat and thermal conductivity of the host material. By this reasonable approximation, it is seen that the LDT is independent of the impurity properties [45].

7.3.3. Bulk Damage

As mentioned earlier, the intrinsic bulk-damage thresholds is related to the dielectric breakdown strengths (Eqn.7.1.). Since the surface damage is a more important factor in laser related optics, bulk damages are only of importance in the study of the damage phenomenon. Generally, the bulk damage is preceded by the surface damage in most cases. One process of bulk damage is due

to the reduction of the damage threshold due to multiple reflections. It is seen that microscopic cracks, grooves, and bubbles account for the apparent lowering of the surface breakdown intensity with respect to the bulk damage threshold [2].

The electric field inside the discontinuity (E_{in}) can be represented as,

$$E_{in} = \frac{E_0}{1 + \left(\frac{1 - \epsilon}{\epsilon} \right) L} \quad \dots\dots(7.12)$$

where, L is the appropriate depolarization factor and ϵ the dielectric constant being equal to n^2 , and E_0 is the electric field associated with the laser beam.

The effect of the breakdown field for a sharp scratch is,

$$P = \frac{E^2 \eta}{Z} \approx \frac{E^2 \eta}{Z_0} \quad \dots\dots(7.13)$$

and is highly dependent on the refractive index. Fig.7.1. shows the effective electric fields at the different types of discontinuities that are encountered by the laser. These arguments are applicable to both internal and surface cracks, grooves or pores, and is the main reason why the laser damage threshold for surfaces are less than their bulk values. It is seen that the LDT decreases with increase in the number of pulses for materials in which electron avalanching effect is temperature dependent. This is due to the fact that since damage is a cumulative process, successive pulses increase the temperature and subsequently due to electron avalanche, the threshold is reduced.

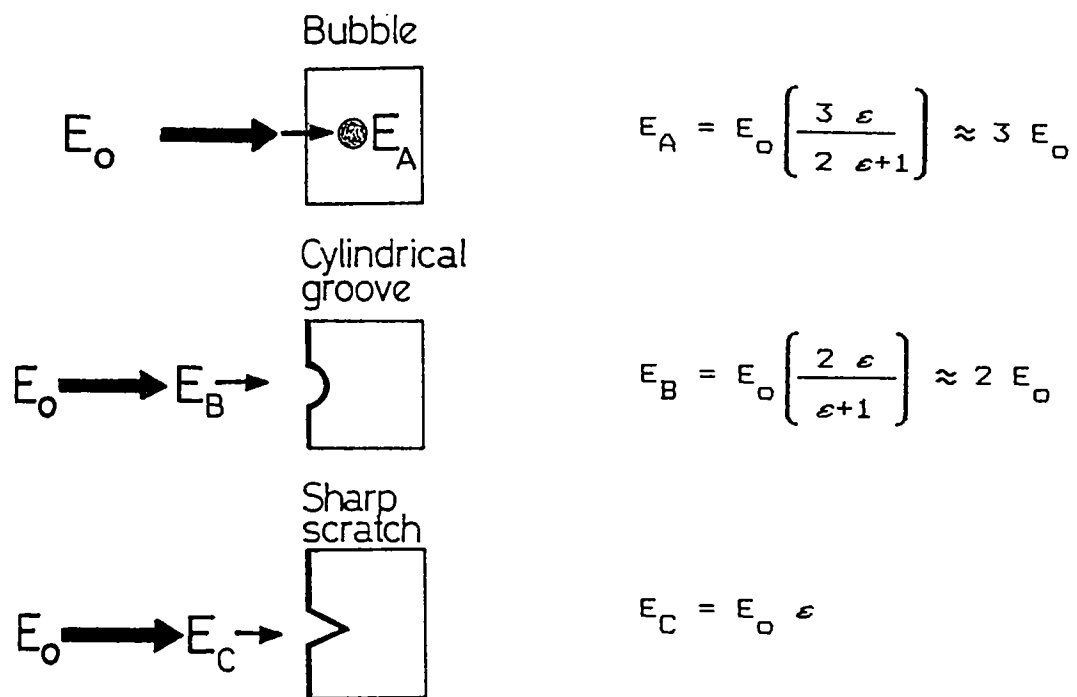


Fig.7.1. The schematic of the different discontinuities encountered by the laser beam and the effective electric fields associated with the discontinuities

7.4. Laser Induced Damage in Metals

The laser damage process in metals is not as complex as in the case of dielectric materials. This process is theoretically quite well understood in the case of metals [47,48]. The damage process is mainly due to absorption of the radiation and subsequent melting or cracking of the surface of the target due to thermally induced strain [49]. A small amount of the incident radiation penetrates the target to a distance called the 'skin depth' where this radiation is absorbed by the free carriers, which, under special circumstances, can lead to the above mentioned damage processes [43]. The LDT in the case of metals is found to depend on the absorptivity, surface and thermal properties of the target [50]. The energy density for laser damage in metals can be estimated to be [51],

$$E_0 = \frac{(T_m - T_0)(k\rho C_m)^{1/2}}{\alpha_0} \quad \dots\dots(7.14)$$

Where, T_m is the melting temperature, T_0 the ambient temperature, k is the coefficient of thermal conductivity, ρ the density, C_m the specific heat and α_0 the absorptivity at T_0 for the laser wavelength.

7.5. Laser Induced Damage in Polymeric Materials

With the advent of the use of the so-called "organic glasses" ie, transparent polymeric materials for laser optics, laser damage threshold measurements in various bulk and thin films of polymeric materials such as those in the methacrylate series like polymethylmethacrylate (PMMA) and their co-polymers as well as polymers containing additives in the form of various plastics like

dimethylphthalate have gained great importance. Many of these materials are now being used as laser optical elements and thus the need exists to study the laser induced damage process in these polymeric materials [52]. Thin, protective coatings of Polytetrafluoroethylene (PTFE), commonly known as TEFLO^N are often used in many applications such as protective coatings in passive components of the excimer laser cavity where highly corrosive halogen environment exists [53]. For the production of thin films of this polymer by laser ablation technique, the damage and ablation measurements in the bulk samples need to be carried out. Again, as mentioned earlier, though many mechanisms have been proposed, none has provided a universal and completely satisfactory explanation of the actual damage processes in polymers. Moreover, the method of increasing the optical strength of polymers is still a developing field. A few relevant cases are presented below.

The effect of high power lasers on transparent polymeric materials is different from that of transparent dielectrics. The former has a lower LDT as compared to the dielectric crystals, a strong dependence of the optical strength on the micro-elastic properties and temperature, a wide range of radiation intensities below damage threshold in which cumulative effects are observed, the occurrence of micro damage of dimensions $\geq 10\mu\text{m}$, not accompanied by bright spark, and the absence of formation of highly absorbing products like soot during damage process [54-58]. Another characteristic feature of the polymer materials that distinguishes them from other transparent dielectric materials (glasses and crystals) is the higher optical strength of the surfaces of polymers as compared to their bulk [57,59]. It was seen that this relationship between the two damage thresholds holds good irrespective of the method of surface treatment. This is important from a practical point of view because it is usually

the surface strength that is the limiting factor in its use as laser optical elements.

The damage in polymeric materials has been attributed to various mechanisms depending on the kind of results obtained. Multiphoton photodestruction of the polymer chains is one of the major causes leading to damage in these materials [60]. Another possibility for damage to occur in polymers is due to the mechanisms involving the formation of highly absorbing products and inclusions resulting from chemical changes at high temperatures produced following irradiation by laser beam [57,61,62].

Anomalous micro-elastic properties of polymers can lead to damage in these materials even when the heating of absorbing inclusions is negligible [56]. A mechanism of non-linear absorption of the incident laser radiation associated with triboproceses in the matrix surrounding the inclusion accompanied by the formation of micro cracks in the matrix has been proposed by Danileiko *et al* [63]. This mechanism could explain the formation of visible damage of dimensions $> 1\mu\text{m}$ initiated by small inclusions ($\leq 0.1\mu\text{m}$). This essentially involves surface electronic states being formed during the micro crack formation process, and these are capable of absorbing the incident light energy to cause damage. The existence of such states have been shown by the sub-threshold luminiscences in the VIS-near-UV regions due to radiative de-excitations [64]. In this analysis, the damage mechanism for a spherically symmetric absorbing defect comprising of a small region of dimension (smaller than the wavelength) and having an absorption coefficient appreciably larger than the surroundings, under irradiation for a short pulse is considered. This induced thermo-elastic stresses increase with time in the matrix. At the damage threshold, these stresses reach micro-breaking magnitudes leading to micro cracks. A

further increase in the laser energy causes the increased density of these micro cracks and thus the concentration of electronic states capable of further absorption of the laser energy increases. Assuming the thermo-elastic stress near an inclusion to be proportional to its temperature, the process of non-linear heating in the matrix can be described in terms of a heat conductive equation which describes the absorption of laser energy by the inclusion and possibly by the electronic states formed at the damage sites, the solution of which gives the expression for the temperature at the centre of the defect. The LDT can be estimated from the conditions of loss of stability of the steady state solution of the equation for the temperature with respect to time. This mechanism accounts for damage mechanisms like micro-cracks and micro-damages [65].

7.6. Photoacoustic Detection of Laser Induced Damage

The interaction of high power lasers with matter can be studied by methods that can be grouped into two categories viz, by the properties of the etch products detected in the gas phase above the ablated surface at some time after the ablation process [66-70] and by monitoring the PA response of the sample being ablated [71-77]. Laser induced fluorescence, mass spectroscopy, and optical spectroscopy can be used to characterize the ablated species from the sample. In these methods, it is often not possible to separate these results which relate to the nascent species generated in the ablation process from those which relate to the subsequent collisional expansion. This expansion is supersonic in nature and leads to a re-distribution of the internal energy into translational energy directed normal to the target thereby yielding little direct information about the ablation process itself, or secondary ionization, plasma formation etc. further complicating the interpretation of the results. In

contrast, the PA technique is relatively insensitive to this expansion of gaseous products and can yield direct information relating to the damage and ablation process [78].

High power lasers are becoming increasingly important for controlled removal and etching of organic surfaces in both industrial and medical sectors. In order to obtain the required amount of etching of the sample surface, the laser energy has to be controlled quite accurately, depending on the laser damage threshold of the sample. Removal of polymeric materials under intense laser irradiation can be termed as 'ablative photodecomposition' [72]. Some transparent polymeric materials are also widely used in the fabrication of high power laser optical components like prisms, lenses and beam-splitters and also in nonlinear optics while opaque polymers find applications in areas like photolithography. It would therefore be of considerable significance to investigate the optical strength of polymeric materials. The determination of the optical damage threshold of polymers is thus important for determining the laser energy density required for controlled etching of the material surfaces. Most of the data on laser damage are obtained through microscopic and other methods of visual inspection of the laser damaged surface, which is a tedious and not an *in-situ* process. Techniques based on phenomena like photothermal deflection and photoacoustic effects have also been proven recently to be very effective in evaluating laser ablation thresholds of both transparent and opaque samples [67,73-77,79-81].

It is well known that the interaction of laser beam with matter produces acoustic pulses in the target material. The absorption of the incident pulsed radiation gives rise to transient thermal variations due to the heat released through non-radiative channels of de-excitations in the sample [82,83]. Since the acoustic signal is linearly-proportional to the energy

absorbed [82] so long as transducer saturation does not set in, the detection of the LDT involves only the monitoring of the acoustic signal pulse resulting from the irradiation of the target by the laser pulse. At lower laser intensities, acoustic waves are generated essentially by thermo-elastic stress. The analysis of the acoustic pulses produced at comparatively lower laser energies can be used for non-destructive testing (NDT) and evaluation of materials [84] At higher laser energies, where damage of the surface occurs, resulting in plasma formation, the ablation of the material from the surface causes a reactive force which acts as an intense source of acoustic waves [84]. During dielectric breakdown resulting from the optical energy absorbed in the illuminated volume results in local heating, thus producing a thermal expansion. The boundary conditions for a free space stipulate that this expansion be followed by a tension pulse. This shock wave, having a bipolar waveform [78], propagates with a velocity appropriate for a longitudinal wave in a direction opposite to that of the laser [85,86]. The velocity v of this shock wave is [87],

$$v = \sqrt{\frac{E_{\text{eff}}}{\rho}} \quad \dots\dots(7.15)$$

where, E_{eff} is the effective elastic constant for the longitudinal excitation and ρ the material density. The acoustic pulse duration τ_a is determined by the laser pulse width τ_L and the acoustic transient time τ_t of the acoustic signal in the sample, so that [88],

$$\tau_a = \sqrt{\tau_L^2 + \tau_t^2} \quad \dots\dots(7.16)$$

For an opaque solid, $\tau_t \approx l/c_0$, where, l is the optical absorption

length and c_0 the velocity of sound. In the case of the teflon samples used (7.5mm thick) in the results presented here, the value of τ_t and τ_a were determined to be $\sim 940\text{m/sec}$ and $7.9\mu\text{sec}$ respectively. The time (t) required for this acoustic response to develop is of the order of 10^{-10} sec [19] after which it begins to propagate through the medium to the transducer. For free lasing and Q-switched pulses, where τ_L is greater than t , the damage threshold power density is independent of the pulse length. For a single mode-locked pulse the power density for damage increases with decreasing pulse length. A mode-locked pulse train, however does give enough response time and damage therefore occurs at similar power density as for longer pulses.

This shock wave can either be detected by an acoustic transducer placed in contact or in the vicinity of the sample or by other techniques like the photothermal deflection (PTD) technique which involves the detection of the deflection of a probe beam grazing the sample surface due to the refractive index gradient developed in the air above the irradiation spot on the sample. These two techniques not only have the advantage of sensitivity over conventional damage detection techniques, but can also be used *in-situ* for LDT measurements. Among the two, the PA measurements involving the transducer placed in firm contact with the sample is more sensitive than the PTD technique since the latter requires that the layer of air above the irradiation site be sufficiently heated so as to cause detectable deflection in the probe beam. In the former case, since the transducer is in firm contact with the sample, there is good acoustic impedance matching between the sample and the transducer and thus it is sensitive to even sub-threshold levels of laser energy [82]. PA technique also has the added advantage that it can effectively distinguish between bulk and surface sources of heating and thus the respective thresholds. Moreover, the PA transducer output

produced being highly dependent on the amount of energy absorbed, can respond to the anomalous absorption induced by inclusions and impurities in the sample. IR lasers give rise to multiphoton excitation over the vibrational manifolds of the ground electronic states of the polymeric sample which is then followed by thermal decomposition resulting in the ablation or damage of the target surface. Such multiphoton absorptions and subsequent damage studies using PA technique have been studied by Van Stryland *et al* [85]. It has the added advantage that in the use of PA technique, the amount of energy absorbed is directly measured rather than monitoring the reflected or transmitted energy [85]. For ablation to take place, there exists a threshold laser energy density beyond which irreversible damage of the sample surface occurs. Many of the material parameters influencing the thermal balance of the system are also significantly altered during the ablation process.

The amplitude of the PA signal generated by the heat transfer from the target to air can be estimated as follows [89]. The heating of the air is small due to the comparatively small thermal conductivity of air. The heat flux from the target into the surrounding air can be represented as, $H(T_m - T_o)$, where T_o is the ambient temperature and T_m the target material temperature, and H is the heat transfer coefficient. For a sample of surface reflection coefficient R_s , the increase in the temperature of the air surface layer of thickness l next to the target as a result of this heating will be,

$$T_m = \frac{H (1-R_s) I_o (\tau_L)^{1/2}}{C_v l \left(k_m C_m \rho_m \right)^{1/2}} \quad \dots \dots (7.17)$$

Here, I_o is the laser intensity, τ_L , k_m , C_m and ρ_m are as defined

in section 7.3.2. C_v is the specific heat at constant volume of the air. Consequently, its boundary is shifted by an amount $\Delta l = \beta_t l T_a$, where, β_t is the thermal coefficient of expansion of air. The pressure amplitude P in the far wave field ($r \gg a^2/c\tau_L$ a is the beam radius on the target) will be,

$$P = \rho \frac{(1-R_s) \beta_t H W}{r \left[k_m C_m \rho_m \right]^{1/2}} \quad \dots \dots (7.18)$$

W is the power of the laser irradiation and ρ the density of air. In the near field,

$$P = \frac{(1-R_s) I_0 (\tau_L)^{1/2} H \beta_t}{\left[k_m C_m \rho_m \right]^{1/2}} \quad \dots \dots (7.19)$$

The far field detection of the signal using PA or PT techniques is less sensitive and sub-threshold signals cannot be effectively detected. This pressure response cannot be compared to the experimental values due to the bandwidth limitations of the acoustic transducer and the possible dependence of H on the pulse duration of the laser. For high power IR sources, the problem that could arise is that the target surface gets heated up due to the high peak power of the laser and other sound generation mechanisms like evaporation or desorption of surface impurity layers, microscopic breakdown events or explosion of microscopic inclusions on the surface become important [90,91]. In the measurements made here, the acoustic transducer is placed in tight contact with the sample and thus the terms H and β_t do not play an important role in the signal generation. At the same time, for plasma monitoring measurements, the transducer is placed away from the sample and only then does these parameters influence the PA

signal.

The acoustic signals generated in solids due to interaction with pulsed laser beam is used to determine the ablation threshold of bulk polymer samples of teflon and nylon under the irradiation from a Q-switched Nd:YAG laser at $1.06\mu\text{m}$ wavelength. A suitably designed piezoelectric transducer is employed for the detection of photoacoustic (PA) signals generated in this process. It has been observed that an abrupt increase in the amplitude of the PA signal occurs at the ablation threshold. Also it has been shown that there exist distinct values for the threshold corresponding to different mechanisms operative in producing damages due to surface morphology, bond breaking and melting processes at different laser energy densities.

7.6.1. Experimental Technique

The schematic diagram of the experimental setup for evaluation of the damage threshold of bulk polymer samples using PA technique is given in fig.7.2. The sample, in the shape of a disk of diameter 2.5cms and thickness $\sim 7\text{mm}$ (sample surface is polished with 400 grade silicon carbide powder) is pressure contacted on to the piezoelectric transducer using silicon grease [82]. Since the PZT transducer is mounted inside a steel enclosure (fig.7.3), the 1mm thick steel between sample and the transducer helps in minimizing the acoustic reflection at the interface and gives a delay time limited by the transit time of the longitudinal waves in the transducer casing [84]. Also, care is taken to ensure that the laser beam itself does not fall on the transducer casing. The $1.06\mu\text{m}$ laser radiation (pulse width $\sim 10\text{ nsec}$, single shot) from a Q-switched Nd:YAG laser (Quanta Ray, DCR-11) is focused to a diameter of $\sim 1\text{mm}$ using a convex lens on to the surface of the sample kept inside a stainless steel irradiation chamber

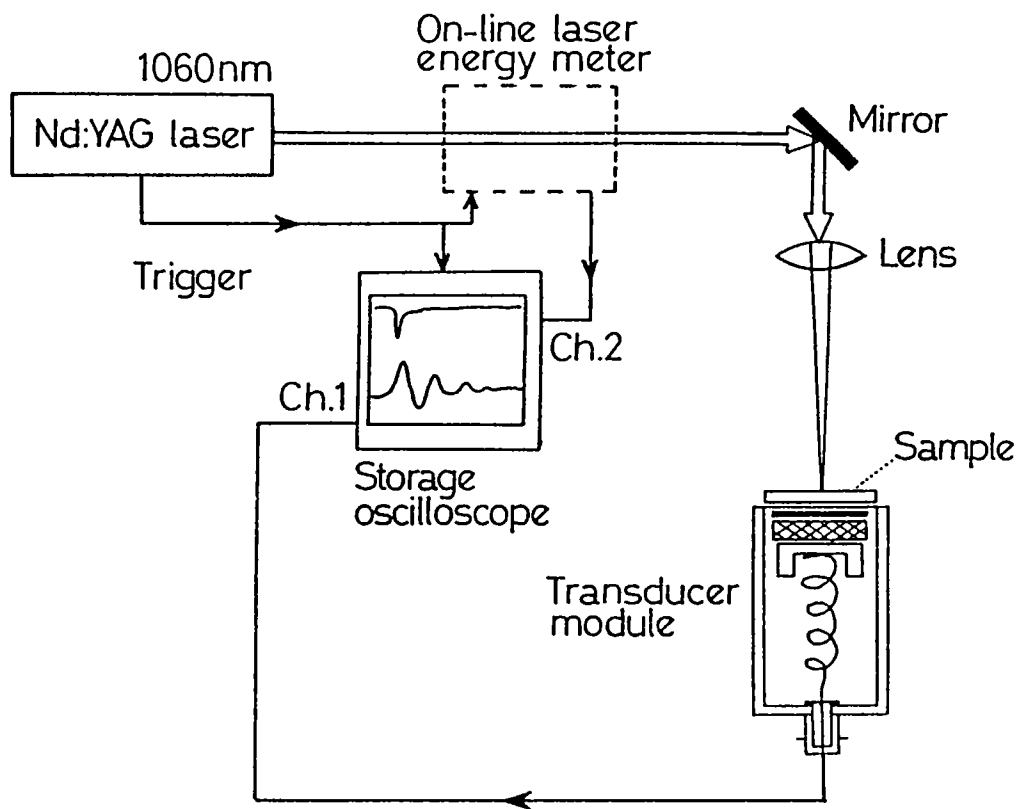


Fig.7.2. Schematic diagram of the experimental setup for PA-LDT measurements

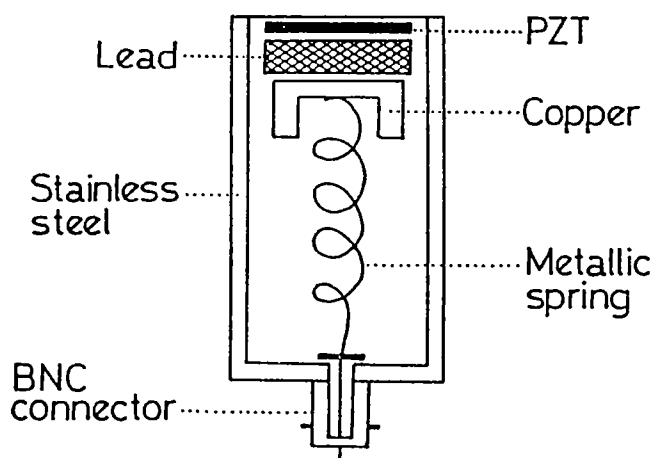


Fig.7.3. The schematic diagram of the transducer module used for PA-LDT measurements

provided with quartz windows. The laser spot size was estimated by microscopic measurement of the burn-pattern of the focused laser and the values correlated by the calculation,

$$\frac{a}{b} = \frac{f}{D - f} \quad \dots \dots \dots (7.20)$$

where, a is the unfocused beam diameter, f the focal length of the lens and b the focused diameter of the beam at a distance D , ($\geq f$) from the lens.

The laser energy, which was changed from pulse-to-pulse was monitored for each laser pulse using an on-line, pulsed laser energy meter, triggered in synchronization with the laser pulse. Each data point was taken with the laser pulse falling on a fresh surface of the sample by rotating the same about its axis while the distance between the illuminated spot and the centre of the transducer is kept constant.

7.6.2. Results and Discussion

The resultant PA signal from the PZT transducer is observed on a 200 MHz digital storage oscilloscope (DSO) using 50 ohm termination. Fig.7.4. shows the typical traces of the oscilloscope outputs of the PA pulse shapes from the PZT acoustic transducer for laser energies below, at and above the laser damage threshold for teflon sample. The PA pulse obtained has a delay with respect to the laser pulse because of the transit time of the acoustic signal through the sample material. The negative peak observed in the pattern is a result of the rarefaction due to cooling of the sample following the compression wave caused by the heating of the same at laser fluence near damage threshold [67,85,86]. The amplitude of these peaks are monitored on the DSO. The variation of the PA signal with the laser energy is studied and the plot of laser energy density versus the PA

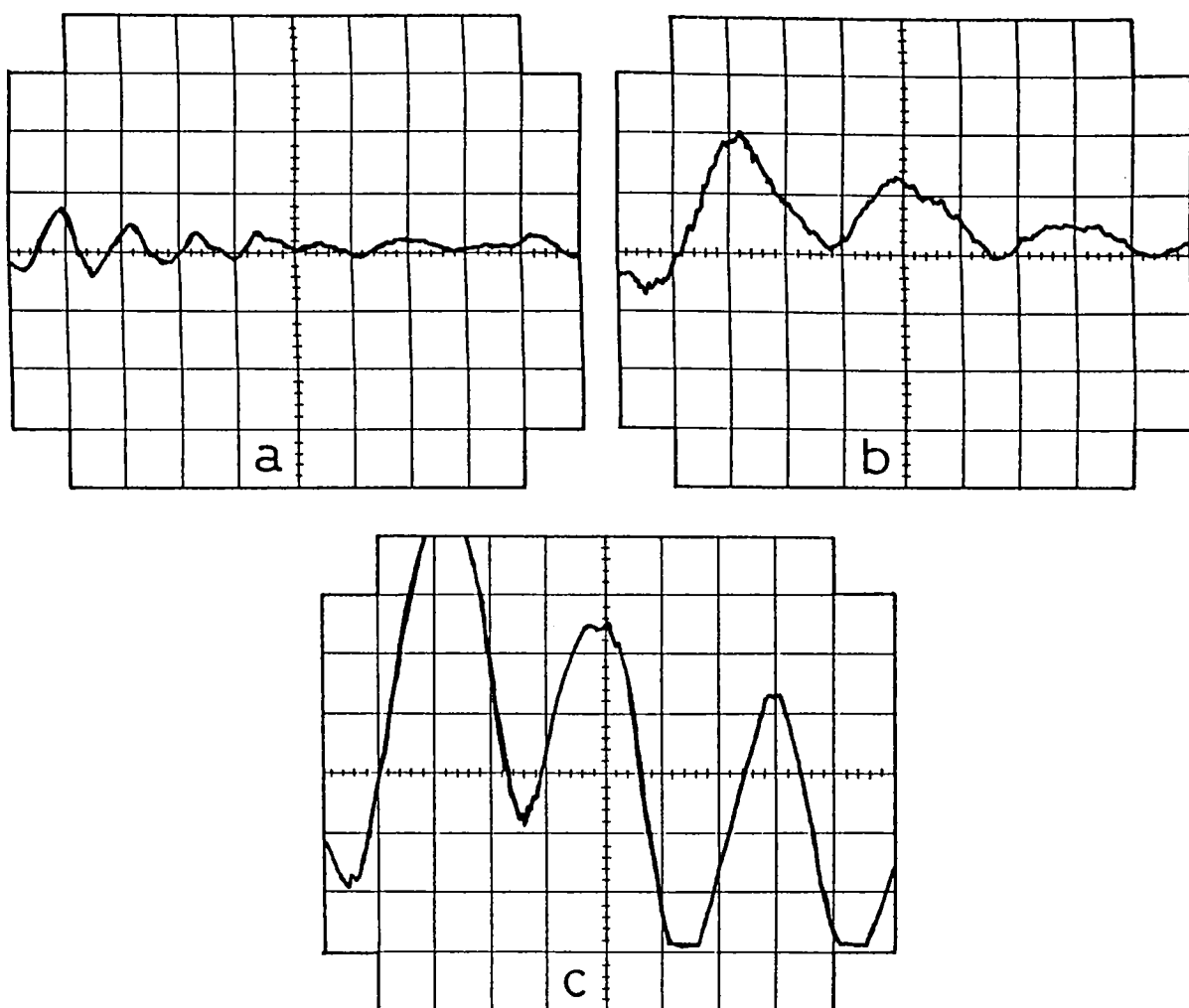


fig.7.4. The typical PA pulse shapes from the acoustic transducer (PZT) at (a) sub-threshold, (b) damage threshold, and (c) plasma formation for TEFLON sample (5 μ sec & 5mV/div)

signal for teflon and nylon bulk samples are given in fig.7.5.(a,b). These show a clear and abrupt increase in the PA signal amplitude in the region of the damage threshold in full agreement with the observations of the previous workers [67,72,73,79,84]. Table 7.1. shows the values of the ablation thresholds evaluated for the two polymer samples teflon and nylon at $1.06\mu\text{m}$ wavelength. At the same wavelength, using multiple beam technique, Milam (1977) [92] determined the damage thresholds for bulk PMMA (acrylic) and polystyrene samples to be of the order of 1.6J/cm^2 and 0.8J/cm^2 respectively which is of the same order of magnitude of damage thresholds for the polymeric materials under the present investigation.

The mechanisms of laser induced damage in polymeric materials have not yet been understood clearly. The damage threshold generally depends on visco-elastic properties of polymers as well as on the molecular structure of the monomers. It has been suggested that [93] laser induced damages in low absorbing dielectric materials like polymers are initiated through bond breaking phenomenon which will act as an acoustic source exhibiting the abrupt enhancement of the PA signal near the threshold. A significant fraction of the light energy above the threshold is utilized in the disruption of chemical bonds and also contributes to the thermal and kinetic energy the ablated fragments [71]. The results for bulk nylon and teflon samples as given in fig.7.5a and 7.5b respectively, show that variation in slope occurs at region (A) (at lower laser energy density), as well as at (B) (higher laser energy density). Abrupt increase in the amplitude of the PA signal occurs at both these points. This shows the existence of two separate thresholds for the laser induced surface damage occurring apparently due to different causes [72,84].

The damage threshold will also depend on possible

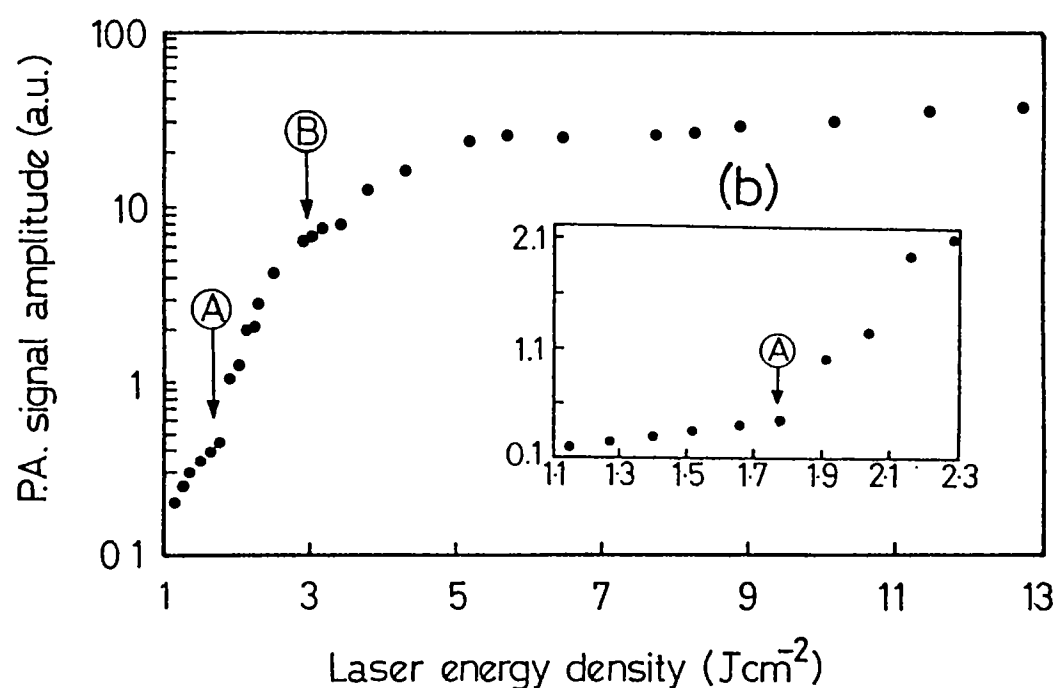
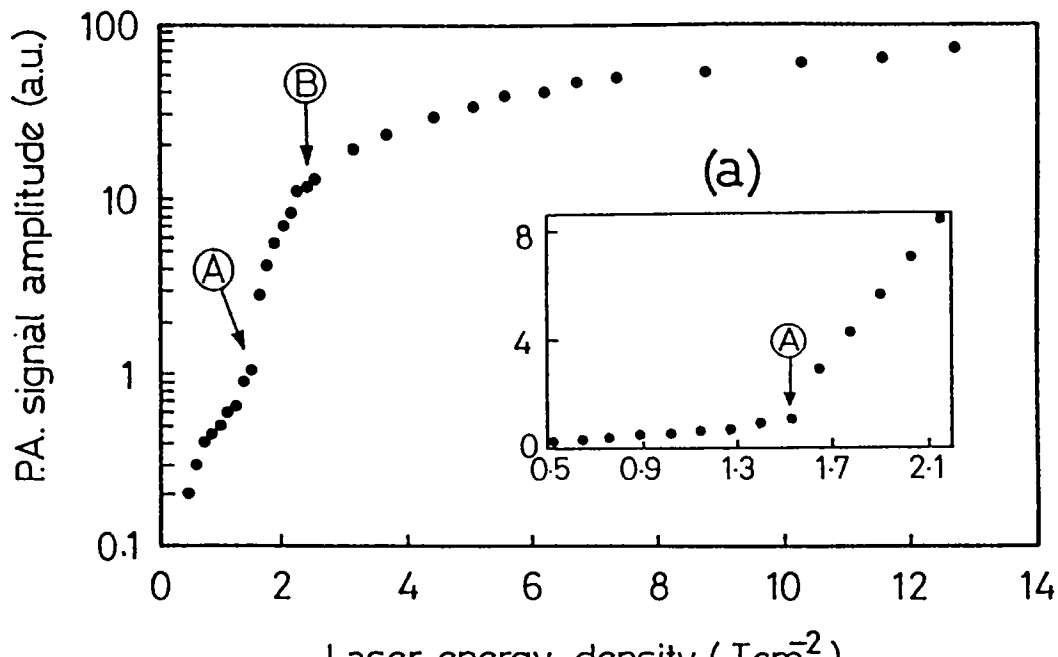


Fig.7.5. The plot of laser energy density vs PA signal amplitude for bulk (a) Nylon and (b) Teflon samples in air.
Inset : The expanded graph showing region (A) in detail.

Table 7.1. The photoacoustically detected surface and bulk laser damage thresholds in Nylon and Teflon samples at $1.06\mu\text{m}$ laser wavelength compared to PTD detected values

SAMPLE	PA TECHNIQUE [#]		PTD TECHNIQUE [@]	
	REGION (A) J/cm ²	REGION (B) J/cm ²	REGION (A) J/cm ²	REGION (B) J/cm ²
TEFLON [#]	1.78	2.85	2.2	3.25
NYLON [#]	1.53	2.25	1.8	2.50
PMMA*	1.60	-----	-----	-----
POLYSTYRENE*	0.80	-----	-----	-----

[#]Ref.[81], [#]Ref.[74], *Ref.[92]

Estimated error ~ 20 %

absorptive inclusions [93] and surface polishing of the sample as mentioned in the earlier parts of this chapter. The laser threshold at (A) is very sensitive to the sample surface conditions unlike the threshold at (B). This observation leads to the conclusion that the threshold at (A) is determined by the surface morphology of the sample. The threshold (A) will characterize damage due to inclusions, impurities and surface inhomogeneity, while that at (B) should correspond to the initiation of bond breaking processes resulting in plasma formation and melting of the sample surface. This observation has been confirmed by recording the PA signal from various points at random on the sample surface at laser energy densities corresponding to the surface (A) and bulk damage (B) thresholds for nylon (ie, near 1.53 and 2.25 J/cm^2 respectively). Fig.7.6 shows that the magnitude of the PA signal corresponding to threshold A varies from point to point whereas that corresponding to threshold B is practically constant. This implies that the threshold A is sensitive to surface conditions while that at B is virtually independent of the nature of the surface. The endothermic phase change occurring at the region of melting can cause a change in the response of the PA signal amplitude (note the change in slope near B). There is a significant absorption of photons by the sample at the damage site or within the plasma produced at the damage, and this added energy being transferred to the sample via electrons. Thus, where laser damage is accompanied by mechanical damage, but with no significant increase in the optical absorption, the PA signal will not increase dramatically [73]. At laser fluences much higher than that at (B), the PA signal tends to saturate due to possible re-absorption of the laser beam by the plasma plume [84]. Visually, there is little or no plasma formation below (A), and as the laser energy crosses the damage threshold, the plasma plume begins to appear and it grows with further increase in laser energy density.

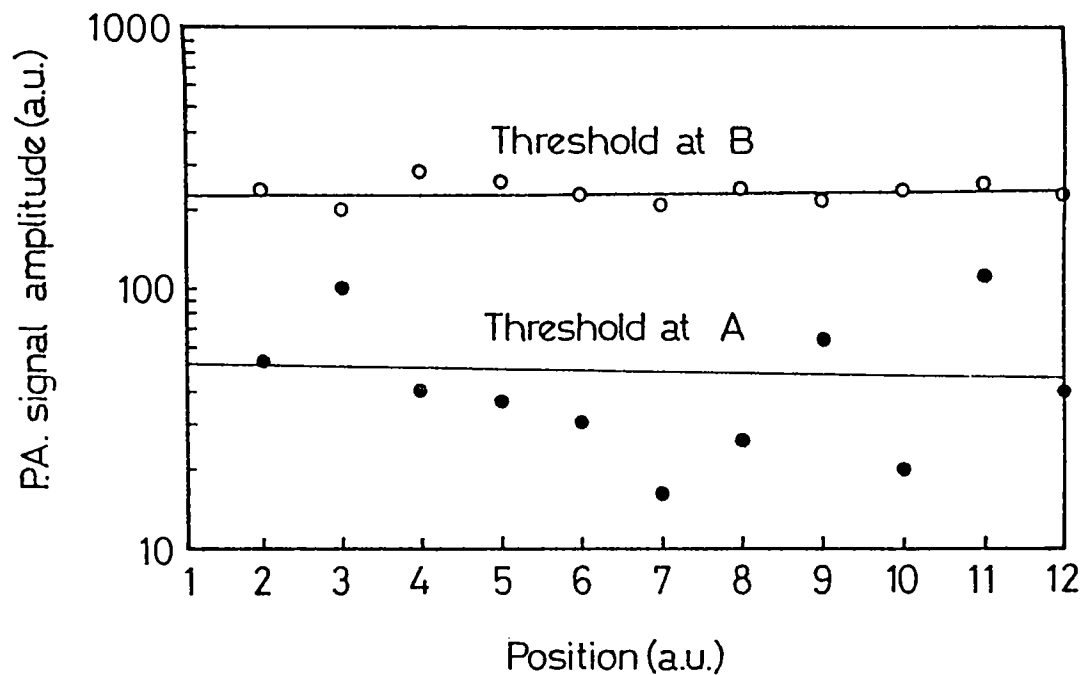


Fig.7.6. The plot of the variation of the PA signal at various points on the sample (nylon) at the two thresholds corresponding to A ($\sim 1.53 \text{ J/cm}^2$) and B ($\sim 2.25 \text{ J/cm}^2$)

Fig.7.10. shows the plasma plume from a bulk sample of teflon at laser energy density $\sim 3\text{J/cm}^2$. Both in the case of nylon and teflon, the profile of the variation of the PA signal with laser energy density is identical. The relatively larger uncertainty in the slopes above region (A) could be due to the presence of spatial hot spots in the beam profile which gives rise to scatter in the data points above (A). This is a consequence of the strongly non-linear behavior of the PA signal above threshold (A) [73]. The lack of efficient beam diagnostic equipment for accurate monitoring of the laser beam shape and pulse width for each pulse, and methods to accurately determine the surface characteristics (like surface finish etc.) of the sample all add to increasing the error margin in these experimental data.

The PA detection of laser damage has also been used to study the LID of a few different samples like stainless steel (fig.7.7), TiO_2 thin film on quartz substrate (fig.7.8.), SiO_2 thin film, aluminium and commercially available transparent acrylic. The obtained values measured using the present technique are listed in Table 7.2. The fig.7.8. shows clearly two abrupt variations in the PA signal, the first one due to the film damage and the second one, possibly due to the quartz substrate damage. The value of the damage threshold for quartz ($\sim 9/\text{cm}^2$) corresponds to previously reported bulk damage value ($\sim 10-15\text{J/cm}^2$) for the same [49].

Figure.7.9. shows the damaged site on the surface of bulk nylon clearly showing the pitting that has occurred due to ablation of the surface. From the micrographs of the damaged surfaces in transparent samples, some of the different damage patterns that occur on laser irradiation are evident. Fig.7.11. shows the damage sites on the surface of a transparent acrylic. Two forms of damage, ie, ripple formation and microcrack formation are clearly seen in the above micrographs These tend to occur away

Table 7.2. The photoacoustically estimated laser damage threshold for a few bulk and thin film samples at $1.06\mu\text{m}$ laser wavelength

SAMPLE	SAMPLE THICKNESS	SURFACE DAMAGE THRESHOLD (J/cm ²)
Stainless steel	~ 1mm	0.27
TiO ₂ thin film	~ 4000 Å	0.58
SiO ₂ thin film	~ 4000 Å	4.8
Aluminium	~ 3mm	0.32
Quartz flat	~ 3mm	9.03
Transparent* Acrylic	~ 3mm	3.25

*All other samples are polished with 400 grade silicon carbide abrasive. Estimated error ~ 20 %

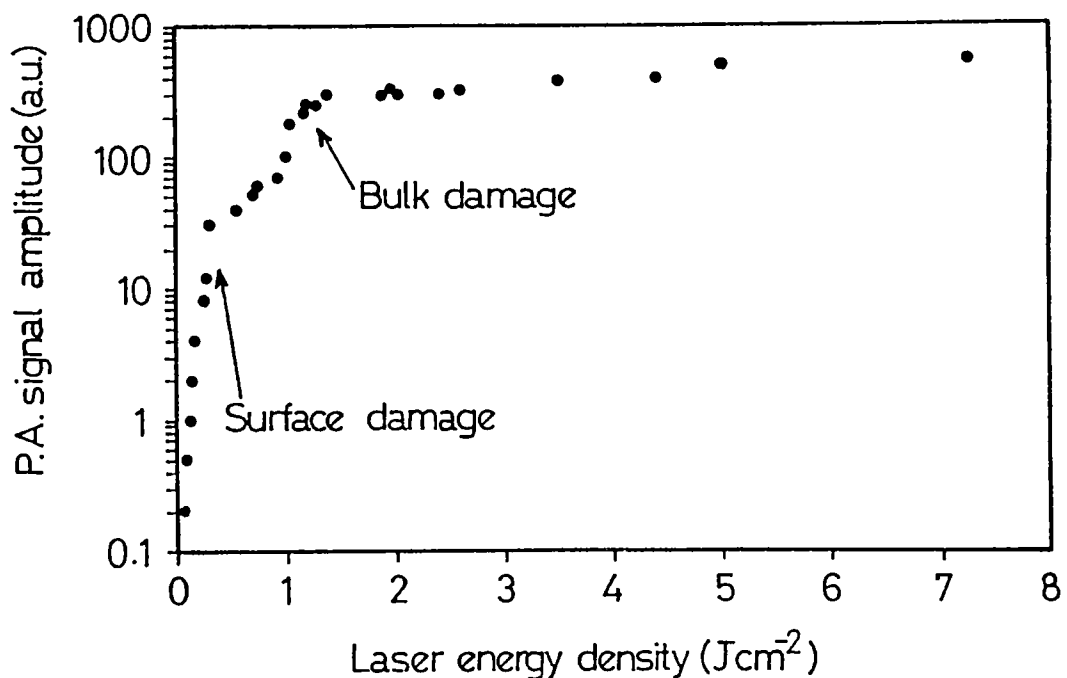


Fig.7.7. The Plot of the PA signal vs the laser energy density for a 1mm thick stainless steel target

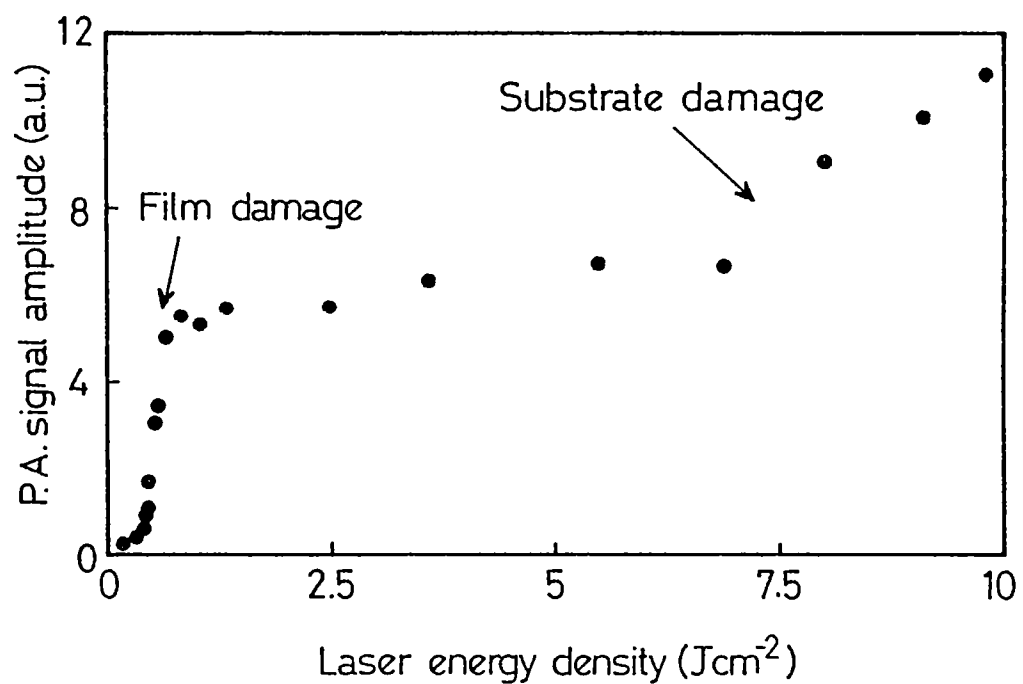


Fig.7.8. The Plot of the PA signal vs the laser energy density for a 400nm A thick TiO_2 thin film sample on quartz substrate

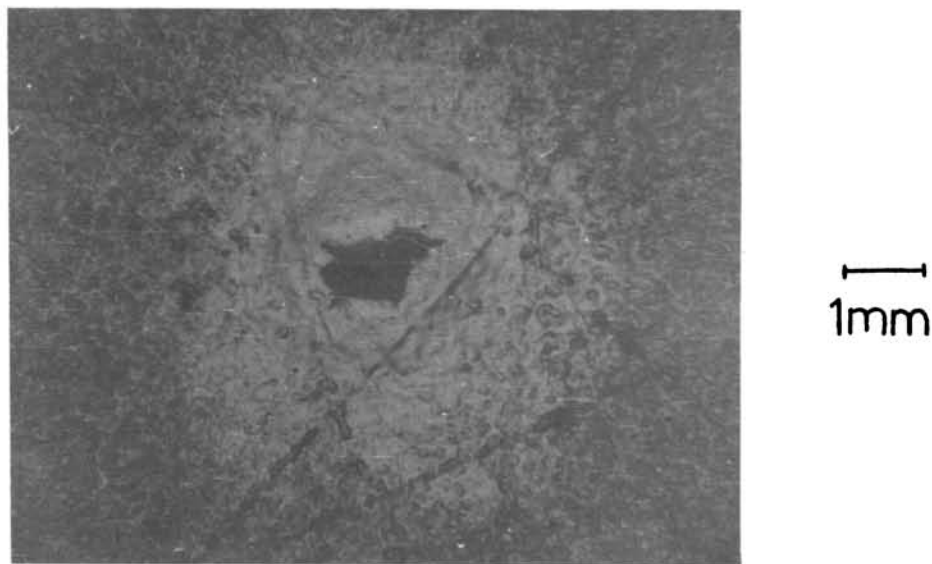


Fig.7.9. The photograph of the damaged surface of nylon at a laser energy density of $\sim 3\text{J/cm}^2$ (Photographed in the reflection mode of the microscope)

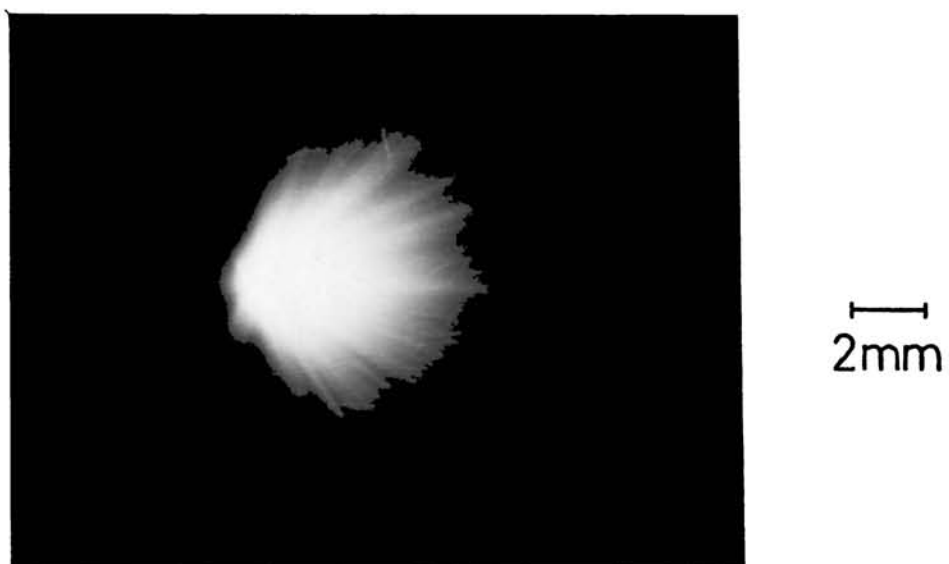
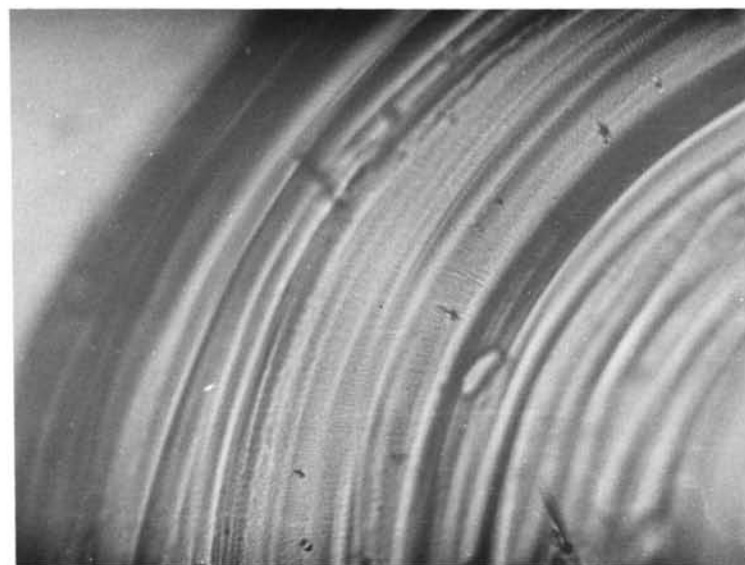
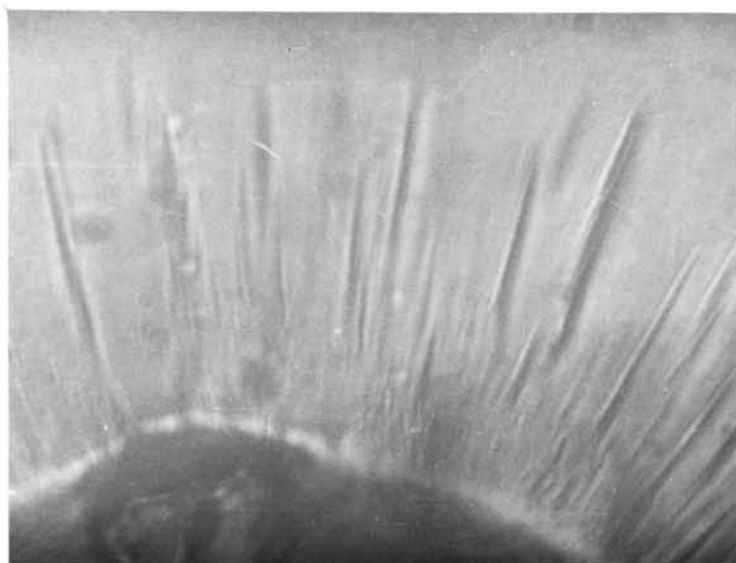


Fig.7.10. The photograph of the plasma plume from bulk teflon sample in air at a laser energy density of $\sim 3\text{J/cm}^2$ in air.



(a)



(b)

Fig.7.11. The transmission micrographs of the damage site in transparent acrylic showing (a) the ripple formation (66x), and (b) Microcracks (132x)

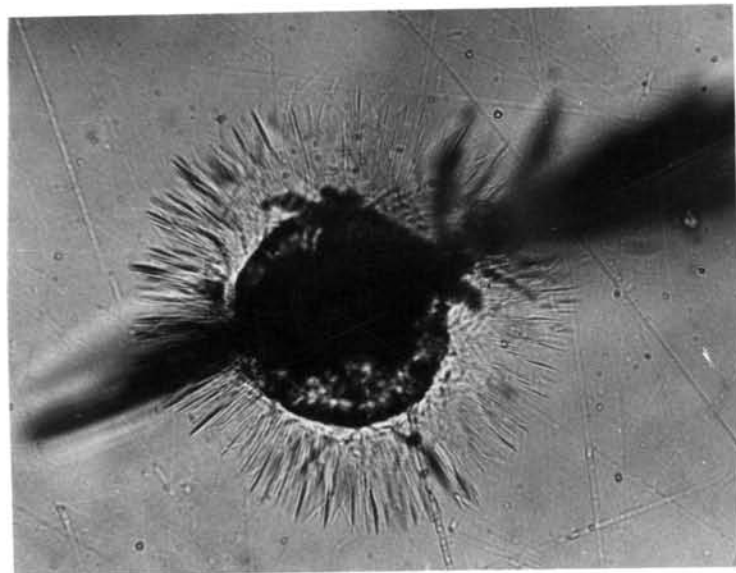
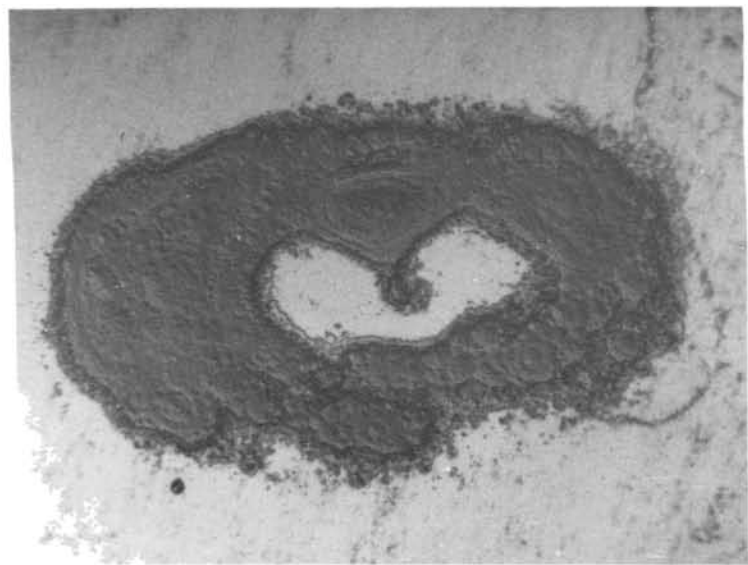
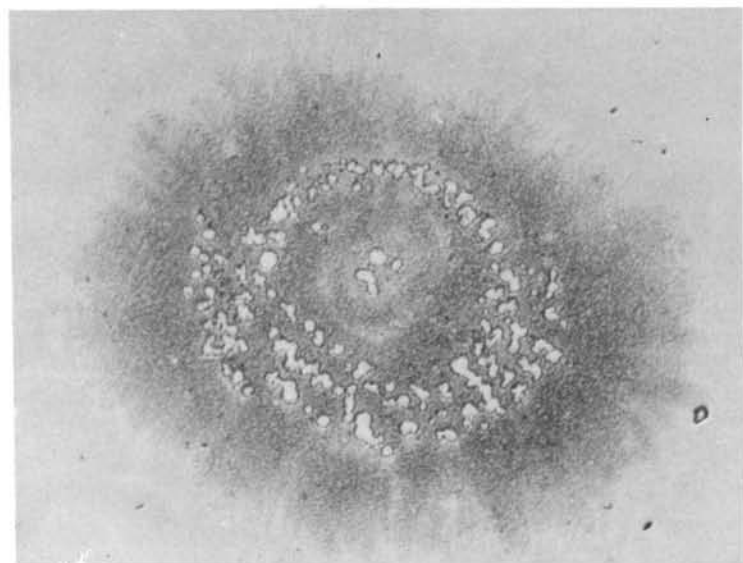


Fig.7.12. The transmission micrograph of the damage on transparent acrylic sample initiated by a sharp scratch on the surface (66x). The dark line across the micrograph is the scratch on the surface. (The microcracks are also visible here)



(a)



(b)

Fig.7.13. The transmission micrographs of the damage sites in (a) TiO_2 (66x) and (b) SiO_2 (66x) thin film samples

from the irradiation site and is possibly due to the propagation of the intense shock waves that originate from the irradiation site. The damage at a scratch on the surface of the transparent acrylic material is seen in fig.7.12. Similar observations were made by Wood *et al* on scratch-initiated damage on germanium surface using $10.6\mu\text{m}$ laser beam radiation [94]. The melt pattern on the surface of the TiO_2 and SiO_2 thin film in the vicinity of the laser damage threshold are shown in fig 7.13. The melt profiles are made prominent using Normaski prism facility in the metallurgical microscope (Versamet-2) used to obtain the micrographs.

7.7. Photoacoustic Monitoring of Laser Ablation Process

One of the widely used applications of laser induced plasma is the synthesis of thin films. Laser ablation provides an ideal method to vaporize materials like ceramics, high temperature superconductors [95], metals [96] for deposition on suitable substrates and for selective photoablation of polymers [67], and applications to microelectronics and medicine. This technique offers a better control of the parameters that determine the nature of ablation unlike conventional vaporization techniques. The PA technique can be applied for *in-situ* monitoring of the laser ablation process and its related parameters such as the laser energy and emission intensity in laser plasma experiments like those mentioned above [97,98]. To correct the pulse-to-pulse variations in the laser generated plumes, one has to know the total amount of the material vapourized during each pulse. It was shown by Chen and Yeung, that the magnitude of the PA pulse associated with the plasma generation was linearly associated to the emission intensity of the plasma constituent elements and it was also shown that the acoustic signal could track the emission signal over four orders of magnitude [99]. In

laser ablation experiments, sub-threshold signals are not relevant since the incident energy density is much above the damage threshold. The experimental setup for the detection of emission intensity and the acoustic pulse is shown in fig.7.14. A miniature electret microphone (Knowles BT 1759) placed in the vicinity of the target monitors the PA signal pulse and a monochromator-PMT combination (0.2m McPherson monochromator with Hamamatsu R928 PMT) detects the emission intensity of a particular species (C_2 molecules, 561.2nm extended region of the plasma) in the plasma plume [69]. The typical CRO traces of the output signal from the microphone and the PMT output for the plasma emission are given in fig.7.15. for a laser energy density of $\sim 1.8 \text{ J/cm}^2$ for teflon sample. By calibrating the PA signal amplitude and the emission intensity against the laser energy density, (fig.7.16.) an *in-situ* monitoring of the latter is possible. From Fig.6. it can be seen that the PA signal and the emission intensity vary linearly with the laser energy densities up to $\sim 5 \text{ J/cm}^2$ after which saturation of the microphone signal occurs. The PA signal increases when the pressure in the chamber is increased, but at the same time, the plasma plume intensity decreases.

One disadvantage of this method of laser energy monitoring is that the microphone needs to be placed either in contact or in the vicinity of the target sample. Moreover, the PA signal intensity decreases as the pressure in the plasma chamber is decreased. The limited frequency response of the microphone is another limiting factor. An alternative is to use the PTD method of detection [79-81] which reduces these drawbacks, but then, the alignment of the probe beam is critical and the signal is sensitive to the air temperature in the region between the sample and the probe beam, and this temperature is strongly affected by the ablation process. It was seen that by using a focused PZT

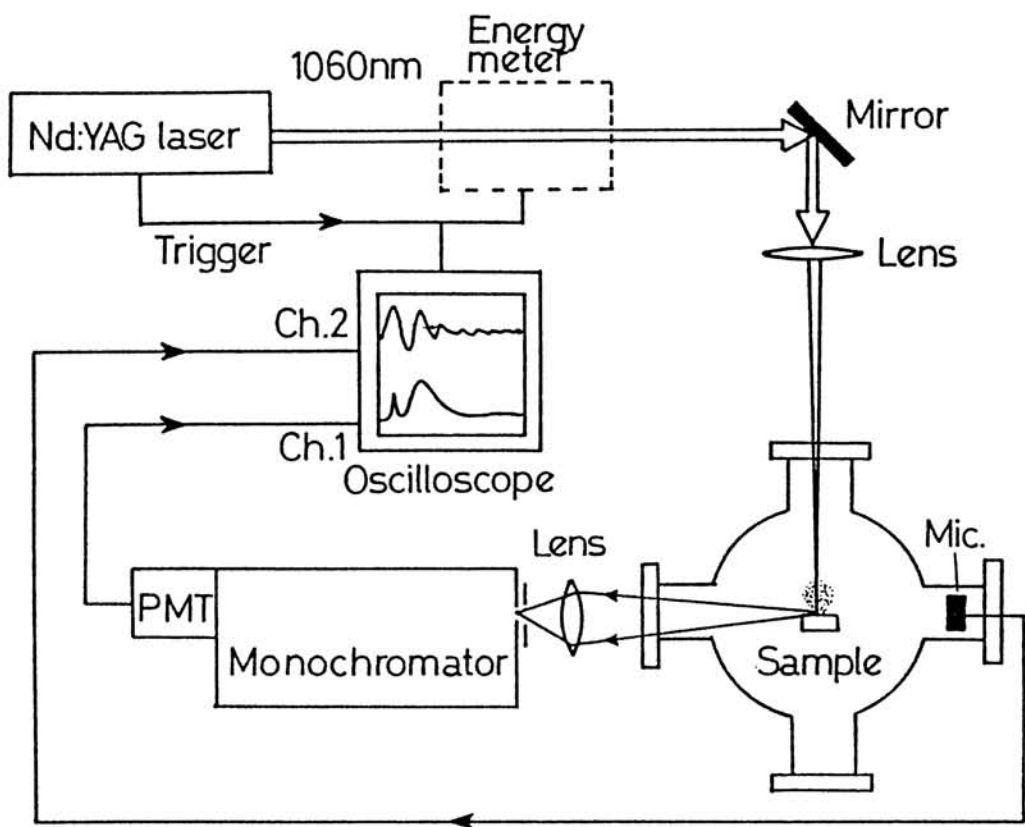


fig.7.14. The experimental setup for monitoring the PA signal and the emission intensity of the plasma plume during ablation process

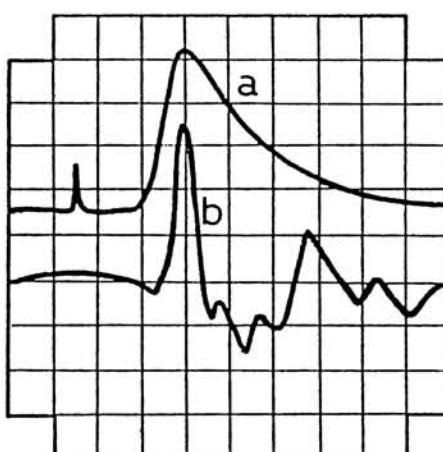


fig.7.15. CRO traces of the (a) PA signal (50mV & 2 μ sec/div.) (b) PMT response (10mV & 1 μ sec/div.) of the emission from C_2 species ($\lambda = 561.2\text{nm}$) in the extended region of the laser induced plasma from TEFILON. Laser energy density $\sim 1.8\text{J/cm}^2$

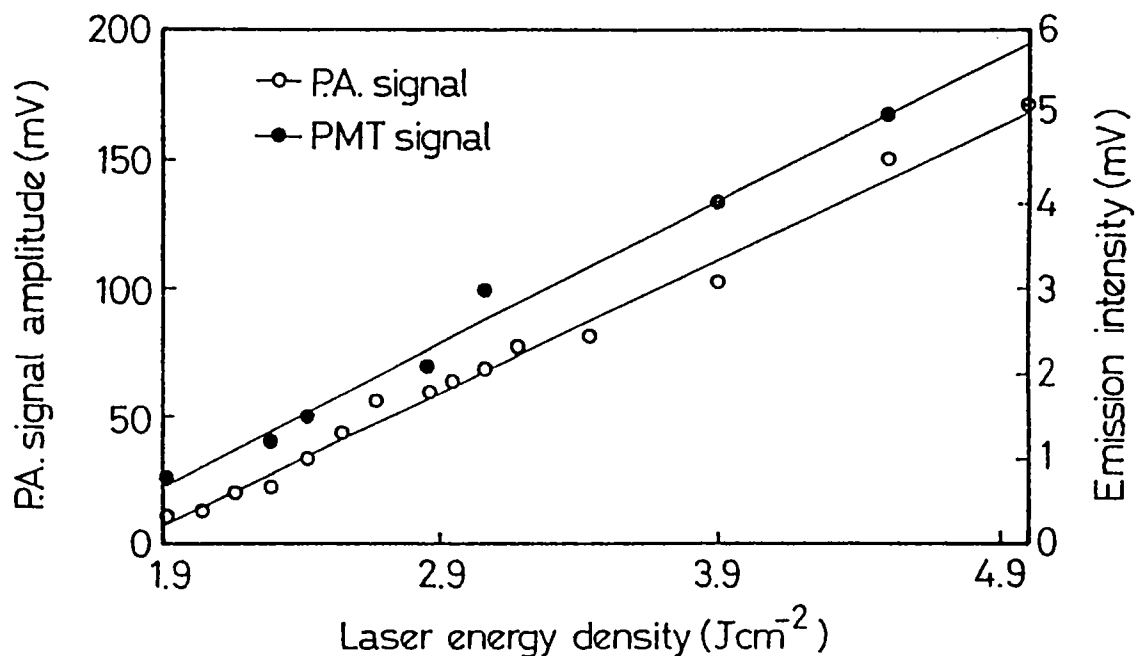


fig.7.16. Plot of the PA signal pulse and the emission intensity for the C_2 species in the extended region of the laser plasma plume of TEFLON

detector having a curved surface and located away from the sample, the above drawback of PA detection could be minimized [100]. The center of curvature of the concave transducer is made to coincide with the ablation spot on the target. The acoustic pulses are detected over a large solid angle of observation and with a high frequency bandwidth. Unlike the PTD technique, the PA non-contact technique is relatively insensitive to the variations in the ambient conditions like temperature or air currents. Since the attenuation of the acoustic sound depends little on the temperature, the PA signal was found to be very stable over a larger temperature range than the PTD technique. Gentle cross air flow across the sample does not affect the signal, though a strong cross air flow shifts the direction of propagation of the sound and the transducer needs to be repositioned. This is an added advantage since in many plasma related experiments (especially in laser plasma deposition of thin films), a particular gas is required to flow across the target, in the region of the plasma. Though this technique only monitored the emission of the plasma and the PA signal with laser energy, this can be efficiently applied to other spectroscopic techniques like atomic absorption [101], fluorescence [102], and to cases where the ablated material is swept to another site [103] or re-deposited onto a collector for further excitation [104].

7.8. Conclusions

The various aspects of laser induced damage process have been discussed in detail. the PA effect has been applied to the estimation of the laser damage threshold in various materials. There exists abrupt changes in the PA signal in the region of laser damage threshold energy density for both surface and bulk damages. Different kinds of damage processes were also observed using microscopic techniques. The PA effect was also utilized to

monitor successfully the laser induced plasma process.

7.9. References

- [1] R M Wood, *GEC.J.Sci.& Tech.*, **45**, 109, (1978)
- [2] Bloembergen N, *Appl.Opt.*, **12**, 661, (1973)
- [3] Milam D, SPIE proceedings, Vol.140, "Optical Coatings - Applications & Utilization - II" p.52, (1978)
- [4] Newnam B E and Gill D H, "Laser Induced Damage in Optical Materials" NBS special publication # 462, p292, (1976)
- [5] Soileau M J, et al, "Laser Induced Damage in Optical Materials" NBS special publication # 541, p. 309, (1978)
- [6] House R A, et al, "Laser Induced Damage in Optical Materials" NBS special publication # 435, p305, (1976)
- [7] Apfel J H et al, "Effects of barrier layers and surface smoothness on, 1060nm laser damage of AR coatings on glass" Proceedings of the Laser Damage Conference, Boulder,USA, (1977)
- [8] Guenther K H et al, *Appl.Opt.*, **23**, 3743, (1984)
- [9] Mansour N et al, "Laser Induced Damage in Optical Materials" NBS special publication # 727, p. 137, (1984)
- [10] Bass M and Barret H H, *Appl.Opt.*, **12**, 690, (1973)
- [11] Bloembergen N, *IEEE J.Quant.Electron.*, **QE10**, 375, (1974)
- [12] Warlock J M, "Two-Photon Spectroscopy" in Laser Handbook Vol.2, p.1323, (North-Holland, (1972)
- [13] Pidgeon C R et al, *Phy.Rev.Lett.*, **42**, 1785, (1979)
- [14] Groshkov B G et al, "Laser Induced Damage in Optical Materials" NBS special publication # 541, p. 299, (1978)
- [15] Keldysh L V, *Sov.Phys.JETP*, **20**, 1307, (1965)
- [16] Jones H D and Reiss F I R, *Phys.Rev:B*, **16**, 2466, (1977)
- [17] Adduci F et al, *Phys.Rev:B*, **15**, 926, (1977)
- [18] Soileau M J et al, "Laser Induced Damage in Optical Materials" NBS special publication # 638, p. 589, (1981)
- [19] Bliss E S, *Opto-Electronics*, **3**, 99, (1971)
- [20] Soileau M J, et al, "Laser Induced Damage in Optical Materials" NBS special publication # 727, p. 394, (1984)

- [21] Milam D, et al, "Laser Induced Damage in Optical Materials" NBS special publication # 509, (1977)
- [22] Sharma S K, Wood R M and Ward R C, "Laser Induced Damage in Optical Materials" NBS special publication # 509, (1977)
- [23] Fauchet P M and Siegman A E, "Laser Induced Damage in Optical Materials" NBS special publication # 727, p. 147, (1984)
- [24] Martin von Allmen, in Springer Series in Material Science 2, "Laser Beam Interaction with Materials", (Springer-Verlag, Berlin, 1987) p41
- [25] Emmony D C, et al, *Appl.Phys.Lett.*, 23, 598, (1973)
- [26] Young J F, et al, *Appl.Phys.Lett.*, 41, 261, (1982)
- [27] Temple P A and Soileau M J, *IEEE J.Quant.Electron.*, QE-17, 2067, (1981)
- [28] Sipe J E, et al, *Phys.Rev.B*, 27, 1141, (1983)
- [29] Sipe J E, et al, *Phys.Rev.B*, 30, 2001, (1984)
- [30] Guosheng Z, et al, *Phys.Rev.B*, 26, 5366, (1982)
- [31] Bruech S R J and Ehrlich D J, *Phys.Rev.Lett.*, 48, 1678, (1982)
- [32] Ehrlich D J, et al, *Appl.Phys.Lett.*, 41, 630, (1982)
- [33] Keilmann F and Bai Y H, *Appl.Phys.A*, 29, 9, (1982)
- [34] Leamy H J, et al, *Appl.Phys.Lett.*, 32, 535, (1978)
- [35] Boyd I W, et al, *Appl.Phys.Lett.*, 45, 80, (1984)
- [36] Koo J C and Slusher R E, *Appl.Phys.Lett.*, 28, 614, (1976)
- [37] M von Allmen, et al, *Appl.Phys.Lett.*, 33, 824, (1978)
- [38] Baltzer N, et al, *Appl.Phys.Lett.*, 32, 535, (1978)
- [39] Gorodetsky G et al, *Appl.Phys.Lett.*, 46, 547, (1985)
- [40] Kreuz E W et al, in Springer series in Chemical Physics, 39, "Laser Processing and Diagnostics", Ed. Bauerle D, (Springer-Verlag, Berlin, 1984), p 107
- [41] Hill C, in "Laser Annealing of Semiconductors", Ed. Poate and Mayer J W, (Academic Press, New York, 1982) p 479
- [42] Keilmann F, *Phys.Rev.Lett.*, 51, 137, (1976)
- [43] Ready J F, *IEEE J.Quant.Electron.*, QE12, 137, (1976)
- [44] Kovalev V I and Faizullov F S, "Laser Induced Damage in Optical Materials" NBS special publication # 541, p.318, (1984)
- [45] Walker T M, PhD thesis, Airforce Institute of Technology, Ohio, USA, (1979)

- [46] Lange M R et al, *SPIE Proc.*, **380**, 450, (1983)
- [47] Sparks M and Loh E, *J.Opt.Soc.Am.*, **69**, 847, (1979)
- [48] Porteus J O et al, *IEEE J.Quant.Electron.*, **QE17**, 2078, (1981)
- [49] Wood R M, Sharma S K and Waite P, *SPIE.Proc.*, **369**, 84, (1983)
- [50] Gibbs R and Wood R M, "Laser Induced Damage in Optical Materials" NBS special publication # 462, p. 181, (1976)
- [51] Ready J F, *J.Appl.Phys.*, **36**, 462, (1965)
- [52] Dyumaev K M et al, *Sov.J.Quantum.Electron.*, **13**, 503, (1983)
- [53] Hect J, *Laser Focus*, **28**, no.6, 63, (1992)
- [54] Manenkov A A, Nechitailo V S and Tsaprilov A S, *Sov.J.Quantum.Electron.*, **11**, 502, (1981)
- [55] Ashkinadze B M et al, *Sov.Phys.JETP.*, **23**, 788, (1966)
- [56] Aldoshin M I et al, *Sov.J.Quantum.Electron.*, **9**, 1102, (1979)
- [57] Bebchuk A S et al, *Sov.J.Quantum.Electron.*, **6**, 986, (1976)
- [58] Butenin A V and Kogan B Y, *Sov.J.Quantum.Electron.*, **6**, 611, (1976)
- [59] Manenkov A A and Nechitailo V S, *Sov.J.Quantum.Electron.*, **10**, 347, (1980)
- [60] Agranat M B et al, *Sov.Phys.JETP*, **33**, 944, (1971)
- [61] Liberman M A and Tribelskii M I, *Sov.Phys.JETP*, **47**, 99, (1978)
- [62] Kovalev A A et al, *Sov.Tech.Phys.Lett.*, **6**, 142, (1980)
- [63] Danileiko Y K et al, Proceedings of the "4th All Union Conference on Non-linear Interaction of Optical Radiation"
- [64] Manenkov A A et al, *Izv.Akad.Nauk.SSSR*, **44**, 1770, (1980)
- [65] Radhakrishnan P, PhD. thesis, "Nd:glass Laser Induced Damage Studies", Cochin University, 1985
- [66] Srinivasan R, Braren B, Seeger D E and Dreyfus R W, *Macro Molecules*, **19**, 916, (1986)
- [67] Srinivasan R and Braren B, *Chem.Rev.*, **89**, 1303, (1989)
- [68] Padmaja G, et al, *J.Phys.D:Appl.Phys.*, **22**, 1558, (1989)
- [69] Padmaja G, et al, *J.Phys.D:Appl.Phys.*, **25**, in press, (1992)
- [70] Koren G and Yeh J T C, *Appl.Phys.Lett.*, **44**, 1112, (1986)
- [71] Gorodetsky G et al, *Appl.Phys.Lett.*, **46**, 828, (1985).
- [72] Dienstbier M et al, *Appl.Phys.B*, **51**, 137 (1990)
- [73] Rosencwaig A and Willis J B, *Appl.Phys.Lett.*, **36**, 667 (1980)

- [74] Ravi Kumar A V, et al, *Pramana*, **37**, 345, (1991)
- [75] Aver'yanov N E et al, *Sov.Phys.Tech.Phys.*, **32**, 1050, (1987)
- [76] Petzoldt S et al, *Appl.Phys.Lett.*, **53**, 2005, (1988)
- [77] Hordvik A and Skolink L, *Appl.Opt.*, **16**, 2919, (1977)
- [78] Ghosh A P and Hurst J E, *J.Appl.Phys.*, **64**, 287, (1988)
- [79] Sell J A, et al, *Appl.Phys.Lett.*, **55**, 2435 (1989)
- [80] Sell J A, et al, *J.Appl.Phys.*, **69**, 1330, (1991)
- [81] Rajasree K, et al, *Bull.Mater.Sci.*, **15**, 183, (1992)
- [82] Patel C K N and Tam A C, *Rev.Mod.Phys.*, **53**, 517, (1981)
- [83] Rosencwaig A, *J.Appl.Phys.*, **49**, 2905, (1978)
- [84] Harada Y et al, *J.Phys. D: Appl. Phys.*, **22**, 569, (1989)
- [85] E W Van Stryland et al, "Laser Induced Damage in Optical Materials" NBS special publication # 589, p.557, (1981)
- [86] Basov N G, Krokhin O N and Sklikov G V, *JETP Lett.*, **6**, 168, (1967)
- [87] Eesley G L, Clemens B M and Paddock C A, *Appl.Phys.Lett.*, **50**, 717, (1987)
- [88] Sullivan B and Tam A C, *J.Acoust.Soc.Am.*, **75**, 437, (1984)
- [89] Benditskii A A et al, *Sov.Phys.Acoust.*, **34**, 240, (1988)
- [90] Benditskii A A and Gromov G L, *Poverkh.Fiz.Khim.Mekh.*, No.12, (1986)
- [91] Babadzhan B I et al, *Poverkh.Fiz.Khim.Mekh.*, No.1, (1987)
- [92] Milam D, *Appl. Opt.*, **16**, 1204, (1977)
- [93] Golberg S M, et al, *Appl.Phys.B*, **31**, 85, (1983)

- [94] Wood R M, Waite P and Sharma S K, proceedings of the "NBS Laser Damage Conference", Boulder, USA, November, 1983
- [95] Dikkjamp D et al, *Appl.Phys.Lett.*, **51**, 619, (1987)
- [96] Sankur S et al, *J.Vac.Sci.Tech.*, **5**, 15, (1987)
- [97] Dijkkamp D et al, *Appl.Phys.Lett.*, **51**, 619, (1987)
- [98] Niefeld R A et al, *Appl.Phys.Lett.*, **53**, 703, (1988)
- [99] Chen G and Yeung E S, *Anal.Chem.*, **60**, 2258, (1988)
- [100] Leung W P and Tam A C, conference proceedings, "7th International Topical Meeting on PA and PT Phenomena", The Netherlands, p.365, (1991)
- [101] Manabe R M and Piepmeyer E H, *Anal.Chem.*, **51**, 2066, (1979)

- [102] Measures R M and Kwong H S, *Appl.Opt.*, 18, 281, (1979)
 [103] Kantor T et al, *Spect.Chem.Acta:B*, 34B, 341, (1979)
 [104] Rudnevsky N K et al, *Spect.Chem.Acta:B*, 39B, 5, (1984)

7.10. Symbols and Notations

a_0	Laser beam radius
a	Laser beam diameter at sample surface
α_0	Absorptivity at T_0 for the laser wavelength
b	Beam diameter at a distance D from lens ($D > f$)
β_t	Thermal coefficient of expansion of air
c_0	Velocity of sound
C_m	Specific heat of sample
C_v	Specific heat at constant volume
Δ	Ionization potential
D_h	Thermal conductivity
E	Electric field associated with the laser
E_B	Electric breakdown strength
E_b	Bandgap energy
E_D	Threshold energy density
E_{in}	Electric field inside the discontinuity
E_0	Electric field associated with the laser
E_{eff}	Effective elastic constant
ϵ	Dielectric constant
f	Focal length of lens
$h\nu$	Photon energy
H	Heat flux from target surface to surrounding air
I	On-axis intensity of damage threshold
k, k_m	Coefficient of thermal conductivity of sample
K	Constant determined by sample properties
l	Optical absorption length
L	Depolarization factor
λ	Laser wavelength

λ_0	Vacuum wavelength
ρ_m	Density of sample
M	Mass of molecule
m, e	Mass and charge of electron
η	Refractive index
P	Pressure amplitude
P_1, P_n	Probability of damage in the 1 st and n th pulse
$p(E)$	Probability of breakdown when 1 initial electron is present
$p'(E)$	Probability of breakdown when n initial electrons are sampled
P_D	Optical power density
Q	Total energy
Q_{in}	Incident energy on the focussing lens
R	Radius of inclusion
R_s	Surface reflection coefficient
r_o	Radius at which laser intensity falls by $1/e^2$
r_d	Radius at which first damage occurs
ρ_v	Vapour density
ρ	Density
σ	Cross section of collision of electrons with molecules
t	Time for the acoustic response to develop
τ_L	Laser pulse width
T_L, T_s	Transmission of the focal lens and sample
T_m, T_o	Melting and ambient temperature
τ_T	Acoustic signal transit time
τ_a	Acoustic pulse duration
T	temperature of the sample
u_e	mean electron velocity
v_e	Frequency of free electron with neutral molecules
v	Velocity of shear wave
ω	Laser frequency
z', z_o	Impedances of dielectric and free space

CHAPTER VIII

GENERAL CONCLUSIONS

CHAPTER VIII

GENERAL CONCLUSIONS

The work presented in this thesis is essentially an attempt to study the laser induced photoacoustic effect in solid and gaseous samples. Both cw and pulsed lasers have been made use of for this purpose. The optimization of the experimental setup and the of the PA cell design for both pulsed and cw PA studies have been achieved. For cw PA studies, a dual cavity, differential PA cell was designed and fabricated and was found to perform well within a permissible low noise factor. Several parameters of the PA cell linked to its resonance characteristics such as the resonance frequency, resonance bandwidth, Quality factor etc. have been investigated in the course of this work. Interesting observations on the variation of the resonance frequency of the cell with gas pressure were made in this context. For cw PA studies, appropriate software was also developed for automated instrument control and data acquisition, thus making measurements much faster and more accurate.

PA studies in gaseous samples were made, with special reference to gases such as NO_2 and formaldehyde, which play a vital role in the environmental chemistry. The many-fold advantages of the PA technique make it a versatile tool for trace detection and analysis of gaseous species. Pulsed PA spectra of formaldehyde vapour and both cw as well as pulsed PA spectra of nitrogen dioxide samples have been studied in some detail in this thesis. Multiphoton absorption processes, observed by PA technique can be used to detect samples like formaldehyde

vapour which does not normally exhibit absorption in the wavelength region of interest (visible). It has been observed that one photon absorption occurs in formaldehyde at low laser energies whereas the two photon absorption process predominates at higher laser energies in both the 564nm and 1060nm wavelength regions. The absorption spectra of formaldehyde in the liquid phase provided information regarding the occurrence of different combination bands in the wavelength regions of interest. The dependence of the PA signal with pressure and the laser energy were also studied. The PA signal varies linearly with gas pressure and laser energy for lower values of pressure and energy but saturates at higher gas pressures and laser energies. The two photon PA spectrum of formaldehyde has been reported for the first time in this thesis.

The significance of studies on NO_2 , especially in the context of atmospheric pollution and the detection of NO_2 by PA technique, using both pulsed and cw dye lasers have been described. The pulsed PA signature spectra of NO_2 in the 560-580nm has been established for the first time to the best of the author's knowledge and the nature of variation of the PA signal with the gas pressure and laser energy/power has been determined. It is seen that the PA signal tends to saturate easily for high concentration samples. The cw PA spectrum of NO_2 in the 570-600nm wavelength region was established using the differential PA detection technique. This arrangement was found to have a very low noise level as is evident from the PA spectra recorded. The spectrum thus obtained was found to be better resolved than previously reported results in this region using PA technique. The dependence of the PA signal on gas pressure and the laser power was investigated in detail, bringing out the features of PA signal saturation with pressure and laser power. An absolute calibration of the PA system was not done due to the

non-availability of standard, certified gas mixtures and other gas analysis techniques such as gas chromatography. Rather than the detailed spectroscopic analysis of these gas samples, the method of detection of the samples and characterization of the PA system for these species have been given more importance.

In the case of solids, the study of laser-material interactions like laser damage, plasma formation etc are of great current interest from the point of view of characterization of materials. The various aspects of laser induced damage process have also been discussed in detail. The PA effect has been applied to the estimation of the laser damage threshold in various materials. The abrupt change exhibited by the PA signal associated with the laser damage threshold has been used to detect the different kinds of damages occurring both on the surface and in the bulk of different samples, with special reference to polymeric samples. The surface damage occur first, followed by bulk damage, which results in processes like bond scission, melting and finally plasma formation. It was observed that the surface damage threshold was very sensitive to the surface finish of the sample whereas the bulk damage is quite independent of the surface characteristics. The versatility of the PA technique is demonstrated by investigating these parameters in a variety of samples. The different kinds of damage processes on the sample surface like ripples, microcracks and scratch induced damage observed in the course of these studies have also been presented.

The PA effect was also used to monitor the laser induced plasma process. The variation of the plasma emission intensity and the acoustic signal generated due to the ablation process were found to be linear with respect to the laser energy density within the region of interest. Thus it is shown that by monitoring the PA signal, it is possible to monitor *in-situ*, the laser energy

density.

Future Work

Since the PA system for gas detection has been optimized, the next step towards *in-situ* trace analysis is to calibrate the PA system with standard, calibrated gas samples and to compare the results obtained by PA studies with other techniques such as the gas chromatography and normal absorption methods. A compact and portable PA cell using a semiconductor diode laser operating in the 670nm region, and appropriate electronics can be built to detect traces of NO₂ in *in-situ* conditions such as automobile exhausts and factory premises. Further, this technique can be applied to other samples in other wavelength regions using lasers of appropriate wavelengths.

The PA detection of the laser damage threshold can also be used to study *in-situ*, the damage process in high power laser optics. By constantly monitoring and processing, using appropriate electronics the the PA signal from a standard laser optics component, it is possible to restrict the power of the laser to within the damage threshold.

-----o000o-----